

Hanne Svergja

Anilines in acid catalyzed amination with 4-chloro-7*H*-pyrrolo[2,3-*d*] pyrimidine

Master's thesis in Organic Chemistry

Supervisor: Bård Helge Hoff

Co-supervisor: Cecilie Elisabeth Olsen

August 2023

Hanne Svergja

Anilines in acid catalyzed amination with 4-chloro-7*H*-pyrrolo[2,3-*d*] pyrimidine

Master's thesis in Organic Chemistry
Supervisor: Bård Helge Hoff
Co-supervisor: Cecilie Elisabeth Olsen
August 2023

Norwegian University of Science and Technology
Faculty of Natural Sciences
Department of Chemistry



Acknowledgements

Firstly, I want to express my immense gratitude to my supervisor Professor Bård Helge Hoff and my co-supervisor PhD student Cecilie Elisabeth Olsen for all the guiding, patience, and feedback during this entire research process. Your competence and dedication to the field contributed significantly to shape my thesis and helped me stay motivated and inspired throughout the whole year.

I don't have a count of how many hours I have spent in the D2-102 and D2-106 lab, but I know it would definitely not have been the same without Cecilie, Vijay, Srini, and Nicholas. Countless conversations regarding everything related to science and non-science enabled me to stay committed to the practical work and enjoying it at the same time. Your willingness to always answer my questions also made me feel so well received. I have also cherished the occasional check-ins by Bård in the lab, preferably Friday afternoons, as they brought value to my research and mood. Additionally, being a member of the "Hoff/Sundby family" research group has been a valuable experience with the weekly meetings and the social gatherings.

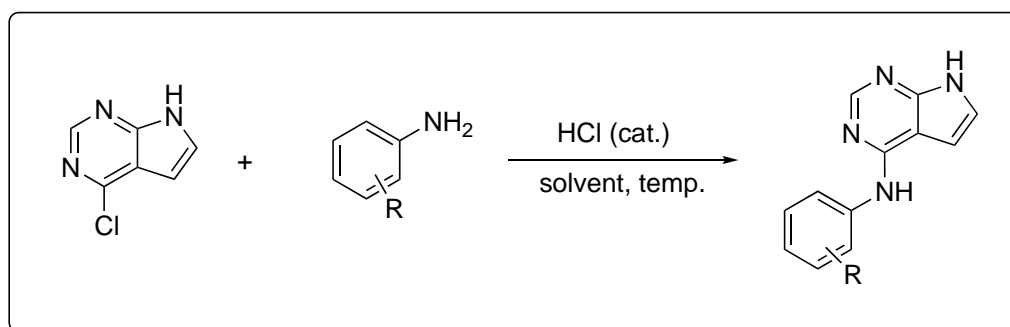
This acknowledgement section would not be complete without mentioning the significant assistance from Roger Aarvik, who have supplied me with countless needles, vials, syringes and last, but not least, DMSO-*d*₆. I am also grateful for Susana Villa Gonzalez and Julie Asmussen for running the MS experiments, and for Torun Margareta Melø for guidance in the NMR lab.

It is no secret that my last semester at NTNU was memorable, but it had its challenges. The horse-riding accident that broke my arm and the following surgery was no doubt a huge setback in my master's journey, and I hope the quality of my work was not compromised. It was a very difficult time, but I was lucky to have amazing friends to both keep me company and do the grocery shopping. These friends have meant a lot to me during my 5 years in Trondheim, and a very special thanks goes out to Liva, Julie, Johan, Simen, Viktoria, Kristin, and Aurora.

Lastly, I want to thank my family, especially my mom (or should I say personal therapist), Ingrid. These last few years have been a journey, both academically and personally. It has been exiting, but also incredibly demanding at times. Without your support, encouragement, and hugs, I genuinely do not know how I would get through it all!

Abstract

Pyrrolopyrimidines have a vast pharmacological profile and are of significant importance in many biologically active compounds. Acid catalyzed amination of such heterocycles is a well-known strategy in synthesizing promising scaffolds in the field of medicinal chemistry. Amination with anilines on 4-chloro-7*H*-pyrrolo[2,3-*d*]pyrimidine under acidic conditions have been reported, however, no in-depth study of such reactions have been found. For this master thesis, 4-chloro-7*H*-pyrrolo[2,3-*d*]pyrimidine and aniline were employed as a model reaction with HCl as the catalyst to optimize conditions and observe the effects of different variables. A secondary objective was to derive a better understanding of the reaction mechanism through NMR analysis.



The protonation site on 4-chloro-7*H*-pyrrolo[2,3-*d*]pyrimidine was investigated through ¹H-NMR analysis. Although it seemed like the compound was protonated in acidic conditions, an exact protonation site was not identified.

Continuing the research of a previous master student, the effect of acid amount was explored with EtOH as the solvent. Acid amounts exceeding 0.1 equivalents had a significant positive effect on conversion but lead to increased solvolysis of 4-chloro-7*H*-pyrrolo[2,3-*d*]pyrimidine. Interestingly, the solvolysis side product 4-ethoxy-7*H*-pyrrolo[2,3-*d*]pyrimidine reacted with aniline in which EtOH was the leaving group, eventually forming the desired product.

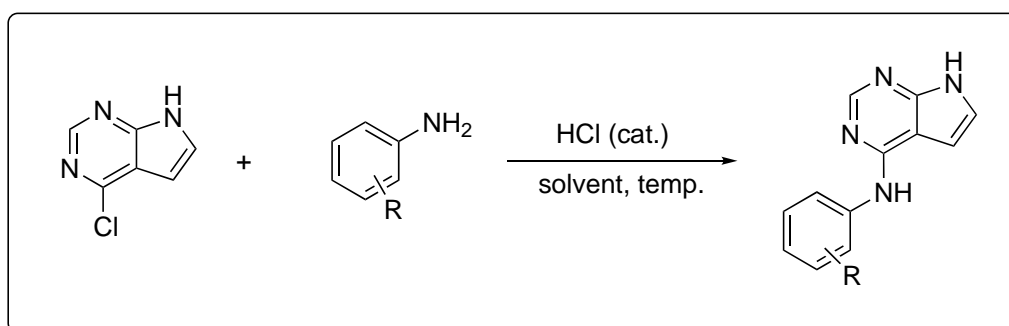
The effect on conversion and side products in the model reaction were studied through reaction variables such as solvent type, acid amount and temperature. The highest conversion in the model reaction was achieved with H₂O at 80 °C with only 0.1 eq. HCl. This procedure was more sustainable and greener than those previously found in the literature and gave full conversion after 6 hours without side products. Simple alcohols were also employed as solvents

but led to either solvolysis or low conversion compared to H₂O. Increasing the acid amount in H₂O did not result in a significant increase of hydrolysis of 4-chloro-7*H*-pyrrolo[2,3-*d*]pyrimidine.

Following identification of a satisfactory procedure, a substrate scope study with different anilines was conducted. It was hypothesized that the reaction could follow two pathways, where either the 4-chloro-7*H*-pyrrolo[2,3-*d*]pyrimidine or nucleophilic amine was protonated based on their p*K*_a. Nevertheless, the S_NAr reaction could proceed in both scenarios. Anilines with weakly deactivating groups, such as halogens and alkyne, posed as great substrates in these conditions followed by anilines with activating groups, such as ethers and alcohol, achieving high initial conversion. The most suited substrates in these two categories gave 70-80% conversion within 1 hour, and mediocre to high yields were obtained on a preparative scale (56-94%). Anilines that did not suffer from steric effects and possessed p*K*_a values in the range of 2.73-5.20 were most suited for acid catalyzed amination to 4-chloro-7*H*-pyrrolo[2,3-*d*]pyrimidine in water. Anilines that fell outside of this p*K*_a range or had bulky *o*-substituents were generally not suitable substrates. Effects such as electron density and steric hindrance on the conversion were observed by comparing similar aniline types. Amines with p*K*_a above 5.20 were also employed, where benzylic amines were almost unreactive, however, one cyclic and one primary amine gave satisfactory conversion rates which even exceeded one literature procedure. Some substrates had difficulties dissolving in H₂O and was one of the main limitations in this procedure as well as steric hindrance in certain substrates.

Sammendrag

Pyrrolopyrimidiner har en omfattende farmakologisk profil og er av stor betydning i mange biologisk aktive forbindelser. Syre-katalysert aminering av slike heterosykliske forbindelser er en velkjent strategi innen syntese av lovende strukturer innen medisinsk kjemi. Aminering med aniliner på 4-kloro-7*H*-pyrrolo[2,3-*d*]pyrimidin under sure betingelser er tidligere blitt rapportert, men en prinsipiell studie har ikke blitt funnet i litteraturen. I dette masterprosjektet ble en modellreaksjon med 4-kloro-7*H*-pyrrolo[2,3-*d*]pyrimidin og anilin benyttet med HCl som katalysator for å optimalisere betingelser og observere effekten av ulike variabler. Et sekundært mål var å oppnå en bedre forståelse av reaksjonsmekanismen gjennom NMR-studier.



Protonering av 4-kloro-7*H*-pyrrolo[2,3-*d*]pyrimidin ble undersøkt ved hjelp av ^1H -NMR. Selv om forbindelsen ble protonert under sure forhold, ble nøyaktig protoneringsposisjon ikke identifisert.

Basert på arbeid utført av en tidligere masterstudent, ble effekten av syremengde utforsket med EtOH som løsningsmiddel. Syremengde over 0.1 ekvivalenter hadde en signifikant effekt på omsetning og førte til økt solvolyse av 4-kloro-7*H*-pyrrolo[2,3-*d*]pyrimidin. Et interessant funn var at solvolyseproduktet 4-etoksy-7*H*-pyrrolo[2,3-*d*]pyrimidin reagerte med anilin, hvor EtOH var utgående gruppe, og dannet det ønskede produktet.

Effekten på omsetning og sekundære reaksjoner i modellreaksjonen ble studert gjennom variabler som løsningsmiddeltype, syremengde og temperatur. Den høyeste omsetningen, full omsetning etter 6 timer, ble oppnådd med H_2O ved $80\text{ }^\circ\text{C}$ med bare 0.1 ekvivalenter HCl. Denne utviklede metoden var mer bærekraftig og grønnere enn de som tidligere er funnet i litteraturen. Små alkoholer ble også testet som løsningsmidler, men solvolyse og lav omsetning ble

observert. Økende syremengde i H₂O førte ikke til en betydelig økning i hydrolyse av 4-kloro-7*H*-pyrrolo[2,3-*d*]pyrimidin.

Etter en mer optimal metode var etablert, ble det gjort en studie på ulike substrater i reaksjonen. Det ble antatt at reaksjonen kunne følge en av to veier, hvor enten 4-kloro-7*H*-pyrrolo[2,3-*d*]pyrimidin eller nukleofilt amin ble protonert basert på p*K*_a-verdi. I begge tilfeller ble det antatt at utgangsstoffene ville reagere *via* S_NAr. Aniliner med svakt deaktivierende grupper, som halogener og alkyn, var gode substrater under disse betingelsene, etterfulgt av aniliner med aktiverende grupper, som eter og alkohol, og oppnådde høy initial omsetning. De best egnede substratene i disse to kategoriene ga 70-80% omsetning innen 1 time, og tilfredsstillende utbytter ble oppnådd på en preparativ skala (56-94%). Aniliner som ikke ble påvirket av sterisk hindring og som hadde p*K*_a-verdi i området 2,73-5,20, var mest egnet for syre-katalysert aminering til 4-kloro-7*H*-pyrrolo[2,3-*d*]pyrimidin i vann. Aniliner som lå utenfor p*K*_a-området eller hadde steriske *o*-substituenten, var generelt ikke egnede substrater. Ved å sammenligne lignende typer aniliner, ble effekter som elektrontetthet og sterisk hindring på konverteringen observert. Aminer med p*K*_a over 5,20 ble også brukt, der bensylliske aminer var nesten ureaktive, men et syklisk amin og et primært amin ga tilfredsstillende omsetning som var høyere enn det som ble funnet i en litteraturprosedyre. Noen substrater var tungtløselig i H₂O som var en av hovedbegrensningene i prosedyren i tillegg til sterisk hindring i enkelte substrater.

Contents

Acknowledgements	I
Abstract	III
Sammendrag	V
Symbols and Abbreviations	X
Numbered compounds	XI
1 Introduction and Theory	1
1.1 Previous work and current aim.....	1
1.2 Pyrrolopyrimidines	3
1.2.1 Structure and biological activity.....	3
1.2.2 Pyrrolopyrimidine chemistry	7
1.2.3 pK _a of pyrrolopyrimidines	10
1.3 Anilines	12
1.3.1 pK _a of anilines	12
1.3.2 Synthesis of anilines	15
1.4 Amination on heterocycles	16
1.4.1 Nucleophilic aromatic substitution	16
1.4.2 Buchwald-Hartwig amination.....	20
2 Results and discussion	24
2.1 NMR-studies	26
2.2 Model reaction.....	29
2.2.1 Initial experiments	30
2.2.2 Effect of solvent type and temperature	33
2.2.3 Effect of acid amount in water	37
2.3 Substrate scope	41
2.3.1 Aniline scope	41
2.3.2 Amine scope	49
2.3.3 Substrate comparison.....	55
2.4 Amination on 500 mg scale.....	56

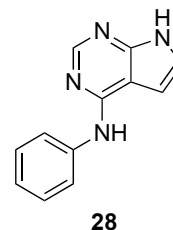
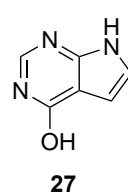
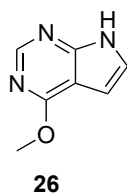
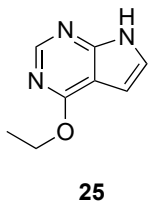
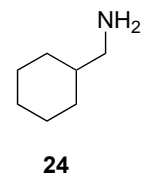
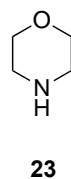
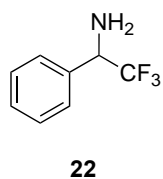
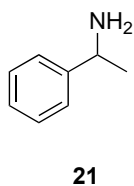
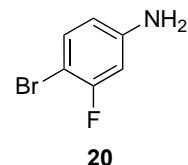
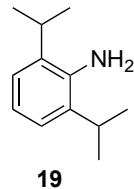
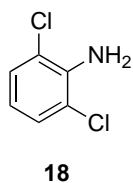
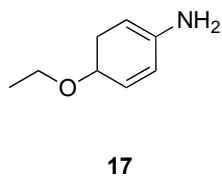
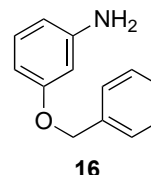
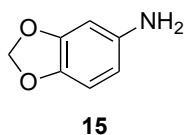
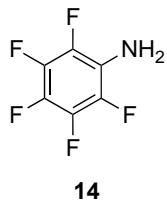
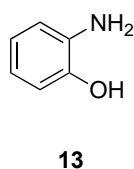
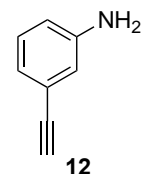
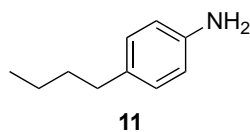
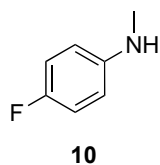
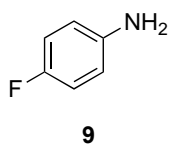
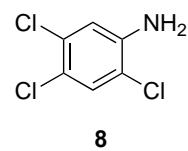
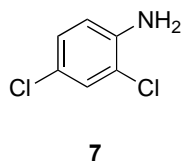
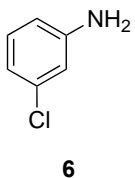
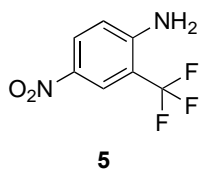
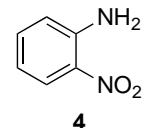
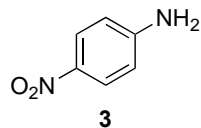
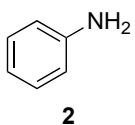
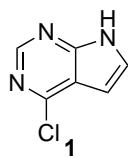
3	Structure elucidation	60
3.1	Pyrrolopyrimidines	60
3.1.1	Elucidation of compound 33.....	62
3.1.2	Elucidation of compound 36.....	64
3.1.3	Elucidation of compound 37.....	66
3.1.4	Elucidation of compound 38.....	68
3.1.5	Elucidation of compound 42.....	70
3.1.6	Elucidation of compound 46.....	72
4	Conclusion.....	74
5	Future work.....	76
6	Experimental	77
6.1	General information.....	77
6.2	Synthetic procedures	78
6.2.1	100 mg scale reaction	78
6.2.2	500 mg scale reaction with NaHCO ₃	78
6.2.3	500 mg scale reaction with K ₂ CO ₃	78
6.2.4	<i>N</i> -Phenyl-7 <i>H</i> -pyrrolo[2,3- <i>d</i>]pyrimidin-4-amine (28)	79
6.2.5	<i>N</i> -(4-Nitrophenyl)-7 <i>H</i> -pyrrolo[2,3- <i>d</i>]pyrimidin-4-amine (29).....	79
6.2.6	<i>N</i> -(3-Chlorophenyl)-7 <i>H</i> -pyrrolo[2,3- <i>d</i>]pyrimidin-4-amine (32)	80
6.2.7	<i>N</i> -(2,4-Dichlorophenyl)-7 <i>H</i> -pyrrolo[2,3- <i>d</i>]pyrimidin-4-amine (33)	80
6.2.8	<i>N</i> -(2,4,5-Trichlorophenyl)-7 <i>H</i> -pyrrolo[2,3- <i>d</i>]pyrimidin-4-amine (34)	80
6.2.9	<i>N</i> -(4-Fluorophenyl)-7 <i>H</i> -pyrrolo[2,3- <i>d</i>]pyrimidin-4-amine (35)	81
6.2.10	<i>N</i> -(4-Fluorophenyl)- <i>N</i> -methyl-7 <i>H</i> -pyrrolo[2,3- <i>d</i>]pyrimidin-4-amine (36)	81
6.2.11	<i>N</i> -(4-Butylphenyl)-7 <i>H</i> -pyrrolo[2,3- <i>d</i>]pyrimidin-4-amine (37)	81
6.2.12	<i>N</i> -(3-Ethynylphenyl)-7 <i>H</i> -pyrrolo[2,3- <i>d</i>]pyrimidin-4-amine (38).....	82
6.2.13	2-((7 <i>H</i> -Pyrrolo[2,3- <i>d</i>]pyrimidin-4-yl)amino)phenol (39)	82
6.2.14	<i>N</i> -(Benzo[<i>d</i>][1,3]dioxol-5-yl)-7 <i>H</i> -pyrrolo[2,3- <i>d</i>]pyrimidin-4-amine (41)	83
6.2.15	<i>N</i> -(3-(Benzyloxy)phenyl)-7 <i>H</i> -pyrrolo[2,3- <i>d</i>]pyrimidin-4-amine (42)	83
6.2.16	<i>N</i> -(4-Ethoxyphenyl)-7 <i>H</i> -pyrrolo[2,3- <i>d</i>]pyrimidin-4-amine (43)	84
6.2.17	<i>N</i> -(4-Bromo-3-fluorophenyl)-7 <i>H</i> -pyrrolo[2,3- <i>d</i>]pyrimidin-4-amine (46).....	84
7	References.....	86
APPENDICES.....		101
A	Spectroscopic data – Compound 28	103
B	Spectroscopic data – Compound 29	107

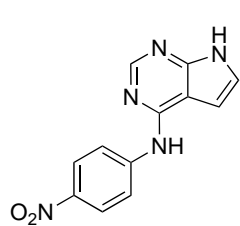
C	Spectroscopic data – Compound 32	111
D	Spectroscopic data – Compound 33	114
E	Spectroscopic data – Compound 34	120
F	Spectroscopic data – Compound 35	121
G	Spectroscopic data – Compound 36	125
H	Spectroscopic data – Compound 37	132
I	Spectroscopic data – Compound 38	139
J	Spectroscopic data – Compound 39	146
K	Spectroscopic data – Compound 41	153
L	Spectroscopic data – Compound 42	160
M	Spectroscopic data – Compound 43	167
N	Spectroscopic data – Compound 46	171
O	Python code for surface plot	178

Symbols and Abbreviations

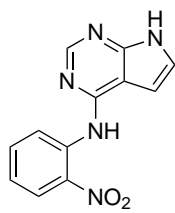
^{13}C NMR	Carbon-13 nuclear magnetic resonance
1D NMR	One dimensional nuclear magnetic resonance
^1H NMR	Hydrogen-1 nuclear magnetic resonance
2D NMR	Two-dimensional nuclear magnetic resonance
bs	Broad singlet
COSY	Correlation spectroscopy
CSF1R	Colony-stimulating factor 1 receptor
DIPEA	Di-isopropyl-ethylamine
EGFR	Epidermal growth factor receptor
eq.	Equivalentents
<i>et al.</i>	Et alii (and others)
FDA	Food and Drug Administration
HER2	Human epidermal growth factor receptor 2
HMBC	Heteronuclear multiple bond correlation
HSQC	Heteronuclear single quantum coherence
IL-17	Interleukin 17
IR	Infrared spectroscopy
J	Coupling constant
m/z	Mass over charge ratio
mp.	Melting point
MS	Mass spectroscopy
NMR	Nuclear magnetic resonance
PDK1	3-Phosphoinositide-dependent kinase 1
ppm	Parts per million
r.t.	Room temperature
R_f	Retention factor
$\text{S}_{\text{N}}\text{Ar}$	Nucleophilic aromatic substitution
TLC	Thin layer chromatography
VEGFR	Vascular endothelial growth factor receptor
δ	Chemical shift

Numbered compounds

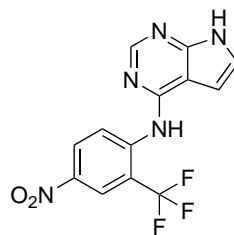




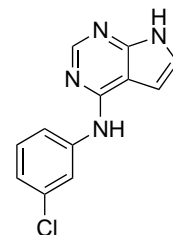
29



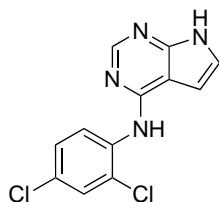
30



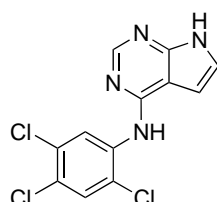
31



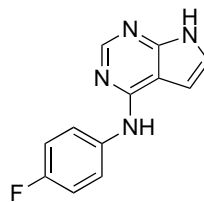
32



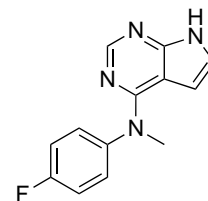
33



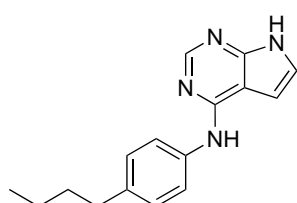
34



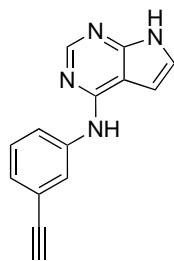
35



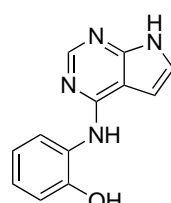
36



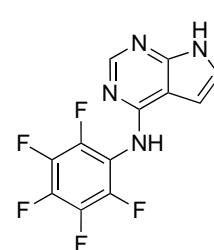
37



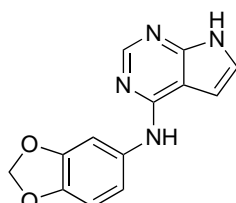
38



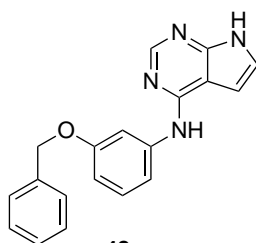
39



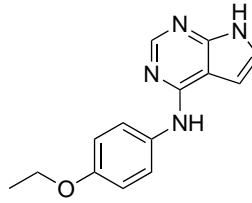
40



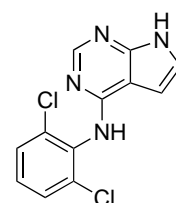
41



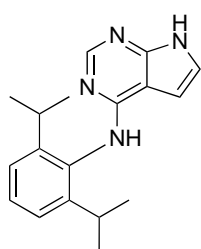
42



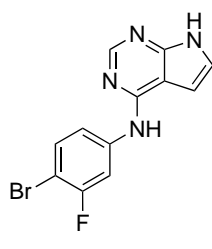
43



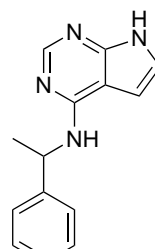
44



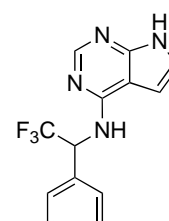
45



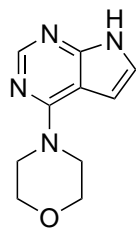
46



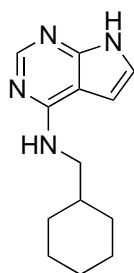
47



48



49



50

1 Introduction and Theory

Heterocyclic compounds, such as fused pyrimidines are part of an interesting class of molecules in the field of medicinal chemistry. This is due to their vast biological activity and potential therapeutic applications.^{1,2} Several fused heterocycles with the privileged pyrimidine scaffold, such as purines, xanthenes, pteridines, quinazolines, pyrrolopyrimidines, pyridopyrimidines, furopyrimidines, thienopyrimidines and thiazolopyrimidines have been evaluated as anti-Alzheimer³, antidepressant⁴, antibacterial^{5, 6}, anticancer⁷, antimalarial⁸, anti-HIV⁹, anti-inflammatory¹⁰ and anti-tuberculosis¹¹ agents, etc.¹

Our research group at NTNU has dedicated extensive efforts into this field, thereby establishing a solid foundation for the background of this current thesis.^{7, 12-15}

1.1 Previous work and current aim

The research group has been working with pyrrolopyrimidines for over 10 years, synthesizing and evaluating several compounds towards treatment of various cancers and autoimmune diseases. This includes inhibitors of the kinases epidermal growth factor receptor (EGFR)^{7, 16, 17} and colony-stimulating factor 1 receptor (CSF1R)¹⁵ and the cytokine interleukin 17 (IL-17) secretion.¹⁸ Several series of disubstituted pyrrolo[2,3-*d*]pyrimidines have been synthesized and assayed towards these applications, some examples are shown in Figure 1.1.

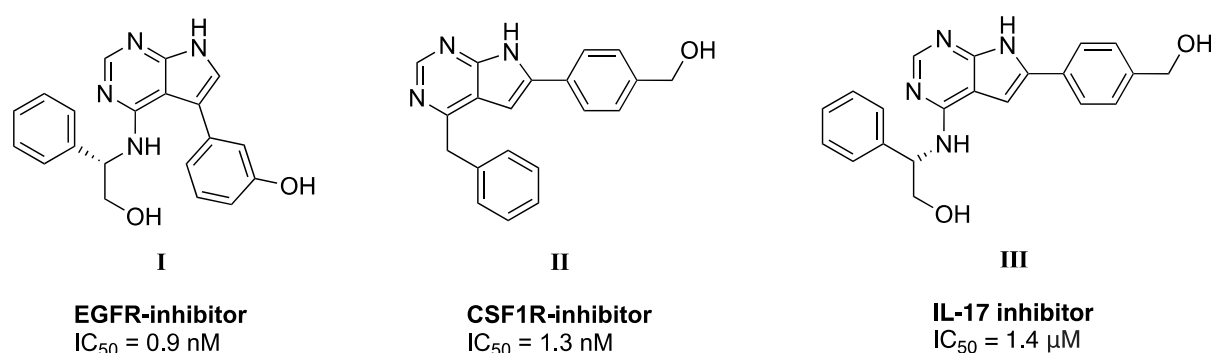


Figure 1.1: Disubstituted pyrrolo[2,3-*d*]pyrimidines **I**, **II** and **III** synthesized by our research group that have shown high activity as antagonists in EGFR, CSF1R and IL-17, respectively.^{13,15, 18}

A more recent project in the group aims to investigate 4-aminosubstituted 7*H*-pyrrolo[2,3-*d*]pyrimidines as low molecular weight inhibitors of human epidermal growth factor receptor 2 (HER2) in breast cancer. Overexpression of HER2 accounts for 25-30%^{19, 20} of all breast cancer

cases and presents an attractive therapeutic target due to its activation mechanism *via* heterodimerization rather than receptor-ligand binding.²¹⁻²³ Additionally, HER2 is overexpressed in several other types of cancer.^{24,25} The structures of Lapatinib²⁶ and Neratinib²⁷ are illustrated in Figure 1.2, which are FDA-approved HER2 inhibitors and characterized by a nitrogen-containing heterocycle and high molecular weight.

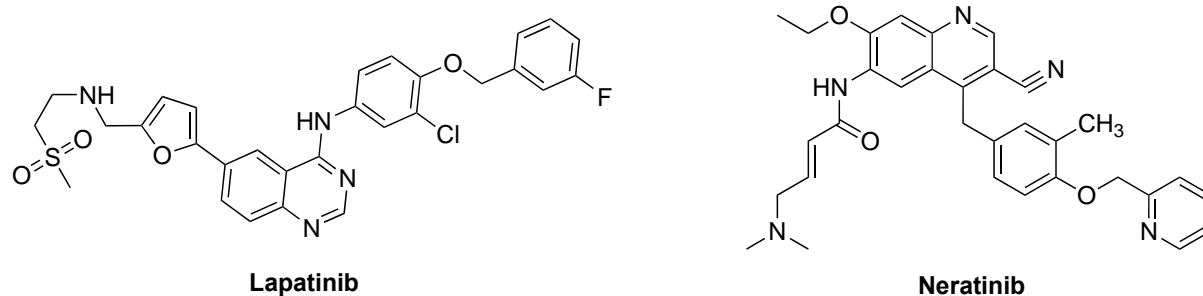


Figure 1.2: Lapatinib and Neratinib as HER2 inhibitors.^{26, 27}

In previous work by Bathen,²⁸ three 4-amino-7*H*-pyrrolo[2,3-*d*]pyrimidines were synthesized as potential HER2 inhibitors, of which some structures showed mediocre, but promising inhibition. The amination of pyrrolopyrimidine was achieved through base and acid catalyzed nucleophilic aromatic substitution (S_NAr). Acid catalyzed S_NAr was the most useful method of the two since basic conditions gave low conversions. In the preferred method, however, the water content had a crucial influence on the formation of side products. Generally acid catalyzed amination is a well-known method, but there has yet to be found any principal studies on amination of heterocycles with anilines.^{11, 24, 29, 30} Therefore, the aim of this project is to identify more optimal conditions for acid catalyzed amination of 7*H*-pyrrolo[2,3-*d*]pyrimidine. A secondary aim is to derive a better understanding of the substrate scope and the mechanism. The general structure of the main target compounds is presented in Figure 1.3.

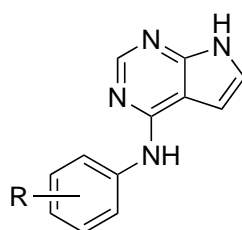


Figure 1.3: Structure of target compounds of 4-amino 7*H*-pyrrolo[2,3-*d*]pyrimidine in this thesis.

1.2 Pyrrolopyrimidines

1.2.1 Structure and biological activity

Pyrrolopyrimidines are nitrogen-containing heterocyclic compounds, made from the electron deficient pyrimidine and the electron rich pyrrole (Figure 1.4). Hence, the pyrimidine can react with nucleophiles while the pyrrole can react with electrophiles, making it a privileged building block. Especially the pyrrolopyrimidine 4-chloro-7*H*-pyrrolo[2,3-*d*]-pyrimidine has several reactive handles.³¹

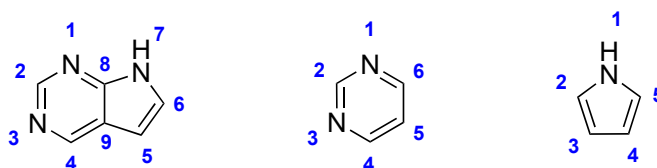


Figure 1.4: Numbered compounds of pyrrolo[2,3-*d*]pyrimidine, pyrimidine, and pyrrole.

Fused nitrogen-containing heterocycles has been a subject of extensive research, as these compounds offer a promising scaffold in medicinal chemistry. This is due to their bioisosteric relationship to purines which enhances their potential in various applications.^{2, 32, 33} These heterocycles were first studied in 1776 when uric acid, a purine derivative, was isolated and identified.³⁴ Pyrrolopyrimidines gained significant attention in the 1950's following the isolation of 6-mercaptopurine³⁵, which exhibited antitumor activity, and toyocamycin³⁶, an antibiotic.^{2, 37} Tubercidin and sangivamycin, which are nucleoside antibiotics, were also discovered during the same timeframe and share the common structural element of 7*H*-pyrrolo[2,3-*d*]pyrimidine.^{2, 33} To date, pyrrolopyrimidines remain a key scaffold and constitute a crucial class of nitrogen-containing heterocycles that play a significant role in medicinal chemistry based on their diverse functions (Figure 1.5).

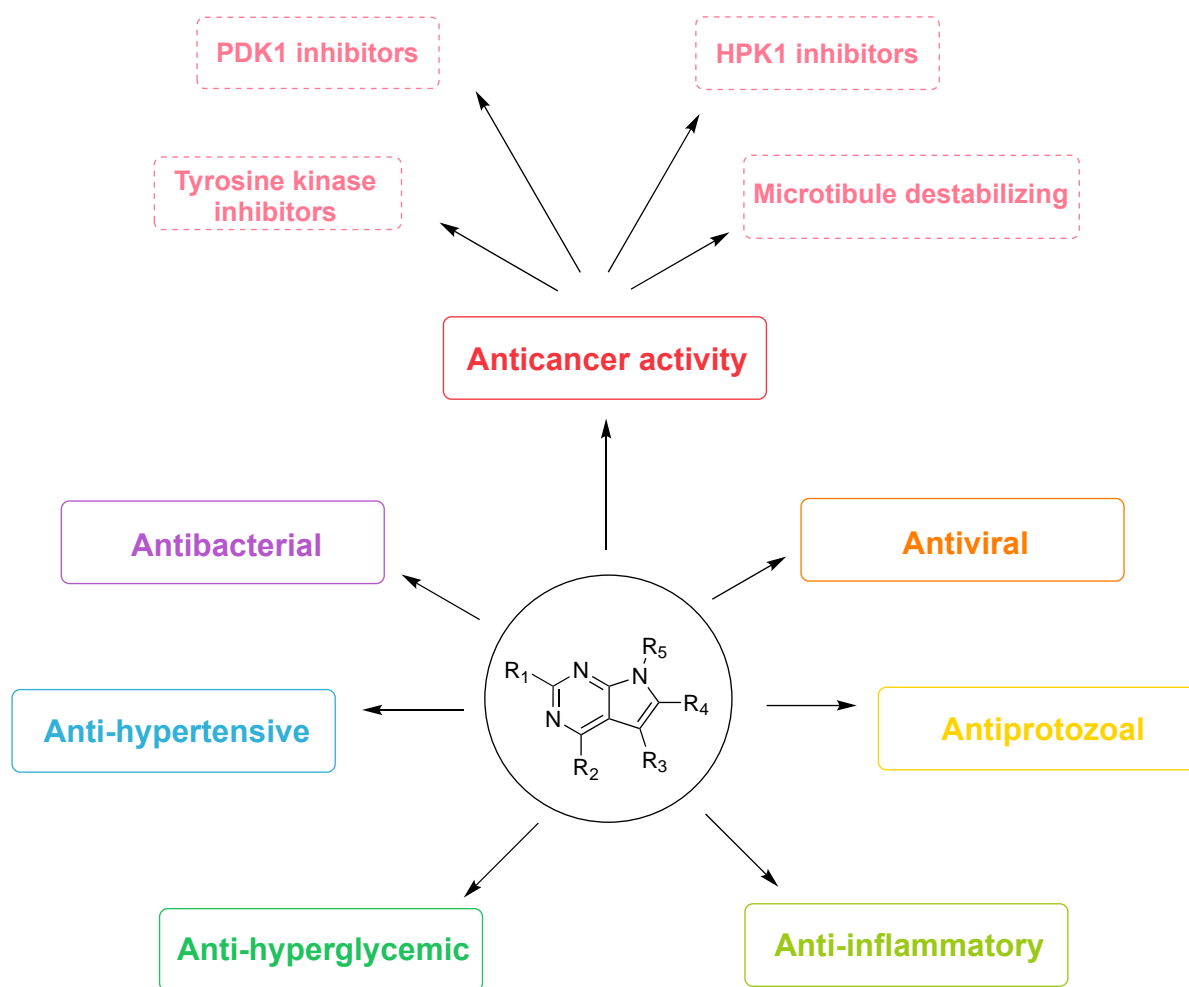


Figure 1.5: An outline of the pharmacological profile of pyrrolopyrimidine: Anticancer activity; Antiviral; Antiprotozoal; Anti-inflammatory; Anti-hyperglycemic; Anti-hypertensive; Antibacterial.

Pyrrolopyrimidines have demonstrated the ability to inhibit critical enzymes involved in signaling pathways as well as microtubule destabilization within the scope of anticancer therapy. Central targets for anticancer therapy are tyrosine kinases, e.g. EGFR, due to their significant role in cell proliferation and differentiation.³⁸ Often, upregulation of these tyrosine kinases results in an impaired apoptotic pathway, leading to extended cancer cell survival and the promotion of aggressive tumor growth.^{21, 38} Finding therapeutic agents in EGFR-mediated disease conditions is therefore of much interest. Fischer *et al.*³⁹ explored novel benzannulated 4-benzylamino pyrrolopyrimidines as dual EGFR and vascular endothelial growth factor receptor 2 (VEGFR2) inhibitors. VEGFR2 is a principal driver of angiogenesis within tumors, and is often found in solid tumors.⁴⁰ In 2016, Han *et al.*⁴¹ synthesized 43 different 6-aryl-7*H*-pyrrolo[2,3-*d*]pyrimidine-4-amines in an effort to develop EGFR inhibitors. Many of these compounds showed high activity and one EGFR inhibitor showed even higher activity than the FDA-approved drug Erlotinib (Figure 1.6).

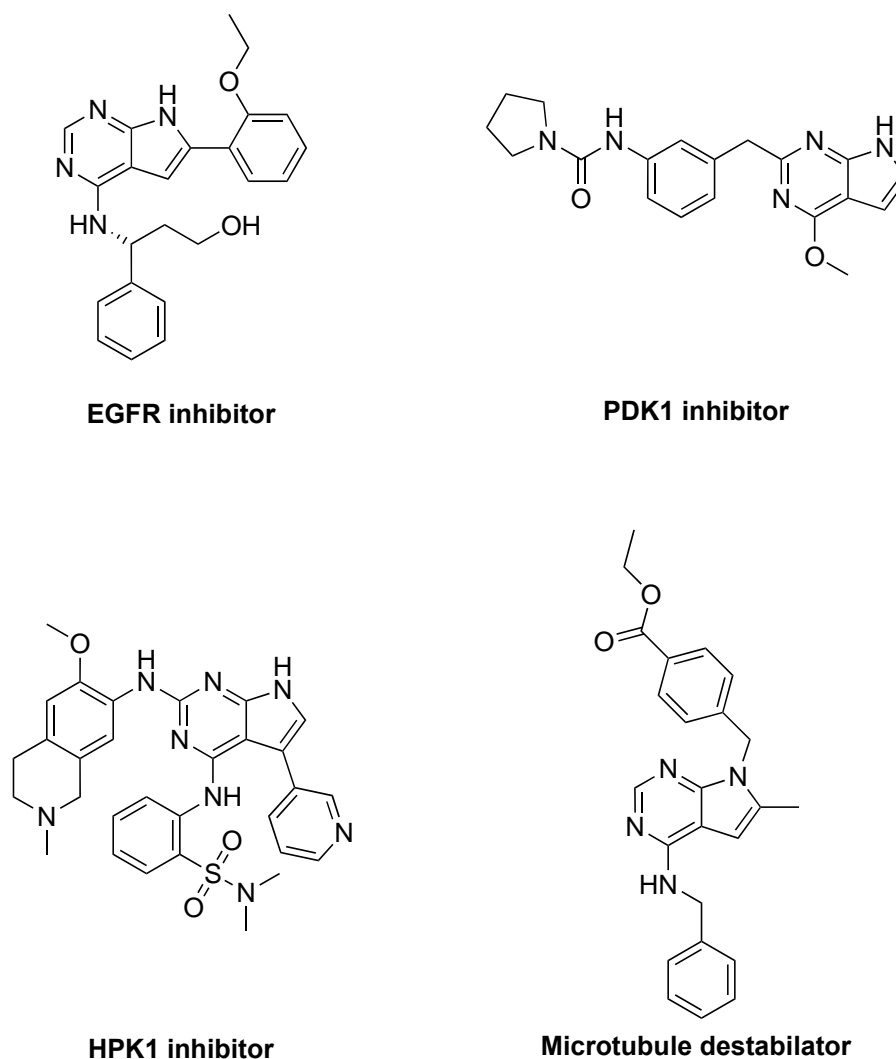


Figure 1.6: Four compounds exhibiting anticancer activity: EGFR inhibitor⁴¹; PDK1 inhibitor⁴²; HPK1 inhibitor⁴³; Microtubule destabilizer⁴⁴.

3-Phosphoinositide-dependent kinase 1 (PDK1) is a kinase that regulates the phosphoinositide-3-kinase (PI3K or Akt) signaling pathway, which regulates cell metabolism, growth, and proliferation.⁴⁵ In several cancer types, this pathway is disrupted.⁴⁶ O'Brien *et al.*⁴² synthesized and evaluated 2-anilino-4-substituted pyrrolopyrimidines as PDK1 inhibitors. They reported an increase in activity with C-4 substitutions of methoxy, exhibiting IC₅₀ value of 1.2 μ M (Figure 1.6).⁴²

Another target for anticancer therapy is the hematopoietic progenitor kinase 1 (HPK1) which is expressed in hematopoietic cells, the stem cells that give rise to other blood cells.⁴⁷ Dysregulation of HPK1 has been implicated in the pathogenesis of various diseases, including cancer, consequently making it a promising therapeutic target. In a recent publication by Wu *et al.*⁴³, 2,4-diaminopyrrolopyrimidines were synthesized and evaluated as potent inhibitors of

HPK1, with one compound exhibiting an IC₅₀ value of 3.5 nM (Figure 1.6). The study also provided valuable insights into the optimization and development of novel HPK1 inhibitors.

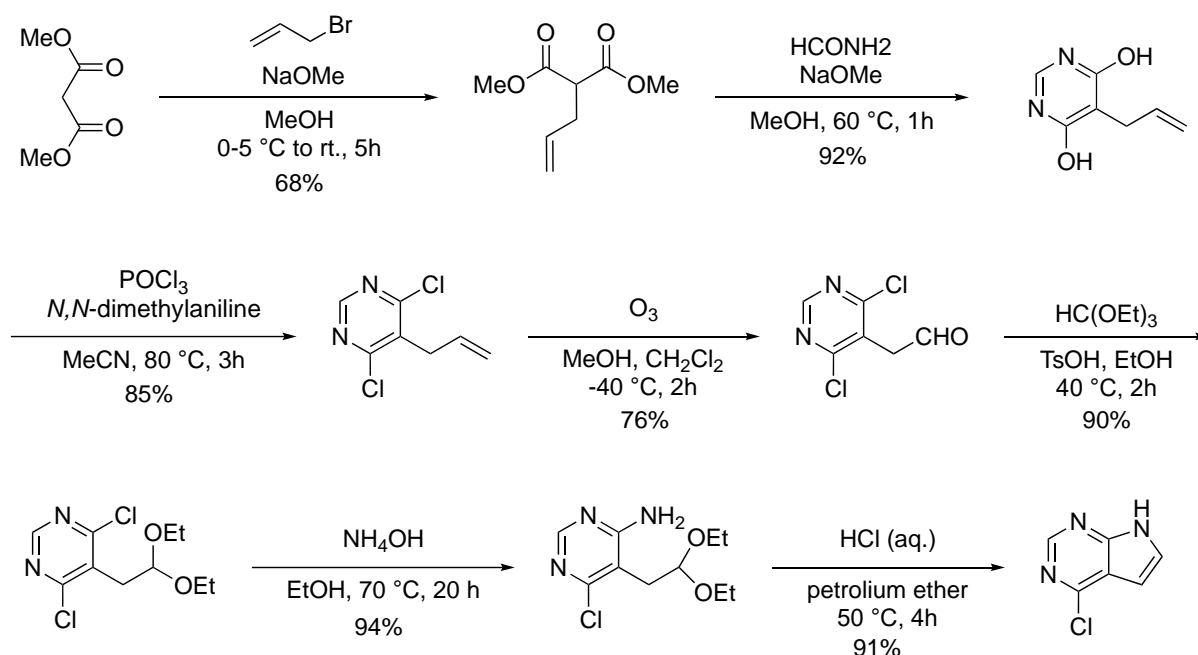
In addition to inhibiting several kinases, pyrrolopyrimidines can also destabilize microtubules. Microtubules are key structural components of the cytoskeleton in cells which is important for cell shape, cell signaling and segregation of chromosomes during cell mitosis.⁴⁸ Defects in the microtubule component may lead to faulty separation of the duplicated chromosomes into the daughter cells, eventually leading to apoptosis or mutation and cancer.⁴⁸ Destabilizing microtubules can make them undergo disassembly.⁴⁹ In cancer treatment, microtubule destabilization is exploited as a therapeutic strategy to inhibit the proliferation of cancer cells, as they are highly dependent on microtubules for successful cell division.⁵⁰ In 2017, Gilson *et al.*⁴⁴ identified new potent pyrrolopyrimidines as microtubule destabilizing agents. The most potent compound was a trisubstituted pyrrolopyrimidine with a 4-amino group, 6-methyl and N7-benzyl group (Figure 1.6).

Similarly, pyrrolopyrimidines exhibit biological activity in many different areas, such as antibacterial^{51, 52}, antiviral⁵², anti-hypertensive⁵³, anti-hyperglycemic⁵⁴, anti-inflammatory⁵⁵ and antiprotozoal^{13, 56}.

1.2.2 Pyrrolopyrimidine chemistry

As shown, pyrrolopyrimidines have a vast pharmacological profile and due to their immense importance, several efforts have been made to establish synthetic pathways.

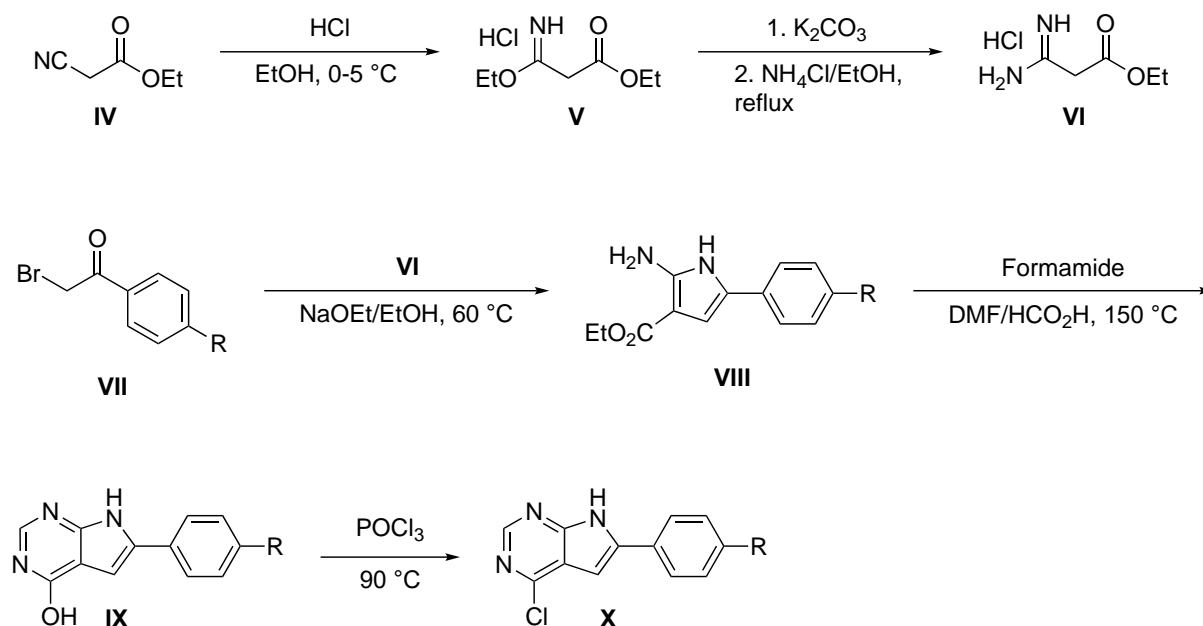
Zhang *et al.*⁵⁷ proposed a synthesis of 4-chloro-7*H*-pyrrolo[2,3-*d*] in seven steps (Scheme 1.1).



Scheme 1.1: Seven step synthesis of 4-chloro-7*H*-pyrrolo[2,3-*d*]pyrimidine, overall yield 31%.⁵⁷

In the fifth step, the aldehyde was protected as diethyl acetal to prevent aldehyde enolization. The aldehyde could undergo direct cyclization under acidic conditions, which gave low yields.⁵⁷ Next, the protected compound was treated with ammonium hydroxide to give a monosubstituted amine, and finally, the hydrolysis and cyclisation under acidic conditions led to the desired product 4-chloro-7*H*-pyrrolo[2,3-*d*]pyrimidine in an overall yield of 31%.⁵⁷

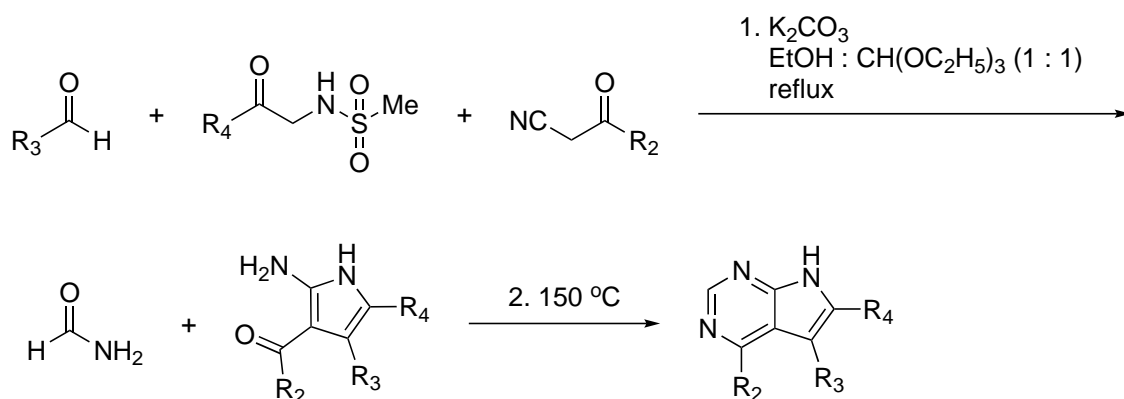
There have been examples of employing ethyl cyanoacetate as the starting material in several synthetic methods towards 4-chloropyrrolopyrimidines with a 6-aryl group.^{13, 16, 58-60} For example, Kaspersen *et al.*¹⁶ employed a five-step synthetic route to the 6-aryl-4-chloropyrrolo[2,3-*d*]pyrimidine (**X**) (Scheme 1.2).



Scheme 1.2: Five step synthesis of 6-aryl-4-chloro-pyrrolo[2,3-*d*]pyrimidine with ethyl cyanoacetate (**IV**) as the starting material.¹⁶

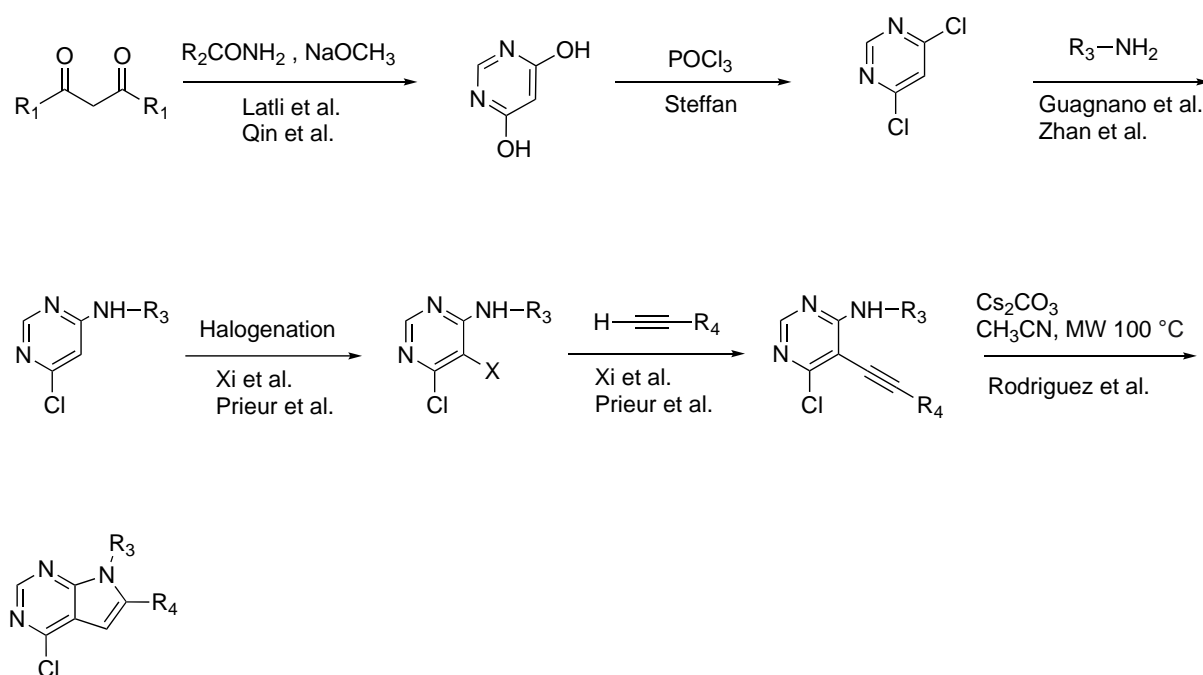
Ethyl cyanoacetate (**IV**) can be reacted with HCl in ethanol to yield ethyl 3-ethoxy-3-iminopropanoate hydrochloride (**V**), followed by free basing with potassium carbonate and treatment with ammonium chloride in ethanol to give ethyl 3-amino-3-iminopropanoate hydrochloride (**VI**). Compound **VI** was then reacted with a α -bromoacetophenone (**VII**) to give the pyrrolidine **VIII**. Finally, condensation of compound **VIII** to the 4-hydroxypyrroropyrimidine (**IX**) and chlorination of the latter gave the product **X** in an overall yield of 42%.^{16, 60}

Another synthetic route was reported by Frolova *et al.*⁶¹ and Scott *et al.*⁶² in which a four-component reaction gave the entire 7*H*-pyrrolo[2,3-*d*]pyrimidine scaffold (Scheme 1.3). The starting materials were reacted with formamide and K_2CO_3 . Then, the formamide was incorporated followed by ring closing of the pyrimidine portion permitted by gradually increasing the temperature.⁶¹



Scheme 1.3: One pot synthesis of pyrrolo[2,3-*d*]pyrimidine with four components.^{61, 62}

A synthetic route to 4-chloro-7*H*-pyrrolo[2,3-*d*]pyrimidine was also suggested by Han⁶³, who combined previously reported syntheses for pyrrolo[2,3-*d*]pyrimidine (Scheme 1.4).⁶⁴⁻⁷¹ However, this synthetic route was not tested.



Scheme 1.4: Synthetic route for the synthesis of 4-chloro-7*H*-pyrrolo[2,3-*d*]pyrimidine suggested by Han⁶³ through combining previously reported syntheses.⁶⁴⁻⁷¹

The pyrrolopyrimidine scaffold is not only found in diverse biological sources, ranging from humans to bacteria, but it can also be isolated from them.^{37, 72} A four-step biosynthetic *in vitro* method, involving four enzymatic steps, has been reported for the synthesis of compounds with the pyrrolopyrimidine core.⁷²

1.2.3 pK_a of pyrrolopyrimidines

Nitrogen containing heterocycles where the lone pair on the nitrogen is not part of the aromatic π -system will react with protons and the pK_a of the heterocycle will determine the equilibrium.⁷³ There has yet to be found reported pK_a values of pyrrolopyrimidines, however, similar compounds have been evaluated which can help establish the pK_a of pyrrolopyrimidine (Figure 1.7).

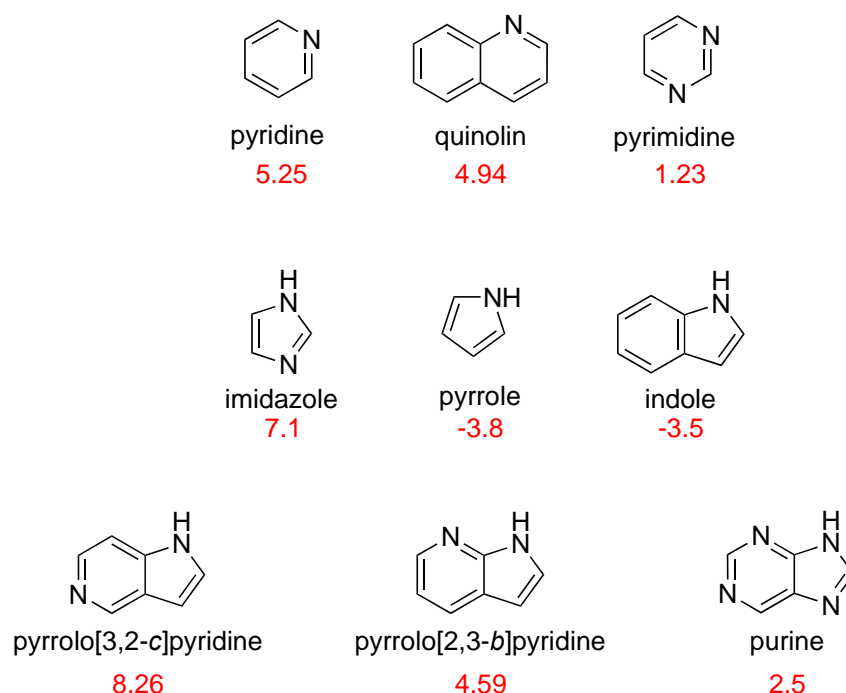


Figure 1.7: Nitrogen containing heterocycles with corresponding pK_a values (red): pyridine (5.25); quinoline (4.94); pyrimidine (1.23); imidazole (7.1); pyrrole (-3.8); indole (-3.5); purine (2.5); pyrrolo[3,2-c]pyridine (8.26); pyrrolo[2,3-b]pyridine (4.59).

Joris *et al.*⁷⁴ reported pK_a values of a series of π -deficient nitrogen heteroaromatics, for instance pyridine with a pK_a of 5.25.⁷⁴ The approximate same value, 5.2, was reported by Joule and Mills⁷³ for the same compound. Quinoline has a similar basicity to pyridine with pK_a 4.94⁷³, while the diazine pyrimidine has a significantly lower pK_a of 1.23-1.3.^{73, 74} The destabilization of the mono-cation formed is likely the explanation for the reduction in basicity, and can be attributed to two factors, inductive withdrawal and mesomeric withdrawal.⁷³

Inductive withdrawal refers to the effect caused by the second nitrogen atom in the pyrimidine ring, which reduces the stability of the positive charge on the protonated cation due to polarization of the σ -bond. Mesomeric withdrawal, on the other hand, refers to the delocalization or distribution of electron density away from the protonated nitrogen atom based

on the relevant resonance structures, further destabilizing the cation. Overall, these combined effects of inductive and mesomeric withdrawal by the second nitrogen atom result in a less stable protonated cation in the diazine, compared to the protonated cation in pyridine and quinoline, hence the decrease in pK_a .⁷³

Imidazole, with pK_a 7.1^{73, 75}, is more basic than pyrrole, pK_a -3.8⁷³. In imidazole, only one of the two nitrogen's lone pair is part of the aromatic system, while the other is not. This allows imidazole to retain its aromaticity and conjugated π -system when protonated.⁷³ In contrast, pyrrole contains only one nitrogen which lone pair is part of the aromatic π -system, which leads to a break in the aromaticity when protonated on C-2.^{73, 76, 77} Imidazole is a stronger base due to the greater availability of the lone pair of electrons compared to pyrrole. This also accounts the weak basicity of indoles, with pK_a -3.5, as the lone pair on the nitrogen atom is part of the aromatic π -system.⁷³

The pK_a values for pyrrolo[2,3-*b*]pyridine and pyrrolo[2,3-*c*]pyridine are 4.59 and 8.26, respectively.⁷³ Considering inductive withdrawal and mesomeric withdrawal, the presence of an extra nitrogen in pyrrolo[2,3-*d*]pyrimidine may result in a significantly lower pK_a compared to the two pyrrolopyridines. This assumption aligns with the difference in pK_a values between pyridine and pyrimidine, where the presence of one extra nitrogen led to a notable decrease in pK_a .

Purine, which has two more nitrogen atoms than the pyrrolopyridine structures, has a pK_a of 2.5 and can be protonated at several positions.⁷³ Comparing imidazole and pyrrole, it is observed that having an extra nitrogen atom whose lone pair is part of the aromatic π -system significantly lowers the pK_a . This might also be the case when comparing purine and pyrrolo[2,3-*d*]pyrimidine, suggesting that the pK_a of pyrrolo[2,3-*d*]pyrimidine could be lower than that of purine. However, to confirm the pK_a value, more detailed analysis of the molecule is needed.

1.3 Anilines

Anilines are aromatic amines that are electron rich due to the free electron pair on nitrogen and can therefore react with electrophiles. Aniline is usually found in dyes, perfumes, and pesticides, and are often used as intermediates in pharmaceutical applications.^{78, 79} They can additionally be found in biologically active products and medicine.⁸⁰ In medicinal chemistry, aniline derivatives are widely used substituents⁸⁰, and multiple research papers have reported on their use in the synthesis and biological evaluation.^{11, 24, 30, 41, 81} Aniline derivatives are also incorporated in the FDA-approved drugs such as Lapatinib²⁶, Gefitinib⁸², Afatinib⁸³ and Erlotinib^{27, 84} (Figure 1.8).

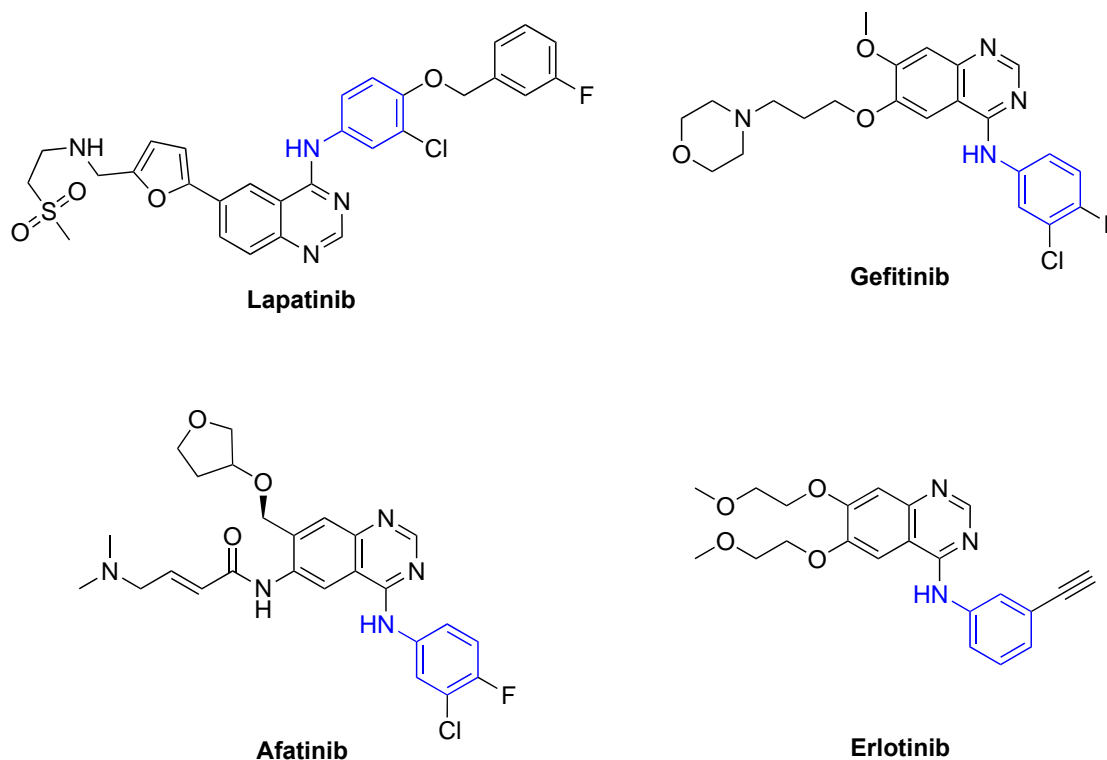


Figure 1.8: Structure of Lapatinib, Gefitinib, Afatinib and Erlotinib with the aniline portion marked in blue.

1.3.1 pK_a of anilines

Anilines, in comparison to aliphatic amines, typically exhibit a lower pK_a value, primarily attributed to the reduced electron density on the nitrogen atom resulting from the presence of a phenyl ring.⁸⁵ Aliphatic amines can typically have pK_a-values between 9-11⁸⁶, while the pK_a of anilines can range from 0-5^{86, 87} depending on the substitution pattern. While there are many experimental pK_a-values of different anilines, several methods have been described for

estimation of their pK_a, utilizing Hammett constants (σ), natural charge (Q_n), proton transfer enthalpy (ΔH_{prot}), average local ionization energy (I) or electrostatic potential (V).⁸⁷

Among these, Hammett constants are considered to be most effective in characterizing the substituent effect on pK_a, while other parameters are comparatively less effective.⁸⁷ Gross and Seybold⁸⁷ have developed simple equations, each employing one of the mentioned parameters, to predict pK_a of anilines. For instance, when Hammett constants are employed, the equation takes the form outlined in Equation 1.

$$\text{pK}_a = -3.03(\pm 0.13) \cdot \sigma + 4.46(\pm 0.06) \quad (\text{Equation 1})$$

Equation 1 was used to estimate the pK_a values of seventeen of the anilines used in this thesis, as shown in Table 1.1. Some values have not been previously reported experimentally but can be estimated using Equation 1. Hammett constants were retrieved from Hansch *et al.*⁸⁸ Experimental values were reported by either Gross and Seybold⁸⁷ or Haynes *et al.*⁸⁹. Most of the estimated values are gathered by using Equation 1⁸⁷, while some are taken from Tehan *et al.*⁸⁶ (superscripted “a”, Table 1.1) where the σ constants did not apply, i.e. *o*-substituted anilines. The pK_a value of two anilines, *N*-methyl-4-fluoroaniline and 2,6-isopropylaniline, is not reported. Neither were applicable in Equation 1 due to *o*-substitution and neither pK_a values were found in the literature.

Table 1.1: Experimental and estimated pK_a values for anilines in this thesis.^{86, 87, 89}

Substituent	pK _a	
	Experimental	Estimated
H (aniline)	4.58	4.46
2,3,4,5,6-pentafluoro	-0.28	-0.49 ^a
2,6-dichloro	0.42	3.44 ^a
4-nitro-2-trifluoromethyl	-	0.80
<i>p</i> -nitro	1.02	2.10
2,4,5-trichloro	1.09	2.02 ^a
2,4-dichloro	2.05	3.11 ^a
<i>o</i> -nitro	2.5	-
4-bromo-3-fluoro	-	2.73
<i>m</i> -chloro	3.34	3.34
<i>m</i> -benzyloxy	-	3.70
<i>m</i> -ethyne	-	3.76
3,4-methylenedioxy	-	4.10
<i>p</i> -fluoro	4.65	4.27
<i>o</i> -hydroxy	4.78	4.52 ^a
<i>p</i> -butyl	-	4.95
<i>p</i> -ethoxy	5.20	5.19

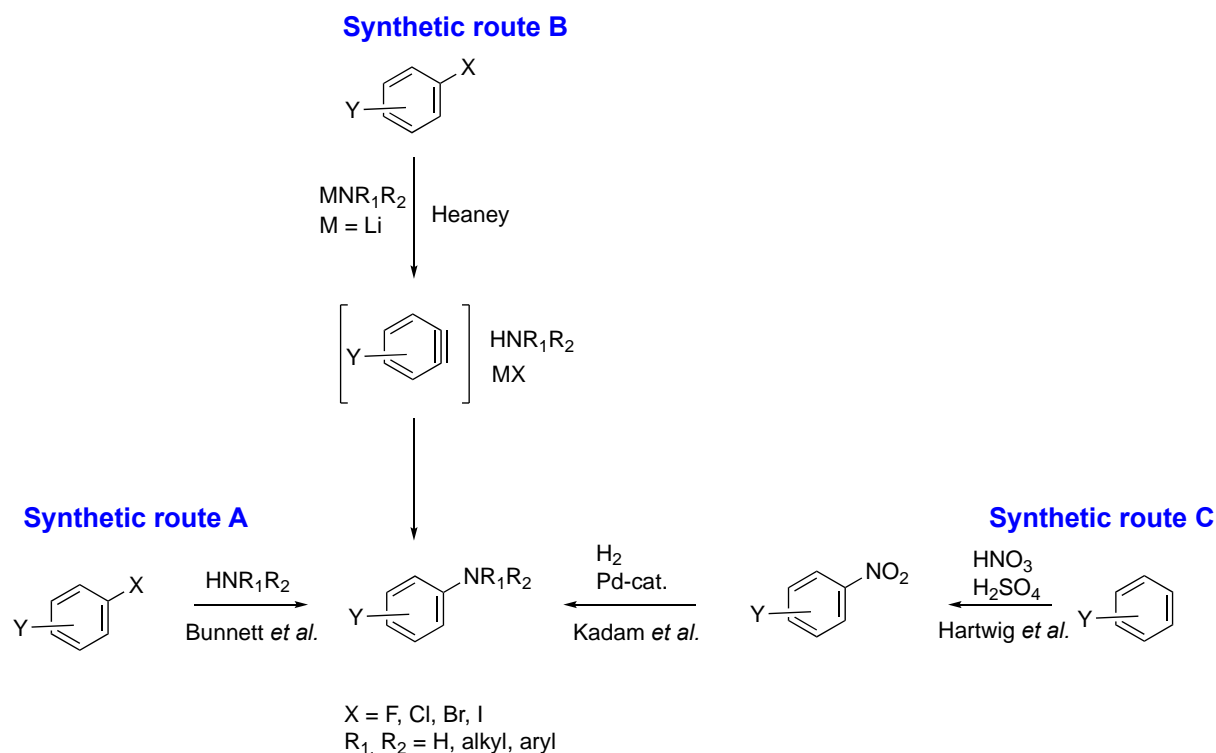
^a Estimated values retrieved from Tehan *et al.*⁸⁶

Anilines will have different pK_a based on the solvent they are in. Rossini *et al.*⁹⁰ have reported estimated pK_a values of aniline in MeCN, MeOH, DMSO and H₂O, spanning from 3.82 to 10.56. The lowest pK_a of 3.82 was reported in DMSO followed by 4.58 in H₂O. For the solvents MeOH and MeCN, the reported pK_a was 6.05 and 10.56, respectively.⁹⁰ The values are calculated using an empirical conversion method, which considers electrostatic effects, namely

an electrostatic transformation method. This method is based on the known pK_a of the organic compound in one solvent, e.g. H_2O , and converts it to an estimated pK_a in another solvent.⁹⁰

1.3.2 Synthesis of anilines

There are several approaches available for synthesizing anilines, and three often used routes are depicted in Scheme 1.5.^{80, 91-93}



Scheme 1.5: Three synthetic routes for synthesizing aniline. Synthetic route A: Halogenated aromatic substituted with an amine *via* S_NAr .⁹¹ Synthetic route B: Lithium amide substituted *via* aryn intermediate.⁹² Synthetic route C: Nitration of an aromatic compound followed by reduction with H_2 and Pd-catalyst.^{80, 93}

One of these routes, described by Bunnett *et al.*⁹¹, involves amine-substitution on halogenated aryls *via* S_NAr (Synthetic route A, Scheme 1.5). However, this method requires high temperatures and often gives low yields. For example, the reaction between chlorobenzene and aqueous ammonia at 300°C only gave aniline in 30% yield.⁹¹ Generally, primary and secondary amines react faster than ammonia in this reaction.⁸⁰ Alternatively, aniline can be synthesized *via* S_NAr through an aryne intermediate using lithium amide (Synthetic route B, Scheme 1.5).⁹² A drawback with this route could be the formation of regioisomers. In a third synthetic route, an aromatic compound is nitrated with concentrated HNO_3 and H_2SO_4 followed by reduction

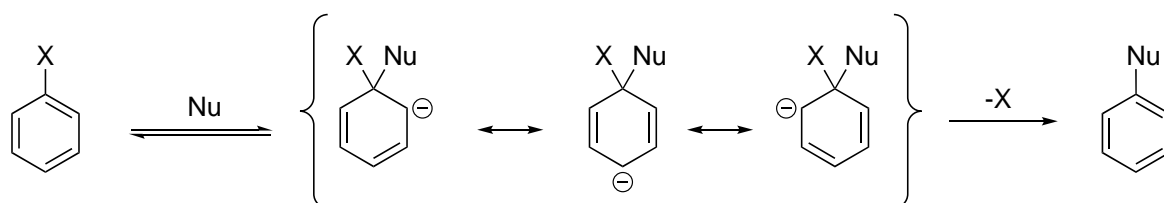
with H₂ and a Pd-catalyst (Synthetic route C, Scheme 1.5).^{80, 93} If the aromatic starting material is electron rich, HNO₃ should be used alone as a nitrating agent as H₂SO₄ may oxidize it.⁸⁰

1.4 Amination on heterocycles

The amination of heterocycles is a key reaction in medicinal chemistry⁹⁴, as several potent drugs are substituted with amino groups, as previously noted. Within this chapter, two common methods are outlined, amination *via* S_NAr and cross-coupling reaction, specifically Buchwald-Hartwig amination.

1.4.1 Nucleophilic aromatic substitution

In nucleophilic aromatic substitution a nucleophile displaces a leaving group on an aromatic ring.⁹¹ The reaction proceeds through an addition-elimination mechanism^{95, 96}, involving the formation of a negatively charged intermediate, the tetrahedral Meisenheimer complex (Scheme 1.6).^{91, 97} After addition of the nucleophile, the carbon atom is assumed to have sp³ hybridization, disrupting the π-system in the aryl. When the leaving group is eliminated, the π-system along with the aromaticity is restored.



Scheme 1.6: Mechanism for S_NAr through addition-elimination with the formation of the negatively charged Meisenheimer complex.^{91, 96, 97}

Generally, second order kinetics are observed and the first step is the rate-determining.^{91, 98} Also, there are a great number of factors that can influence the reactivity of S_NAr reactions⁹⁶, for instance the size of the leaving group and the nucleophile, interactions between leaving group and nucleophile and solvent effects.^{91, 97} Electron deficient aromatic compounds facilitate the reaction as this creates stronger electrophiles and electron withdrawing substituents will stabilize the developing negative charge in the Meisenheimer complex.⁹¹

Pyrimidine is an electron deficient aromatic and has six π-electrons delocalized across six overlapping p-orbitals (Figure 1.9). The presence of two sp²-hybridized nitrogen atoms results

in reduced π -electron density especially in the 2- and 4-position.⁹⁹ On the other hand, the pyrrole heterocycle of the pyrrolopyrimidine also possesses an aromatic system with six π -electrons, but distributed over only five p-orbitals, rendering it more electron-rich compared to pyrimidine (Figure 1.9).⁹⁹ Consequently, pyrimidine would be a more favorable substrate in an S_NAr reaction than pyrrole, being more susceptible to nucleophilic attack.

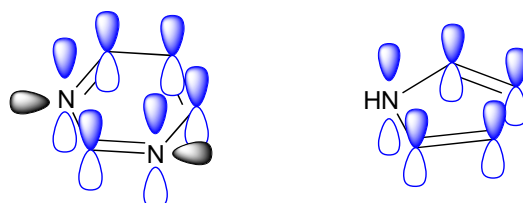


Figure 1.9: Aromatic structures of pyrimidine and pyrrole with p-orbitals (blue) orthogonal to the plane of the rings. Electrons that are not orthogonal to the plane are represented as grey orbitals.

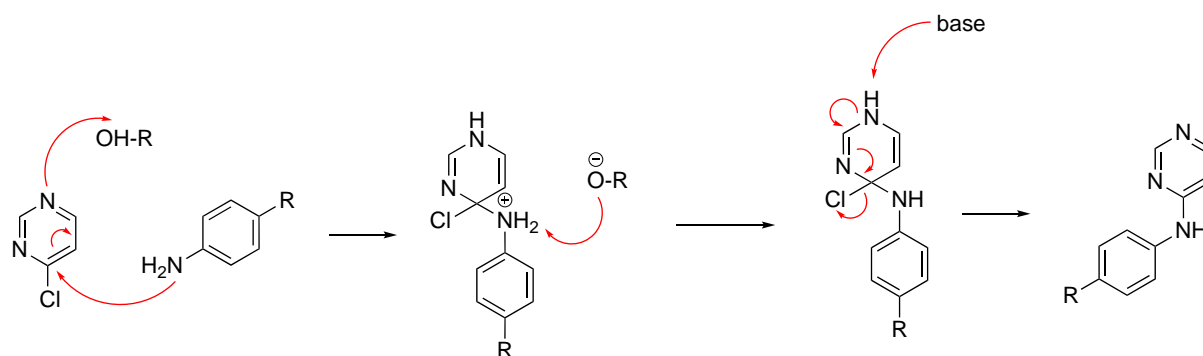
Solvent effects are also to be considered in reactivity of the S_NAr reaction. The polarity of the solvent is crucial for the reactivity, as higher polarity will stabilize the Meisenheimer complex.¹⁰⁰ Hydrogen bond donor and acceptor abilities of the solvent will also influence reactivity, where it is generally observed that the higher degree of hydrogen bond acceptor abilities will increase the reaction rate constant and decrease it when the solvent has high hydrogen bond donor abilities.¹⁰⁰ Dissolution of the starting materials also has a huge influence on reactivity.⁹¹

The strength of the nucleophile is equally an important factor when determining the reactivity. A nucleophile's strength can be considered through its basicity, polarizability, and the presence of unshared alpha electrons to the nucleophilic atom.¹⁰¹ Polarizability is to consider in nucleophilicity, as the more polarizable a molecule is, the better nucleophile it becomes. This is because it reduces electrostatic repulsion between the nucleophile and the substrate, enabling the reactants to approach each other easily.¹⁰¹ In addition, the presence of unshared electron pair on the adjacent atom to the nucleophilic atom, also called the alpha effect, makes stronger nucleophiles.¹⁰¹

Typical leaving groups are halides, but alkoxy, nitro and sulfonyl groups can also act as leaving groups.^{91, 98} Considering the halides, the leaving group order is $F > Cl \approx Br > I$ which is opposite as usually observed for aliphatic halides in S_N2 reactions^{91, 96}, and is often referred to as the elemental effect.¹⁰² This inverted order can be explained by the higher electronegativity of

fluorine compared to the higher halogens, thus adding stability to the negative charge in the Meisenheimer complex. The elemental effect is particularly noticeable for the smaller and polarizable nucleophiles in protic solvents, such as amines. This phenomenon is thought to establish the addition-elimination mechanism in the S_NAr reaction.^{96, 102}

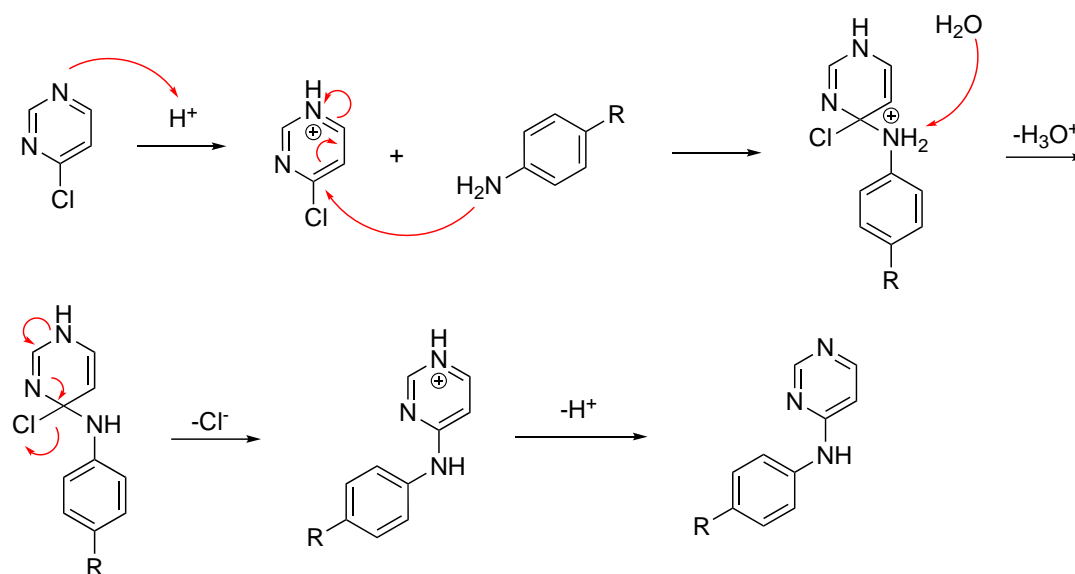
Amination of heterocycles *via* S_NAr can be carried out under basic and acidic conditions. A mechanism for amination of pyrimidine has been proposed for both conditions.¹⁰³ Under weakly basic conditions, the amine in excess, or a co-base can be added to capture acidic protons from the byproduct HCl (Scheme 1.7).¹⁰³



Scheme 1.7: S_NAr mechanism in basic conditions with pyrimidine and aniline.¹⁰³

Amination in basic conditions, more specifically amination to 4-chloro-7*H*-pyrrolo[2,3-*d*]pyrimidine, has been reported several times.^{29, 30, 63} One patent by Traxler *et al.*³⁰ reported aniline added in excess when synthesizing derivatives of 7*H*-pyrrolo[2,3-*d*]pyrimidine. In a thesis by Han⁶³ and a paper by Han *et al.*⁴¹ the amination was carried out with three equivalents of aniline in low to excellent yields (15-91%). A patent by Grotzfeld *et al.*²⁹ described a method to synthesize derivatives of 7*H*-pyrrolo[2,3-*d*]pyrimidine-4-amine with equimolar amounts of the starting materials. Wu *et al.*⁴³ have reported base-mediated S_NAr in the amination to pyrrolopyrimidine, wherein equimolar amounts of the starting materials were employed with either DIPEA or *t*-BuOK as a co-base, which are non-nucleophilic bases that capture protons from the byproduct HCl. Bathen²⁸ also carried out base mediated S_NAr with three equivalents of DIPEA. Unlike typical catalytic reactions, these bases are added in excess due to their inability to regenerate throughout the reaction. As this reaction proceeds, HCl is formed, and the base is consumed by the capture of HCl.

Under acid-mediated S_NAr reactions, only catalytic amounts of the acid is needed as HCl is generated throughout the reaction (Scheme 1.8).¹⁰³



Scheme 1.8: S_NAr mechanism under acidic conditions with pyrimidine and aniline.¹⁰³

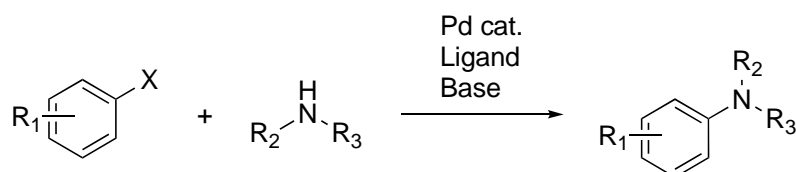
There are several reports of acid catalyzed amination to 7*H*-pyrrolo[2,3-*d*]pyrimidines with aniline. Particularly one method with isopropanol, 2-6 drops of concentrated HCl and three equivalents of aniline is popular.^{11, 24, 81} This method gave low to excellent yields (16-96%) with a large variety of anilines and amines. Bathen²⁸ reported a method with ethanol as the solvent and three drops concentrated HCl, giving full conversions after 3 h. Abou-Shehada *et al.*¹⁰⁴ employed Lewis acids in amination of pyridines, such as Zr(acac) and Zn(NO₃)₂ in 20 molar percentage. The highest conversions were achieved with Zr(acac), namely 81%, but this was also the most expensive catalyst. When switching to the zinc-based catalyst, Zn(NO₃)₂, they developed a greener more sustainable methodology and achieved full conversion and excellent yields with anilines and cyclic amines. Primary amines such as benzylamine, however, did not react. It was also reported that heating of 4-chloropyridine in a polar protic solvent, such as MeOH, EtOH and *n*-PrOH, led to solvolysis of the starting material due to the nucleophilicity of these solvents.¹⁰⁴

Although acid catalyzed amination of this sort is a well-known method, no fundamental studies or optimization of such reactions have been found in the literature. Unpublished work by our research group can give some valuable insights. Both polar protic and aprotic solvents have been successfully employed, where the most polar solvents gave higher conversion in both categories. Previous literature has reported the use of various alcohols as solvent, including MeOH¹⁰⁴, EtOH^{28, 30, 104}, *i*-PrOH^{24, 30, 81, 104} and *n*-BuOH³⁰ in similar reactions. One patent by Traxler *et al.*³⁰ claims that these simple alcohols were inert solvents in this specific reaction,

however, as mentioned, Abou-Shehada *et al.*¹⁰⁴ observed solvolysis under the same reaction conditions.

1.4.2 Buchwald-Hartwig amination

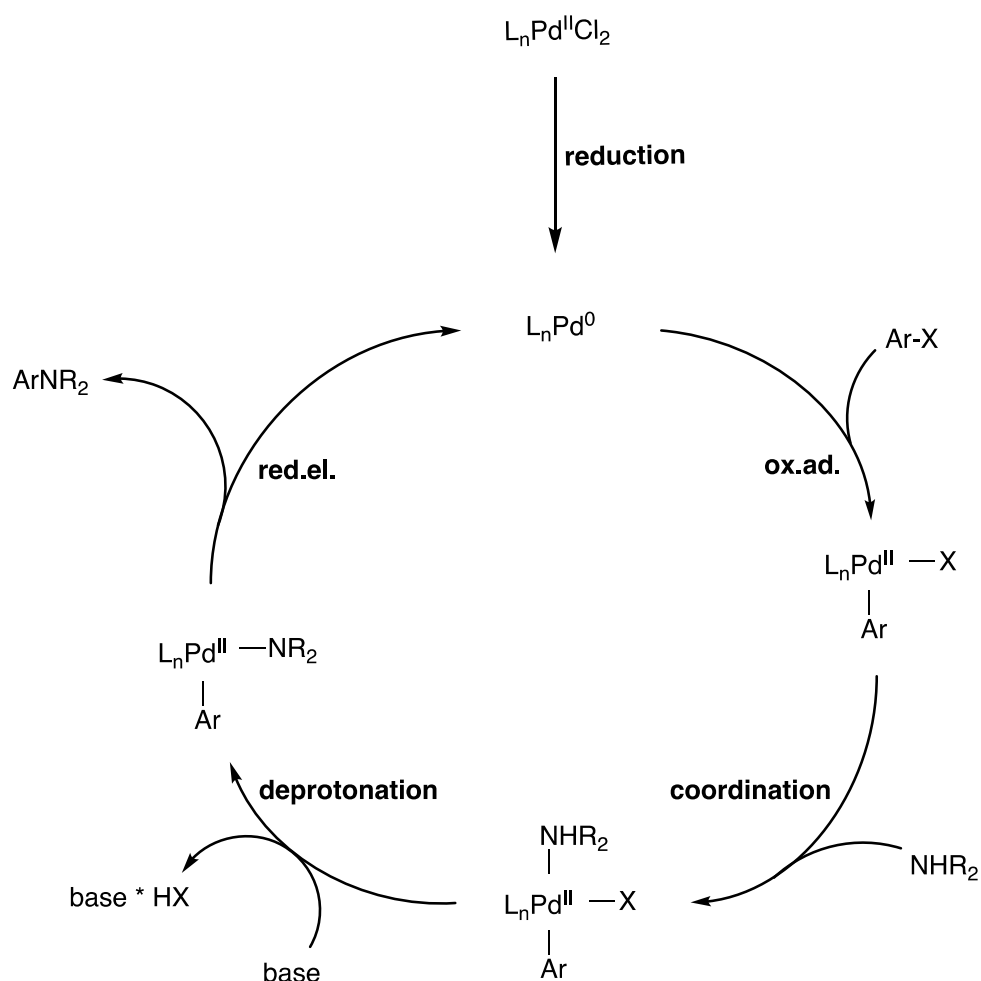
The Buchwald-Hartwig amination is a palladium catalyzed cross-coupling reaction between aryl halides and amines in presence of a base (Scheme 1.9).



Scheme 1.9: General cross coupling, Buchwald-Hartwig amination between a halogenated aryl and an amine with the use of a Pd-catalyst and a base.

The first cross-coupling reaction between sp^2 -carbon and nitrogen was reported separately by Goldberg¹⁰⁵ and Ullmann¹⁰⁶ in the early 1900's using copper as the metal catalyst.¹⁰⁷ Palladium was later employed as the catalyst by Masanori *et al.*¹⁰⁸ for the aromatic amination. Stephen L. Buchwald and John F. Hartwig independently published methods for cross-coupling of aryl bromides and aminostannanes using palladium catalyst for the synthesis of arylamines in 1994.^{109, 110} While effective, these *in situ*-generated aminostannanes suffered from long reaction times and the formation of side products, with additional issues concerning toxicity of organic stannanes and waste disposal.¹⁰⁷ Furthermore, this reaction was not suitable for primary amines which was due to a competitive β -hydride elimination leading to the formation of reduced aryl as the side product.¹¹¹

In 1995, both Buchwald and Hartwig published an improved method for palladium-catalyzed cross-coupling of aryl halides and amines without the use of tin.^{110, 111} This methodology is now commonly known as the Buchwald-Hartwig amination.¹⁰⁷ The Buchwald-Hartwig amination proceeds through a catalytic cycle in which the catalyst Pd^0 is being regenerated in each catalytic turn (Scheme 1.10).^{110, 111}



Scheme 1.10: The Buchwald-Hartwig amination cycle.^{110, 111}

In the first step, the Pd^{II}-complex gets reduced to the unsaturated Pd⁰-complex which subsequently undergoes oxidative addition with the aryl halide. The oxidative addition is favored by electron donating Pd ligands that makes the metal electron rich, also called σ -donor effect, such as phosphines.¹¹² Ligands that are good π -acceptors will slow down this step due to decreased electron density on the metal from π -backbonding, but will ease the reduction elimination.¹¹² After oxidative addition, coordination with the amine NHR₂ will occur followed by a base mediated deprotonation. In the last step, the reductive elimination takes place, the opposite of oxidative addition. For this step to occur, the two groups, NR₂ and Ar must be *cis* to each other, and no reaction will occur if they are *trans* positioned. Reductive elimination is favored by an electron deficient metal Pd, characterized by π -backbonding ligands.¹¹²

Over time, several generations of catalysts have been developed, each with its own set of limitations and advantages. Three ligands that can be used in Buchwald-Hartwig cross coupling are outlined in Figure 1.10, BINAP, XPhos and DPEPhos.¹⁰⁷

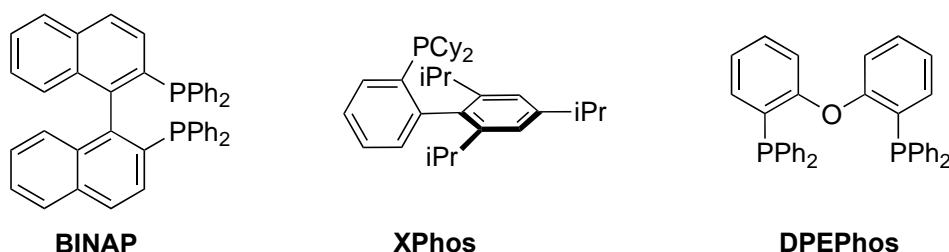


Figure 1.10: Examples of phosphine ligands used in Buchwald-Hartwig amination. BINAP as bidentate ligand, XPhos as monodentate and sterically hindered one, and DPEPhos as a POP-ligand.¹⁰⁷

The use of biphosphines in the Pd-complex, such as BINAP, has enabled successful arylation of primary amines.^{111, 113} The bidentate coordination of both phosphorus to the metal center hinders free rotation of the bonds and makes β -elimination a less favored side reaction.¹¹³ Sterically hindered ligands, such as the monodentate XPhos achieve the same result. Diphosphine ligands with an oxygen atom between the two phosphorus atoms, or so-called POP-ligands, can stabilize the catalyst by creating an additional coordination site.¹¹⁴ POP-ligands, e.g. DPEPhos, are considered highly effective in coupling of aniline and aryl bromide and can in some cases exceed the reactivity of BINAP.¹⁰⁷

Phosphine ligands are one of the most employed in the Buchwald-Hartwig amination. Among the bidentate phosphine ligands, a wider “bite angle” between the ligand and the metal is generally favored and gives the highest reaction rate in this cross-coupling reaction.¹¹³ The backbone of the diphosphine ligand determines the chelation angle, which can be defined as the bite angle (Figure 1.11).¹¹³ The cone angle on the other hand is a measure of the bulk of the phosphine ligand (Figure 1.11). A bigger cone angle will accelerate the reductive elimination step as steric strain is released, but as a consequence of the steric strain, the rate of oxidative addition will decrease.¹¹²

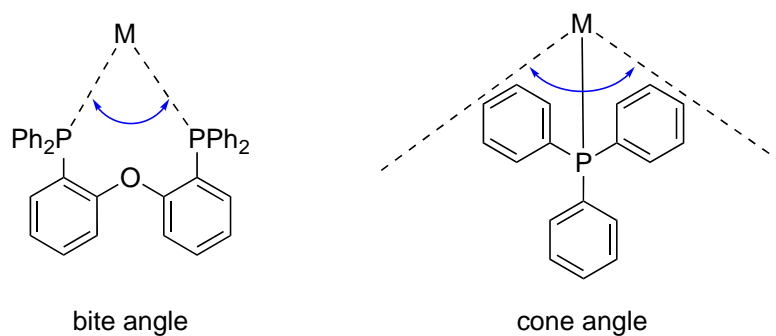
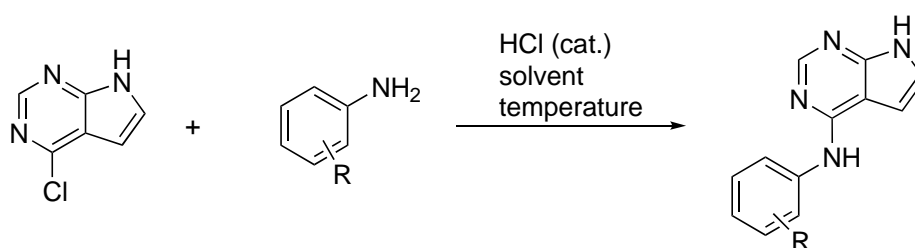


Figure 1.11: Bite angle and cone angle explained.^{112, 113}

Anilines have previously been successfully employed in Buchwald-Hartwig cross-coupling.^{107, 115} Zheng *et al.*¹¹⁵ employed several anilines in a cross-coupling with aryl ester phenyl benzoate, in some cases reaching excellent yields. Two 2,6-disubstituted anilines were successfully employed in 89-93% yield, and 2-isopropylaniline in 97% yield. Cross-coupling between pyrrolopyrimidines and anilines has previously been reported in the literature. O'Brien *et al.*⁴² synthesized six different 2,4-substituted 7*H*-pyrrolo[2,3-*d*]pyrimidine employing different anilines in good yields, 72-87%, with the use of XPhos as the ligand.

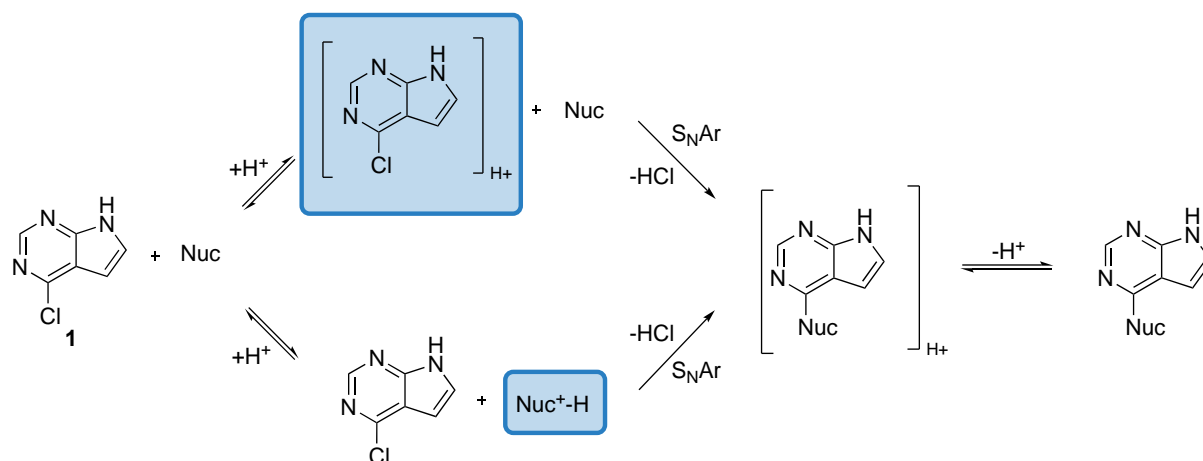
2 Results and discussion

The objective of this study was to optimize the acid catalyzed amination of 4-chloro-7*H*-pyrrolo[2,3-*d*]pyrimidine (**1**) by identifying more efficient and sustainable reaction conditions. A model reaction involving **1** and aniline (**2**) was conducted to investigate the effects of solvent type, acid amount and temperature on the reaction conversion. Once an optimal reaction procedure was developed for the model reaction, a substrate scope study was conducted on nineteen anilines (**2-20**), two chiral benzylic amines (**21**, **22**), one cyclic amine (**23**) and one primary amine (**24**) to validate the reaction conditions. The general reaction for all anilines in this thesis is outlined in Scheme 2.1.



Scheme 2.1: General reaction and reaction conditions for acid catalyzed amination of 4-chloro-7*H*-pyrrolo[2,3-*d*]pyrimidine (**1**).

The S_NAr reaction can be hypothesized to proceed through one of two proposed pathways, which are determined by the basicity of the starting materials (Scheme 2.2). In the first pathway, the pyrrolopyrimidine **1** is protonated initially, as the weak nucleophile has a lower pK_a value. This protonation makes **1** a stronger electrophile, enabling it to still react with the weaker nucleophile *via* S_NAr. In the second pathway, the nucleophilic amine is protonated before the pyrrolopyrimidine **1**, due to the amine being a better nucleophile with higher pK_a. In this pathway, the S_NAr reaction can still proceed because the nucleophile is thought to react prior to protonation, forcing the protonation equilibrium to the non-protonated form.

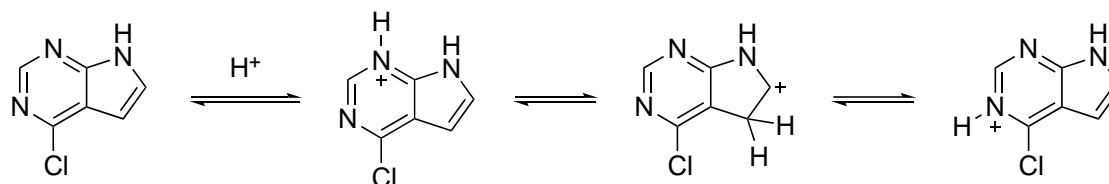


Scheme 2.2: Two suggested protonation pathways in the S_NAr reaction between pyrrolopyrimidine **1** and a nucleophilic amine. In the first pathway, the pyrrolopyrimidine **1** is protonated first, while in the second pathway, the amine is protonated first. The S_NAr reaction is still thought to proceed in both pathways.

To assess the reaction efficiency, test reactions were carried out at a 100 mg scale where samples were collected at specific time intervals. In total, twenty-three substrates were tested. Subsequently, eight anilines were employed in an upscaled reaction of 500 mg with the same conditions. In addition, NMR was employed in an attempt to give insights to the reaction mechanism. The ensuing section comprises the findings from the NMR study, the model reaction, and the substrate scope.

2.1 NMR-studies

NMR-studies were executed to investigate protonation sites on **1** to get a better understanding of the mechanism in the acid catalyzed amination of pyrrolopyrimidine **1**. Previous studies on related compounds have provided mechanistic information. For instance, Guo *et al.*¹⁰³ proposed a mechanism for the acid catalyzed amination to pyrimidine (Scheme 1.8, Section 1.4.1), suggesting protonation occurs on N-1. As the lone pairs on N-1 and N-3 are not part of the aromatic π -system in pyrrolopyrimidine **1**, these sites could be protonated.⁷³ C-5 was also thought to be a potential protonation site.^{17, 73} We hoped that by analyzing the chemical shifts under various acidic conditions obtained from ¹H-NMR spectra¹¹⁶ we could identify the specific site of protonation on compound **1**. Three suggested protonated structures are presented in Scheme 2.3.



Scheme 2.3: Pyrrolopyrimidine **1** and three suggested protonated structures.

Initially, compound **1** was dissolved in DMSO-*d*₆ and treated with 1 drop of concentrated HCl, but negligible changes in Δ ppm were observed. Instead, an unidentified peak at 11.01 ppm emerged as the water peak at 3.33 ppm disappeared. This unidentified peak was therefore thought to belong to H₃O⁺, which aligned with previously reported chemical shifts for the same species.¹¹⁷ Due to the limited Δ ppm changes in DMSO-*d*₆, the NMR-solvent was switched to acetonitrile-*d*₃, which gave significant changes in ppm when HCl was added. In total, 9 different parallels were made with varied amounts of HCl to enable a comparative analysis of the H-2 protons.¹¹⁶ The NMR-signals of H-2 are depicted with estimated amounts of HCl in Figure 2.1. Since pH is a scale used in only aqueous solutions, the estimated quantities of HCl are reported in equivalents. This estimation involved weighing a single drop of HCl (37%) and adding it to a known volume of acetonitrile-*d*₃, followed by further dilution. All samples were added approximately 10 \pm 2 mg of compound **1**.

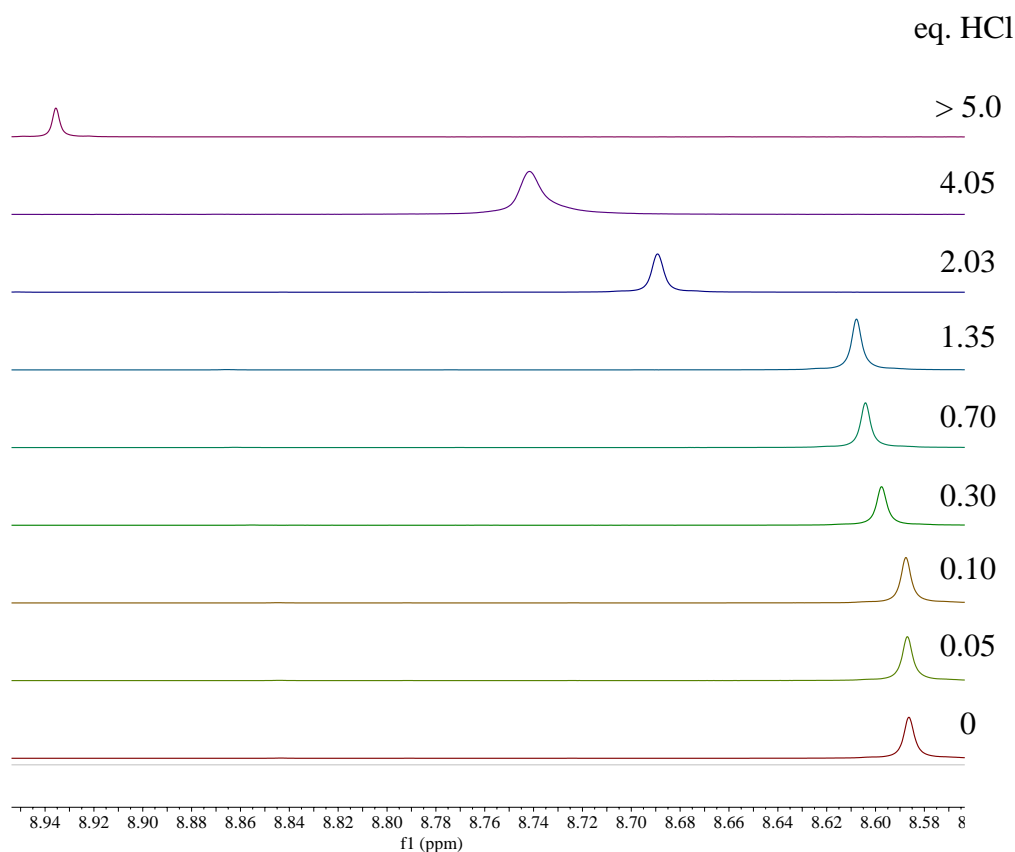


Figure 2.1: ¹H-NMR spectra (400 MHz, acetonitrile-*d*₃) of starting material **1**, displaying only H-2 with estimated amounts of HCl in each sample.

When 0-0.05 eq. HCl was added, no significant changes in Δ ppm was observed, and the H-2 resonated at 8.56 ppm. The first notable change occurred when adding 0.10 eq. HCl, leaving a slightly downshifted signal, Δ ppm = 0.01 ppm. Between 0.10 and 1.35 eq. HCl the changes are small, all Δ ppm = 0.01. However, when adding 2.03 eq. HCl the signal of H-2 was shifted downfield by 0.10 ppm. The biggest value of Δ ppm was observed when adding >5.00 eq. HCl with Δ ppm = 0.38 ppm. Chemical shifts for all protons in pyrrolopyrimidine **1** are presented in Table 2.1, displaying signals from the samples with 0 eq. HCl and 5 eq. HCl. The biggest difference in Δ ppm was observed for the proton on N-7 (H-7) with a value of Δ ppm = 2.28 (Table 2.1).

Table 2.1: Chemical shifts for all protons in compound **1** in two different conditions, 0 eq. and >5 eq. HCl, and the corresponding Δ ppm.

Proton	δ [ppm]		Δ ppm
	0 eq. HCl	> 5 eq. HCl	
H-2	8.56	8.93	0.37
H-5	6.60	7.01	0.41
H-6	7.47	7.88	0.41
H-7	10.20	12.48	2.28

With the similar Δ ppm observed for all C-H protons, namely H-2, H-5 and H-6, the position of protonation on pyrrolopyrimidine **1** is inconclusive. However, this may indicate that the compound can be protonated in more than one position. For example, when considering H^+ as an electrophile, it is previously reported that C-5 is most susceptible for electrophilic attack.¹⁷ By observing the change in splitting pattern of H-5 and H-6, it indicates that H-7 is being exchanged more rapidly as the solution gets more acidic. In neutral solution of acetonitrile- d_3 , the two signals appear as doublet of doublets and are both coupled to H-7. In acidic solution, the two signals are observed as doublets and have no coupling with H-7. This indicates that H-7 is being exchanged in the NMR time frame under acidic conditions (Figure 2.2).

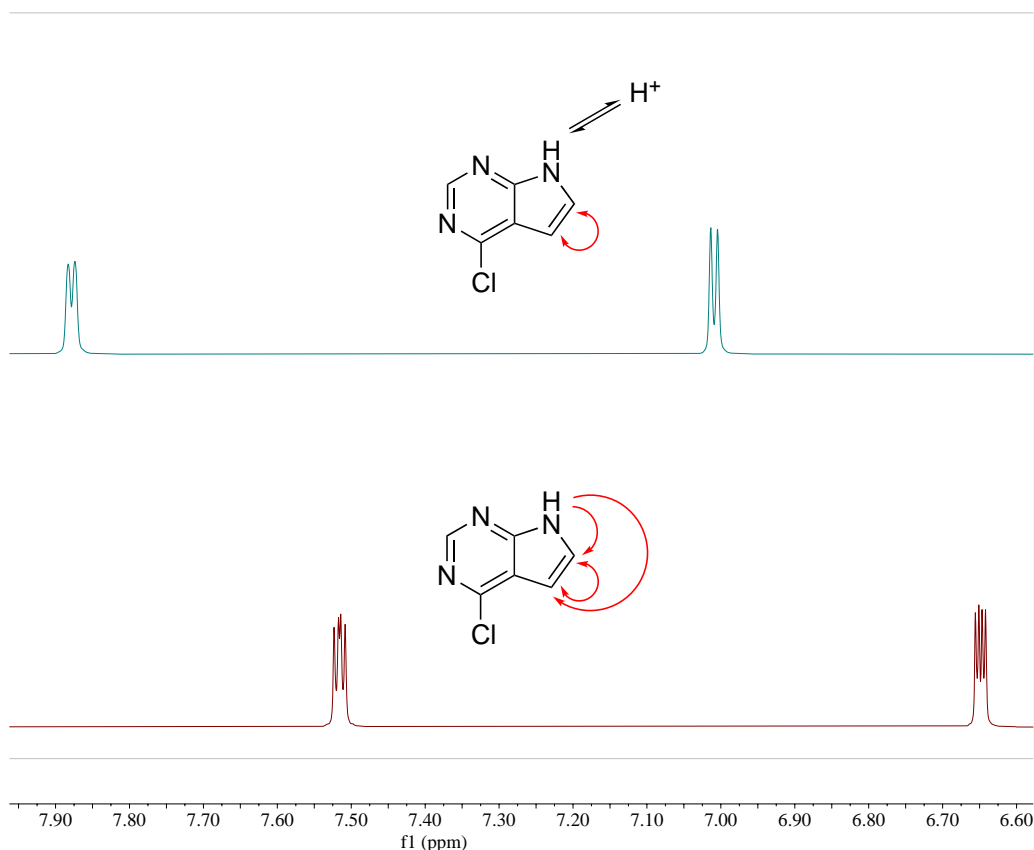


Figure 2.2: $^1\text{H-NMR}$ signals for H-5 and H-6 in neutral (dark red) and acidic (blue) conditions with compound **1** and corresponding couplings (red arrows) for these protons.

To support this assumption, a decrease in the integral for H-7 was expected, however, this was not observed and the integral for H-7 stayed consistent in the range of 0.22-0.25. Based on these results, site of protonation could not be concluded.

2.2 Model reaction

The model reaction consisted of the starting materials 4-chloro-7*H*-pyrrolo[2,3-*d*]pyrimidine (**1**) and aniline (**2**) that reacted *via* $\text{S}_{\text{N}}\text{Ar}$ to form the product *N*-(4-phenyl)-7*H*-pyrrolo[2,3-*d*]pyrimidine-4-amine (**28**). Conversion rate and side product profile have been studied through testing variables such as solvent type, temperature, and acid amount.

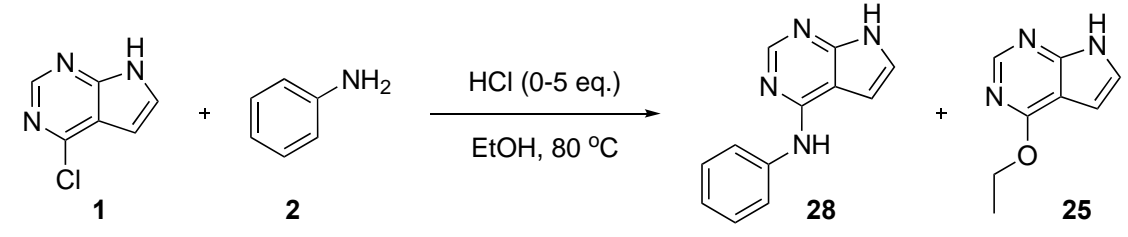
The conversion rate and side product profile were determined from $^1\text{H-NMR}$ and the reactions were also analyzed through TLC. Samples were taken from the reaction mixture at specific time intervals in all experiments. All samples were neutralized, extracted, and concentrated *in vacuo* before NMR-analysis to achieve a more readable spectrum as the protonated products gave

overlapping signals. When the specific solvent was not miscible in water, the samples were neutralized with NaHCO_3 and extracted with EtOAc before evaporative work-up. When the solvent was miscible in water, however, an additional step of concentration *in vacuo* was done before the neutralizing step to prevent the reaction components from mixing with the water phase. Mostly, the aniline **2** was lost during evaporative work-up and the conversion was therefore solely calculated from the H-2 on the starting material **1** and the product **28**, having signals at 8.56 ppm and 8.27 ppm respectively. Because of lacking $^1\text{H-NMR}$ signals from the starting material **2**, >97 % is used when indicating full conversion.

2.2.1 Initial experiments

Based on the experiments of previous master student Bathen²⁸, who employed a system with EtOH as solvent at reflux temperature, different amounts of acid were initially tested in the same system. Acid catalyzed amination to pyrrolopyrimidines *via* $\text{S}_{\text{N}}\text{Ar}$ has previously only been reported with dropwise amounts of HCl, as already stated. Therefore, specific amounts of HCl were added to observe the effects thereof. The concentration of the reaction mixture was increased from 0.10 mmol/mL as described by Bathen²⁸ to 0.26 mmol/mL to enhance the reaction rate.¹¹⁸ In total, six experiments were conducted with the model reaction in different amounts of HCl, from 0 eq. to 5 eq. (Table 2.2). Samples were taken at 1 h, 2 h, 3 h, 4 h and 6 h for all experiments. In addition to the expected product **28**, a side product from alcoholysis, 4-ethoxy-7*H*-pyrrolo[2,3-*d*]pyrimidine (**25**), was observed. The side product was not isolated but identified through comparing $^1\text{H-NMR}$ spectra of compound **28** from a previous project in our research group.

Table 2.2: Different amounts of HCl, 0-5 eq., in the model reaction of 7*H*-pyrrolo[2,3-*d*]pyrimidine (**1**) and aniline (**2**) led to formation of the expected product *N*-phenyl-7*H*-pyrrolo[2,3-*d*]pyrimidin-4-amine (**28**) and the alcoholysis side product 4-ethoxy-7*H*-pyrrolo[2,3-*d*]pyrimidine (**25**).



Entry	HCl [eq.]	Conv. 1 h [%]	Molar percentage, 6 h [%]	
			Product, 28	Side product, 25
1	0	0	69	0
2	0.1	51	>97	0
3	0.5	74	90	10
4	1.0	81	86	14
5	3.0	82	85	15
6	5.0	86	83	17

The conversion in the initial 1 h is reported to compare the initial rates of the experiments. To illustrate the influence of acid amount on the rate of the side reaction, alcoholysis, the molar percentages of both the desired product **28** and the side product **25** are reported after 6 h.

Without HCl, no conversion was observed within 1 h (Entry 1, Table 2.2). However, after 6 h, a molar percentage of 69% of the desired product **28** was observed, mainly explained by HCl being the byproduct of the reaction.¹⁰³ The initial conversion was significantly higher when adding 0.1 eq. HCl, reaching 51% after 1 h (Entry 2, Table 2.2). In this experiment, the starting materials were fully converted after 6 h and no side product **25** was observed. A significant increase in conversion and formation of the side product was observed when adding more than 0.1 eq. HCl. With 0.5 eq. HCl, 74% conversion was observed after 1 h, and after 6 h the molar percentages of the compounds **28** and **25** were 90% and 10%, respectively (Entry 3, Table 2.2). Increased amounts of **25** was observed when adding 1 eq. HCl, reaching 14% after 6 h (Entry 4, Table 2.2). In this experiment, the conversion also increased, with 81% after 1 h. Comparable results were observed when adding 3.0 eq. HCl (Entry 5, Table 2.2). The highest conversion was observed when adding 5.0 eq. HCl (Entry 6, Table 2.2). Within 1 h, the conversion was 86% and after 6 h the molar percentages of **28** and **25** was 83% and 17%, respectively.

The increased molar percentage of compound **25** can be attributed to aniline **2** being a weaker nucleophile under acidic conditions due to protonation. In water, aniline **2** has a pK_a of 4.58⁸⁷ and for the conjugate acid of EtOH, the ethyl oxonium ion, the pK_a is -2.3.¹¹⁹ Even though these experiments are conducted in EtOH and not H₂O, aniline **2** will still protonate first under these acidic conditions. Consequently, it is rendered a weaker nucleophile which allows alcoholysis with EtOH as the nucleophile instead.

Alcoholysis was identified as the main competing side reaction, however, it was observed that the side product **25** was reacting with aniline **2** to give the desired product **28**. This observation was made from ¹H-NMR analysis, and the molar percentage of compound **25** was highest at 2 h and decreased in the following 3-6 h. A 3D surface plot based on the experiments from Table 2.2 illustrates this trend (Figure 2.3). See Listing O.1 in Appendix O for details.

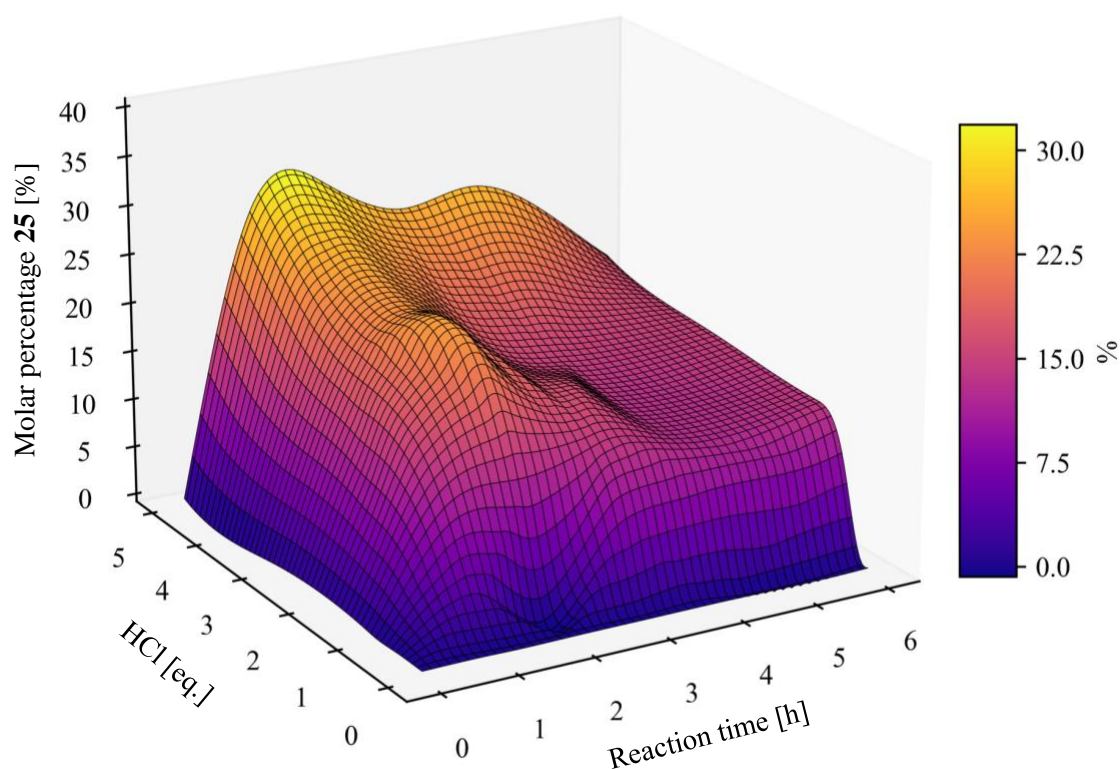
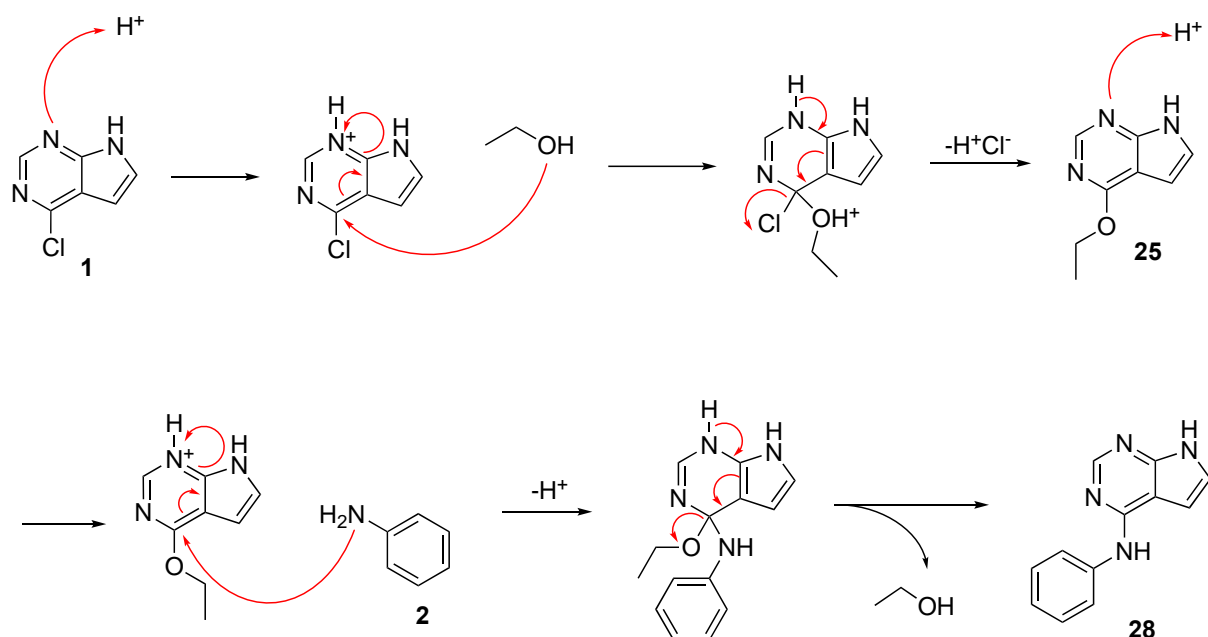


Figure 2.3: 3D-plot of side product profile, **25** from alcoholysis with EtOH, in acid catalyzed amination to pyrrolopyrimidine **1**. The plot consists of molar percentage of **25**, equivalents of the catalyst HCl and reaction time.

A suggested mechanism is presented in Scheme 2.4 where EtOH attacks compound **1** *via* S_NAr with chlorine as the leaving group, followed by another S_NAr where EtOH is the leaving group and aniline **2** is the nucleophile.



Scheme 2.4: Suggested mechanism of alcoholysis of the starting material **1**, followed by S_NAr between the side product **25** and aniline **2** with ethanol as the leaving group to form the desired product **28**.

2.2.2 Effect of solvent type and temperature

Next, the effect of different solvent types was investigated in the model reaction. Five different protic solvents have been employed, namely H_2O , MeOH, EtOH, *i*-PrOH and *t*-BuOH. All reactions were run with 0.1 eq. HCl and observed by 1H -NMR and TLC for 22 h. The reactions were run at 60 °C due to the lower boiling point of MeOH (bp. 64 °C¹²⁰). All calculated molar percentage of **28** at different reaction times are outlined in Figure 2.4.

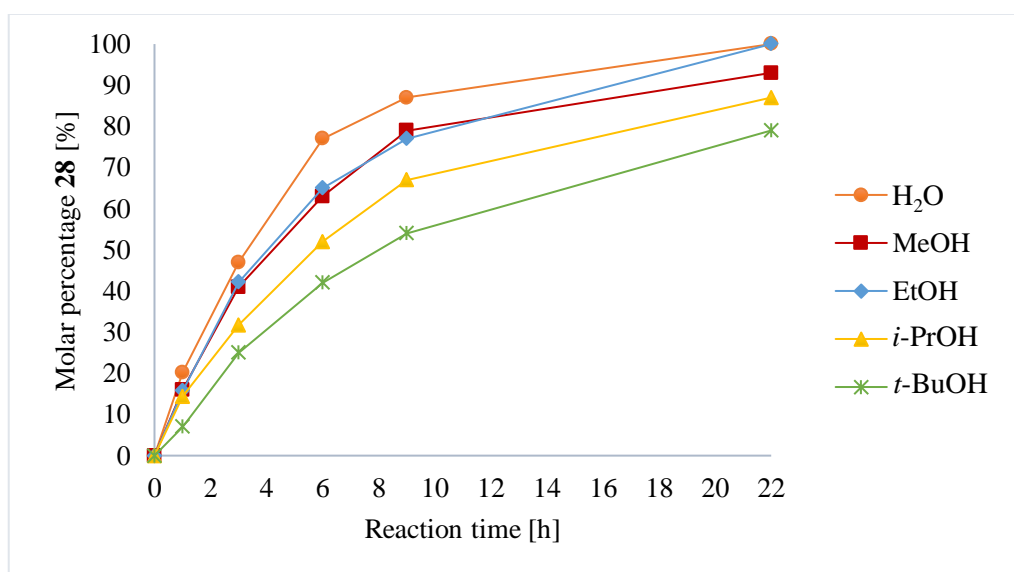


Figure 2.4: Molar percentage of product **28** at different reaction times in different solvents: H_2O (orange), MeOH (red), EtOH (blue), *i*-PrOH (yellow), *t*-BuOH (green). All reactions were run at 60 °C.

Employing H₂O and EtOH lead to full conversion of **28** after 22 h. With MeOH the molar percentage of **28** after 22 h was 95% due to solvolysis of the starting material, leading to a 5% formation of 4-methoxy-7*H*-pyrrolo[2,3-*d*]pyrimidine (**26**). Although the starting materials were not fully converted with *i*-PrOH and *t*-BuOH, no side product was observed.

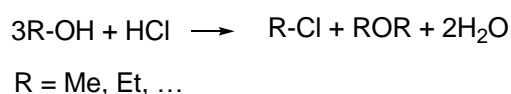
Solvents such as alcohols have the potential to act as nucleophiles when the nucleophilicity of the anilines are sufficiently reduced, due to factors such as hydrogen bonding with the solvent or protonation of the aniline.¹⁰⁰ Generally, within the initial 3-6 h, no side product from solvolysis with MeOH were detected. The side product was being formed after 6 h, which can be attributed to generation of HCl during the reaction, leading to protonation of the aniline and eventually permitting solvolysis of the starting material **1**. MeOH is a slightly stronger nucleophile than EtOH¹²¹ and H₂O is a weaker nucleophile compared to the two^{121, 122}, which can explain why only solvolysis by MeOH was observed. Additionally, MeOH is a better hydrogen bond donor than EtOH which is one factor that will decrease the reaction rate.¹⁰⁰ There are also strong hydrogen bonding interactions between aniline and MeOH which further reduces the reactivity of the aniline.^{100, 123} Solvolysis of **1** was not observed with *i*-PrOH or *t*-BuOH, as they are weaker nucleophiles compared to the smaller alcohols due to steric effects.

The variation in the pK_a of anilines in different solvents may explain why there was no observation of hydrolysis in H₂O. Rossini *et al.*⁹⁰ have provided calculated pK_a-values of aniline **2** in various solvents. In MeOH the pK_a was reported 6.05 whereas in H₂O it was 4.58.⁹⁰ The protonation of aniline in MeOH occurs at a higher pH than in H₂O, which could imply that the aniline behaves as a weaker nucleophile in the reaction with MeOH. Furthermore, due to the lower pK_a of aniline **2** in H₂O, the aniline retains its nucleophilicity for a longer time during the reaction, which could explain the absence of the hydrolysis side product. The higher pK_a of aniline **2** in MeOH could explain the presence of alcoholysis. Likewise, the basicity of pyrrolopyrimidine **1** will also vary in the different solvents. Further, hydrogen bonding in the different alcohols^{124, 125} and reactivity of the alcohols¹²⁶ can influence the reactivity.

The hydrogen bonding of the different solvents varies. H₂O has the most hydrogen bonds per molecule followed by methanol and then ethanol.¹²⁴ The number of branched methyl groups, such as in *i*-PrOH and *t*-BuOH, decreases the intermolecular hydrogen bonding.¹²⁵ The presence of hydrogen bonds might help dissolution of the starting materials **1** and **2**, which can

explain the decreasing conversion as the alkyl portion of the solvent gets bigger. Also, the density of the liquid solvents decreases with increased bulk of the alkyl portion.¹²⁵ Additionally, HCl can also form hydrogen bonds with the solvents.

Another competing side reaction is the chlorination of the alcohols (Scheme 2.5).¹²⁶ The chlorination side product and the ether formed are generally low boiling compounds and would not be detected with the analyses performed in these experiments. However, as HCl is being consumed in this side reaction, the conversion to the desired product **28** may decrease as was observed in the initial experiment in EtOH that was run without acid (Section 2.2.1).



Scheme 2.5: Chlorination of alcohol derivatives leads to the chlorinated product as well as ether and H₂O.¹²⁶

Upon comparing the polarity of the solvents employed, a clear trend emerged where the more polar solvents resulted in higher conversion rates. This observation was consistent with the theory that a greater polarity in the solvent enhances the stabilization of the Meisenheimer complex.¹⁰⁰ In this thesis, only polar protic solvents were utilized. Previous experiments by our research group using polar aprotic solvents gave moderate conversion rates, one of the solvents tested was MeCN. The precipitation of the protonated product **28** in MeCN during the reaction hindered effective stirring. One possible solution to the stirring difficulties would be to employ a more diluted reaction mixture, although this would counteract the goal of developing a more sustainable method. It is worth noting that also with employment of the aprotic solvents, higher conversions were observed when increasing the polarity, which are attributed to the stabilizing of the Meisenheimer complex.¹⁰⁰

The temperature effect was also investigated by comparing the model reaction at 80 °C and 60 °C (Figure 2.5).

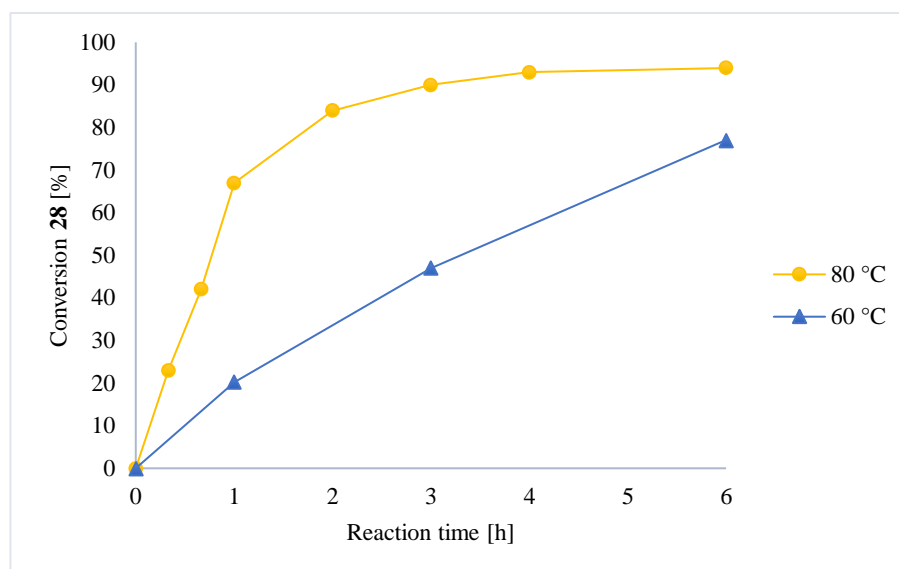
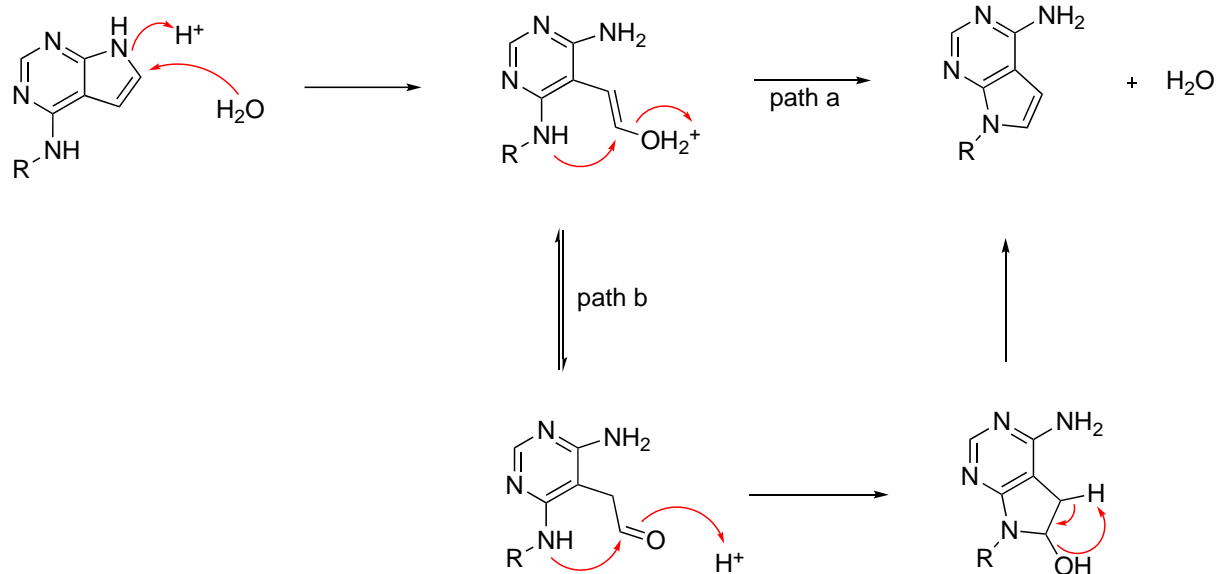


Figure 2.5: Temperature effect on the model reaction: 60 °C and 80 °C.

The reaction proceeded faster in 80 °C than in 60 °C. After 1 h, the reaction in 80 °C had reached 67% conversion whereas the reaction in 60 °C reached 20%. This is explained by Arrhenius equation (Equation 2), which implies that the rate of a reaction is dependent on activation energy and temperature.¹²⁷

$$k = A \cdot e^{-\frac{E_a}{RT}} \quad \text{Equation 2}$$

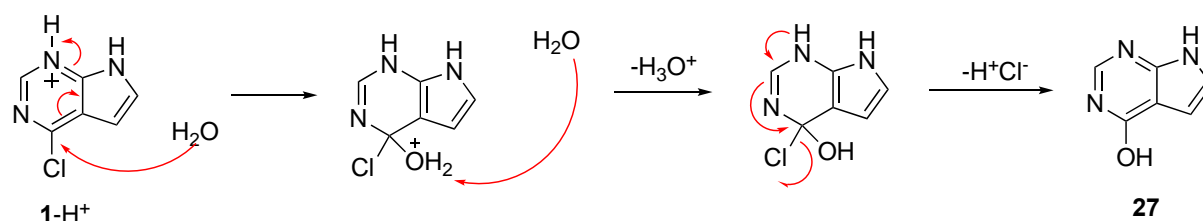
Considering Equation 2, decreasing the temperature will result in lower conversions and *vice versa*. With H₂O as the solvent, the reaction could be run at reflux temperature, 100 °C. This was not tested as one goal was to develop a more sustainable procedure and increasing the temperature by 20 °C requires a lot of energy on an industrial scale. There are also reports of decomposition of pyrrolopyrimidines at temperatures exceeding 100 °C²⁸ and under similar conditions.¹²⁸ The decomposition stems from a type of Dimroth rearrangement, as it comprises cleavage between a ring nitrogen atom and an adjacent sp² carbon (Scheme 2.6).¹²⁹ Water attacks as the nitrogen is protonated leading to a ring-opening reaction followed by nucleophilic attack of the amine moiety on C-4 with H₂O as the leaving group, making a ring-closing reaction (path a, Scheme 2.6). Another alternative is tautomerization followed by nucleophilic attack and dehydration (path b, Scheme 2.6). The rearranged side product has a free amine group and a new pyrrole ring.



Scheme 2.6: One type of Dimroth rearrangement of 4-amino substituted pyrrolopyrimidine **1** with cleavage between a nitrogen atom and the adjacent sp² carbon.^{28, 129} Path a: Nucleophilic attack by nitrogen with H₂O as the leaving group. Path b: tautomerization to aldehyde followed by nucleophilic attack by nitrogen and dehydration.

2.2.3 Effect of acid amount in water

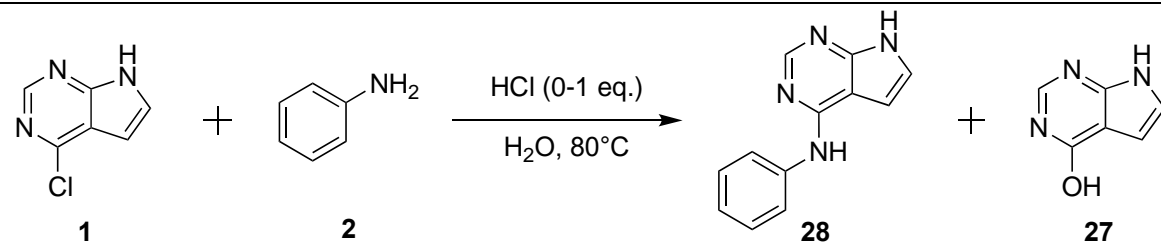
Several procedures of acid catalyzed amination on 4-chloro-7*H*-pyrrolo[2,3-*d*]pyrimidine (**1**) described in the literature employs dropwise amounts of HCl.^{11, 24, 28, 81} Hence, it was interesting to study the effect of acid amount in the model reaction. All reactions were carried out in H₂O, as the effect of acid in EtOH was already established in the initial experiments (Section 2.2.1) and H₂O was considered the most suitable solvent. One side product from hydrolysis, 7*H*-pyrrolo[2,3-*d*]pyrimidin-4-ol (**27**), was identified by comparing ¹H-NMR spectra with the commercially available compound. A proposed mechanism of the hydrolysis is presented in Scheme 2.7 based on the mechanism provided by Guo *et al.*¹⁰³



Scheme 2.7: Proposed mechanism for the hydrolysis of compound **1**, starting with the protonated pyrrolopyrimidine (**1-H⁺**) leading to the formation of the side product 7*H*-pyrrolo[2,3-*d*]pyrimidin-4-ol **27**.

Six experiments with different amounts of HCl were conducted for 22 h at 80 °C (Table 2.3).

Table 2.3: Different amounts of HCl in the model reaction with H₂O. Molar percentage of product **28** at 20 minutes and 22 h are displayed as well as molar percentage of the side product **27** at 22 h.



Entry	HCl [eq.]	Molar percentage [%]		
		28 (20 min)	28 (22 h)	27 (22 h)
1	0	1	90	0
2	0.1	23	> 97	0
3	0.2	31	> 97	1
4	0.5	48	> 97	2
5	0.8	58	> 97	1
6	1	54	97	3

The molar percentage of **28** was only 1% after 20 minutes when adding 0 eq. HCl (Entry 1, Table 2.3), but reached 90% conversion after 22 h. This was the lowest conversion observed but proves that the reaction also proceeds without acid. Since HCl is the byproduct of the reaction¹⁰³, as previously noted (Chapter 1.4.1, Scheme 1.6), it leads to an increasing activation of the pyrrolopyrimidine **1** allowing the reaction to proceed. When adding 0.1-0.8 eq. HCl (Entry 2-5, Table 2.3) the molar percentage of **28** after 20 minutes was increasingly higher, and full conversion to the desired product was reached after 22 h. This suggests that the pyrrolopyrimidine **1** can be activated towards S_NAr with only small amounts of HCl which will kick-start the reaction. However, a marginal decrease in conversion was observed upon addition of 1 eq. HCl (Entry 6, Table 2.3). This result deviates from the expected trend and could possibly be attributed to saturation of the reaction system. As HCl is generated during the reaction¹⁰³, the resulting lowering of pH may lead to protonation of the aniline, rendering it as a less effective nucleophile as explained in the suggested pathway in Scheme 2.2. Also, when increasing the acidity of the reaction, higher molar percentages of the side product **27** was observed. With H₂O as the solvent, a maximum of 3% side product **27** was observed by ¹H-NMR (Entry 6, Table 2.3). Adding more than 1 eq. HCl is likely to increase the conversion to

the side product **27**, as already observed for alcoholysis to **25** in EtOH (Section 2.2.1), however hydrolysis seems to be a much slower reaction than alcoholysis under these conditions.

Solubility of the starting materials was another important consideration. Outlined in Figure 2.6 are all calculated molar percentages of **28** at different reaction times from 1-6 h based on the experiments in Table 2.3.

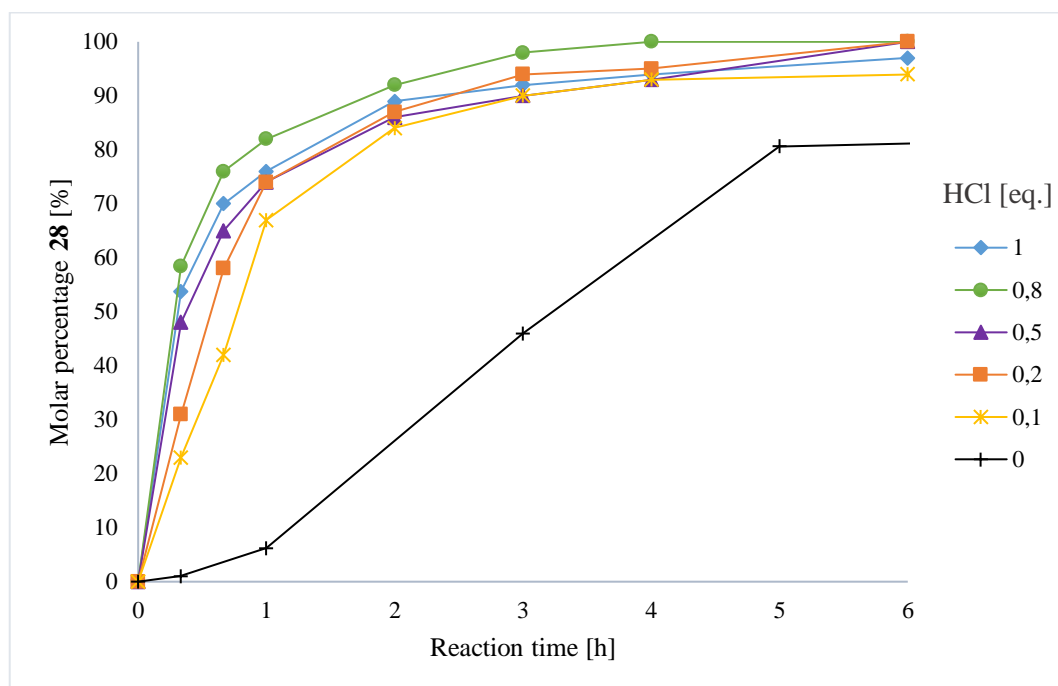


Figure 2.6: Plot of molar percentage of compound **28** against reaction time in different amounts of HCl added: 1 eq. (blue); 0.8 eq. (green); 0.5 eq. (purple); 0.2 eq. (orange); 0.1 (yellow); 0 eq. (black).

For reactions with 1 eq. and 0.8 eq. HCl, the substrates were completely dissolved when the reaction temperature reached 80 °C. In contrast, when adding 0.1-0.5 eq. HCl the initial conversion was lower due to incomplete dissolution of the starting materials. Comparably high conversions were achieved after some time, from 2 h to 3 h (Figure 2.6), when the reaction mixtures were fully dissolved. This was not the case for the reaction with 0 eq. HCl, which reached full dissolution between 9-22 h. These results suggest that higher amounts of acid results in faster solvation and hence higher conversion rates initially, whereas lower acid amounts require more time for complete dissolution but ultimately achieves similar conversion levels. Therefore, further test reactions were carried out in 0.1 eq. HCl.

The reaction mixture, consisting of the starting materials **1** and **2** and the product **28**, can capture acid through protonation, giving the reaction mixture a buffer capacity. When adding 0.1 eq. HCl to H₂O in this procedure, the calculated pH value of the reaction mixture without considering the starting materials would be 1.87. The buffer capacity of the system was demonstrated by measuring the pH of the reaction with 0.1 eq. HCl. At the starting time of the reaction, the pH was measured 4.72. After 3 h, the pH had decreased to 2.23, and after 22 h the pH had further decreased to 1.97.

The utilization of H₂O and a small quantity of HCl in this procedure represents a more environmentally sustainable approach compared to previous reports that employ various alcohols as solvents along with dropwise additions of HCl and up to three equivalents of aniline. The current procedure has enhanced sustainability, as evidenced by comparable reaction times and conversions.

The model reaction was conducted on a 500 mg scale, which gave an excellent yield of 91% (see details in Section 2.4 later). This successful reaction served as the basis for subsequent reactions in a substrate scope study, where it was a variety of substrates were used to observe potential strengths and limitations of the method.

2.3 Substrate scope

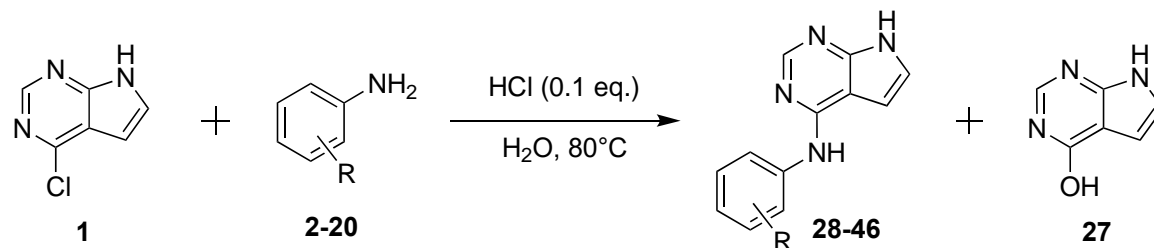
The substrate scope study consisted of nineteen different anilines, two benzylic amines, one aliphatic amine and one cyclic amine. The test reactions were run with H₂O as the solvent at 80 °C with 0.1 eq. HCl, at a 100 mg scale with equimolar amounts of the starting materials. Molar percentages and conversions have been calculated from ¹H-NMR. For the desired products, H-2 resonated in the range 8.15-8.29 ppm which integral were compared with that of H-2 on the starting material **1** at 8.56 ppm. Some substrates gave extremely poor to no yields, in which isolation and elucidation of the compounds were not possible. Molar percentages of these compounds have been calculated based on the chemical shifts observed in the H-2 range of 8.15-8.29, which did not correspond to any identified side products.

2.3.1 Aniline scope

By examining both electron-rich and electron-deficient anilines, the aim was to identify the essential characteristics required for anilines to successfully execute a nucleophilic attack on **1** under acidic conditions. The test reactions were all sampled at specific intervals, namely 1 h, 3 h, 6 h, 9 h, and 22 h. Performing a work-up was essential for the identification and elucidation of the final product structures, however, due to the comprehensive sampling, the yields were not expected to be excellent.

Table 2.4 provides an overview of all experiments, primarily sorted by pK_a-values and substituent effects. Outlined are the substitution pattern of the aniline (R), followed by the initial conversion achieved after 1 h. The total reaction time and the molar percentage of the desired product at that specific time are also reported. Furthermore, one side product **27** from hydrolysis was observed during these experiments, and its molar percentages at the total reaction time is reported.

Table 2.4: Test reactions at 100 mg scale with 19 different anilines. The conversion after 1 h is outlined for each reaction, as well as the time the reaction was stopped or reached full conversion and molar percentages of the desired product and the side product **27** at that specific time. Yields are also included.



Entry	R	Conv. 1 h [%]	Reaction time [h]	Product [%] ^a	Side product 27 [%] ^a	Yield [%]	Product no.
1	H	67	6	> 97	0	91 ^b	28
2	2,3,4,5,6-F	0	22	3	15	0	40
3	<i>o</i> -CF ₃ , <i>p</i> -NO ₂	0	22	0	15	0	31
4	<i>o</i> -NO ₂	0	22	5	17	traces	30
5	<i>p</i> -NO ₂	18	9	> 97	2	88 ^b	29
6	2,6- <i>i</i> -Pr	0	22	0	17	0	45
7	2,6-Cl	0	22	0	17	0	44
8	2,4,5-Cl	0	22	15	12	traces	34
9	2,4-Cl	19	22	94	3	37	33
10	<i>m</i> -Cl	80	6	> 97	0	68	32
11	3-F, 4-Br	84	3	> 97	0	57	46
12	<i>m</i> -ethyne	81	6	> 97	0	59	38
13	<i>p</i> -F	75	6	> 97	0	56	35
14	N-Me, <i>p</i> -F	16	22	94	1	54	36
15	<i>m</i> -OBn	86	6	> 97	0	58	42
16	<i>p</i> -OEt	76	9	> 97	0	94 ^b	43
17	3,4-methylenedioxy	74	22	97	3	58	41
18	<i>o</i> -OH	46	22	94	2	59	39
19	<i>p</i> -butyl	66	9	> 97	0	48	37

^a Calculated molar percentages at "Reaction time"

^b Yield achieved on a 500 mg scale reaction (see Section 2.4 later)

The model reaction with aniline **2** gave 67% conversion to the desired product **28** after 1 h (Entry 1, Table 2.4). This reaction was fully converted within 6 h and gave no side products. The yield of 91% was achieved from a 500 mg scale reaction, as already mentioned. Due to the absence of any substitutions on the aniline **2**, this test reaction can be considered as the reference reaction in this aniline scope study.

Among the electron deficient anilines investigated, 2,3,4,5,6-pentafluoroaniline (**14**) exhibited the lowest pK_a value of -0.28. In the initial 1 h of the reaction, no desired product was observed, and 3% of the desired product was detected after 22 h (Entry 2, Table 2.4). The primary explanation for the low conversion is the electron deficiency, however, steric effects may also contribute to some degree as both *o*-positions are occupied by fluorine atoms.

Similar trends were observed with other electron deficient anilines, such as 4-nitro-2-(trifluoromethyl)aniline (**5**), 2-nitroaniline (**4**) and 4-nitroaniline (**3**) (Entries 3-5, Table 2.4). Aniline **4** and **5** exhibited no reactivity within 1 h, and the conversion was only 0-5% after 22 h. Aniline **3** however, showed a slight increase in conversion, reaching 18% within 1 h. Aniline **4** has an experimental pK_a value of 2.5 whilst aniline **3** has an experimental pK_a of 1.02. One could expect that aniline **4** would achieve higher conversion than aniline **3** considering its pK_a is closer to aniline **2**. However, this is not the case and suggests that steric effects can significantly limit this reaction. When bulky substituents are further removed from the reaction center, the reactivity increases.¹³⁰ Thus, the large NO₂ group on aniline **4** or the CF₃ group on aniline **5**, both in *o*-position, may block the nucleophilic nitrogen from attacking, leading to a decreased reactivity compared to aniline **3** that has a *p*-NO₂ group. The molar percentages of the desired products are reported at specific reaction times in Figure 2.8.

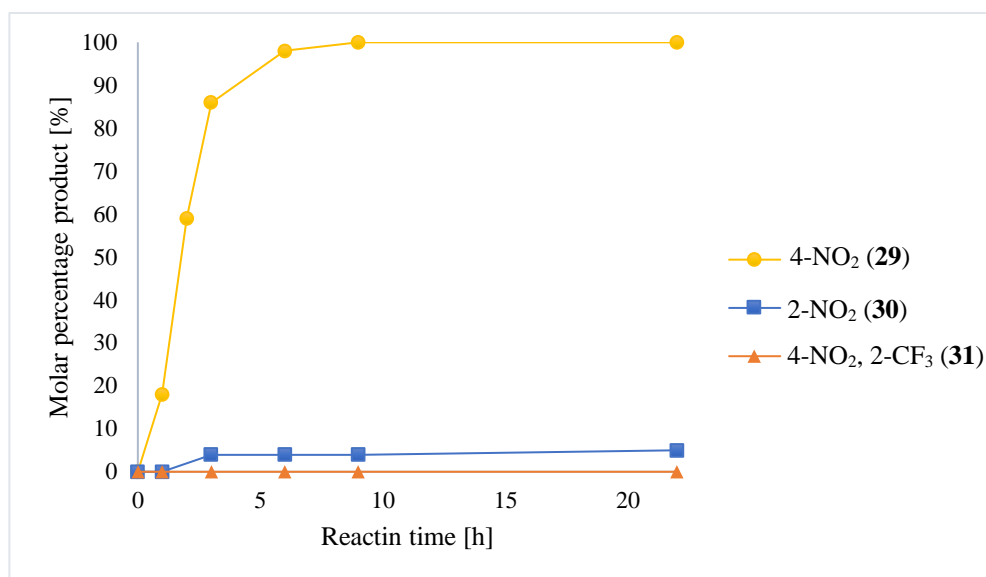


Figure 2.7: Comparison of the nitroanilines **3**, **4** and **5**, with molar percentages of the desired products *N*-(4-nitrophenyl)-7*H*-pyrrolo[2,3-*d*]pyrimidin-4-amine (**29**, yellow), *N*-(2-nitrophenyl)-7*H*-pyrrolo[2,3-*d*]pyrimidin-4-amine (**30**, blue) and *N*-(4-nitro-2-(trifluoromethyl)phenyl)-7*H*-pyrrolo[2,3-*d*]pyrimidin-4-amine (**31**, orange), respectively, at different reaction times.

The consequences of steric hindrance were also observed for 2,6-dichloroaniline (**18**) and 2,6-diisopropylaniline (**19**) as they did not react (Entries 6 and 7, Table 2.4). With both *o*-positions occupied, the conversion to the desired products decreased significantly, which is explained by the slower reaction rates of sterically hindered nucleophiles.¹³¹

For the experiments that reached the lowest conversions in this aniline scope study, i.e. anilines that were very electron deficient or sterically hindered anilines (Entries 2-4, 6 and 7, Table 2.4), significant molar percentages of the hydrolysis side product **27** were observed, 15-17%. No amounts of the side product **27** was observed in the first 9 h of the reactions, implying that hydrolysis of compound **1** competes slowly with the desired amination due to the very weak nucleophilicity of H₂O.¹³² Under acidic conditions, these electron deficient anilines failed to react effectively as nucleophiles, which can be attributed to increased activation energy needed due to the decreased electron density on the nucleophilic nitrogen.¹³³ To improve the conversion rates, alternative strategies can be considered, for instance increasing the acidity of the reaction by adding more acid could enhance the electrophilicity of pyrrolopyrimidine **1**. Employing an organic solvent, such as an alcohol, could also improve the conversion, considering the solubility issues encountered with H₂O.

In addition to the dichloroaniline **18**, three chloro-substituted anilines were tested, 2,4,5-trichloroaniline (**8**), 2,4-dichloroaniline (**7**) and 3-chloroaniline (**6**) (Entries 8-10, Table 2.4). Aniline **6** was the least electron deficient aniline of the three and reached 80% conversion after 1 h and full conversion after 6 h to the desired product. The initial conversion after 1 h decreased drastically with aniline **7** which reached 19% after 1 h, but 94% conversion was observed after 22 h to the desired product. The most electron deficient trichloroaniline **8** was unreactive within 1 h and reached 15% conversion to the product. The decreasing reactivity can be explained by the decreased electron density on nitrogen by the increasing amount of chlorine substituents (Figure 2.9).

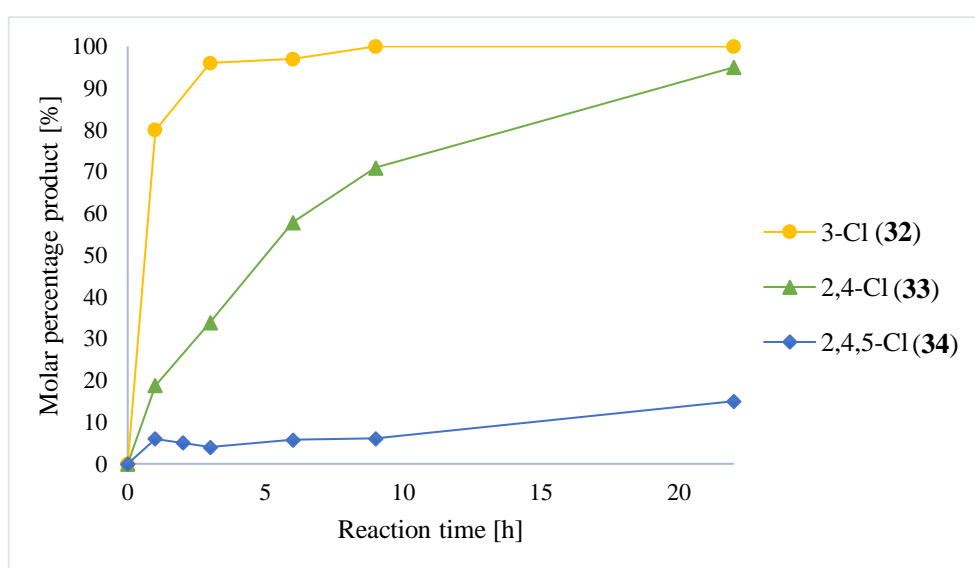


Figure 2.8: Comparison of three chloro-substituted anilines, **6**, **7** and **8**, with molar percentages of the desired products *N*-(3-chlorophenyl)-7*H*-pyrrolo[2,3-*d*]pyrimidin-4-amine (**32**, orange), *N*-(2,4-dichlorophenyl)-7*H*-pyrrolo[2,3-*d*]pyrimidin-4-amine (**33**, grey) and *N*-(2,4,5-trichlorophenyl)-7*H*-pyrrolo[2,3-*d*]pyrimidin-4-amine (**34**, blue), respectively, at different reaction times.

The trichloroaniline **8**, with pK_a 1.09, demonstrated higher reactivity compared to the 2-nitroaniline **4** (pK_a 2.5) and the trifluoromethylaniline **5** (pK_a 0.80) even though its pK_a value falls in between the two latter. This can be attributed to the stronger electron-withdrawing ability of the nitro group in both aniline **4** and **5** compared to the chlorine substituent on **8**, as well as steric effects associated with the larger size of the nitro- and trifluoromethyl group compared to chlorine. Aniline **5** possesses two strong electron-withdrawing substituents, NO_2 and CF_3 , with the *o*-trifluoromethyl group potentially hindering the nucleophilic attack.

Including 3-chloroaniline **6**, some of the highest conversions were obtained with weakly deactivated anilines, such as 4-bromo-3-fluoro-aniline (**21**), 4-fluoro-aniline (**9**), and 3-ethyne-

aniline (**12**). When aniline **21** was employed, 84% conversion to the desired product was achieved after 1 h and the reaction completed within 3 h (Entry 11, Table 2.4). Aniline **9** and **12** gave molar percentages of 75-81% within 1 h and reached full conversion to the desired products after 6-9 h (Entries 12 and 13, Table 2.4). These anilines were originally thought to be less reactive than aniline in the model reaction as electron withdrawing groups reduce the electron density on the nucleophilic nitrogen, creating weaker nucleophiles.¹³³ However, that was not the case here. Aniline **6**, **9**, **12** and **21** are slightly deactivated with substituents such as halogens and alkyne and have estimated pK_a values in the range of 2.73-4.27 whereas aniline **2** has pK_a 4.58 (Section 1.3.1, Table 1.1). Rate of protonation of weakly deactivated anilines in this pK_a range is slower compared to anilines with higher pK_a, which can allow higher conversions. Additionally, the free electron pair is sufficiently available to still react with the starting material **1** compared to the very electron poor anilines. These observations align with the suggested pathway as presented in Scheme 2.2 (Section 2).

N-Methyl-4-fluoroaniline (**10**), structurally similar to the 4-fluoroaniline **9**, gave low initial conversion to the desired product at 16% after 1 h and reached 94% after 22 h (Entry 14, Table 2.4). Despite being sterically hindered by a methyl group on the nitrogen atom, it still exhibited high conversion as opposed to other sterically hindered anilines in this scope study. This observation may be attributed to the electron density on the nucleophilic nitrogen, as aniline **10** has only one weakly deactivating fluorine in the *p*-position, and no strong withdrawing groups such as NO₂ or CF₃. The *N*-methylated fluoroaniline **10** and the non-methylated fluoroaniline **9** are compared in terms of molar percentages to the desired products **35** and **36** and reaction time in Figure 2.10. The difference in conversion rates may be attributed to the nucleophilicity and the availability of the lone pair on the nucleophilic nitrogen. Considering solubility, the *N*-methyl group will make dissolution of aniline **10** a slower process compared to aniline **9** that has a hydrogen in the same position.

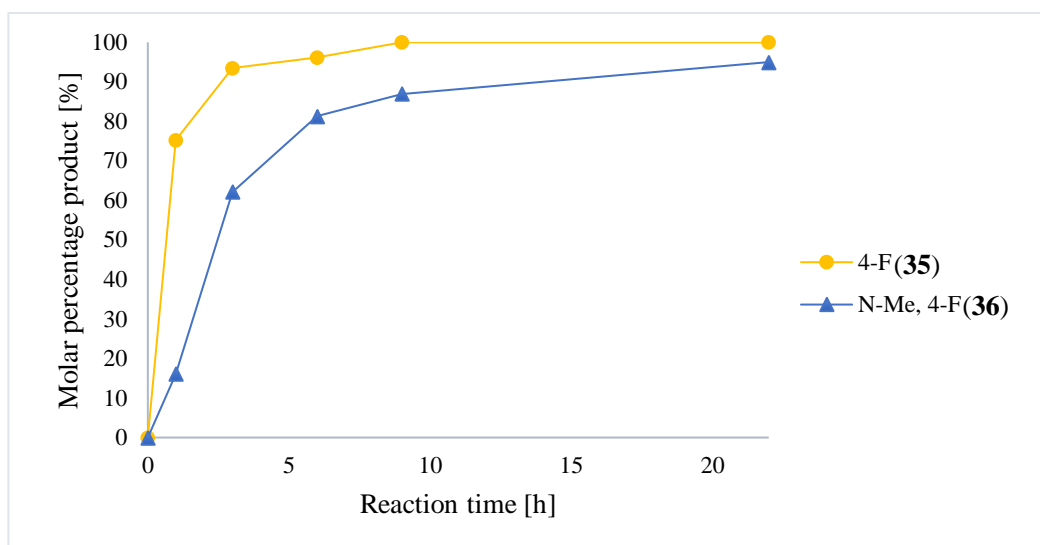


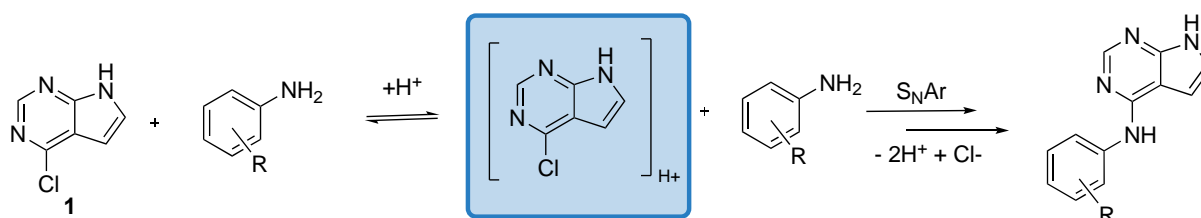
Figure 2.9: Comparison of fluoroaniline **9** and **10**, molar percentages of the desired products **35** (orange) and **36** (blue) respectively, is plotted against reaction time.

High conversions were also achieved with the electron rich anilines as expected, employing 3-benzyloxyaniline (**15**) and 4-ethoxyaniline (**17**) (Entries 15 and 16, Table 2.4). After 1 h, 76-86% conversion was observed, and full conversion was reached within 6-9 h. There was no observation of the side product **27**. Electron donating substituents increases the electron density on the aniline nitrogen, making them better nucleophiles.¹³³ Also, 2-aminophenol (**13**) and 3,4-methylenedioxyaniline (**15**) gave high conversion after 22 h, and 94-97 % was observed (Entries 17 and 18, Table 2.4). A molar percentage of 2-3% of the hydrolysis product **27** were observed when employing aniline **13** and **15**, which was expected due to the reaction taking more than 9 h to complete. 4-Butyl-aniline (**11**) gave comparable high conversions to the desired product and reached full conversion after 9 h despite the aniline being weakly activated (Entry 19, Table 2.4).

The electron rich anilines without steric hindrance in this scope study had pK_a values in the range of 3.70-5.20 (Section 1.3.1, Table 1.1). Aminophenol **13** has a pK_a of 4.78 which would make it a good candidate for acid catalyzed amination considering its pK_a lies in between 3.70-5.20. However, with an alcohol substituent in *o*-position, steric effects could account for the reaction not reaching full conversion within 9 h. The OH-group can impact the nucleophilicity in blocking the free electron pair on the nitrogen atom and making the nucleophilic site too big to fit the attack on C-4 in the pyrrolopyrimidine **1**. This may be contributing to the 3% molar percentage of the hydrolysis side product **27**. In the reactions with the electron rich anilines (Entries 15-19, Table 2.4), the side product **27** was only observed if the reactions had not

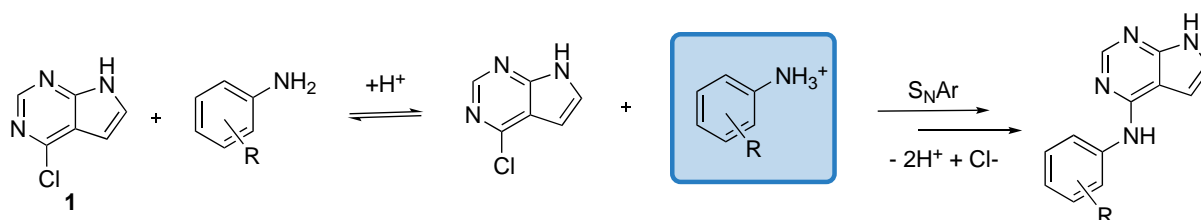
reached full conversion at the 9 h mark, indicating again that hydrolysis is a slow competing reaction.

In this substrate scope, anilines with pK_a between 2.73-5.20 gave the highest conversions. The reaction is thought to follow one of two pathways based on the pK_a of the nucleophile (see Scheme 2.2, Section 2). When assuming the deactivated anilines have pK_a value below that of pyrrolopyrimidine, the latter will protonate first (Scheme 2.8). When pyrrolopyrimidine **1** is protonated, it is rendered a stronger electrophile due to the positive charge allowing the deactivated anilines to react effectively even though they are considered weaker nucleophiles due to the decreased electron density on the nitrogen atom.



Scheme 2.8: One suggested pathway of the acid catalyzed amination of pyrrolopyrimidin **1**, where **1** is rather protonated than the aniline.

In the case of the electron rich anilines, if assuming they have a higher pK_a value than pyrrolopyrimidine, they are protonated before pyrrolopyrimidine **1** (Scheme 2.9). In contrast to the electron poor anilines, the electron rich ones are stronger nucleophiles due to the electron donating substituents that makes the electron density on nitrogen increase. The high conversions of the electron rich anilines can therefore be attributed to the stronger nucleophilicity. Even though they are assumed protonated before pyrrolopyrimidine **1** in the reaction time frame, the unprotonated portion of the substrate will react, pushing the equilibrium of protonation towards the unprotonated form.



Scheme 2.9: A second suggested pathway of the acid catalyzed amination of pyrrolopyrimidin **1**, where the aniline is rather protonated than pyrrolopyrimidine **1**.

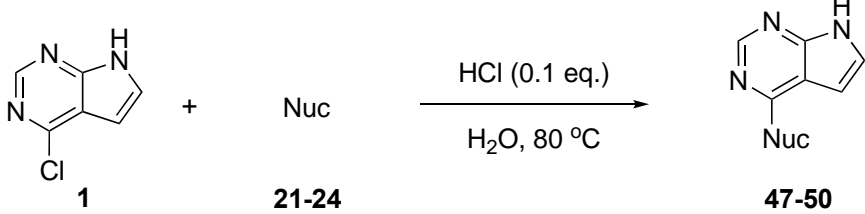
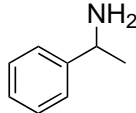
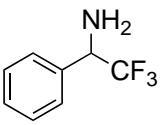
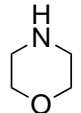
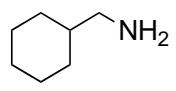
Anilines with pK_a values below the optimal range of 2.73-5.20, generally reacted poorly. No anilines with pK_a higher than 5.20 were tested. The reactivity was affected by steric effects and solubility. As steric effects increased, the conversion decreased significantly. This was especially observed for the electron deficient anilines, and the *o*-substitution of the electron rich anilines did not affect the reactivity as much. Since the reaction is conducted in H₂O, some reaction mixtures also had difficulty in achieving complete dissolution, and some anilines precipitated during the reaction. This had especially an impact on the initial reaction rates, and the accuracy of conversion values after 1 h may be compromised. Additionally, sampling from a heterogeneous reaction mixture could introduce inaccurate values, although no inconsistencies have been observed, such as negative changes in molar percentages of starting materials, products, or side products. Several test reactions could have been carried out in different solvents to investigate how solubility was affecting the reaction rates. Some of the substrates that did not react could have achieved higher conversion in organic solvents, such as small alcohols (Section 2.2.2), as this would provide a homogenous reaction mixture which eventually could facilitate the reaction.⁹¹

2.3.2 Amine scope

In an amine scope study, the reactivity of four amines was observed in the optimized reaction system with H₂O. Two benzylic amines, 1-phenylethane-1-amine (**21**) and 2,2,2-trifluoro-1-phenylethane-1-amine (**22**), were chosen as substrates based on their pK_a -values. Amine **21** have a pK_a of 9.45¹³⁴ and amine **22** was expected to have a lower pK_a due to the electron withdrawing CF₃-group although no pK_a -value was found for the compound. One cyclic amine, morpholine (**23**), and one primary, cyclohexanemethylamine (**24**) was also included in the scope as they have been successfully employed in a literature method.¹¹ In addition to the scope study, the conversion of these two amines were compared through three different methods, of which one was a literature method.¹¹ This section comprises the results from the amine scope study and the comparison of the different methods.

Outlined in Table 2.5 are experiments with the four different amines, **21-24**, in the optimized procedure with H₂O.

Table 2.5: Test reactions with four different amines (**21-24**). The conversion after 1 h is reported as well as total reaction time and molar percentages of product and side products after 22 h.

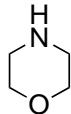
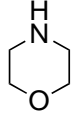
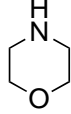
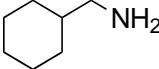
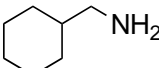
				
Entry	Nuc	Conv. 1 h [%]	Molar percentage, 22 h [%]	
			Product	Side product
1		0	13	0
2		0	6	17 ^a
3		46	61	0
4		7	24	0

For the reaction with 1-phenylethylamine (**21**), the conversion was 13% after 22 h (Entry 1, Table 2.5). This amine has an experimental pK_a of 9.45¹³⁴, which may lead to protonation of the amine in acidic conditions, hence the low conversion. It was anticipated that 2,2,2-trifluorophenylethylamine (**22**) would give higher conversion compared to **21**, due to the expectedly lower pK_a attributed to the electron withdrawing CF_3 -group. This was not the case, as amination with **23** only led to 6% conversion after 22 h (Entry 2, Table 2.5). Additionally, three unknown side products were observed in the reaction with **23**. The unexpected low conversions may be due to incomplete dissolution in H_2O . Also, benzylic amines have been employed in acid catalyzed amination to pyrimidine previously, but no reaction was observed.¹⁰⁴ In one procedure, acetonitrile was employed as the solvent with a zinc-based Lewis acid catalyst, and it was hypothesized that binding of the benzylic amine to the catalyst hindered the reaction.¹⁰⁴ Although zinc was not employed under these experiments, it might suggest that benzylic amines are not very reactive in acid catalyzed amination. This can be supported by Jesumoroti *et al.*¹¹ where benzylic amines gave low yields (34-48%).

Morpholine (**23**) gave 46% conversion to the desired product in 1 h and 61% conversion was achieved after 22 h (Entry 3, Table 2.5). Despite low conversion, no side product from hydrolysis was observed. When employing the primary amine **24**, 7% conversion to the desired product was achieved after 1 h and 24% conversion was observed after 22 h (Entry 4, Table 2.5). The cyclic amine **23** gave higher conversion than the primary amine **24**, which can be explained by their pK_a values and their molecular structures. As the primary amine **24** has a higher pK_a of 10.49¹³⁵, it will be protonated at an earlier stage compared to the cyclic amine **23** with pK_a 8.49¹³⁶. Furthermore, cyclic amines tend to be more nucleophilic than acyclic ones.¹⁰⁴ In this case, the alkyl groups of amine **23** are pinned back and locked in position, giving it a beneficial steric effect which can facilitate the nucleophilic attack.¹⁰⁴

Next, the cyclic amine **23** and the primary amine **24** were employed in a literature procedure to compare conversion rates to the developed method with H₂O. These two amines were chosen as Jesumoroti *et al.*¹¹ have reported excellent yields when employing them. In total, three different methods were tested. Hereby called method A is the optimized procedure developed in this thesis, with H₂O in a 0.26 mmol/mL concentration with 1 eq. amine and 0.1 eq. HCl. The two test reactions with amine **23** and **24** under these conditions are already reported in Table 2.5 (Entry 3 and 4, Table 2.5), but are reported again in Table 2.6 (Entry 1 and 4, Table 2.6) to ease the comparison between the different methods. In the procedure from Jesumoroti *et al.*¹¹, called method B, *i*-PrOH is employed as the solvent in a 1.04 mmol/mL concentration with 3 eq. amine and 3 drops of HCl per 5 mL solvent. One experiment was conducted with a method similar to method A, employing H₂O with an increased concentration of the starting materials, 0.52 mmol/mL, with 3 eq. amine and 0.1 eq. HCl, hereby called method A*. The results from the different methods are presented in Table 2.6.

Table 2.6: Morpholine (**23**) and cyclohexylamine (**24**) employed in different methods. Conversion after 1 h is reported as well as total reaction time and conversion to the desired products at that time. Method A: H₂O (0.26 mmol/mL), 1 eq. amine, 0.1 eq. HCl. Method A*: H₂O (0.52 mmol/mL), 3 eq. amine, 0.1 eq. HCl. Method B: *i*-PrOH (1.04 mmol/mL), 3 eq. amine, 3 drops HCl per 5 mL.

Entry	Nuc	Method	Conv. 1 h [%]	Reaction time [h]	Conv. [%]
1		A	46	22	61
2		B	70	6	>97
3		A*	85	6	>97
4		A	7	22	24
5		B	16	22	93

Morpholine (**24**) was employed in three different experiments. In method A with 1 eq. amine, 46% conversion to the desired product was observed after 1 h (Entry 1, Table 2.6). In method B, 85% conversion was observed after 1 h (Entry 2, Table 2.6). This conversion was significantly higher compared to method A and can be attributed to the difference in concentration of reaction mixtures.¹¹⁸ One additional experiment with method A* was conducted, which resulted in 85% conversion after 1 h (Entry 3, Table 2.6) and exceeded what was observed for both preceding experiments. Employing an excess amount amine will give an increased buffer capacity in the reaction system and a higher amount of the amine can remain unprotonated due to the excess amounts. This means that Method A has a lower buffer capacity than method B and A* because the amine is added in equimolar amounts. Molar percentages

of the desired product are plotted against reaction time for these three experiments in Figure 2.11.

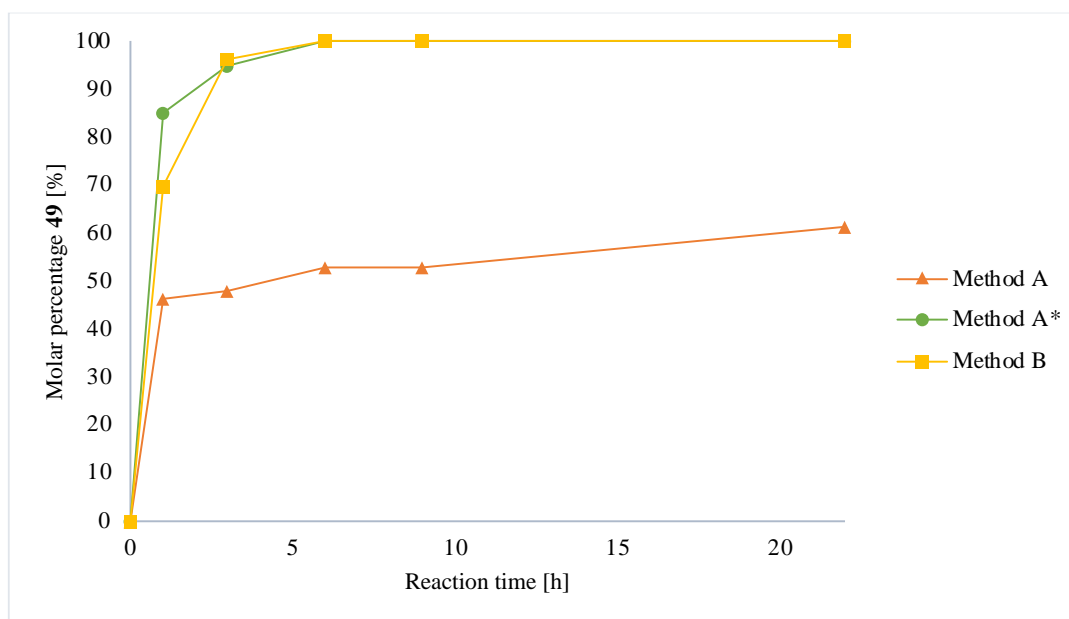


Figure 2.10: Comparison of the three different methods, Method A (orange), A* (green) and B (yellow), on conversion to compound **49** from morpholine **24**.

Solvent polarity will, as mentioned, stabilize the Meisenheimer complex¹⁰⁰, and the increased concentration of the amine increases both reaction rate¹²⁷ (Section 2.2.2, Equation 2) and buffer capacity of the reaction system. Morpholine **24**, with a pK_a 8.49¹³⁶, can act as a buffer in the reaction system, capturing the generated HCl as observed in the model reaction (Section 2.2.3). With only 1 eq. of amine **24** in method A, the amine captures HCl, but has lower buffer capacity compared to when it is added in excess. The reduced buffer capacity renders the amine protonated and unreactive at an earlier stage in the reaction time frame compared to method B and method A* in which 3 eq. amine is employed. This might explain why the conversion in method A plateaus at 61% conversion (Figure 2.11). In method B, the concentration of the starting materials is 1.04 mmol/mL, and in method A* it is 0.52 mmol/mL. Considering the two experiments employ the same equivalents of amine, H₂O is a more suitable solvent than *i*-PrOH in this reaction. These results emphasize the positive effects of increased solvent polarity and increased reaction concentration.

Two reactions were conducted with the primary amine cyclohexanemethylamine (**24**) using method A and method B (Entry 4-5, Table 2.6). After 1 h, 7% conversion was observed and 24% was achieved after 22 h with method A (Entry 4, Table 2.6). With method B, a slightly

higher conversion, 17%, was observed after 1 h, and the reaction reached 93% conversion after 22 h (Entry 4, Table 2.6). The amine **24** has a predicted pK_a 10.49, and the difference in conversion can again be explained by the concentration of the starting materials and the buffer capacity of the reaction systems. Incomplete dissolution of the starting materials in H_2O could also have influenced the conversion, as precipitate was observed in the reaction mixture throughout the whole reaction time. Molar percentages of product **50** from two experiments with method A and B are plotted against reaction time in Figure 2.12.

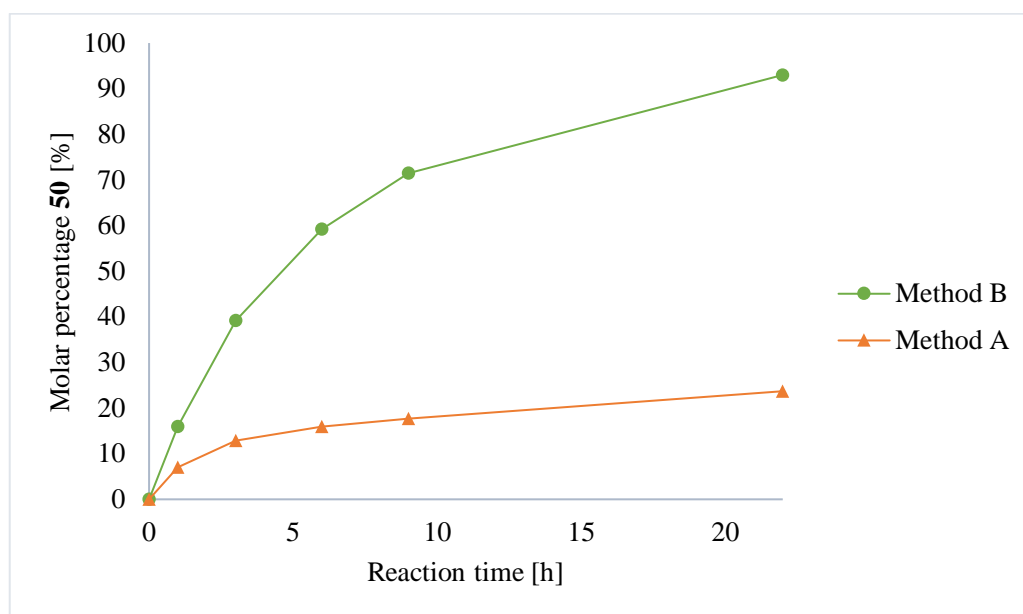


Figure 2.11: Employing the primary amine **24** in Method A and B, molar percentage of the desired product **50** is plotted against reaction time.

The results from the different methods might suggest that the benzylic amines could be more reactive in a more concentrated reaction mixture. Employing organic solvents with the benzylic amines could also enhance conversion. The comparisons of the three different methods might also give insights on possible strategies to tackle reactivity-challenges related to acid catalyzed amination of pyrrolopyrimidines.

2.3.3 Substrate comparison

The results from the substrate scope study are outlined in Figure 2.13, where the initial conversion after 1 h is plotted against pK_a-values in the optimized reaction conditions. A trend line of moving average is also displayed. The 2-nitroaniline **4**, 2-trifluoromethyl nitroaniline **5**, *o*-hydroxy aniline **13** and dichloroaniline **19** gave low conversions due to steric effects and are marked as red triangles in the plot. These values in red are not included in the moving average line as they were defined as outliers when compared to the other values. The unsubstituted aniline **2** is marked in green for reference.

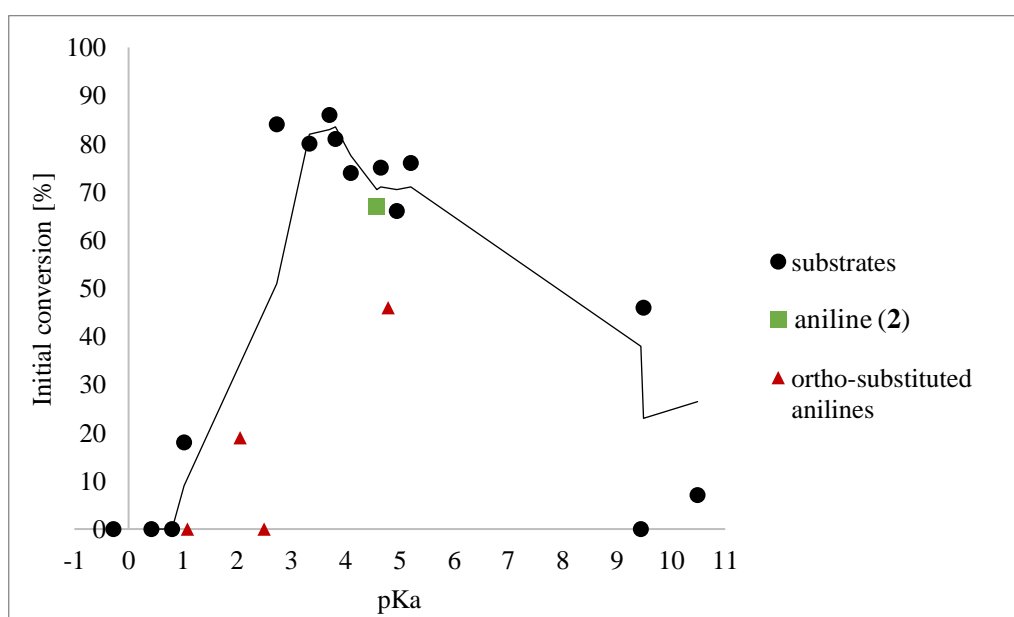


Figure 2.12: Initial conversion is plotted against reaction time for the test reactions, and moving average line is of 19 amines, thereof 18 anilines and 1 primary amine. *o*-Substituted anilines (red) are shown but not included in the moving average and aniline **2** (green) is also marked for reference.

Considering the substrates marked as black dots, anilines with pK_a below 2.5 gave the lowest initial conversions. The highest initial conversions were observed for anilines within the pK_a range of 2.73-5.20. No anilines with pK_a above this range were tested in the substrate scope study. However, four amines, the benzylic amines **21** and **22**, the cyclic amine **23** and the primary amine **24** were tested, but the initial conversions were not as high as observed for the anilines. This may emphasize the suitability of anilines in acid catalyzed amination of **1** under these conditions.

The pK_a values for the *N*-methylated fluoroaniline **10**, the diisopropylaniline **19**, and the benzylic trifluoroamine **22** were not available in the existing literature, and no established

equations were found for their estimation, consequently, they are not included in this plot. Aniline **10** may have a slightly higher pK_a value than the non-methylated 4-fluoroaniline **9** based on that *N*-methylaniline demonstrates a slightly higher pK_a compared to aniline **2**. Aniline **9** has a reported pK_a value of 4.65 and aniline **10** would therefore be expected to fall within an intermediate range on the plot but not aligning with the experimental findings as the initial conversion was only 16%. Experimental data for the aniline **20** is omitted due to the challenges associated with estimating its pK_a value using Equation 1 (Section 1.3.1), primarily attributable to the presence of *o*-substitution. Moreover, the pK_a value for the benzylic amine **22** has not been reported in the literature. A commercial website¹ offering the compound suggests a predicted pK_a value of 6.15 ± 10 ; however, given the absence of a peer reviewed source, this prediction is not considered in the present plot.

In addition to the pK_a values, there are other factors to consider when interpreting this plot, such as the solubility of the starting materials. The different rates of dissolution of the different substrates inevitably impacted the initial conversion and employing an alcoholic solvent could be beneficial. Nevertheless, while quantifying and comparing all substrates in one manner was challenging, this plot effectively displays the reactivity of each aniline and some amines when employed in this specific procedure, giving insights to which substrates are suitable for acid-catalyzed amination of compound **1** in H_2O , and which are not.

2.4 Amination on 500 mg scale

Following the substrate scope, eight anilines were employed on a 500 mg scale to verify if the optimized procedure was suited on a larger scale. Some of the best anilines from the scope study were chosen for these experiments. All syntheses were run with the optimal conditions found in the model reaction. The aniline was added in slight excess, 1.1 eq., to ease the product purification. The aminated pyrrolopyrimidine products were polar and certain structures had long retention time. The R_f value of the anilines differed more from the products compared to pyrrolopyrimidine **1**, and by adding 0.1 eq. more aniline, mixed fractions were avoided.

¹ <https://www.chembk.com/en/chem/2,2,2-Trifluor-1-phenylethanamin>

Presented in Table 2.7 are experiments with the different anilines on 500 mg scale with corresponding yields and product number. The yield of five compounds had previously been reported and are also presented with respective authors and reaction scale.

Table 2.7: Anilines characterized by R-group employed in 500 mg scale under acidic conditions to yield desired products.

Entry	R-group	Yield [%]	Lit. yield [%]	Product nr.
1	H	91	84 ^a	28
2	H	70	"	"
3	<i>p</i> -NO ₂	88	31 ^b	29
4	<i>m</i> -Cl	81	95 ^a	32
5	<i>p</i> -butyl	56	-	37
6	<i>m</i> -ethyne	85	-	38
7	3,4-methylenedioxy	85	15 ^c	41
8	<i>p</i> -OEt	91	20 ^c	43
9	4-Br, 3-F	72	-	46

^a Kurup *et al.*²⁴ (300 mg scale)

^b Jesumoroti *et al.*¹¹ (200 mg scale)

^c Nozal *et al.*¹³⁷ (unknown scale)

Aniline **2** was employed in two experiments on 500 mg scale which resulted in 91% and 70% yield (Entries 1 and 2, Table 2.7). The neutralization of the reaction mixture was the only methodic difference between the two syntheses. In the experiment that gave the highest yield (Entry 1, Table 2.7), a saturated aqueous solution of K₂CO₃ was used to neutralize the reaction mixture, which had a pH of 11 and gave 687 mg crude product. In the experiment that gave the lower yield (Entry 2, Table 2.7), a saturated aqueous solution of NaHCO₃ with pH of 8-9 was used instead. This gave a crude product weight of 543 mg, which was significantly lower compared to the first crude weight. The solution of NaHCO₃ with pH 8 may not be basic enough to deprotonate all the product **28** to its neutral form, whereas the solution of K₂CO₃ can

deprotonate it more easily. The highest yield for compound **28** found in the literature was 84%.²⁴

Both the nitroaniline **3** and chloroaniline **6** gave good yields on 500 mg scale, 88% and 81% respectively (Entries 3 and 4, Table 2.7). The two anilines employed, **3** and **6**, have lower pK_a than aniline **2**, and neutralizing with NaHCO₃ may be sufficient potentially explaining why such high yields were obtained. Both products, **29** and **32** have been synthesized before in 31%¹¹ and 95%²⁴ yield, respectively. The lowest yield of 56% was achieved when employing butylaniline **11** (Entry 5, Table 2.7). This value was in the same range as for the test reaction, which gave 48% yield (Table 2.3, Section 2.3.1). Even though the yield in the test reaction was lower compared to other similar anilines, 52% yield on the preparative scale was lower than expected. The butylaniline **11** has a higher pK_a than aniline **2** and neutralization with NaHCO₃ might not suffice in this experiment. Instead, K₂CO₃ could be employed. During work-up and purification, no side product was observed, and all steps were carefully monitored to make sure no product was lost. The weight of the crude product was 751 mg, while only 488 mg of the purified product was isolated with flash chromatography, indicating that the product stuck to the silica gel in the column.

Satisfactory yields were achieved when employing the ethyaneaniline **12**, methylenedioxyaniline **15** and ethoxyaniline **17**, ranging from 85-91% (Entries 6-9, Table 2.7). The methylenedioxy pyrrolopyrimidine **41** and the ethoxy pyrrolopyrimidine **43** had both been synthesized by Nozal *et al.*¹³⁷ in 15% and 20% yield, respectively. The dihalogen aniline **20** was expected to give a high yield considering this aniline gave the second highest conversions in the substrate scope. However, aniline **20** resulted in 72% yield of the desired compound **46** (Entry 10, Table 2.7). The crude product weighed 884 mg, which was reasonable, indicating that NaHCO₃ might suffice in the neutralization process as aniline **20** possess a lower pK_a than aniline **2**. In the purification step, 165 mg was lost which may be attributed to it being stuck on the column due to the crystalline structure of the purified product. Additionally, the product had very long retention time and was distributed in 56 fractions. A more suitable purification method could be recrystallization.

This optimized procedure with H₂O generally gave high conversions on the 500 mg scale reactions. However, some unexpected low yields might imply that each work-up needs fine tuning. Switching the neutralizing agent from NaHCO₃ to K₂CO₃ or using recrystallization as

the purification step instead of flash chromatography are two solutions that can maximize these yields. Despite the limitations and potential for improvement in this procedure, several yields obtained in the 500 mg scale reactions exceed those found in the literature. This highlights the efficiency of the optimized method. Two values from the literature were comparable to yields achieved in this project, compound **28** and **32** (Entries 1 and 4, Table 2.7). However, the procedure provided by Jesumoroti *et al.*¹¹ is not as sustainable and green compared to this procedure with H₂O since *i*-PrOH is employed as the solvent and more acid is added.

3 Structure elucidation

Some of the compounds synthesized in this thesis have not been synthesized before, and 1D and 2D NMR-spectroscopy as well as HRMS analysis were used to elucidate these structures. Regarding the compounds that had already been reported in the literature, comparing signals from ^1H -NMR and ^{13}C -NMR spectra was done to confirm the structures. IR-analysis was performed to characterize vibrational modes.

3.1 Pyrrolopyrimidines

There has previously been reported NMR data for 4-amino-6-aryl substituted pyrrolopyrimidines in $\text{DMSO-}d_6$.⁶⁰ These data were used in the elucidation of the new compounds synthesized in this thesis. HMBC couplings typical for pyrrolopyrimidines⁶⁰ are shown in Figure 3.1.

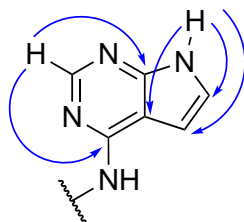


Figure 3.1: Pyrrolopyrimidine moiety with typical HMBC couplings.⁶⁰

For all NMR samples, $\text{DMSO-}d_6$ was used as the solvent. Mostly, proton H-5 and H-6 appeared as doublets in ^1H -NMR spectrum, but occasionally they appeared as doublet of doublets due to coupling with H-7 on the nitrogen.

Seven of the isolated aniline-products had not been previously reported. Kurup *et al.*²⁴ have previously synthesized *N*-phenyl-7*H*-pyrrolo[2,3-*d*]-pyrimidine-4-amine (**28**). Chemical shifts for *N*-(4-nitrophenyl)-7*H*-pyrrolo[2,3-*d*]pyrimidin-4-amine (**29**), *N*-(3-chlorophenyl)-7*H*-pyrrolo[2,3-*d*]pyrimidin-4-amine (**32**) and *N*-(4-fluorophenyl)-7*H*-pyrrolo[2,3-*d*]pyrimidin-4-amine (**35**) were retrieved from Jesumoroti *et al.*¹¹, and 2-((7*H*-pyrrolo[2,3-*d*]pyrimidin-4-yl)amino)phenol (**39**), *N*-(4-ethoxyphenyl)-7*H*-pyrrolo[2,3-*d*]pyrimidin-4-amine (**43**) and *N*-(benzo[*d*][1,3]dioxol-5-yl)-7*H*-pyrrolo[2,3-*d*]pyrimidin-4-amine (**41**) have previously been synthesized by Nozal *et al.*¹³⁷

Regarding the amine-products, the spectroscopic data for 4-(7*H*-pyrrolo[2,3-*d*]pyrimidin-4-yl)morpholine (**49**) and *N*-(cyclohexylmethyl)-7*H*-pyrrolo[2,3-*d*]pyrimidin-4-amine (**50**) have been provided by Jesumoroti *et al.*¹¹

Some products, such as *N*-(2-nitrophenyl)-7*H*-pyrrolo[2,3-*d*]pyrimidin-4-amine (**30**), *N*-(4-nitro-2-(trifluoromethyl)phenyl)-7*H*-pyrrolo[2,3-*d*]pyrimidin-4-amine (**31**), *N*-(2,4,5-trichlorophenyl)-7*H*-pyrrolo[2,3-*d*]pyrimidin-4-amine (**34**), *N*-(perfluorophenyl)-7*H*-pyrrolo[2,3-*d*]pyrimidin-4-amine (**40**), *N*-(2,6-dichlorophenyl)-7*H*-pyrrolo[2,3-*d*]pyrimidin-4-amine (**44**), *N*-(2,6-diisopropylphenyl)-7*H*-pyrrolo[2,3-*d*]pyrimidin-4-amine (**45**), *N*-(1-phenylethyl)-7*H*-pyrrolo[2,3-*d*]pyrimidin-4-amine (**46**) and *N*-(2,2,2-trifluoro-1-phenylethyl)-7*H*-pyrrolo[2,3-*d*]pyrimidin-4-amine (**47**) were not isolated (see Section 2.3).

3.1.1 Elucidation of compound 33

The structure of compound **33** with assigned shifts from ^1H -NMR and ^{13}C -NMR, and the correlation between them are shown in Table 3.1. All spectral data for this compound can be found in Appendix E.

Table 3.1: NMR signals for compound **33**, ^1H -NMR (400 MHz, $\text{DMSO-}d_6$) and ^{13}C -NMR (101 MHz, $\text{DMSO-}d_6$), as well as COSY and HMBC couplings.

Position	^1H [ppm]	multiplet	integral	^{13}C [ppm]	COSY	HMBC
1	-	-	-	-	-	-
2	8.15	s	1	151.1	-	4, 8
3	-	-	-	-	-	-
4	-	-	-	151.7	-	-
5	6.60	dd	1	99.0	6	4, 6, 9
6	7.22	dd	1	122.9	5	4, 5, 9
7	11.76	bs	1	-	-	5, 6, 9
8	-	-	-	154.5	-	-
9	-	-	-	103.3	-	-
10	9.10	s	1	-	-	-
11	-	-	-	136.2	-	-
12	-	-	-	130.5	-	-
13	7.70	d	1	129.7	15	12, 14
14	-	-	-	129.8	-	-
15	7.45	dd	1	127.9	13, 16	11, 12
16	7.75	d	1	129.4	15	11, 12

The signal at 8.15 ppm was assigned H-2, which was confirmed by long range coupling (HMBC) to C-4 and C-8. This correlation also accounted for assignment of chemical shifts for C-2 and C-4, which resonated at similar shifts. Proton H-6 was expected to resonate at a higher shift than H-5 due to the deshielding effect of the nitrogen N-7.¹³⁸ Hence, the signal at 7.22

ppm was assigned H-6, and 6.60 ppm was assigned H-5, confirmed by HMBC signals. These two signals appear as doublet of doublets rather than a doublet, which is caused by long range coupling with H-7 resonating at 11.76 ppm. Assignment of C-8 and C-9 was accomplished by observation of long-range coupling to H-2 and the pyrrolo protons H-6 and H-5, respectively.

Assignment of shifts in the aniline moiety of the compound was accomplished by analyzing ^1H - ^1H coupling constants typical for *o*, *m* and *p*-coupling (Figure 3.2). H-15 and H-16 are positioned *p* to each other, and they are correlated with a coupling constant of 8.7 Hz, which is expected for protons in *p*-position.¹³⁸ Similarly, H-15 couple with H-13 with a coupling constant of 2.4 Hz, typical for protons in *m*-position to each other.

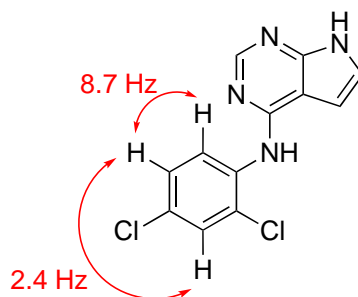


Figure 3.2: COSY coupling (red) between aromatic protons in the amine moiety of compound **32**.

3.1.2 Elucidation of compound 36

The structure of compound **36** with assigned shifts from $^1\text{H-NMR}$ and $^{13}\text{C-NMR}$, and the correlation between them are shown in Table 3.2. All spectral data for this compound can be found in Appendix H.

Table 3.2: NMR signals for compound **36**, $^1\text{H-NMR}$ (400 MHz, $\text{DMSO-}d_6$) and $^{13}\text{C-NMR}$ (101 MHz, $\text{DMSO-}d_6$), as well as COSY and HMBC couplings.

Position	^1H [ppm]	multiplet	integral	^{13}C [ppm]	COSY	HMBC
1	-	-	-	-	-	-
2	8.27	s	1	151.3	151.3	4, 8
3	-	-	-	-	-	-
4	-	-	-	156.5	-	-
5	4.66	d	1	100.8	6	6, 8, 9
6	6.99	d	1	121.5	5	5, 8
7	11.61	bs	1	-	-	9
8	-	-	-	151.8	-	-
9	-	-	-	103.3	-	-
10	-	-	-	-	-	-
11	3.50	s	3	39.4	-	4, 12
12	-	-	-	142.5	-	-
13/13'	7.43	m	2	130.6	-	12, 14/14', 15
14/14'	7.34	m	2	117.0	-	12, 13/13', 15,
15	-	-	-	161.3	-	-

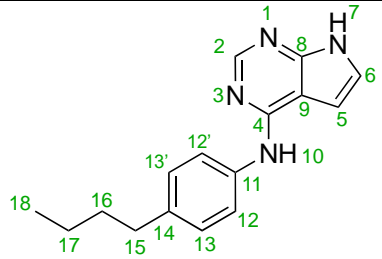
Assignment of shift in the heterocycle was done as previously described. Long-range correlation was not observed between H-11 and C-5 or C-6, however, a signal which corresponded with long-range coupling to C-9 was observed. The methyl group on N-10 was assigned shift 39.4 ppm for C-11 and 3.50 ppm for H-11 due to the expected low shifts. For

proton H-13/13' and H-14/14', the shifts were assigned based on the splitting patterns of the two multiplets in the ^{13}C -NMR spectrum due to the presence of the fluorine atom. C-14/14' was expected to have a significantly higher coupling constant than C-13/13', which was the case as $^2J_{\text{CF}} = 22.7$ Hz and $^3J_{\text{CF}} = 8.4$ Hz. Therefore, it was concluded that H-13/13' resonated at 7.43 ppm and H14/14' resonated at 7.34 ppm.

3.1.3 Elucidation of compound 37

The structure of compound **37** with assigned shifts from ^1H -NMR and ^{13}C -NMR, and the correlation between them are shown in Table 3.3. All spectral data for this compound can be found in Appendix I.

Table 3.3: NMR signals for compound **37**, ^1H -NMR (400 MHz, $\text{DMSO-}d_6$) and ^{13}C -NMR (151 MHz, $\text{DMSO-}d_6$), as well as COSY and HMBC couplings.



Position	^1H [ppm]	multiplet	integral	^{13}C [ppm]	COSY	HMBC
1	-	-	-	-	-	-
2	8.24	s	1	151.3	-	8
3	-	-	-	-	-	-
4	-	-	-	151.3	-	-
5	6.75	dd	1	99.0	6, 7	6, 4, 9
6	7.20	dd	1	122.4	5, 7	5, 4, 9
7	11.70	bs	1	-	6	5, 9
8	-	-	-	154.1	-	-
9	-	-	-	104.0	-	-
10	9.20	s	1	-	-	8, 9, 12 / 12'
11	-	-	-	138.5	-	-
12 / 12'	7.75	d	2	121.0	13 / 13'	14, 13 / 13'
13 / 13'	7.14	d	2	128.6	12 / 12'	11, 12 / 12', 15
14	-	-	-	136.5	-	-
15	2.54	t	2	34.8	16	13 / 13', 14, 16, 17
16	1.55	p	2	33.8	15, 16	14, 15, 17, 18
17	1.31	h	2	22.2	16, 18	15, 18
18	0.90	t	3	14.3	17	16, 17

Assignment of shifts for the pyrrolopyrimidine was done as previously described. Protons in the aromatic ring H-12/12' and H-13/13' were assigned shifts based on the deshielding effect

of N-10 compared to that of the butyl chain on C-14,¹³⁸ concluding that H-12/12' resonate at 7.75 ppm and H-13/13' at 7.14 ppm. This was confirmed by long-range coupling between C-12/12' and H-10. For the alkyl chain, shifts were assigned based on splitting pattern and the expected decrease in chemical shift away from the aromatic ring.

3.1.4 Elucidation of compound 38

The structure of compound **38** with assigned shifts from ^1H -NMR and ^{13}C -NMR, and the correlation between them are shown in Table 3.4. All spectral data for this compound can be found in Appendix J.

Table 3.4: NMR signals for compound **38**, ^1H -NMR (400 MHz, $\text{DMSO-}d_6$) and ^{13}C -NMR (101 MHz, $\text{DMSO-}d_6$), as well as COSY and HMBC couplings.

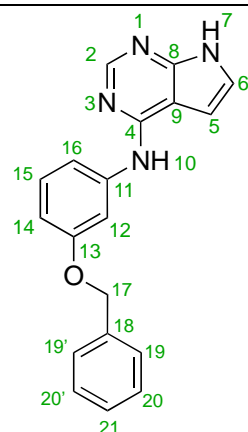
Position	^1H [ppm]	multiplet	integral	^{13}C [ppm]	COSY	HMBC
1	-	-	-	-	-	-
2	8.32	s	1	150.9	-	8
3	-	-	-	-	-	-
4	-	-	-	151.4	-	-
5	6.82	d	1	99.2	6	4, 6, 9
6	7.28	d	1	122.9	5	4, 5
7	11.81	bs	1	-	-	6, 9
8	-	-	-	153.7	-	-
9	-	-	-	104.3	-	-
10	9.40	bs	1	-	-	6, 8, 9
11	-	-	-	141.2	-	-
12	8.16	t	1	123.1	14, 16	11, 14, 15, 17
13	-	-	-	122.2	-	-
14	7.11	dt	1	125.5	12, 15	12, 15, 16, 17
15	7.34	t	1	129.6	14, 16	11, 13
16	7.91	ddd	1	120.9	12	11, 14
17	-	-	-	84.3	-	-
18	4.15	s	1	80.7	-	13

Assignment of signals in the pyrrolopyrimidine was done as previously described. The ethyne portion of the compound had the lowest shifts with C-17 resonating at 84.3 ppm and C-18 at 80.7 ppm with H-18 at 4.15 ppm. Long range coupling from HMBC was used to determine H-15 and H-16, where H-15 had a three-bond correlation with C-13 and H-16 had a three-bond correlation with C-14. From COSY, a correlation between H-15 and H-14 was observed and H-14 was assigned the shift 7.11 ppm. H-12 was assigned due to a lack of COSY signals to H-15.

3.1.5 Elucidation of compound **42**

The structure of compound **42** with assigned shifts from $^1\text{H-NMR}$ and $^{13}\text{C-NMR}$, and the correlation between them are shown in Table 3.5. All spectral data for this compound can be found in Appendix L.

The NMR spectra of compound **42** had overlapping signals which made them difficult to distinguish, especially long-range correlations. The pyrrolopyrimidine heterocycle was assigned shifts as previously described. However, H-6 shift, 7.19-7.28 ppm, was overlapping with signals from H-15 but was assigned due to correlation with C-4, C-5, and C-9. H-15 was assigned shift within the same multiplet of 7.19-7.28 ppm based on long-range correlation with C-11, C-12, and C-13. Proton H-5 and H-6 appeared as a doublet of doublets due to coupling with H-7. The signal at 6.80 ppm had coupling constants of 8.2 Hz and 2.6 Hz indicating that it is an aromatic proton with adjacent protons in *o*- and *m*-position, hence it belonged to H-16. This was confirmed by long-range coupling to C-12 and C-14 as well as one weak signal indicating a four-bond-correlation with C-13.

Table 3.5: NMR signals for compound **42**, $^1\text{H-NMR}$ (400 MHz, $\text{DMSO-}d_6$) and $^{13}\text{C-NMR}$ (101 MHz, $\text{DMSO-}d_6$), as well as COSY and HMBC couplings.

Position	^1H [ppm]	multiplet	integral	^{13}C [ppm]	COSY	HMBC
1	-	-	-	-	-	-
2	8.31	s	1	151.2	-	4, 8
3	-	-	-	-	-	-
4	-	-	-	151.3	-	-
5	6.82	dd	1	99.2	6, 7	4, 6, 9
6	7.19-7.28	m	1	122.7	5, 7	4, 5, 9
7	11.78	bs	1	-	5, 6	-
8	-	-	-	153.4	-	-
9	-	-	-	104.3	-	-
10	9.28	bs	1	-	-	8, 9, 12, 16
11	-	-	-	142.2	-	-
12	7.80	m	1	107.4	14	11, 13
13	-	-	-	159.1	-	-
14	6.68	dd	1	108.5	12, 15	12, 13, 16
15	7.19-7.28	m	1	129.7	14	11, 12, 13
16	7.44-7.52	m	1	113.1	16	14
17	5.12	s	1	69.7	-	13, 18, 19 / 19'
18	-	-	-	137.6	-	-
19 / 19'	7.44-7.52	m	2	128.2	in. ^a	21
20 / 20'	7.34-7.48	m	2	128.9	in. ^a	18
21	7.29-7.38	m	1	128.3	in. ^a	19/19'

^a Inconclusive

3.1.6 Elucidation of compound 46

The structure of compound **46** with assigned shifts from ^1H -NMR and ^{13}C -NMR, and the correlation between them are shown in Table 3.6. All spectral data for this compound can be found in Appendix N.

Table 3.6: NMR signals for compound **46**, ^1H -NMR (400 MHz, $\text{DMSO-}d_6$) and ^{13}C -NMR (101 MHz, $\text{DMSO-}d_6$), as well as COSY and HMBC couplings.

Position	^1H [ppm]	multiplet	integral	^{13}C [ppm]	COSY	HMBC
1	-	-	-	-	-	-
2	8.37	s	1	150.5	-	4, 8, 9
3	-	-	-	-	-	-
4	-	-	-	152.9	-	-
5	6.82	dd	1	98.6	6, 7	6, 8, 9
6	7.31	dd	1	122.9	5, 7	5, 8, 9
7	11.89	bs	1	-	5, 6	-
8	-	-	-	151.0	-	-
9	-	-	-	104.1	-	-
10	9.61	s	1	-	-	4, 9, 12, 16
11	-	-	-	141.9	-	-
12	8.27	m	1	107.5	15, 16	11, 13, 14, 16
13	-	-	-	158.0	-	-
14	-	-	-	98.6	-	-
15	7.58 - 7.68	m	1	132.8	12	11, 12, 13, 14
16	7.58 - 7.68	m	1	116.9	12	11, 12, 13, 14

Chemical shifts in the pyrrolopyrimidine portion of the compound were assigned as previously described. Next, the typical coupling constants between C and F nuclei was used to assign ^{13}C

shifts in the phenyl portion. The large coupling constant $^1J_{C,F} = 241$ Hz was used to determine C-13 and H-13. C-12 was assigned shift 107.5 ppm based on the coupling constant of $^2J_{CF} = 27.5$ Hz, and the same was done for C-11 ($^3J_{CF} = 10.6$ Hz). C-14 also had a coupling constant equal to C-12 with $^2J_{C,F} = 21.3$ Hz, but resonated at a lower frequency which was expected due to Br being the neighboring nucleus.¹³⁸ Some signals were overlapping, for instance H-15 and H-16, and coupling between H-10 and H-12 and H-16 through HMBC was crucial for determining the structure.

4 Conclusion

In this master project, the effects of solvent type, acid amount and temperature were investigated in the acid catalyzed amination to 4-chloro-7*H*-pyrrolo[2,3-*d*]pyrimidine. One aim was to develop a green and sustainable method that led to high conversions and no side products. A substrate scope study consisting of twenty-three substrates, thereof nineteen anilines, were conducted with the best conditions found. A secondary aim was to derive a better understanding of the reaction mechanism.

¹H-NMR was utilized to investigate the protonation site on 4-chloro-7*H*-pyrrolo[2,3-*d*]pyrimidine. The greatest value of Δ ppm was observed for H-7, and an alternative splitting pattern emerged for H-5 and H-6 suggesting that the H-7 proton is exchanged under acidic conditions. Other Δ ppm did not provide definitive clues regarding the protonation site as these values were approximately the same, indicating that the compound could potentially be protonated at several positions.

In the model reaction, solvolysis was a significant drawback when employing EtOH as the solvent. Increasing amounts of HCl led to an increased amount of the side product 4-ethoxy-7*H*-pyrrolo[2,3-*d*]pyrimidine from alcoholysis. Other protic solvents were tested with the observed trend based on conversion $\text{H}_2\text{O} > \text{MeOH} \sim \text{EtOH} > i\text{-PrOH} > t\text{-BuOH}$. Increasing acid amounts in H_2O did not significantly increase formation of the hydrolysis side product 7*H*-pyrrolo[2,3-*d*]pyrimidin-4-ol, nor did it alter the conversion rate significantly. Small differences were observed when employing different amounts of HCl, primarily attributed to the dissolution rate of the starting materials. Higher temperature gave increased conversion rates, but the reactions were run at a maximum temperature of 80 °C to prevent Dimroth rearrangement. The highest conversion without formation of side products was achieved with H_2O as the solvent and 0.1 eq. HCl at 80 °C and was further used in the substrate scope study.

Anilines with pK_a in the range of 2.73-5.20 gave moderate to high conversions. Weakly deactivated anilines and activated anilines were the most suitable substrates and achieved up to 86% conversion within 1 h. Sterically hindered anilines, gave low conversions even though they possessed pK_a -values in the optimum range. High electron deficiency and bulky *o*-substituents were two of the main limitations in this procedure. Dissolution of the starting materials were also a drawback.

Benzylic amines proved to be almost unreactive. However, morpholine and cyclohexanemethylamine were well-suited substrates despite their high pK_a -values. Comparison of three different methods showed the positive effect of reaction concentration on conversion. With equal amounts of the starting materials H_2O proved to be a more suitable solvent compared to *i*-PrOH even with lower concentration of the reaction mixture.

Two anilines that gave high conversion in the scope study, such as the 4-bromo-4-fluoroaniline and the 4-butyraniline, were not isolated in satisfactory yields on the preparative scale. One suggestion to fine-tune the work-up was to neutralize the reaction mixture with K_2CO_3 instead of $NaHCO_3$ due to the difference in pK_a of the desired products. Switching the neutralizing agent gave an approximate 20% difference in yield when synthesizing *N*-phenyl-7*H*-pyrrolo[2,3-*d*]pyrimidin-4-amine.

The developed method presented in this thesis is greener, more sustainable, and, in some cases, more effective compared to methods found in existing literature for aminating 4-chloro-7*H*-pyrrolo[2,3-*d*]pyrimidine under acidic conditions. This research also gives valuable insights to further optimization work and synthesis of potential biologically active compounds with the pyrrolopyrimidine scaffold.

5 Future work

Many substrates were well suited in the acid catalyzed amination to 4-chloro-7*H*-pyrrolo[2,3-*d*]pyrimidine in H₂O with minimal amounts of HCl. It is possible to explore the reaction further with a broader range of substrates, including different functional groups to assess the applicability of the substrates. Further, this amination reaction could be enhanced in the sense of conversion rates and yields. Some conversions were very low, and exploring more variables such as solvents, different acid catalysts and reaction temperatures could be interesting. Two pathways were suggested, where one of the starting materials, the pyrrolopyrimidine or the nucleophile, was protonated based on their pK_a preceding the S_NAr reaction. Through experimental and theoretical analyses, this reaction mechanism could be confirmed and validated.

It could also be interesting to expand the reaction scope by applying the developed procedure to other related heterocyclic systems. If conducting this reaction scope expansion, however, it is important to consider the hydrophilicity of the starting materials as the solvent is H₂O.

Even though this developed procedure is greener, the purification method could be further optimized as flash chromatography is not a green method. One possible alternative could be to run the reaction with 1 eq. of both starting materials and let it reach full conversion. Then, after neutralizing with an aqueous solution of appropriate pH (e.g. NaHCO₃ and K₂CO₃) and filtration, washing the precipitate. The washing step could for example be done with H₂O and pentane, as the products do not seem to dissolve significantly.

The future work for this research may involve exploring further improvements for the amination reaction, as mentioned. However, the most significant future work may be the application of these results in developing new and potential biologically active compounds.

6 Experimental

6.1 General information

All commercial chemicals and solvents were purchased from Sigma Aldrich or VWR chemicals. No further purification of solvents or reagents was performed, but all solvents except H₂O were stored over molecular sieves (4 Å) for a minimum of 24 h. Oil baths were used to control reaction temperatures and magnets were used for even heating and stirring of the reaction mixtures.

Thin-layer chromatography (TLC) was employed to monitor the progress of the reactions. Silica plates (Silica gel 60 F254) from Merck were visualized under UV light (254 nm). For flash chromatography silica gel 40-63 µm from VWR chemicals was used, and the eluent system was optimized for each crude product being purified. In cases where the crude product was applied in its dry form, it was first immobilized on Celite® (545, 0.002-0.1 mm) from Merck.

¹H-NMR spectroscopy was also used to monitor the progress of the reactions, using a Bruker Avance III HD Spectrometer operating at 400 MHz. ¹³C-NMR spectroscopy was performed on the same spectrometer at a frequency of 101 MHz. All chemical shifts are reported in ppm (parts per million). In this project, only DMSO-*d*₆ was used as the solvent, and the reference signals in ¹H-NMR (2.50 ppm) and ¹³C-NMR (39.52 ppm) were utilized. Accurate mass determination was performed on a "Synapt G2-S" Q-TOF instrument from Waters TM. Samples were ionized by the use of an ESI probe. No chromatographic separation was used previous to the mass analysis. Calculated exact mass and spectra processing was done by Waters TM Software Masslynx V4.1 SCN871. Infrared spectroscopy (IR) was conducted using an ALPHA FTIR Spectrometer, and the IR spectra were processed using OPUS software. Melting point analyses were performed using the Stuart automatic melting point apparatus SMP40 or the manual apparatus Stuart SMP3. Measuring pH of the reaction mixtures in H₂O was done with the JENWAY 3510 pH meter, and the pH of two basic solutions was measured with MQuant® pH strips from Sigma-Aldrich.

6.2 Synthetic procedures

6.2.1 100 mg scale reaction

The 7*H*-pyrrolo[2,3-*d*]pyrimidines **28-45** were synthesized on a 100 mg scale *via* acid catalyzed S_NAr of 4-chloro-7*H*-pyrrolo[2,3-*d*]pyrimidine (**1**, 100 mg, 0.65 mmol, 1 eq.) with the appropriate amines (**2-24**, 1 eq.). The starting materials were dissolved in H₂O (5 mL) and added HCl (0.61 M, 0.1 eq.). The reaction mixtures were stirred for 22 h at 80 °C. After cooling to room temperature, the reaction mixtures were suspended in aqueous sat. NaHCO₃ (2 mL) and vacuum filtered. The residue was air dried overnight to give the crude product which was then immobilized on celite. The crude products were purified using flash chromatography.

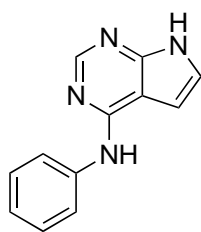
6.2.2 500 mg scale reaction with NaHCO₃

Eight compounds were additionally synthesized on a 500 mg scale with the same reaction conditions as above. 4-Chloro-7*H*-pyrrolo[2,3-*d*]pyrimidine (**1**, 500 mg, 3.26 mmol, 1. eq) and the appropriate anilines (1.1 eq.) were mixed with H₂O (25 mL) and HCl (0.61 M, 0.1 eq.). The reaction mixtures were stirred at 80 °C for 12-22 h. After cooling to room temperature, the reaction mixtures were suspended in sat. NaHCO₃ (aq. 10 mL) and vacuum filtered. The filtrate was extracted with EtOAc until no product was observed from TLC in the water phase. The combined organic phases were dried with brine (2 x 20 mL) and anhydrous Na₂SO₄ followed by filtration and concentration *in vacuo*. The residue from the filtrate and precipitate were combined and dried *in vacuo* to give the crude product, which was then immobilized with celite and purified using flash chromatography.

6.2.3 500 mg scale reaction with K₂CO₃

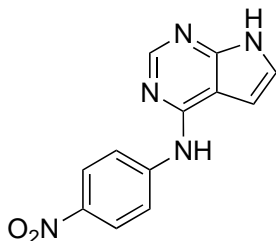
One compound was synthesized on a 500 mg scale with the same reaction conditions and procedure as described in 6.2.2. The only difference being the neutralization of the reaction mixture was done with sat. K₂CO₃ (aq., 10 mL) instead of sat. NaHCO₃ (aq.).

6.2.4 *N*-Phenyl-7*H*-pyrrolo[2,3-*d*]pyrimidin-4-amine (28)



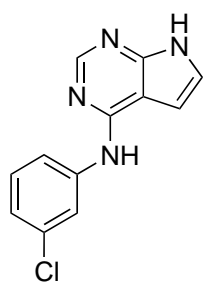
Compound **28** was synthesized on 500 mg scale with NaHCO₃ as the neutralizing agent, as described in Section 6.2.2. The crude (543 mg) was purified using flash chromatography (EtOAc/*n*-pentane, 2:1 → 100% EtOAc, *R_f* = 0.21 in EtOAc/*n*-pentane, 2:1). This yielded 481 mg (2.29 mmol, 71%) of compound **27** as a white powder. The same product was also synthesized on a 500 mg scale with K₂CO₃ as the neutralizing agent as described in Section 6.2.3, which gave 687 mg of crude product. After purifying using flash chromatography (EtOAc/*n*-pentane, 2:1 → 100% EtOAc, *R_f* = 0.21 in EtOAc/*n*-pentane, 2:1), 626 mg (2.98 mmol, 91%) of the product was isolated, mp. 240 – 243 °C (lit. 241 °C)^{11, 24}, ¹H NMR (400 MHz, DMSO-*d*₆) δ 11.74 (s, 1H), 9.28 (s, 1H), 8.27 (s, 1H), 7.93 – 7.85 (m, 2H), 7.38 – 7.28 (m, 2H), 7.23 (dd, *J* = 3.5, 2.3 Hz, 1H), 7.01 (tt, *J* = 7.3, 1.2 Hz, 1H), 6.78 (dd, *J* = 3.5, 1.8 Hz, 1H). ¹³C NMR (101 MHz, DMSO-*d*₆) δ 153.5, 150.9, 150.7, 140.4, 128.4 (2C), 122.1, 122.0, 120.2 (2C), 103.7, 98.8, 31.2, 26.9, 26.8. HRMS (ES+, *m/z*): detected 211.0986, calcd. for C₁₂H₁₁N₄ [M+H]⁺: 211.0984 (Appendix A). The spectroscopic data correspond to those previously found in the literature.^{11, 24}

6.2.5 *N*-(4-Nitrophenyl)-7*H*-pyrrolo[2,3-*d*]pyrimidin-4-amine (29)



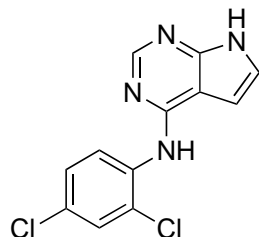
Compound **29** was synthesized on a 500 mg scale as described in Section 6.2.2. The crude product (816 mg) was purified using flash chromatography (EtOAc/*n*-pentane, 2:1 → MeOH/EtOAc, 1:10, *R_f* = 0.27 in EtOAc/*n*-pentane, 2:1). This yielded 732 mg (2.87 mmol, 88%) of compound **29** as a yellow powder, mp. 335-337 °C (lit. 331 °C)¹¹, ¹H NMR (400 MHz, DMSO-*d*₆) δ 11.99 (s, 1H), 9.99 (s, 1H), 8.44 (s, 1H), 8.25 (s, 4H), 7.37 (dd, *J* = 3.5, 2.3 Hz, 1H), 6.89 (dd, *J* = 3.5, 1.9 Hz, 1H). ¹³C NMR (101 MHz, DMSO-*d*₆) δ 152.9, 151.9, 150.8, 147.7, 141.1, 125.4, 124.0, 119.1, 105.2, 99.2. HRMS (ES+, *m/z*): detected 256.0839, calcd. for C₁₂H₁₀N₅O₂ [M+H]⁺: 256.0834 (Appendix B). The spectroscopic data correspond to those previously found in the literature.¹¹

6.2.6 *N*-(3-Chlorophenyl)-7*H*-pyrrolo[2,3-*d*]pyrimidin-4-amine (**32**)



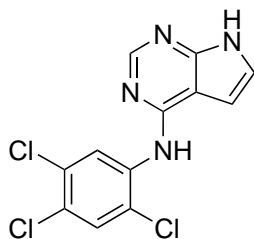
Compound **32** was synthesized on a 100 mg scale as described in Section 6.2.1. The crude product (109 mg) was purified using flash chromatography (EtOAc/*n*-pentane, 4:1, $R_f = 0.27$). This yielded 104 mg (0.43 mmol, 64%) of compound **32**. The same compound was also synthesized on a 500 mg scale as described in Section 6.2.2. The crude product (704 mg) was purified using flash chromatography EtOAc/*n*-pentane, 4:1, $R_f = 0.27$). This yielded 659 mg (2.69 mmol, 81%) of compound **32** as a white powder, mp. 226-227 °C (lit. 227 °C)¹¹, ¹H NMR (400 MHz, DMSO-*d*₆) δ 11.85 (s, 1H), 9.46 (s, 1H), 8.35 (s, 1H), 8.22 (t, $J = 2.1$ Hz, 1H), 7.81 (dd, $J = 8.2, 2.4$ Hz, 1H), 7.35 (t, $J = 8.1$ Hz, 1H), 7.28 (d, $J = 3.4$ Hz, 1H), 7.03 (dd, $J = 7.8, 2.4$ Hz, 1H), 6.82 (d, $J = 3.4$ Hz, 1H). ¹³C NMR (101 MHz, DMSO-*d*₆) δ 153.6, 151.5, 151.1, 142.6, 133.3, 130.5, 123.1, 121.8, 119.6, 118.6, 104.4, 99.1 (Appendix C). The spectroscopic data correspond to those previously found in the literature.¹¹

6.2.7 *N*-(2,4-Dichlorophenyl)-7*H*-pyrrolo[2,3-*d*]pyrimidin-4-amine (**33**)



Compound **33** was synthesized on a 100 mg scale as described in Section 6.2.1. The crude product (114 mg) was immobilized on celite and purified using flash chromatography (EtOAc/*n*-pentane, 4:1, $R_f = 0.23$). This yielded 74 mg (0.27 mmol, 37%) of compound **33** as a white powder, the melting point was not measured, ¹H NMR (400 MHz, DMSO-*d*₆) δ 11.76 (s, 1H), 9.10 (s, 1H), 8.15 (s, 1H), 7.75 (d, $J = 8.7$ Hz, 1H), 7.70 (d, $J = 2.4$ Hz, 1H), 7.45 (dd, $J = 8.6, 2.4$ Hz, 1H), 7.22 (dd, $J = 3.5, 2.3$ Hz, 1H), 6.60 (dd, $J = 3.5, 2.0$ Hz, 1H). ¹³C NMR (101 MHz, DMSO-*d*₆) δ 153.6, 151.5, 151.1, 142.6, 133.3, 130.5, 123.1, 121.8, 119.6, 118.6, 104.4, 99.1 (Appendix D).

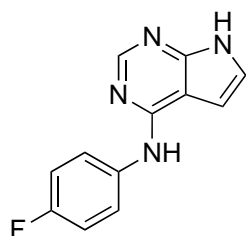
6.2.8 *N*-(2,4,5-Trichlorophenyl)-7*H*-pyrrolo[2,3-*d*]pyrimidin-4-amine (**34**)



Compound **34** was synthesized on a 100 mg scale as described in Section 6.2.1. The crude product (150 mg) was immobilized on celite and purified using flash chromatography (EtOAc/*n*-pentane, 4:1, $R_f = 0.28$). This yielded 7 mg of the product in an impure mixture. ¹H NMR (400 MHz, DMSO-*d*₆) δ 11.84 (s, 1H), 9.16 (s, 1H), 8.21 (s, 1H), 8.15 (s, 1H), 7.95

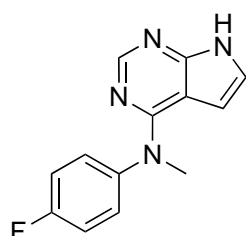
(s, 1H), 7.27 (dd, $J = 3.6, 2.3$ Hz, 1H), 6.69 (s, 1H). (Appendix E). Insufficient material was obtained for a ^{13}C -NMR spectrum.

6.2.9 *N*-(4-Fluorophenyl)-7*H*-pyrrolo[2,3-*d*]pyrimidin-4-amine (35)



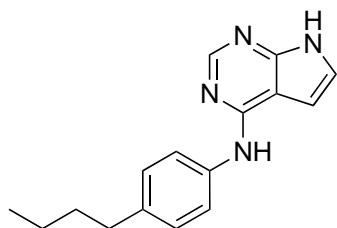
Compound **35** was synthesized on a 100 mg scale as described in Section 6.2.1. The crude product (119 mg) was immobilized on celite and purified using flash chromatography (EtOAc/*n*-pentane, 4:1, $R_f = 0.17$). This yielded 90 mg (0.39 mmol, 56%) of compound **33** as a white powder, mp. 251-253 °C (lit. 253 °C)¹¹, ^1H NMR (400 MHz, DMSO- d_6) δ 11.76 (s, 1H), 9.34 (s, 1H), 8.27 (s, 1H), 7.92 – 7.86 (m, 2H), 7.23 (d, $J = 3.5$ Hz, 1H), 7.20 – 7.13 (m, 2H), 6.76 (d, $J = 3.4$ Hz, 1H). ^{13}C NMR (101 MHz, DMSO- d_6) δ 159.2, 156.8, 154.0, 151.3, 151.2, 137.2, 137.2, 122.6, 122.5, 122.4, 115.6, 115.3, 104.0, 99.2. HRMS (ES+, m/z): detected 229.0892, calcd. for $\text{C}_{12}\text{H}_{10}\text{N}_4\text{F}$ $[\text{M}+\text{H}]^+$: 229.0889 (Appendix F). The spectroscopic data correspond to those previously found in the literature.¹¹

6.2.10 *N*-(4-Fluorophenyl)-*N*-methyl-7*H*-pyrrolo[2,3-*d*]pyrimidin-4-amine (36)



Compound **36** was synthesized on a 100 mg scale as described in Section 6.2.1. The crude product (102 mg) was immobilized on celite and purified using flash chromatography (EtOAc/*n*-pentane, 4:1, $R_f = 0.1$). This yielded 80 mg (0.33 mmol, 54%) of compound **36** as a white powder, mp. 250-252 °C, ^1H NMR (400 MHz, DMSO- d_6) δ 11.61 (s, 1H), 8.27 (s, 1H), 7.48 – 7.28 (m, 3H), 6.90 (d, $J = 3.5$ Hz, 1H), 4.66 (d, $J = 3.5$ Hz, 1H), 3.50 (s, 3H). ^{13}C NMR (101 MHz, DMSO- d_6) δ 162.5, 160.1, 156.4, 151.8, 151.2, 142.6, 142.5, 130.7, 130.6, 121.5, 117.0, 116.7, 103.3, 100.8, 39.4. HRMS (ES+, m/z): detected 243.1051, calcd. for $\text{C}_{13}\text{H}_{12}\text{N}_4\text{F}$ $[\text{M}+\text{H}]^+$: 243.1046 (Appendix G).

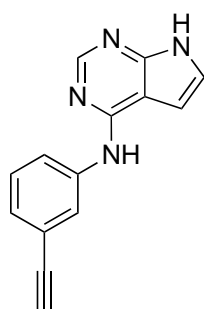
6.2.11 *N*-(4-Butylphenyl)-7*H*-pyrrolo[2,3-*d*]pyrimidin-4-amine (37)



Compound **37** was synthesized on a 100 mg scale as described in Section 6.2.1. The crude product (93 mg) was immobilized on celite and purified using flash chromatography (EtOAc/*n*-pentane, 4:1, $R_f = 0.17$). This yielded 79 mg (0.30 mmol, 48%) of compound

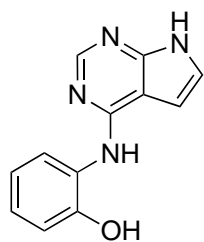
37 as a white powder. Compound **37** was also synthesized on a 500 mg scale as described in section 6.2.2. The crude product (751 mg) was purified using flash chromatography (EtOAc/*n*-pentane, 4:1, $R_f = 0.17$ in EtOAc/*n*-pentane, 4:1). This yielded 488 mg (1.83 mmol, 56%) of compound **37** as a white powder, mp. 195-197, $^1\text{H NMR}$ (400 MHz, DMSO- d_6) δ 11.71 (s, 1H), 9.21 (s, 1H), 8.25 (s, 1H), 7.80 – 7.72 (m, 2H), 7.21 (dd, $J = 3.5, 2.2$ Hz, 1H), 7.18 – 7.11 (m, 2H), 6.76 (dd, $J = 3.5, 1.8$ Hz, 1H), 2.55 (t, $J = 7.7$ Hz, 2H), 1.62 – 1.50 (m, 2H), 1.39 – 1.25 (m, 2H), 0.91 (t, $J = 7.3$ Hz, 3H). $^{13}\text{C NMR}$ (101 MHz, DMSO- d_6) δ 154.1, 151.3, 151.3, 138.4, 136.5, 128.7, 122.4, 121.0, 104.0, 99.3, 34.7, 33.8, 22.2, 14.3. HRMS (ES+, m/z): detected 267.1614, calcd. for $\text{C}_{16}\text{H}_{19}\text{N}_4$ $[\text{M}+\text{H}]^+$: 267.1610 (Appendix H).

6.2.12 *N*-(3-Ethynylphenyl)-7*H*-pyrrolo[2,3-*d*]pyrimidin-4-amine (**38**)



Compound **38** was synthesized on a 100 mg scale as described in Section 6.2.1. The crude product (120 mg) was immobilized on celite and purified using flash chromatography (EtOAc/*n*-pentane, 4:1, $R_f = 0.23$). This yielded 91 mg (0.39 mmol, 59%) of compound **38** as a white powder. Compound **38** was also synthesized on a 500 mg scale as described in section 6.2.2. The crude product (1042 mg) contained some water but was purified using flash chromatography (EtOAc/*n*-pentane, 4:1, $R_f = 0.23$). This yielded 627 mg (2.77 mmol, 83%) of compound **38** as a white powder, mp. 228-230 °C, $^1\text{H NMR}$ (400 MHz, DMSO- d_6) δ 9.40 (s, 1H), 8.32 (s, 1H), 8.16 (t, $J = 2.0$ Hz, 1H), 7.91 (ddd, $J = 8.4, 2.4, 1.0$ Hz, 1H), 7.34 (t, $J = 7.9$ Hz, 1H), 7.26 (d, $J = 3.5$ Hz, 1H), 7.11 (dt, $J = 7.6, 1.3$ Hz, 1H), 6.80 (d, $J = 3.5$ Hz, 1H), 4.15 (s, 1H). $^{13}\text{C NMR}$ (101 MHz, DMSO- d_6) δ 153.7, 151.4, 151.1, 141.2, 129.4, 125.5, 123.2, 122.9, 122.2, 121.0, 104.3, 99.2, 84.3, 80.7. HRMS (ES+, m/z): detected 235.0987, calcd. for $\text{C}_{14}\text{H}_{11}\text{N}_4\text{F}$ $[\text{M}+\text{H}]^+$: 235.0984 (Appendix I).

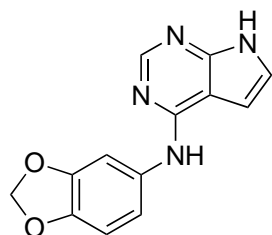
6.2.13 2-((7*H*-Pyrrolo[2,3-*d*]pyrimidin-4-yl)amino)phenol (**39**)



Compound **39** was synthesized on a 100 mg scale as described in Section 6.2.1. The crude product (115 mg) was immobilized on celite and purified using flash chromatography (EtOAc/*n*-pentane, 4:1, $R_f = 0.21$). This yielded 88 mg (0.33 mmol, 59%) of compound **39** as a light-yellow powder, mp. 232-234 °C (lit. 233-235 °C).¹³⁷ $^1\text{H NMR}$ (400 MHz, DMSO- d_6) δ 11.81 (s, 1H), 10.60 (s, 1H), 8.89 (s, 1H), 8.21 (s, 1H), 7.56 (dd, $J = 7.9, 1.7$ Hz, 1H), 7.21 (dd, $J = 3.5, 2.2$ Hz, 1H), 7.02 (td, $J = 7.3, 1.7$ Hz, 1H), 6.92 (dd, $J = 8.1, 1.6$ Hz, 1H), 6.84 (td, $J = 7.5, 1.6$ Hz,

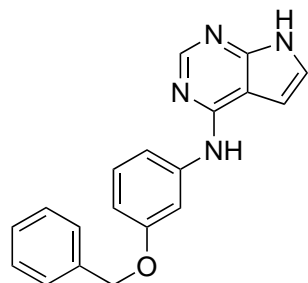
1H), 6.70 (dd, $J = 3.5, 1.6$ Hz, 1H). ^{13}C NMR (101 MHz, DMSO- d_6) δ 154.3, 151.1, 150.7, 150.1, 128.3, 125.5, 124.8, 122.7, 119.6, 117.9, 103.6, 99.5, 40.7. HRMS (ES+, m/z): detected 227.0937, calcd. for $\text{C}_{12}\text{H}_{11}\text{N}_4\text{O}$ $[\text{M}+\text{H}]^+$: 227.0933 (Appendix J). The spectroscopic data correspond to those previously found in the literature.¹³⁷

6.2.14 *N*-(Benzo[*d*][1,3]dioxol-5-yl)-7*H*-pyrrolo[2,3-*d*]pyrimidin-4-amine (41)



Compound **41** was synthesized on a 100 mg scale as described in Section 6.2.1. The crude product (126 mg) was immobilized on celite and purified using flash chromatography (EtOAc/*n*-pentane, 4:1 \rightarrow 100 % EtOAc, $R_f = 0.20$ in EtOAc/*n*-pentane, 4:1). This yielded 101 mg (0.40 mmol, 58%) of compound **41** as a light red powder. Compound **41** was also synthesized on a 500 mg scale as described in section 6.2.2. The crude product (728 mg) was purified using flash chromatography (EtOAc/*n*-pentane, 4:1 \rightarrow 100% EtOH \rightarrow MeOH/EtOAc 1:10, $R_f = 0.20$ in EtOAc/*n*-pentane, 4:1). This yielded 701 mg (2.77 mmol, 85%) of compound **41** as a light red powder, mp. 282 °C (decomp.) (lit. 282-283 °C)¹³⁷, ^1H NMR (400 MHz, DMSO- d_6) δ 11.71 (s, 1H), 9.18 (s, 1H), 8.23 (s, 1H), 7.59 (d, $J = 2.2$ Hz, 1H), 7.20 (ddd, $J = 6.1, 3.0, 1.6$ Hz, 2H), 6.89 (d, $J = 8.4$ Hz, 1H), 6.71 (dd, $J = 3.5, 1.9$ Hz, 1H), 6.00 (s, 2H). ^{13}C NMR (101 MHz, DMSO- d_6) δ 154.1, 151.3, 151.2, 147.4, 142.8, 135.2, 122.4, 113.8, 108.3, 103.8, 103.5, 101.3, 99.2. HRMS (ES+, m/z): detected 255.0887, calcd. for $\text{C}_{13}\text{H}_{11}\text{N}_4\text{O}_2$ $[\text{M}+\text{H}]^+$: 255.0882 (Appendix K). The spectroscopic data correspond to those previously found in the literature.¹³⁷

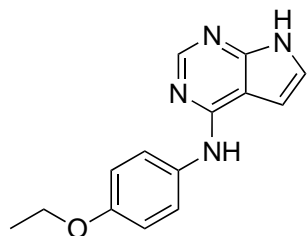
6.2.15 *N*-(3-(Benzyloxy)phenyl)-7*H*-pyrrolo[2,3-*d*]pyrimidin-4-amine (42)



Compound **42** was synthesized on a 100 mg scale as described in Section 6.2.1. The crude product (144 mg) was immobilized on celite and purified using flash chromatography (EtOAc/*n*-pentane, 4:1, $R_f = 0.25$). This yielded 127 mg (0.40 mmol, 58%) of compound **42** as a light brown powder, mp. 194-196 °C, ^1H NMR (400 MHz, DMSO- d_6) δ 11.77 (s, 1H), 9.27 (s, 1H), 8.30 (s, 1H), 7.79 (t, $J = 2.3$ Hz, 1H), 7.52 – 7.44 (m, 3H), 7.47 – 7.33 (m, 3H), 7.37 – 7.29 (m, 1H), 7.27 – 7.19 (m, 2H), 6.81 (dd, $J = 3.5, 1.9$ Hz, 1H), 6.67 (ddd, $J = 8.2, 2.6, 0.9$ Hz, 1H), 5.11 (s, 2H). ^{13}C NMR (101 MHz, DMSO- d_6) δ 159.1, 153.9, 151.3, 151.2, 142.2, 137.7, 129.6, 128.9, 128.3, 128.2, 122.7, 113.1, 108.5, 107.4, 104.3,

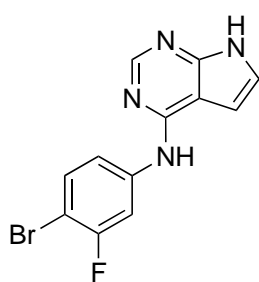
99.2, 69.6. HRMS (ES⁺, m/z): detected 317.1407, calcd. for C₁₉H₁₇N₄O [M+H]⁺: 317.1402 (Appendix L).

6.2.16 *N*-(4-Ethoxyphenyl)-7*H*-pyrrolo[2,3-*d*]pyrimidin-4-amine (43)



Compound **43** was synthesized on a 500 mg scale as described in Section 6.2.2. The crude product (790 mg) was immobilized on celite and purified using flash chromatography (EtOAc/*n*-pentane, 2:1, *R_f* = 0.16). This yielded 781 mg (3.07 mmol, 94%) of compound **43** as a white powder, mp. 240-242 °C (lit. 241-242 °C)^{24,137}, ¹H NMR (400 MHz, DMSO-*d*₆) δ 11.66 (s, 1H), 9.13 (s, 1H), 8.20 (s, 1H), 7.70 (d, *J* = 9.0 Hz, 2H), 7.18 (d, *J* = 3.5 Hz, 1H), 6.91 (d, *J* = 9.0 Hz, 1H), 6.67 (d, *J* = 3.4 Hz, 1H), 4.00 (q, *J* = 6.9 Hz, 2H), 1.32 (t, *J* = 6.9 Hz, 3H), ¹³C NMR (101 MHz, DMSO-*d*₆) δ 154.5, 154.3, 151.4, 151.2, 133.7, 122.9, 122.2, 114.7, 103.7, 99.2, 63.6, 15.2. HRMS (ES⁺, m/z): detected 255.1249, calcd. for C₁₄H₁₅N₄O [M+H]⁺: 255.1246 (Appendix M). The spectroscopic shifts from ¹H-NMR and ¹³C-NMR correspond to those previously found in the literature.^{24,137}

6.2.17 *N*-(4-Bromo-3-fluorophenyl)-7*H*-pyrrolo[2,3-*d*]pyrimidin-4-amine (46)



Compound **46** was synthesized on a 100 mg scale as described in Section 6.2.1. The crude product (135 mg) was immobilized on celite and purified using flash chromatography (EtOAc/*n*-pentane, 4:1, *R_f* = 0.27). This yielded 111 mg (0.36 mmol, 57 %) of compound **46** as white crystals. Compound **46** was also synthesized on a 500 mg scale as described in section 6.2.2. The crude product (884 mg) was purified using flash chromatography (EtOAc/*n*-pentane, 4:1, *R_f* = 0.27). This yielded 719 mg (2.34 mmol, 72 %) of compound **46** as white crystals, mp. 308-309 °C, ¹H NMR (400 MHz, DMSO-*d*₆) δ 11.88 (s, 1H), 9.61 (s, 1H), 8.37 (s, 1H), 8.26 (dd, *J* = 12.2, 2.4 Hz, 1H), 7.67 – 7.56 (m, 2H), 7.30 (dd, *J* = 3.6, 2.0 Hz, 1H), 6.82 (dd, *J* = 3.5, 1.5 Hz, 1H). ¹³C NMR (101 MHz, DMSO-*d*₆) δ 159.2, 156.8, 152.9, 151.0, 150.5, 142.0, 141.9, 132.8, 122.9, 116.9, 116.9, 107.6, 107.3, 104.1, 98.7, 98.6, 98.5. HRMS (ES⁺, m/z): detected 307.0000, calcd. for C₁₂H₉N₄FBr [M+H]⁺: 307.9995 (Appendix N).

7 References

1. Vyas, A.; Sahu, B.; Pathania, S.; Nandi, N. K.; Chauhan, G.; Asati, V.; Kumar, B., An insight on medicinal attributes of pyrimidine scaffold: An updated review. *J Heterocycl Chem* **2022**, 1081-1121.
2. Pathania, S.; Rawal, R. K., Pyrrolopyrimidines: An update on recent advancements in their medicinal attributes. *Eur J Med Chem* **2018**, *157*, 503-526.
3. Pant, S.; Kapri, A.; Nain, S., Pyrimidine analogues for the management of neurodegenerative diseases. *Eur J Med Chem Report* **2022**, *6*, Article 100095.
4. Wang, S.-B.; Deng, X.-Q.; Zheng, Y.; Yuan, Y.-P.; Quan, Z.-S.; Guan, L.-P., Synthesis and evaluation of anticonvulsant and antidepressant activities of 5-alkoxytetrazolo[1,5-c]thieno[2,3-e]pyrimidine derivatives. *Eur J Med Chem* **2012**, *56*, 139-144.
5. Blindheim, F. H.; Olsen, C. E.; Krogh Søgaaard, C.; Otterlei, M.; Sundby, E.; Hoff, B. H., Synthetic Strategies towards Imidazopyridinones and 7-Azaoxindoles and their Evaluation as Antibacterial Agents. *Eur J Org Chem* **2021**, *2021* (18), 2701-2712.
6. Al-Adiwish, W. M.; Tahir, M. I. M.; Siti-Noor-Adnalizawati, A.; Hashim, S. F.; Ibrahim, N.; Yaacob, W. A., Synthesis, antibacterial activity and cytotoxicity of new fused pyrazolo[1,5-a]pyrimidine and pyrazolo[5,1-c][1,2,4]triazine derivatives from new 5-aminopyrazoles. *Eur J Med Chem* **2013**, *64*, 464-476.
7. Kaspersen, S. J.; Han, J.; Nørsett, K. G.; Rydså, L.; Kjøbli, E.; Bugge, S.; Bjørkøy, G.; Sundby, E.; Hoff, B. H., Identification of new 4-N-substituted 6-aryl-7H-pyrrolo[2,3-d]pyrimidine-4-amines as highly potent EGFR-TK inhibitors with Src-family activity. *Eur J Med Chem* **2014**, *59*, 69-82.
8. Maurya, S. S.; Khan, S. I.; Bahuguna, A.; Kumar, D.; Rawat, D. S., Synthesis, antimalarial activity, heme binding and docking studies of N-substituted 4-aminoquinoline-pyrimidine molecular hybrids. *Eur J Med Chem* **2017**, *129*, 175-185.
9. Romeo, R.; Iannazzo, D.; Veltri, L.; Gabriele, B.; Macchi, B.; Frezza, C.; Marino-Merlo, F.; Giofrè, S. V., Pyrimidine 2,4-Diones in the Design of New HIV RT Inhibitors. *Molecules* **2019**, *24* (9), 1718-1732.

REFERENCES

10. Wang, H.; Cui, E.; Li, J.; Ma, X.; Jiang, X.; Du, S.; Qian, S.; Du, L., Design and synthesis of novel indole and indazole-piperazine pyrimidine derivatives with anti-inflammatory and neuroprotective activities for ischemic stroke treatment. *Eur J Med Chem* **2022**, *241*, 114597.
11. Jesumoroti, O. J.; Beteck, R. M.; Jordaan, A.; Warner, D. F.; Legoabe, L. J., Exploration of 4-aminopyrrolo[2,3-d]pyrimidine as antitubercular agents. *Mol Div* **2022**, 753–765.
12. Han, J.; Kaspersen, S. J.; Nervik, S.; Nørsett, K. G.; Sundby, E.; Hoff, B. H., Chiral 6-aryl-furo[2,3-d]pyrimidin-4-amines as EGFR inhibitors. *Eur J Med Chem* **2016**, *119*, 278–299.
13. Kaspersen, S. J.; Sundby, E.; Charnock, C.; Hoff, B. H., Activity of 6-aryl-pyrrolo [2, 3-d] pyrimidine-4-amines to Tetrahymena. *Bioorg Chem* **2012**, *44*, 35-41.
14. Blindheim, F. H.; Olsen, C. E.; Krogh Sjøgaard, C.; Otterlei, M.; Sundby, E.; Hoff, B. H., Synthetic Strategies towards Imidazopyridinones and 7-Azaoxindoles and their Evaluation as Antibacterial Agents. *Eur J Med Chem* **2021**, *2021* (18), 2701-2712.
15. Aarhus, T. I.; Teksum, V.; Unger, A.; Habenberger, P.; Wolf, A.; Eickhoff, J.; Klebl, B.; Wolowczyk, C.; Bjørkøy, G.; Sundby, E.; Hoff, B. H., Negishi Cross-Coupling in the Preparation of Benzyl Substituted Pyrrolo[2,3-d]pyrimidine Based CSF1R Inhibitors. *Eur J Org Chem* **2023**, *26* (12), 93-104.
16. Kaspersen, S. J.; Sørum, C.; Willassen, V.; Fuglseth, E.; Kjøbli, E.; Bjørkøy, G.; Sundby, E.; Hoff, B. H., Synthesis and in vitro EGFR (ErbB1) tyrosine kinase inhibitory activity of 4-N-substituted 6-aryl-7H-pyrrolo[2,3-d]pyrimidine-4-amines. *Eur J Med Chem* **2011**, *46* (12), 6002-6014.
17. Reiersølmoen, A. C.; Aarhus, T. I.; Eckelt, S.; Nørsett, K. G.; Sundby, E.; Hoff, B. H., Potent and selective EGFR inhibitors based on 5-aryl-7H-pyrrolopyrimidin-4-amines. *Bioorg Chem* **2019**, *88*, 102918.
18. Reiersølmoen, A. C.; Han, J.; Sundby, E.; Hoff, B. H., Identification of fused pyrimidines as interleukin 17 secretion inhibitors. *Eur J Med Chem* **2018**, *155*, 562-578.

REFERENCES

19. Dilday, T.; Yeh, E., 6.03 - HER2-Positive (HER2+) Breast Cancer. In *Comprehensive Pharmacology*, Kenakin, T., Ed. Elsevier: Oxford, 2022; pp 11-34.
20. Guevara-Cuellar, C. A.; Parody-Rúa, E.; Rengifo-Mosquera, M. P.; del Mar Conde-Crespo, M.; Nuñez-Castro, J. M., Cost-Effectiveness Analysis of Pertuzumab Plus Trastuzumab and Docetaxel Compared With Trastuzumab and Docetaxel in the Adjuvant Treatment of Human Epidermal Growth Factor Receptor 2–Positive Metastatic Breast Cancer in Colombia. *Value Health Reg Issues* **2022**, *32*, 109-118.
21. Broekman, F.; Giovannetti, E.; Peters, G. J., Tyrosine kinase inhibitors: Multi-targeted or single-targeted? *World J Clin Oncol* **2011**, *2* (2), 80-93.
22. Hynes, N. E.; Lane, H. A., ERBB receptors and cancer: the complexity of targeted inhibitors. *Nat Rev Cancer* **2005**, *5* (5), 341-354.
23. Pellat, A.; Vaquero, J.; Fouassier, L., Role of ErbB/HER family of receptor tyrosine kinases in cholangiocyte biology. *Hepatology* **2018**, *67* (2), 762-773.
24. Kurup, S.; McAllister, B.; Liskova, P.; Mistry, T.; Fanizza, A.; Stanford, D.; Slawska, J.; Keller, U.; Hoellein, A., Design, synthesis and biological activity of N(4)-phenylsubstituted-7H-pyrrolo[2,3-d]pyrimidin-4-amines as dual inhibitors of aurora kinase A and epidermal growth factor receptor kinase. *J Enzyme Inhib Med Chem* **2018**, *33* (1), 74-84.
25. Noble, M. E.; Endicott, J. A.; Johnson, L. N., Protein kinase inhibitors: insights into drug design from structure. *Science* **2004**, *303* (5665), 1800-1805.
26. Carter, M. C.; Cockerill, G. S.; Guntrip, S. B.; Lackey, K. E.; Smith, K. J. Bicyclic heteroaromatic compounds as protein tyrosine kinase inhibitors. CA2317589A1, 15.07.1999.
27. Wong, K. K.; Fracasso, P. M.; Bukowski, R. M.; Lynch, T. J.; Munster, P. N.; Shapiro, G. I.; Jänne, P. A.; Eder, J. P.; Naughton, M. J.; Ellis, M. J.; Jones, S. F.; Mikhail, T.; Zacharchuk, C.; Vermette, J.; Abbas, R.; Quinn, S.; Powell, C.; Burris, H. A., A phase I study with neratinib (HKI-272), an irreversible pan ErbB receptor tyrosine kinase inhibitor, in patients with solid tumors. *Clin Cancer Res* **2009**, *15* (7), 2552-2558.
28. Bathen, M. Synthesis of aniline substituted heterocycles: searching for anticancer agents. Masteroppgave, Norges teknisk-naturvitenskapelige universitet, 2022.

REFERENCES

29. Grotzfeld, R.; Patel, H.; Mehta, S.; Milanov, Z.; Lai, A.; Lochart, D. Pyrrolopyrimidine Derivates and Analogs and their use in the Treatment and Prevention of Diseases. US20050153989A1, 2005.
30. Traxler, P.; Bold, G.; Brill, W. K.-D.; Frei, J. Pyrrolopyrimidines and Processes for the Preparation thereof. WO9702266A1, 26.02.1997.
31. Bjørnstad, F.; Sundby, E.; Hoff, B. H., Directed Lithiation of Protected 4-Chloropyrrolopyrimidine: Addition to Aldehydes and Ketones Aided by Bis(2-dimethylaminoethyl)ether. *Molecules* **2023**, 28 (3), 932-947.
32. Perlíková, P.; Hocek, M., Pyrrolo [2, 3-d] pyrimidine (7-deazapurine) as a privileged scaffold in design of antitumor and antiviral nucleosides. *Med Res Rev* **2017**, 37 (6), 1429-1460.
33. Glushkov, R. G.; Sizova, O. S., Progress in chemistry of-pyrrolo[3,2-d]pyrimidines (Review). *Pharm Chem J* **1986**, 20 (6), 415-426.
34. Lagoja, I. M., Pyrimidine as constituent of natural biologically active compounds. *Chem Biodivers* **2005**, 2 (1), 1-50.
35. Elion, G. B.; Bieber, S.; Hitchings, G. H., The fate of 6-mercaptopurine in mice. *Ann NY Acad Sci* **1954**, 60 (2), 297-303.
36. Nishimura, H.; Katagiri, K.; Satō, K.; Mayama, M.; Shimaoka, N., Toyocamycin, A New Anti-Candida Antibiotics. *J Antibiot* **1956**, 9 (2), 60-62.
37. McCarty, R. M.; Bandarian, V., Biosynthesis of pyrrolopyrimidines. *Bioorg Chem* **2012**, 43, 15-25.
38. Arora, A.; Scholar, E. M., Role of tyrosine kinase inhibitors in cancer therapy. *J Pharmacol Exp Ther* **2005**, 315 (3), 190-198.
39. Fischer, T.; Krüger, T.; Najjar, A.; Totzke, F.; Schächtele, C.; Sippl, W.; Ritter, C.; Hilgeroth, A., Discovery of novel substituted benzo-anellated 4-benzylamino pyrrolopyrimidines as dual EGFR and VEGFR2 inhibitors. *Bioorg Med Chem Lett* **2017**, 27 (12), 2708-2712.

REFERENCES

40. Liang, Y.; Brekken, R. A.; Hyder, S. M., Vascular endothelial growth factor induces proliferation of breast cancer cells and inhibits the anti-proliferative activity of anti-hormones. *Endocr-relat cancer* **2006**, *13* (3), 905-919.
41. Han, J.; Henriksen, S.; Nørsett, K. G.; Sundby, E.; Hoff, B. H., Balancing potency, metabolic stability and permeability in pyrrolopyrimidine-based EGFR inhibitors. *Eur J Med Chem* **2016**, *124*, 583-607.
42. O'Brien, N. J.; Brzozowski, M.; Wilson, D. J. D.; Deady, L. W.; Abbott, B. M., Synthesis and biological evaluation of substituted 2-anilino-7H-pyrrolopyrimidines as PDK1 inhibitors. *Tetrahedron* **2014**, *70* (33), 4947-4956.
43. Wu, F.; Li, H.; An, Q.; Sun, Y.; Yu, J.; Cao, W.; Sun, P.; Diao, X.; Meng, L.; Xu, S., Discovery of 7H-Pyrrolo[2,3-d]pyrimidine Derivatives as potent hematopoietic progenitor kinase 1 (HPK1) inhibitors. *Eur Med Chem* **2023**, 115355.
44. Gilson, P.; Josa-Prado, F.; Beauvineau, C.; Naud-Martin, D.; Vanwonderghem, L.; Mahuteau-Betzer, F.; Moreno, A.; Falson, P.; Lafanechère, L.; Frachet, V.; Coll, J.-L.; Fernando Díaz, J.; Hurbin, A.; Busser, B., Identification of pyrrolopyrimidine derivative PP-13 as a novel microtubule-destabilizing agent with promising anticancer properties. *Sci Rep* **2017**, *7* (1), 10209.
45. Hemmings, B. A.; Restuccia, D. F., PI3K-PKB/Akt pathway. *Cold Spring Harb Perspect Biol* **2012**, *4* (9), 011189.
46. Bart Vanhaesebroeck; Sally J. Leever; Khatereh Ahmadi; John Timms; Roy Katso; Paul C. Driscoll; Rudiger Woscholski; Peter J. Parker; Michael D. Waterfield, Synthesis and Function of 3-Phosphorylated Inositol Lipids. *Ann Rev Biochem* **2001**, *70* (1), 535-602.
47. Sawasdikosol, S.; Burakoff, S., A perspective on HPK1 as a novel immuno-oncology drug target. *Elife* **2020**, *9*, 55122.
48. Ritter, A.; Kreis, N. N., Microtubule Dynamics and Cancer. *Cancers (Basel)* **2022**, *14* (18), 4368-4372.
49. Kavallaris, M., Microtubules and resistance to tubulin-binding agents. *Nat Rev Cancer* **2010**, *10* (3), 194-204.

REFERENCES

50. Prota, A. E.; Bargsten, K.; Diaz, J. F.; Marsh, M.; Cuevas, C.; Liniger, M.; Neuhaus, C.; Andreu, J. M.; Altmann, K. H.; Steinmetz, M. O., A new tubulin-binding site and pharmacophore for microtubule-destabilizing anticancer drugs. *Proc Natl Acad Sci U S A* **2014**, *111* (38), 13817-13821.
51. Hilmy, K. M. H.; Khalifa, M. M.; Hawata, M. A. A.; Keshk, R. M. A., Synthesis of new pyrrolo [2, 3-d] pyrimidine derivatives as antibacterial and antifungal agents. *Eur J Med Chem* **2010**, *45* (11), 5243-5250.
52. Cardozo, T. J., Synthesis and Biological evaluation of pyrrolo [2, 3-d] pyrimidine derivatives as antibacterial and antiviral. *Int J Chem* **2012**, *02*.
53. Boland, S.; Bourin, A.; Alen, J.; Geraets, J.; Schroeders, P.; Castermans, K.; Kindt, N.; Boumans, N.; Panitti, L.; Vanormelingen, J., Design, synthesis and biological characterization of selective LIMK inhibitors. *Bioorg Med Chem Lett* **2015**, *25* (18), 4005-4010.
54. Mohamed, M.; Ali, S.; Abdelaziz, D.; Fathallah, S. S., Synthesis and evaluation of novel pyrroles and pyrrolopyrimidines as anti-hyperglycemic agents. *BioMed Res Int* **2014**, *2014*, 809-817.
55. Kim, W.; Lee, S.-M.; Jeong, P.-H.; Jung, J.-H.; Kim, Y.-C., Synthesis and structure-activity relationship studies of 1, 5-isomers of triazole-pyrrolopyrimidine as selective Janus kinase 1 (JAK1) inhibitors. *Bioorg Med Chem Lett* **2022**, *55*, 128451.
56. Khalaf, A. I.; Huggan, J. K.; Suckling, C. J.; Gibson, C. L.; Stewart, K.; Giordani, F.; Barrett, M. P.; Wong, P. E.; Barrack, K. L.; Hunter, W. N., Structure-based design and synthesis of antiparasitic pyrrolopyrimidines targeting pteridine reductase 1. *J Med Chem* **2014**, *57* (15), 6479-6494.
57. Zhang, Y.-L.; Xu, C.-T.; Liu, T.; Zhu, Y.; Luo, Y., An improved synthesis of 4-chloro-7H-pyrrolo[2,3-d]pyrimidine. *Chem Heterocycl Comp* **2018**, *54* (6), 638-642.
58. Davoll, J., Pyrrolo[2,3-d]pyrimidines. *J Chem Soc* **1960**, (0), 131-138.
59. Chai, X.; Qian, C.; Gould, S. Fused bicyclic pyrimidines as ptk inhibitors containing a zinc binding moiety. WO2008033745A2. 2007.

REFERENCES

60. Sørum, C.; Simić, N.; Sundby, E.; Hoff, B. H., ¹H,¹³C and ¹⁹F NMR data of N-substituted 6-(4-methoxyphenyl)-7H-pyrrolo[2,3-d]pyrimidin-4-amines in DMSO-d₆. *Magn Reson Chem* **2010**, *48* (3), 244-248.
61. Frolova, L. V.; Magedov, I. V.; Romero, A. E.; Karki, M.; Otero, I.; Hayden, K.; Evdokimov, N. M.; Banuls, L. M. Y.; Rastogi, S. K.; Smith, W. R.; Lu, S.-L.; Kiss, R.; Shuster, C. B.; Hamel, E.; Betancourt, T.; Rogelj, S.; Kornienko, A., Exploring Natural Product Chemistry and Biology with Multicomponent Reactions. 5. Discovery of a Novel Tubulin-Targeting Scaffold Derived from the Rigidin Family of Marine Alkaloids. *J Med Chem* **2013**, *56* (17), 6886-6900.
62. Scott, R.; Karki, M.; Reisenauer, M. R.; Rodrigues, R.; Dasari, R.; Smith, W. R.; Pelly, S. C.; van Otterlo, W. A. L.; Shuster, C. B.; Rogelj, S.; Magedov, I. V.; Frolova, L. V.; Kornienko, A., Synthetic and Biological Studies of Tubulin Targeting C₂-Substituted 7-Deazahypoxanthines Derived from Marine Alkaloid Rigidins. *ChemMedChem* **2014**, *9* (7), 1428-1435.
63. Han, J. Investigation of pyrrolo- and furopyrimidines as epidermal growth factor receptor tyrosine kinase inhibitors - Synthesis and activity-ADME profile. Doktorgrad, Norges teknisk-naturvitenskapelige universitet, 2016.
64. Guagnano, V.; Furet, P.; Spanka, C.; Bordas, V.; Le Douget, M.; Stamm, C.; Brueggen, J.; Jensen, M. R.; Schnell, C.; Schmid, H.; Wartmann, M.; Berghausen, J.; Druce, P.; Zimmerlin, A.; Bussiere, D.; Murray, J.; Graus Porta, D., Discovery of 3-(2,6-dichloro-3,5-dimethoxy-phenyl)-1-{6-[4-(4-ethyl-piperazin-1-yl)-phenylamino]-pyrimidin-4-yl}-1-methyl-urea (NVP-BGJ398), a potent and selective inhibitor of the fibroblast growth factor receptor family of receptor tyrosine kinase. *J Med Chem* **2011**, *54* (20), 7066-7083.
65. Latli, B.; Jones, P.-J.; Krishnamurthy, D.; Senanayake, C. H., Synthesis of [¹⁴C]-, [¹³C_{4]-, and [¹³C₄, ¹⁵N₂]- 5-amino-4-iodopyrimidine. *J Label Comp Radiopharmaceut* **2008**, *51* (1), 54-58.}
66. Prieur, V.; Rubio-Martínez, J.; Font-Bardia, M.; Guillaumet, G.; Pujol, M. D., Microwave-Assisted Synthesis of Substituted Pyrrolo[2,3-d]pyrimidines. *Eur J Org Chem* **2014**, *2014* (7), 1514-1524.

REFERENCES

67. Qin, J.; Rao, A.; Chen, X.; Zhu, X.; Liu, Z.; Huang, X.; Degrado, S.; Huang, Y.; Xiao, D.; Aslanian, R.; Cheewatrakoolpong, B.; Zhang, H.; Greenfeder, S.; Farley, C.; Cook, J.; Kurowski, S.; Li, Q.; van Heek, M.; Chintala, M.; Wang, G.; Hsieh, Y.; Li, F.; Palani, A., Discovery of a potent nicotinic Acid receptor agonist for the treatment of dyslipidemia. *ACS Med Chem Lett* **2011**, 2 (2), 171-176.
68. Rodriguez, A. L.; Koradin, C.; Dohle, W.; Knochel, P., Versatile Indole Synthesis by a 5-endo-dig Cyclization Mediated by Potassium or Cesium Bases. *Angew Chem Int Ed* **2000**, 39 (14), 2488-2490.
69. Steffan, G. Patent EP697406A1. 1996.
70. Xi, N.; Wang, L.; Wang, T.; Wu, W. Alkynyl compounds and methods of use. WO2015175579A1. 2015.
71. Zhan, W.; Li, D.; Che, J.; Zhang, L.; Yang, B.; Hu, Y.; Liu, T.; Dong, X., Integrating docking scores, interaction profiles and molecular descriptors to improve the accuracy of molecular docking: toward the discovery of novel Akt1 inhibitors. *Eur J Med Chem* **2014**, 75, 11-20.
72. McCarty, R. M.; Somogyi, Á.; Lin, G.; Jacobsen, N. E.; Bandarian, V., The Deazapurine Biosynthetic Pathway Revealed: In Vitro Enzymatic Synthesis of PreQ0 from Guanosine 5'-Triphosphate in Four Steps. *Biochem* **2009**, 48 (18), 3847-3852.
73. Joule, J. A.; Mills, K., *Heterocyclic Chemistry*. 5th ed ed.; Wiley: 2010.
74. Joris, L.; von RaguéSchleyer, P., π -Deficient N-heteroaromatics as proton acceptors in hydrogen-bonding: Infrared spectral shifts vs. pKa's as measures of "basicity". *Tetrahedron* **1968**, 24 (18), 5991-6005.
75. Alí-Torres, J.; Rodríguez-Santiago, L.; Sodupe, M., Computational calculations of pKa values of imidazole in Cu(ii) complexes of biological relevance. *Phys Chem Chem Phys* **2011**, 13 (17), 7852-7861.
76. Chiang, Y.; Whipple, E. B., The Protonation of Pyrroles. *J Am Chem Soc* **1963**, 85 (18), 2763-2767.

REFERENCES

77. Lorenz, U. J.; Lemaire, J.; Maitre, P.; Crestoni, M.-E.; Fornarini, S.; Dopfer, O., Protonation of heterocyclic aromatic molecules: IR signature of the protonation site of furan and pyrrole. *Int J Mass Spectrom* **2007**, *267* (1), 43-53.
78. Kim, K.-H.; Ihm, S.-K., Heterogeneous catalytic wet air oxidation of refractory organic pollutants in industrial wastewaters: A review. *J Hazard Mater* **2011**, *186* (1), 16-34.
79. Khan, M. F., Splenic Toxicology. In *Encyclopedia of environmental health (Second Edition)*, Nriagu, J., Ed. Elsevier: Oxford, 2019; pp 799-804.
80. Hartwig, J. F.; Shekhar, S.; Shen, Q.; Barrios-Landeros, F., Synthesis of Anilines. In *PATAI'S Chemistry of Functional Groups*, 2009; pp 3-8.
81. Gangjee, A.; Kurup, S.; Ihnat, M. A.; Thorpe, J. E.; Shenoy, S. S., Synthesis and biological activity of N(4)-phenylsubstituted-6-(2,4-dichloro phenylmethyl)-7H-pyrrolo[2,3-d]pyrimidine-2,4-diamines as vascular endothelial growth factor receptor-2 inhibitors and antiangiogenic and antitumor agents. *Bioorg Med Chem* **2010**, *18* (10), 3575-3587.
82. Kris, M. G.; Natale, R. B.; Herbst, R. S.; Lynch, T. J., Jr.; Prager, D.; Belani, C. P.; Schiller, J. H.; Kelly, K.; Spiridonidis, H.; Sandler, A.; Albain, K. S.; Cella, D.; Wolf, M. K.; Averbuch, S. D.; Ochs, J. J.; Kay, A. C., Efficacy of gefitinib, an inhibitor of the epidermal growth factor receptor tyrosine kinase, in symptomatic patients with non-small cell lung cancer: a randomized trial. *Jama* **2003**, *290* (16), 2149-2158.
83. Li, D.; Ambrogio, L.; Shimamura, T.; Kubo, S.; Takahashi, M.; Chirieac, L.; Padera, R.; Shapiro, G.; Baum, A.; Himmelsbach, F., BIBW2992, an irreversible EGFR/HER2 inhibitor highly effective in preclinical lung cancer models. *Oncogene* **2008**, *27* (34), 4702-4711.
84. Carter, P.; Presta, L.; Gorman, C. M.; Ridgway, J.; Henner, D.; Wong, W.; Rowland, A. M.; Kotts, C.; Carver, M. E.; Shepard, H. M., Humanization of an anti-p185HER2 antibody for human cancer therapy. *P Natl A Sci* **1992**, *89* (10), 4285-4289.
85. Folkers, E.; Runquist, O., Correlation of base strengths of aliphatic and N-substituted anilines. *J Org Chem* **1964**, *29* (4), 830-832.

REFERENCES

86. Tehan, B. G.; Lloyd, E. J.; Wong, M. G.; Pitt, W. R.; Montana, J. G.; Manallack, D. T.; Gancia, E., Estimation of pKa Using Semiempirical Molecular Orbital Methods. Part 1: Application to Phenols and Carboxylic Acids. *Quant Struct-Act Rel* **2002**, *21* (5), 457-472.
87. Gross, K. C.; Seybold, P. G.; Peralta-Inga, Z.; Murray, J. S.; Politzer, P., Comparison of Quantum Chemical Parameters and Hammett Constants in Correlating pKa Values of Substituted Anilines. *J Org Chem* **2001**, *66* (21), 6919-6925.
88. Hansch, C.; Leo, A. J.; Taft, R. W., A survey of Hammett substituent constants and resonance and field parameters. *Chem Rev* **1991**, *91*, 165-195.
89. Haynes, W.; Bruno, T.; Lide, D., Dissociation constants of organic acids and bases. *CRC handbook of chemistry and physics, 95th edn. CRC Press, Boca Raton* **2014**, 5-94.
90. Rossini, E.; Bochevarov, A. D.; Knapp, E. W., Empirical Conversion of pKa Values between Different Solvents and Interpretation of the Parameters: Application to Water, Acetonitrile, Dimethyl Sulfoxide, and Methanol. *ACS Omega* **2018**, *3* (2), 1653-1662.
91. Bunnett, J. F.; Zahler, R. E., Aromatic Nucleophilic Substitution Reactions. *Chem Rev* **1951**, *49* (2), 273-412.
92. Heaney, H., The Benzyne and Related Intermediates. *Chem Rev* **1962**, *62* (2), 81-97.
93. Kadam, H. K.; Tilve, S. G., Advancement in methodologies for reduction of nitroarenes. *RSC Advances* **2015**, *5* (101), 83391-83407.
94. Roughley, S. D.; Jordan, A. M., The Medicinal Chemist's Toolbox: An Analysis of Reactions Used in the Pursuit of Drug Candidates. *J Med Chem* **2011**, *54* (10), 3451-3479.
95. Małkosza, M., Electrophilic and nucleophilic aromatic substitution: Analogous and complementary processes. *Russ Chem B+* **1996**, *45* (3), 491-504.
96. Senger, N. A.; Bo, B.; Cheng, Q.; Keeffe, J. R.; Gronert, S.; Wu, W., The element effect revisited: factors determining leaving group ability in activated nucleophilic aromatic substitution reactions. *J Org Chem* **2012**, *77* (21), 9535-9540.
97. Fernández, I.; Frenking, G.; Uggerud, E., Rate-Determining Factors in Nucleophilic Aromatic Substitution Reactions. *J Org Chem* **2010**, *75* (9), 2971-2980.

REFERENCES

98. Carey, F. A.; Sundberg, R. J., *Advanced Organic Chemistry Part B: Reactions and Synthesis*. 5th ed. ed.; Springer: Virginia, 2007.
99. Gilchrist, T. L., *Heterocyclic Chemistry*. 3 ed.; Longman: Essex, England, 1997.
100. El Guesmi, N.; Berionni, G.; Asghar, B. H., Electronic and solvent effects on kinetics of S(N)Ar substitution reactions of substituted anilines with 2,6-bis(trifluoromethanesulfonyl)-4-nitroanisole in MeOH-Me(2)SO mixtures of varying composition: one reaction with two mechanistic pathways. *Monatsh Chem* **2013**, *144* (10), 1537-1545.
101. Edwards, J. O.; Pearson, R. G., The Factors Determining Nucleophilic Reactivities. *J Am Chem Soc* **1962**, *84* (1), 16-24.
102. Bunnett, J.; Garbisch Jr, E. W.; Pruitt, K. M., The "element effect" as a criterion of mechanism in activated aromatic nucleophilic substitution reactions 1, 2. *J Am Chem Soc* **1957**, *79* (2), 385-391.
103. Guo, C.; Dong, L.; Marakovits, J.; Kephart, S., A novel method to enable S_NAr reaction of aminopyrrolopyrazoles. *Tetrahedron Lett* **2011**, *52* (14), 1692-1696.
104. Abou-Shehada, S.; Teasdale, M. C.; Bull, S. D.; Wade, C. E.; Williams, J. M. J., Lewis Acid Activation of Pyridines for Nucleophilic Aromatic Substitution and Conjugate Addition. *ChemSusChem* **2015**, *8* (6), 1083-1087.
105. Goldberg, I., Ueber phenylirungen bei gegenwart von kupfer als katalysator. *Ber Deut Chem Ges* **1906**, *39* (2), 1691-1692.
106. Ullmann, F., Ueber eine neue Bildungsweise von Diphenylaminderivaten. *Ber Dtsch Chem Ges* **1903**, *36* (2), 2382-2384.
107. Dorel, R.; Grugel, C. P.; Haydl, A. M., The Buchwald–Hartwig Amination After 25 Years. *Angew Chem Int Edit* **2019**, *58* (48), 17118-17129.
108. Masanori, K.; Masayuki, K.; Toshihiko, M., Palladium-Catalyzed Aromatic Amination of Aryl Bromides with N,N-diethylaminotributyltin. *Chem Lett* **1983**, *12* (6), 927-928.
109. Guram, A. S.; Buchwald, S. L., Palladium-Catalyzed Aromatic Aminations with in situ Generated Aminostannanes. *J Am Chem Soc* **1994**, *116* (17), 7901-7902.

REFERENCES

110. Louie, J.; Hartwig, J. F., Palladium-catalyzed synthesis of arylamines from aryl halides. Mechanistic studies lead to coupling in the absence of tin reagents. *Tetrahedron Lett* **1995**, *36* (21), 3609-3612.
111. Guram, A. S.; Rennels, R. A.; Buchwald, S. L., A Simple Catalytic Method for the Conversion of Aryl Bromides to Arylamines. *Angew Chem Int Edit* **1995**, *34* (12), 1348-1350.
112. Hegedus, L. S.; Söderberg, B. C. G., *Transition Metals in the Synthesis of Complex Organic Molecules*. 3 ed.; University Science Books: 2010.
113. Birkholz, M.-N.; Freixa, Z.; van Leeuwen, P. W. N. M., Bite angle effects of diphosphines in C–C and C–X bond forming cross coupling reactions. *Chem Soc Rev* **2009**, *38* (4), 1099-1118.
114. Zimina, A. M.; Somov, N. V.; Malysheva, Y. B.; Knyazeva, N. A.; Piskunov, A. V.; Grishin, I. D., 12-Vertex closo-3,1,2-Ruthenadecaboranes with Chelate POP-Ligands: Synthesis, X-ray Study and Electrochemical Properties. *Inorganics* **2022**, *10* (11), 206-211.
115. Zheng, D.-Z.; Xiong, H.-G.; Song, A. X.; Yao, H.-G.; Xu, C., Buchwald–Hartwig amination of aryl esters and chlorides catalyzed by the dianisole-decorated Pd–NHC complex. *Org Biomol Chem* **2022**, *20* (10), 2096-2101.
116. Bezençon, J.; Wittwer, M. B.; Cutting, B.; Smieško, M.; Wagner, B.; Kansy, M.; Ernst, B., pKa determination by ¹H NMR spectroscopy – An old methodology revisited. *J Pharmaceut Biomed* **2014**, *93*, 147-155.
117. Stoyanov, E. S.; Kim, K.-C.; Reed, C. A., The Nature of the H₃O⁺ Hydronium Ion in Benzene and Chlorinated Hydrocarbon Solvents. Conditions of Existence and Reinterpretation of Infrared Data. *J Am Chem Soc* **2006**, *128* (6), 1948-1958.
118. Andersen, J. M.; Starbuck, H. F., Rate and Yield Enhancements in Nucleophilic Aromatic Substitution Reactions via Mechanochemistry. *J Org Chem* **2021**, *86* (20), 13983-13989.
119. Weston, R. E.; Ehrenson, S.; Heinzinger, K., Basicities of methanol and 2-propanol as determined by Raman spectrophotometry. *J Am Chem Soc* **1967**, *89* (3), 481-486.

REFERENCES

120. Kalbassi, M.; Biddulph, M., Surface tensions of mixtures at their boiling points. *J Chem Eng Data* **1988**, *33* (4), 473-476.
121. Kevill, D. N.; Lin, G. M. L., Solvent nucleophilicity. A scale based on triethyloxonium ion solvolysis. *J Am Chem Soc* **1979**, *101* (14), 3916-3919.
122. Minegishi, S.; Kobayashi, S.; Mayr, H., Solvent Nucleophilicity. *J Am Chem Soc* **2004**, *126* (16), 5174-5181.
123. Jamali-Paghaleh, J.; Harifi-Mood, A. R.; Gholami, M. R., Reaction kinetics investigation of 1-fluoro-2, 4-dinitrobenzene with substituted anilines in ethyl acetate–methanol mixtures using linear and nonlinear free energy relationships. *J Phys Org Chem* **2011**, *24* (11), 1095-1100.
124. Padró, J. A.; Saiz, L.; Guàrdia, E., Hydrogen bonding in liquid alcohols: a computer simulation study. *J Mol Struct* **1997**, *416* (1), 243-248.
125. Aida, T.; Aizawa, T.; Kanakubo, M.; Nanjo, H., Relation between Volume Expansion and Hydrogen Bond Networks for CO₂–Alcohol Mixtures at 40 °C. *J Phys Chem B* **2010**, *114* (43), 13628-13636.
126. Hardouin, C.; Lemaitre, S., Safety Case Study. Intrinsic Instability of Concentrated Solutions of Alcoholic Hydrogen Chloride: Potential Hazards Associated with Methanol. *Org Proc Res Dev* **2020**, *24* (5), 867-871.
127. Laidler, K. J., The development of the Arrhenius equation. *J Chem Educ* **1984**, *61* (6), 494-506.
128. Thutewohl, M.; Schirok, H.; Bennabi, S.; Figueroa-Pérez, S., Synthesis of 4-Substituted 7-Azaindole Derivatives via Pd-Catalyzed C-N and C-O Coupling. *Synthesis* **2006**, *2006* (04), 629-632.
129. Wentrup, C.; Mirzaei, M. S.; Kvaskoff, D.; Taherpour, A. A., When a “Dimroth Rearrangement” Is Not a Dimroth Rearrangement. *J Org Chem* **2021**, *86* (12), 8286-8294.
130. Bartoli, G.; Todesco, P.; Ciminale, F.; Fiorentino, M., Electronic and steric effects in nucleophilic aromatic substitution. Kinetic studies on the reactions between ethers and thioethers of 2, 4-dinitrophenol and nucleophiles. *J Org Chem* **1975**, *40* (25), 3777-3778.

REFERENCES

131. Ouellette, R. J.; Rawn, J. D., Nucleophilic Substitution and Elimination Reactions. In *Organic Chemistry Study Guide*, Ouellette, R. J.; Rawn, J. D., Eds. Elsevier: Boston, 2015; pp 169-182.
132. Guo, W.; Martínez-Rodríguez, L.; Martin, E.; Escudero-Adán, E. C.; Kleij, A. W., Highly Efficient Catalytic Formation of (Z)-1,4-But-2-ene Diols Using Water as a Nucleophile. *Angew Chem Int Ed* **2016**, *55* (37), 11037-11040.
133. Henderson Jr, W. A.; Buckler, S. A., The nucleophilicity of phosphines. *J Am Chem Soc* **1960**, *82* (22), 5794-5800.
134. Smith, P. J.; Noble, L. M., A Primary Hydrogen-Deuterium Isotope Effect Study on the Carbonyl Elimination Reaction of 9-Fluorenyl Nitrate with Various Bases. *Canadian J Chem* **1975**, *53* (2), 263-268.
135. Juranic, I., Simple Method for the Estimation of pKa of Amines. *Croatica Chemica Acta* **2014**, *87*, 343-347.
136. Information, N. C. f. B. PubChem Bioassay Record for Bioactivity AID 781327 - SID 103179146 Source: ChEMBL. <https://pubchem.ncbi.nlm.nih.gov/bioassay/781327#sid=103179146> (accessed June 27, 2023).
137. Nozal, V.; Martínez-González, L.; Gomez-Almeria, M.; Gonzalo-Consuegra, C.; Santana, P.; Chaikuad, A.; Pérez-Cuevas, E.; Knapp, S.; Lietha, D.; Ramírez, D.; Petralla, S.; Monti, B.; Gil, C.; Martín-Requero, A.; Palomo, V.; de Lago, E.; Martinez, A., TDP-43 Modulation by Tau-Tubulin Kinase 1 Inhibitors: A New Avenue for Future Amyotrophic Lateral Sclerosis Therapy. *J Med Chem* **2022**, *65* (2), 1585-1607.
138. Silverstein, R. M.; Webster, F. X.; Kiemle, D. J.; Bryce, D. L., *Spectrometric Identification of Organic Compounds*. 8th ed. ed.; Wiley: 2015.

APPENDICES

A Spectroscopic data – Compound 28

Parameter	Value
1 Data File Name	/Volumes/nmrdata/nmr400ny/hammsm/nmr/HS1-7-8/1/fid
2 Title	HS1-7-8.1.fid
3 Comment	
4 Origin	Bruker BioSpin GmbH
5 Owner	nmrsu
6 Site	spect
7 Instrument	DMSO
8 Author	298.4
9 Solvent	zg30
10 Temperature	ID
11 Pulse Sequence	Z116098_0398 (PA BBO 400S1 BBF-H-D-05 Z.SP)
12 Experiment	8
13 Probe	143.5
14 Number of Scans	1.0000
15 Receiver Gain	9.5000
16 Relaxation Delay	
17 Pulse Width	
18 Presaturation Frequency	
19 Acquisition Time	4.0894
20 Acquisition Date	2022-09-14T14:36:36
21 Modification Date	2022-09-14T14:36:36
22 Class	
23 Spectrometer Frequency	400.13
24 Spectral Width	8012.8
25 Lowest Frequency	-1535.4
26 Nucleus	¹ H
27 Acquired Size	32768
28 Spectral Size	65536
29 Digital Resolution	0.12

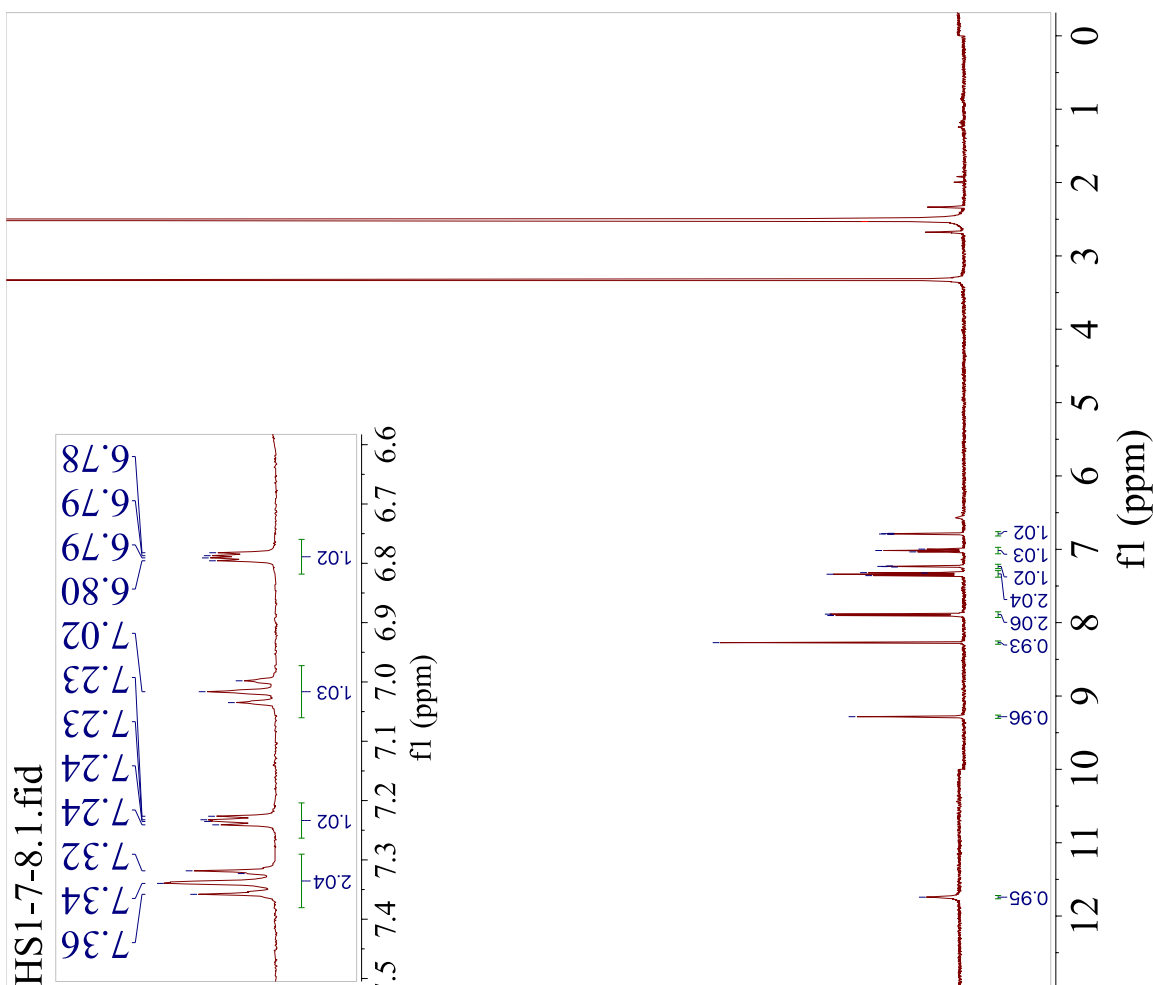
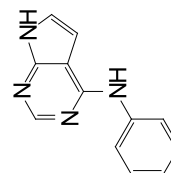


Figure A.1: ¹H-NMR of compound 28.

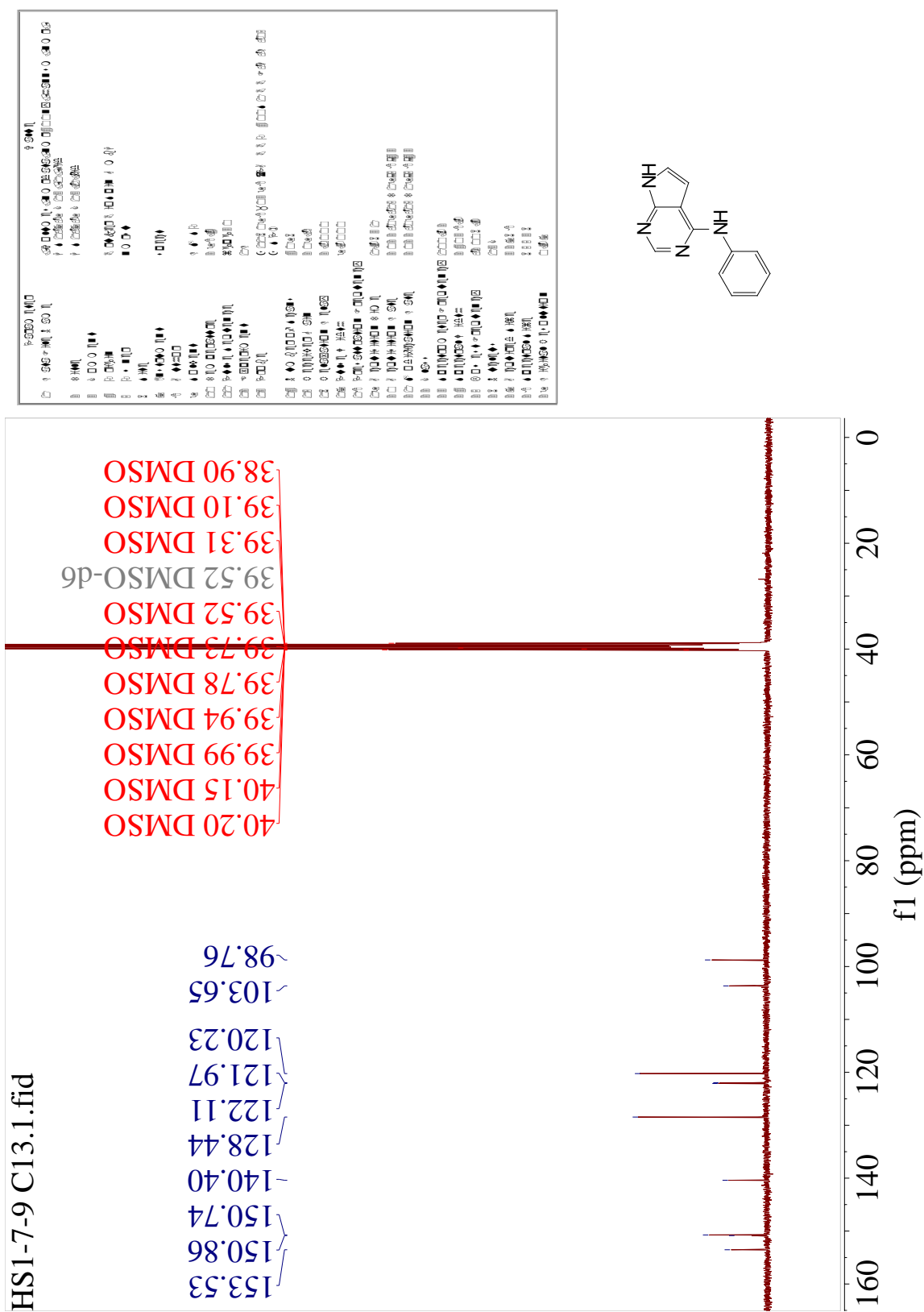


Figure A.2: ¹³C-NMR of compound 28.

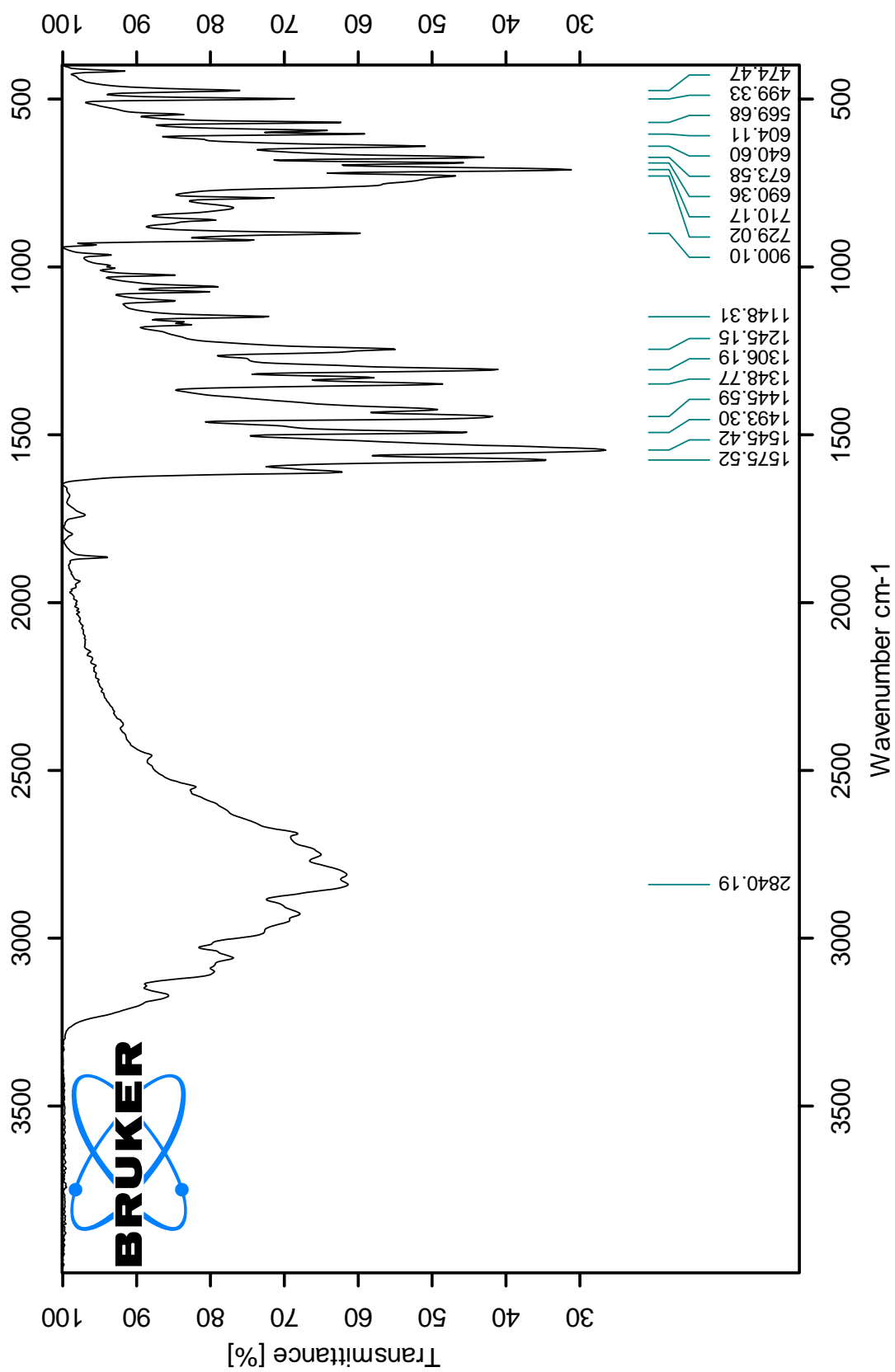


Figure A.3: IR spectrum of compound 28.

Elemental Composition Report

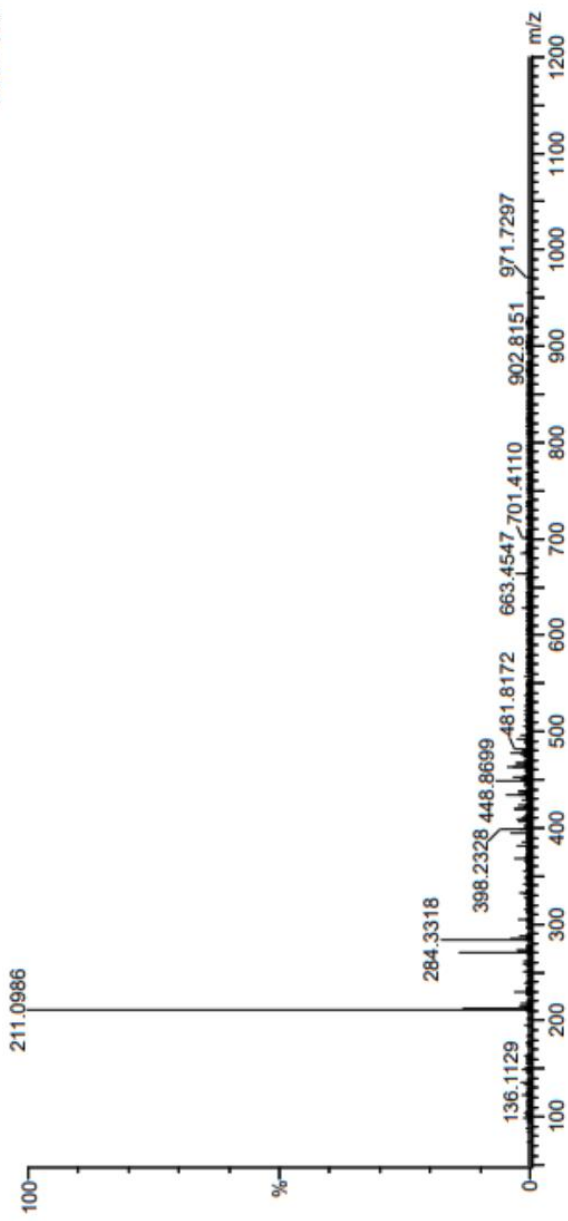
Single Mass Analysis

Tolerance = 5.0 PPM / DBE: min = -1.5, max = 50.0
 Element prediction: Off
 Number of isotope peaks used for i-FIT = 3

Monoisotopic Mass, Even Electron Ions
 184 formula(e) evaluated with 1 results within limits (up to 50 closest results for each mass)
 Elements Used:

C: 0-500 H: 1-1000 N: 0-7 O: 0-20
 recID:1935 137 (1.543)AM2 (Ar,350000.0,0.00,0.00); Cm (133:137)
 1: TOF MS ES+

3.13e+006



Mass	Calc. Mass	mDa	PPM	DBE	i-FIT	Norm	Conf(%)	Formula
211.0986	211.0984	0.2	0.9	9.5	1723.6	n/a	n/a	C12 H11 N4
Minimum:				-1.5				
Maximum:				50.0				

Figure A.4: MS spectrum of compound 28.

B Spectroscopic data – Compound 29

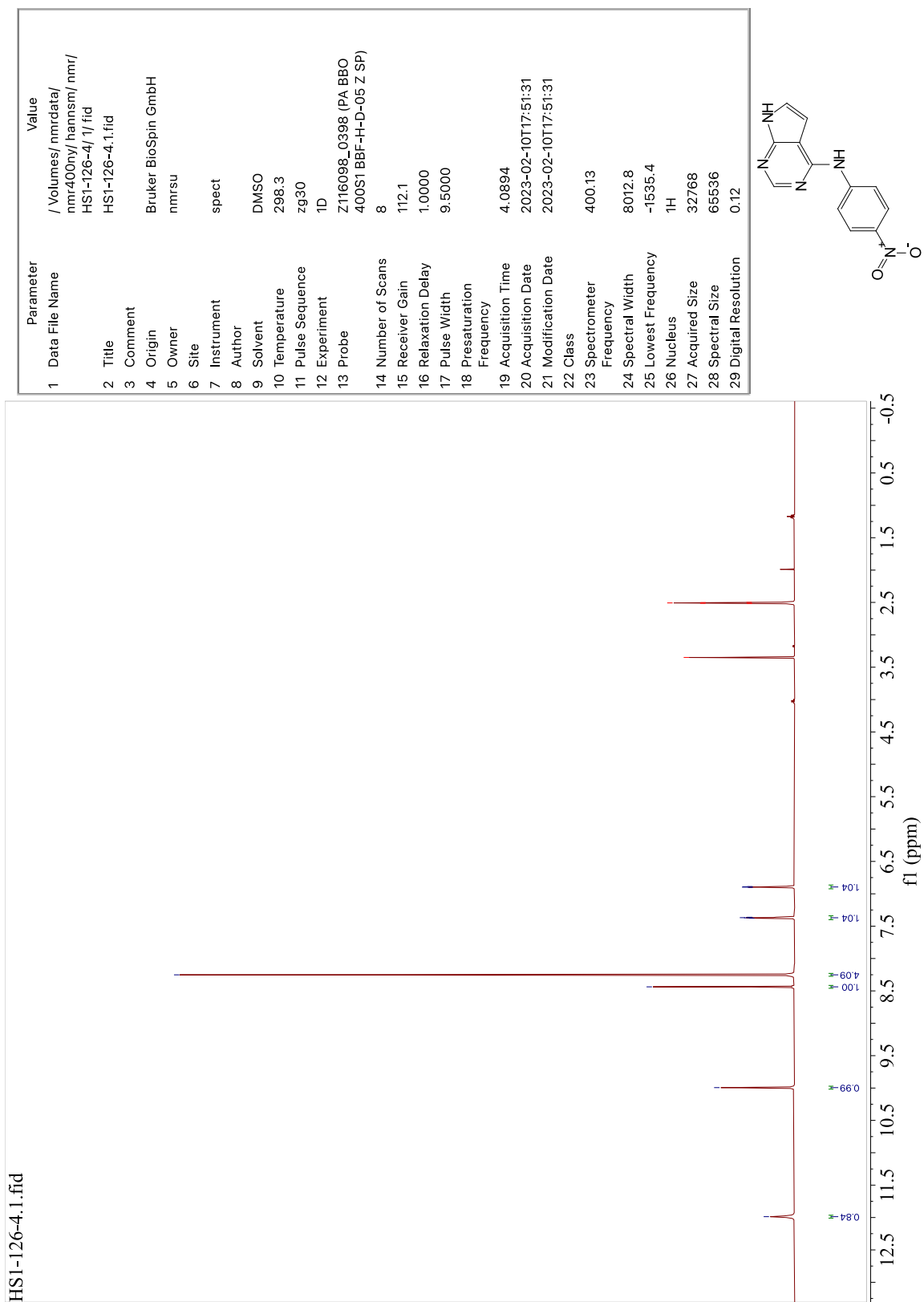


Figure B.1: ¹H-NMR spectrum of compound 29.

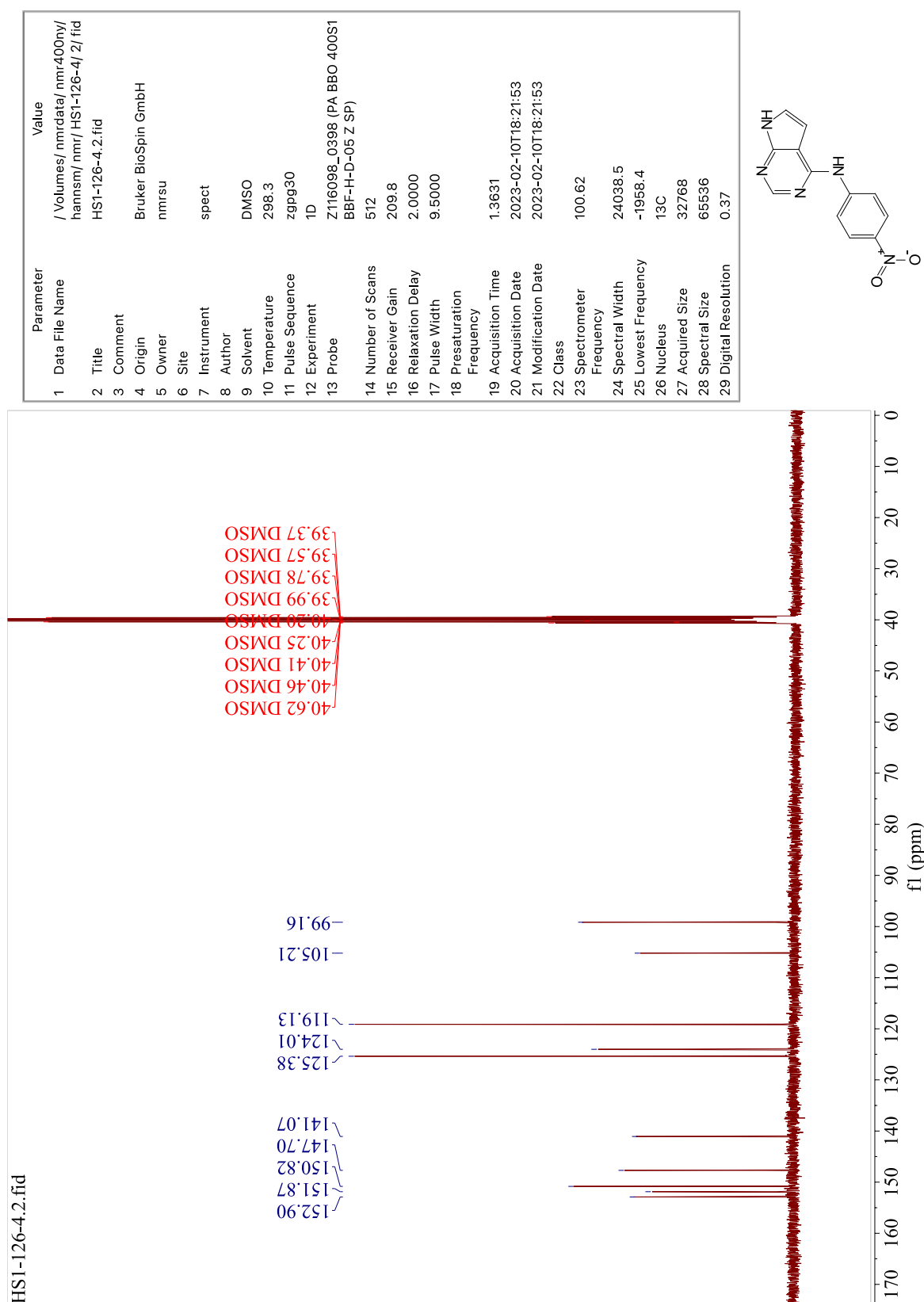


Figure B.2: ¹³C-NMR spectrum of compound 29.

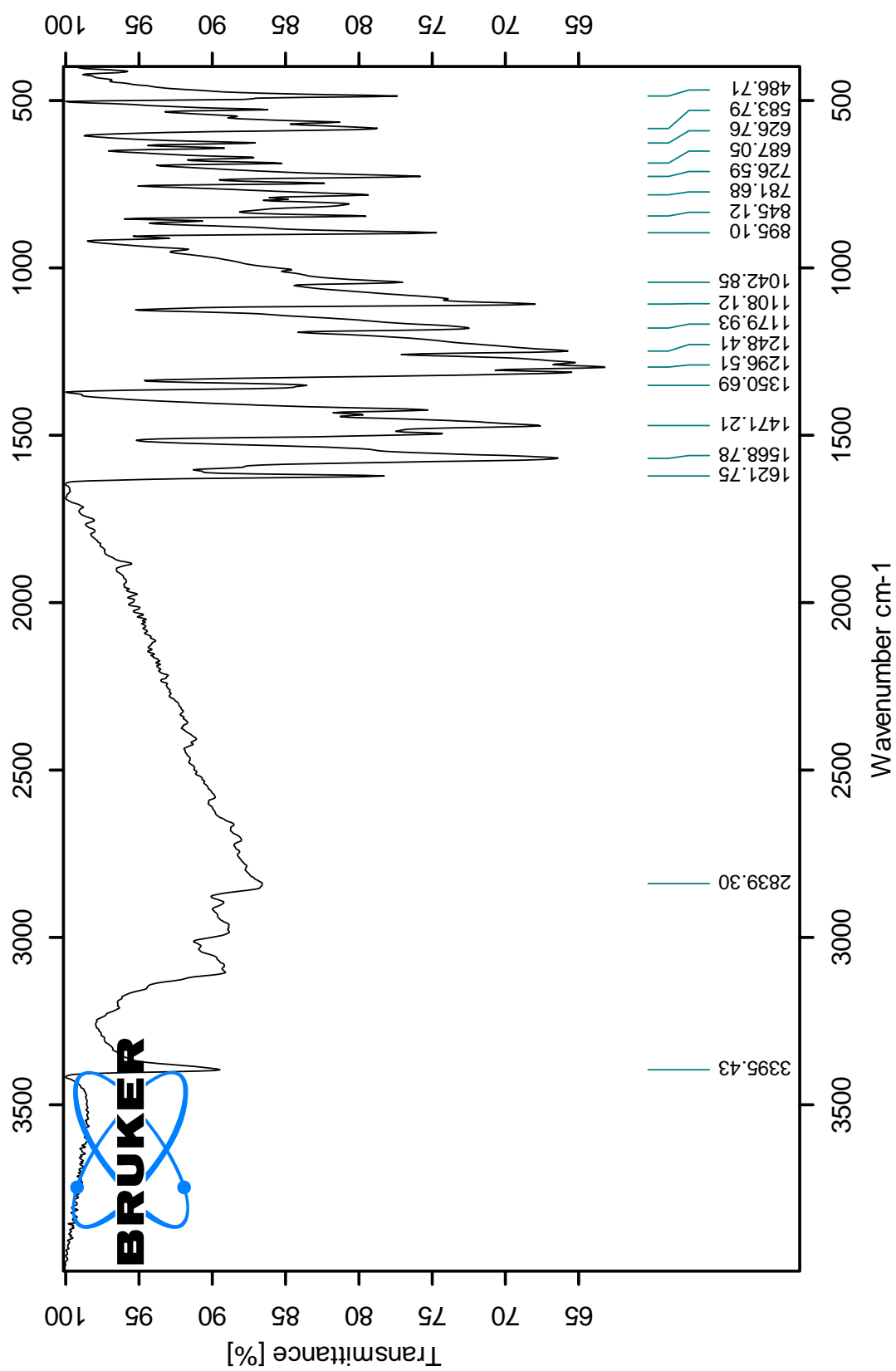


Figure B.3: IR spectrum of compound 29.

Elemental Composition Report

Single Mass Analysis

Tolerance = 5.0 PPM / DBE: min = -1.5, max = 50.0
 Element prediction: Off
 Number of isotope peaks used for i-FIT = 3

Monoisotopic Mass, Even Electron Ions
 183 formula(e) evaluated with 1 results within limits (up to 50 closest results for each mass)
 Elements Used:
 C: 0-60 H: 1-1000 N: 0-8 O: 0-6
 RECID: 2152109 (1.030) AMZ (Ar: 35000.0, 0.00, 0.00); Cm (106:109)
 1: TOF MS ES+

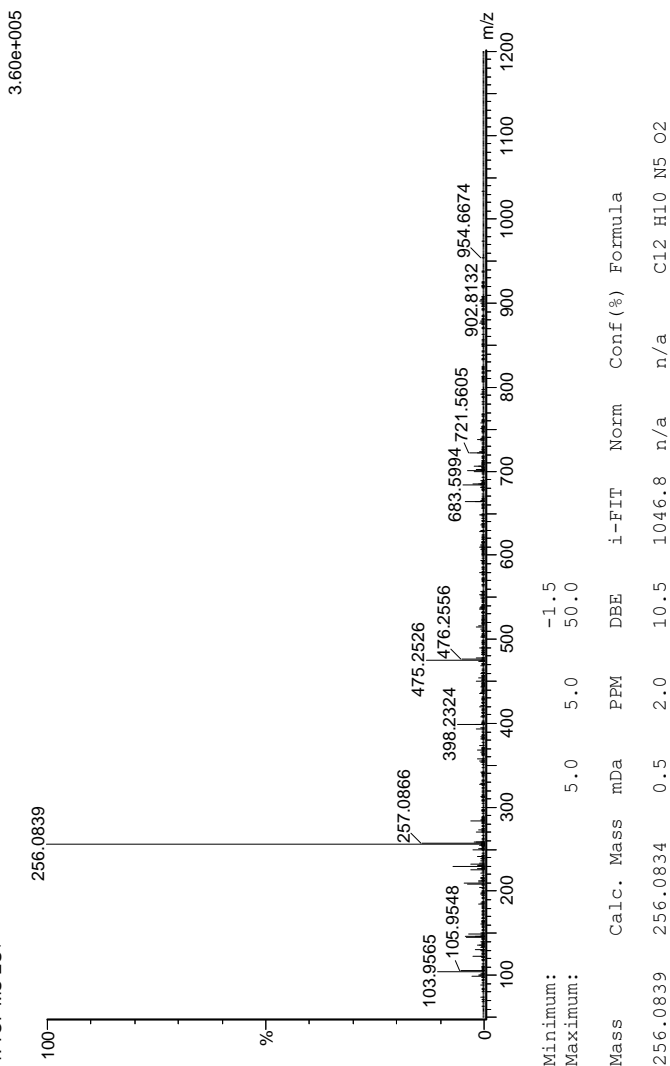


Figure B.4: MS spectrum of compound 29.

C Spectroscopic data – Compound 32

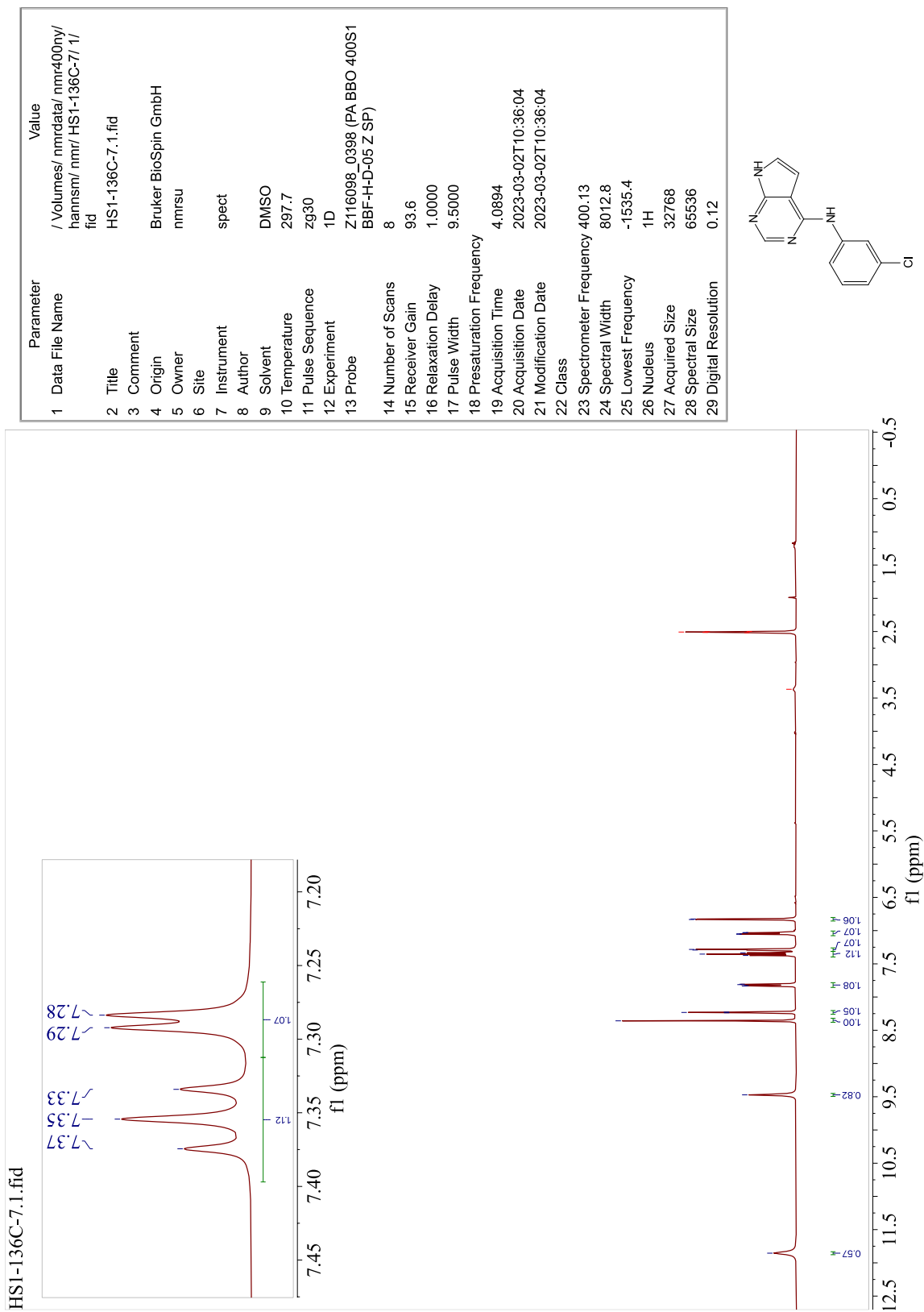
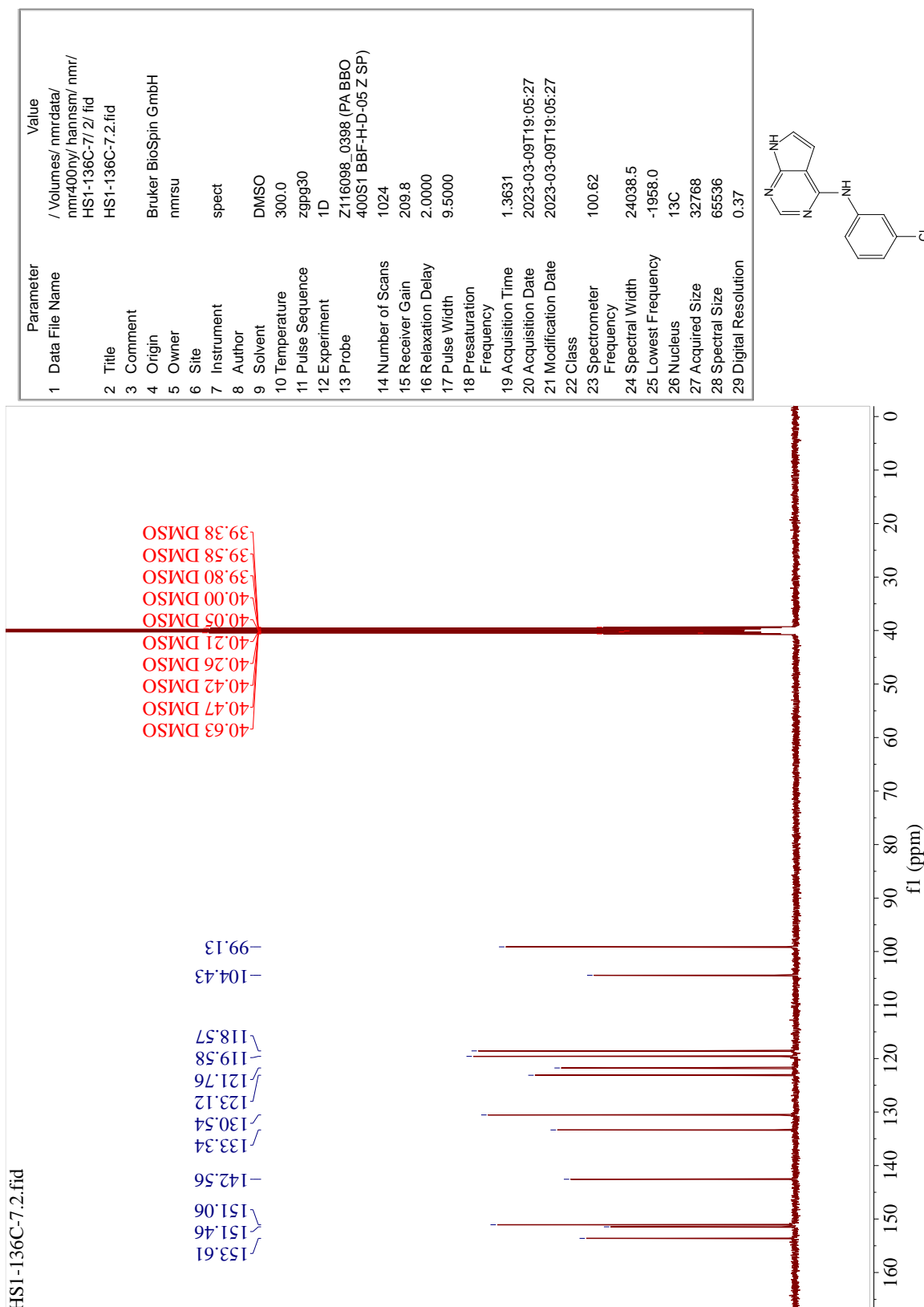


Figure C.1: ¹H-NMR spectrum of compound 32.

Figure C.2: ¹³C-NMR spectrum of compound 32.

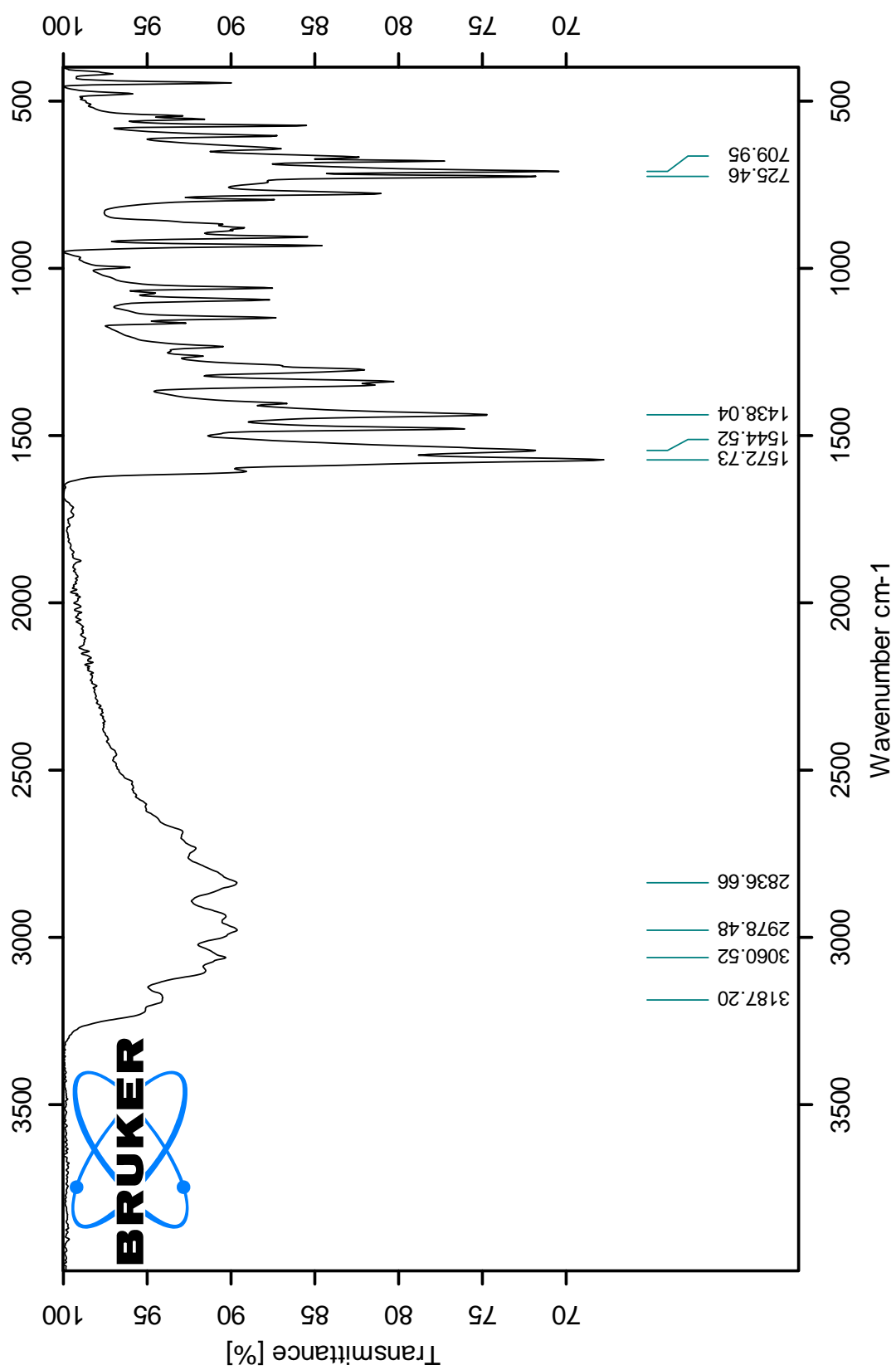


Figure C.3: IR spectrum of compound 32.

D Spectroscopic data – Compound 33

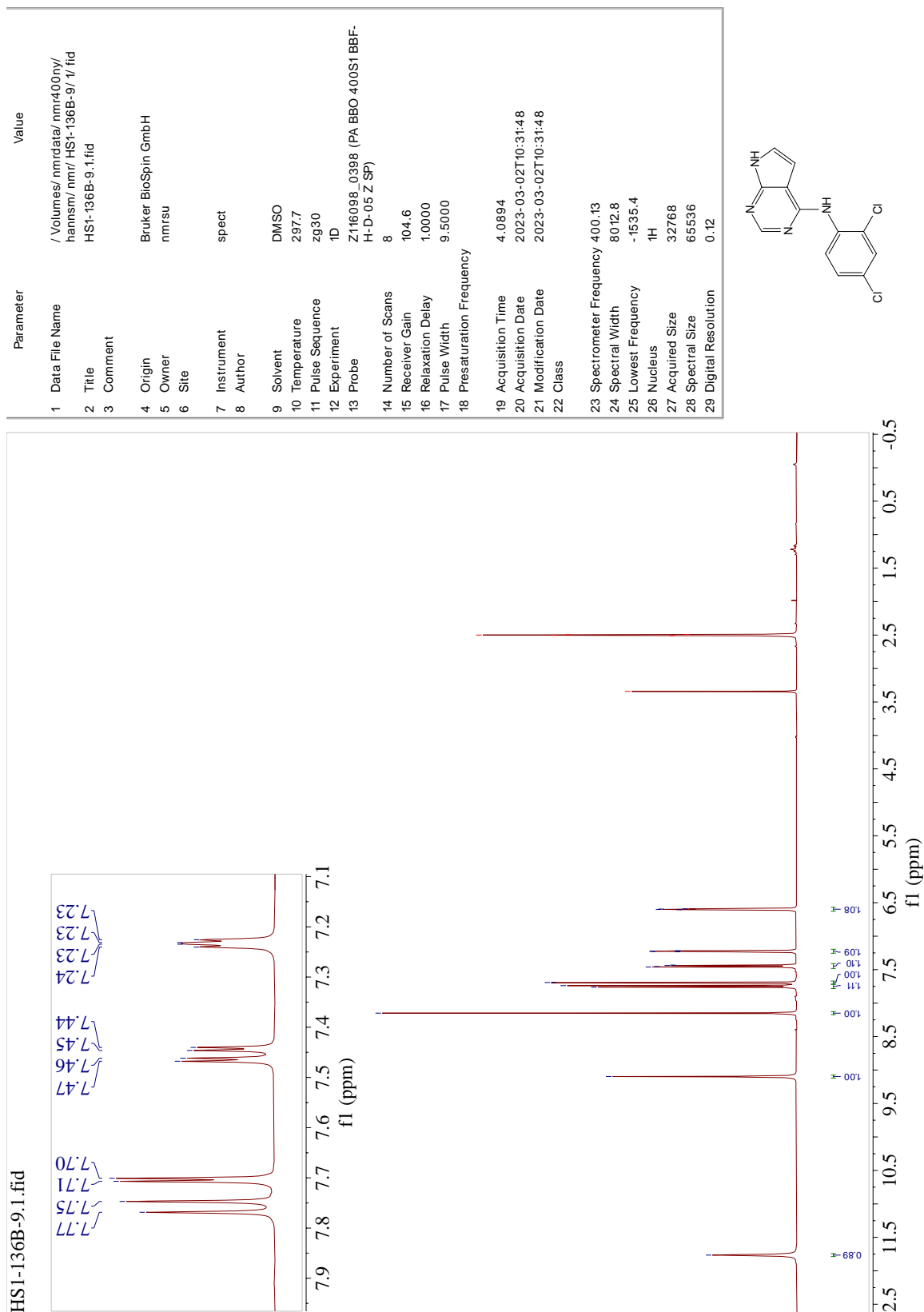


Figure D.1: ¹H-NMR spectrum of compound 33.

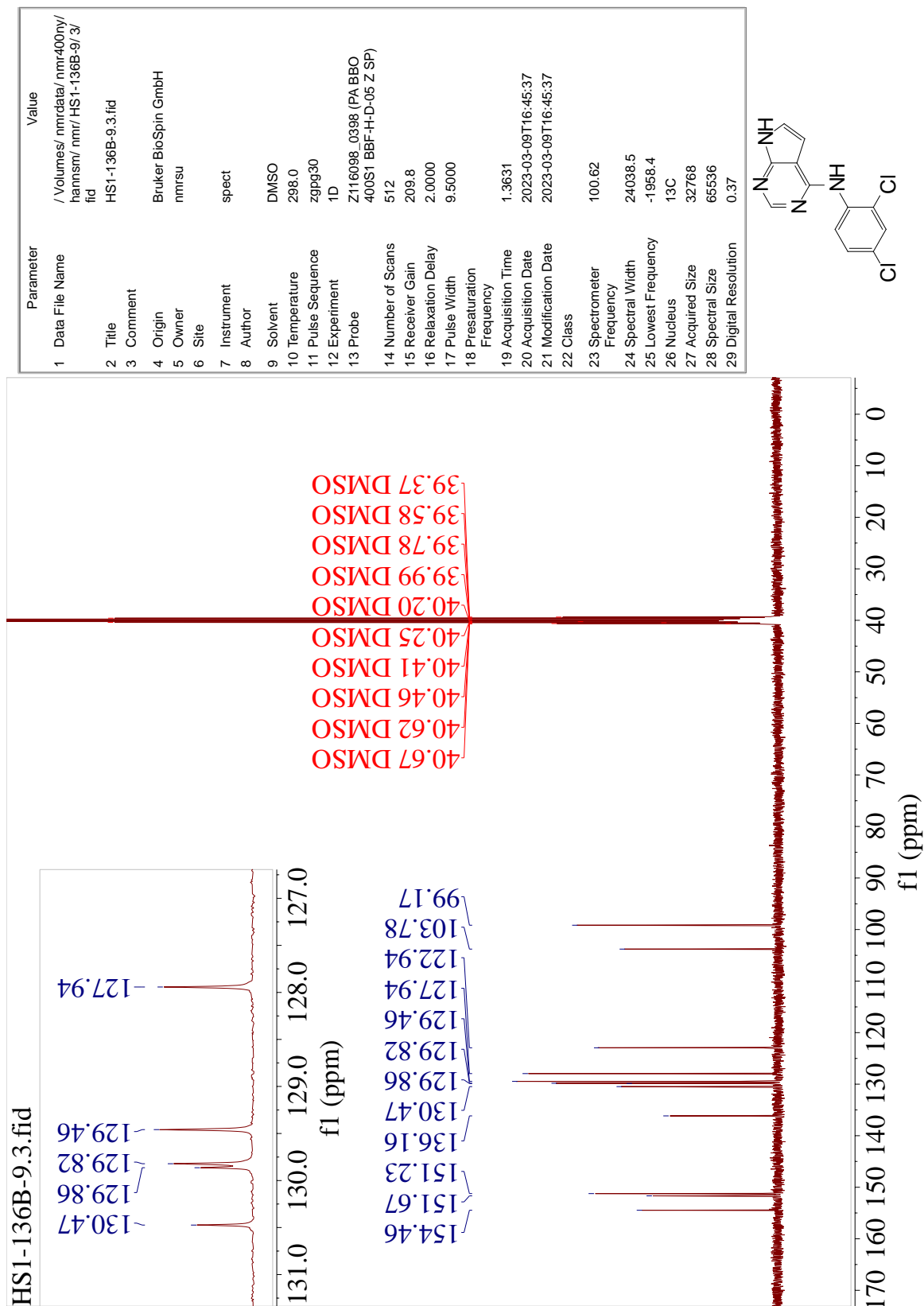


Figure D.2: ¹³C-NMR spectrum of compound 33.

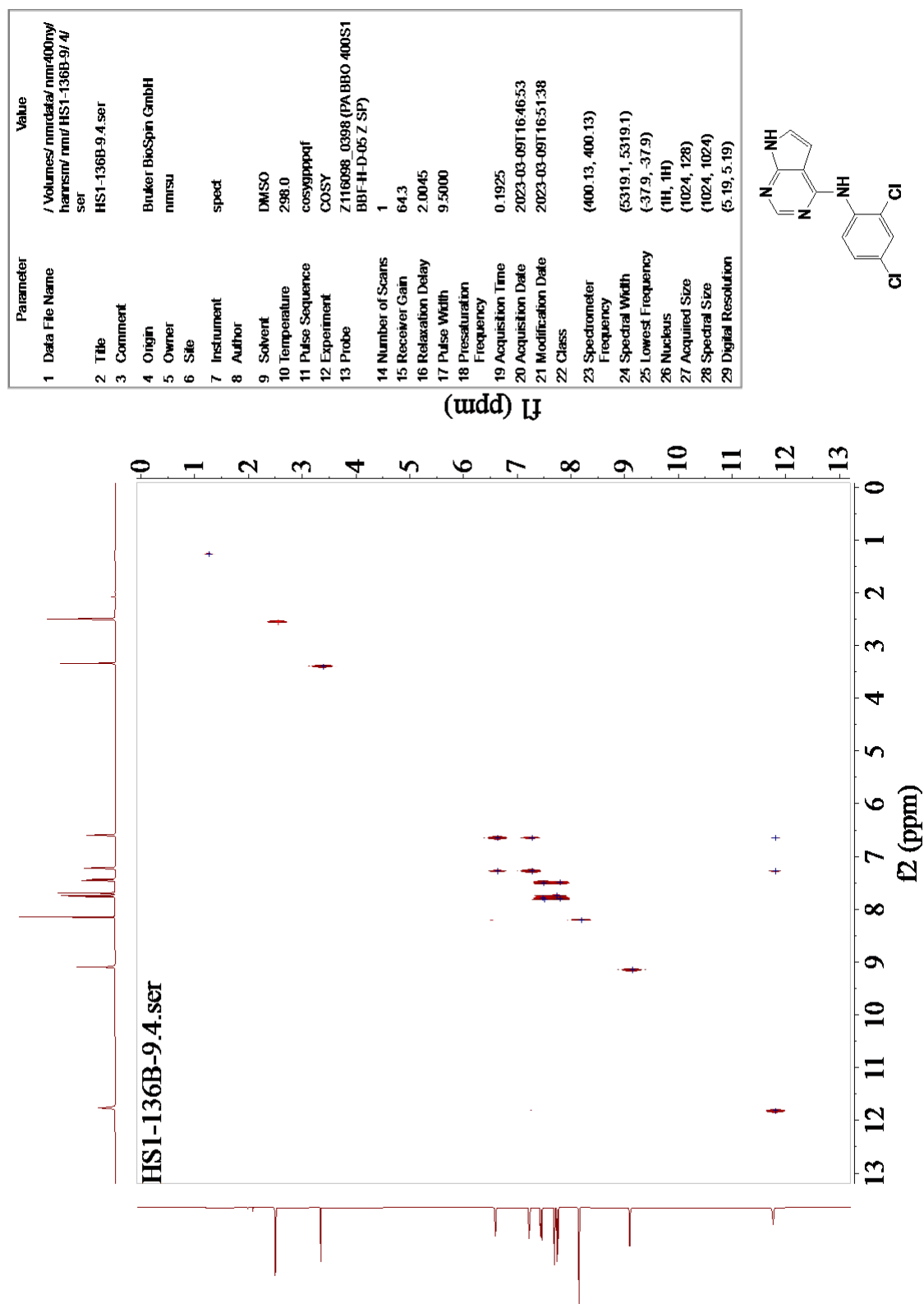


Figure D.3: COSY spectrum of compound 33.

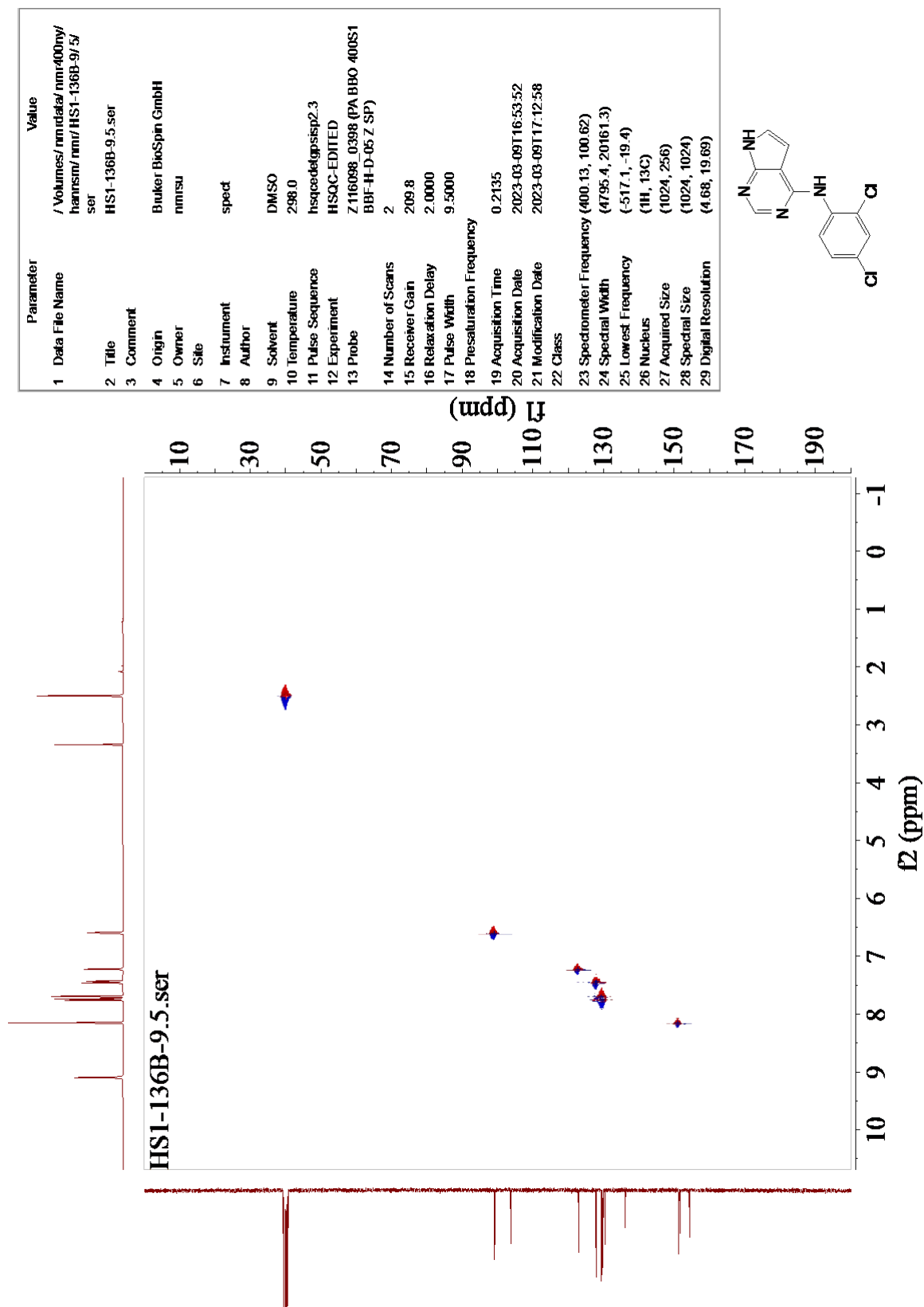


Figure D.4: HSQC spectrum of compound 33.

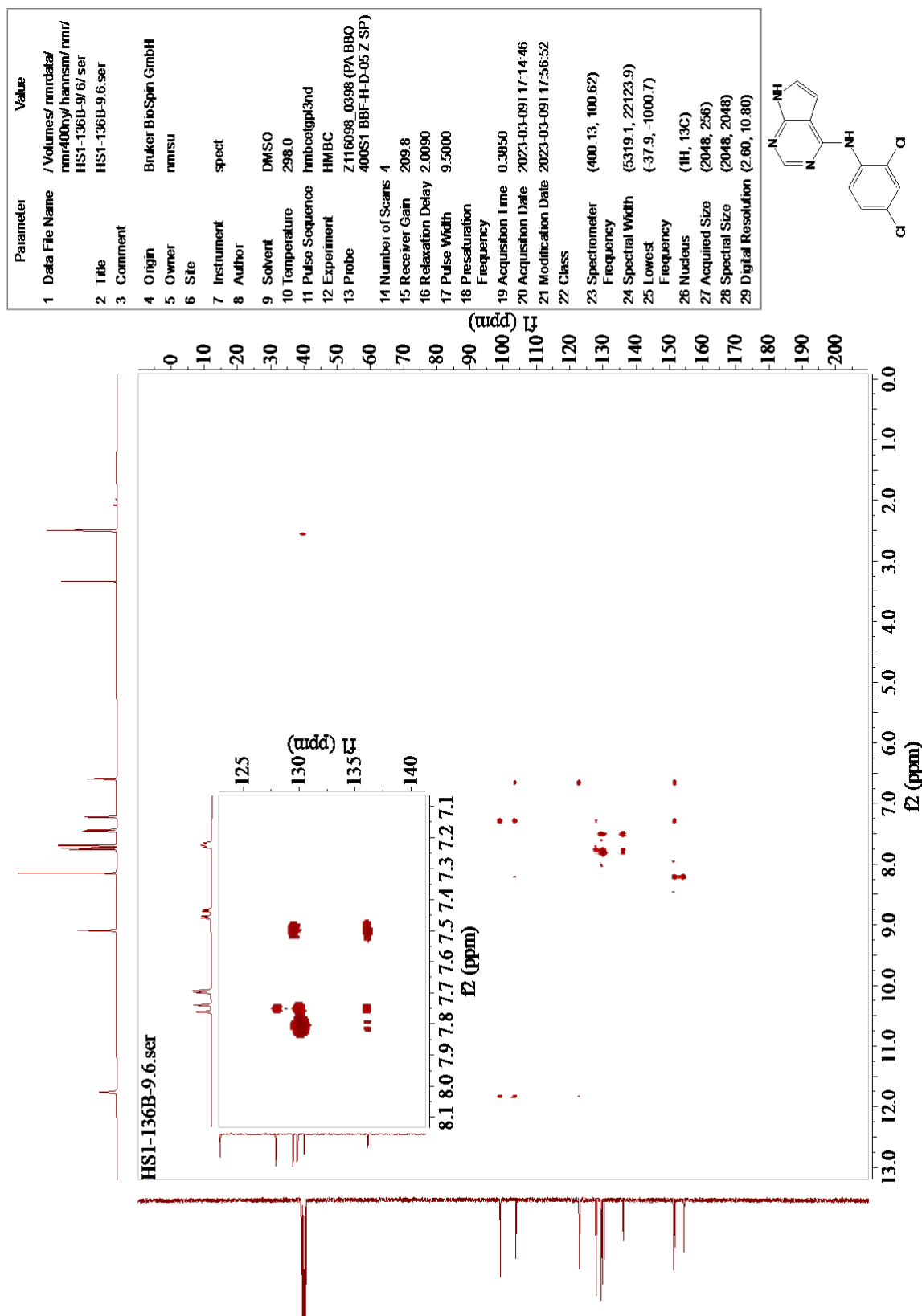


Figure D.5: HMBC spectrum of compound 33.

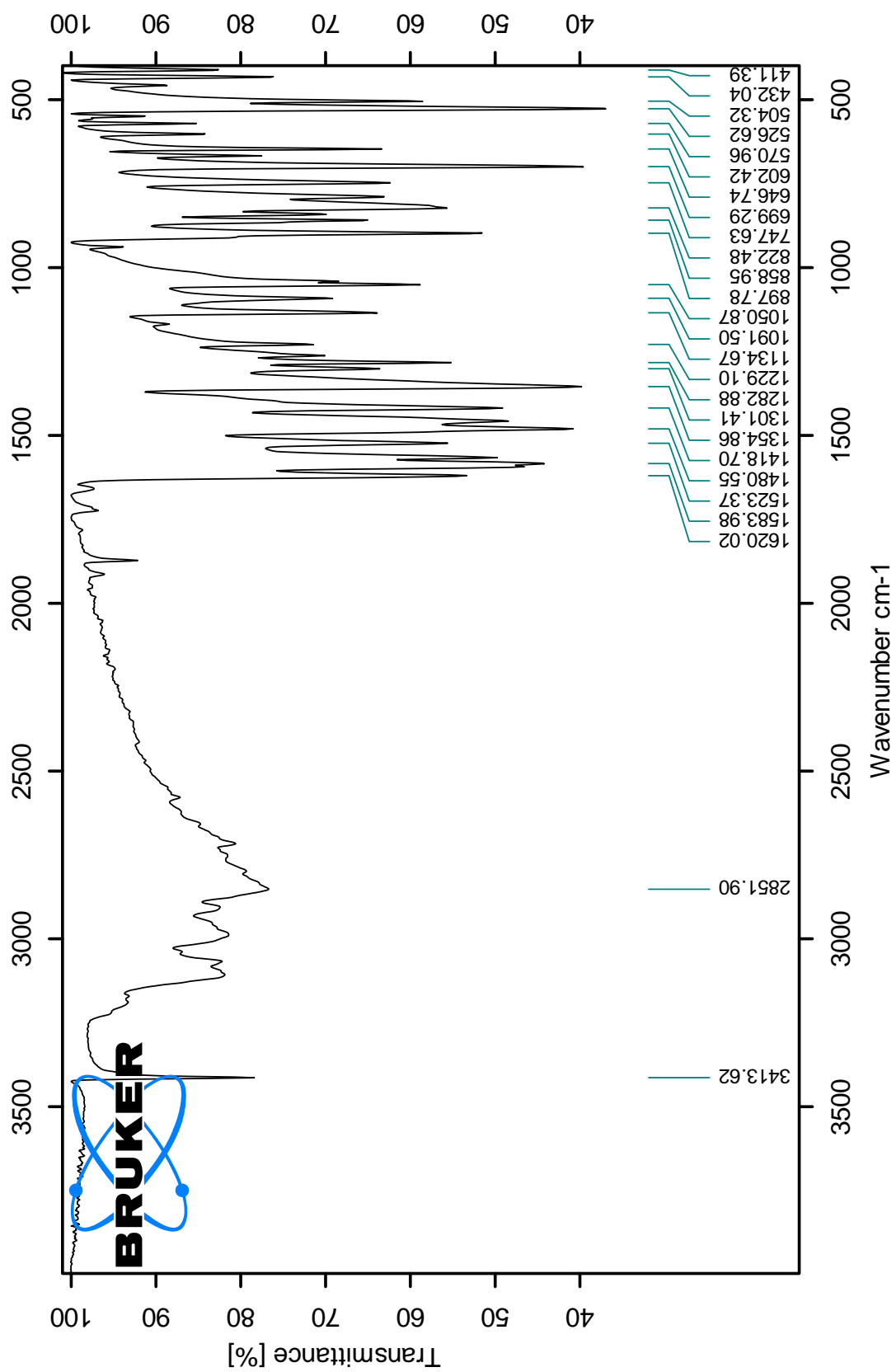


Figure D.6: IR spectrum of compound 33.

E Spectroscopic data – Compound 34

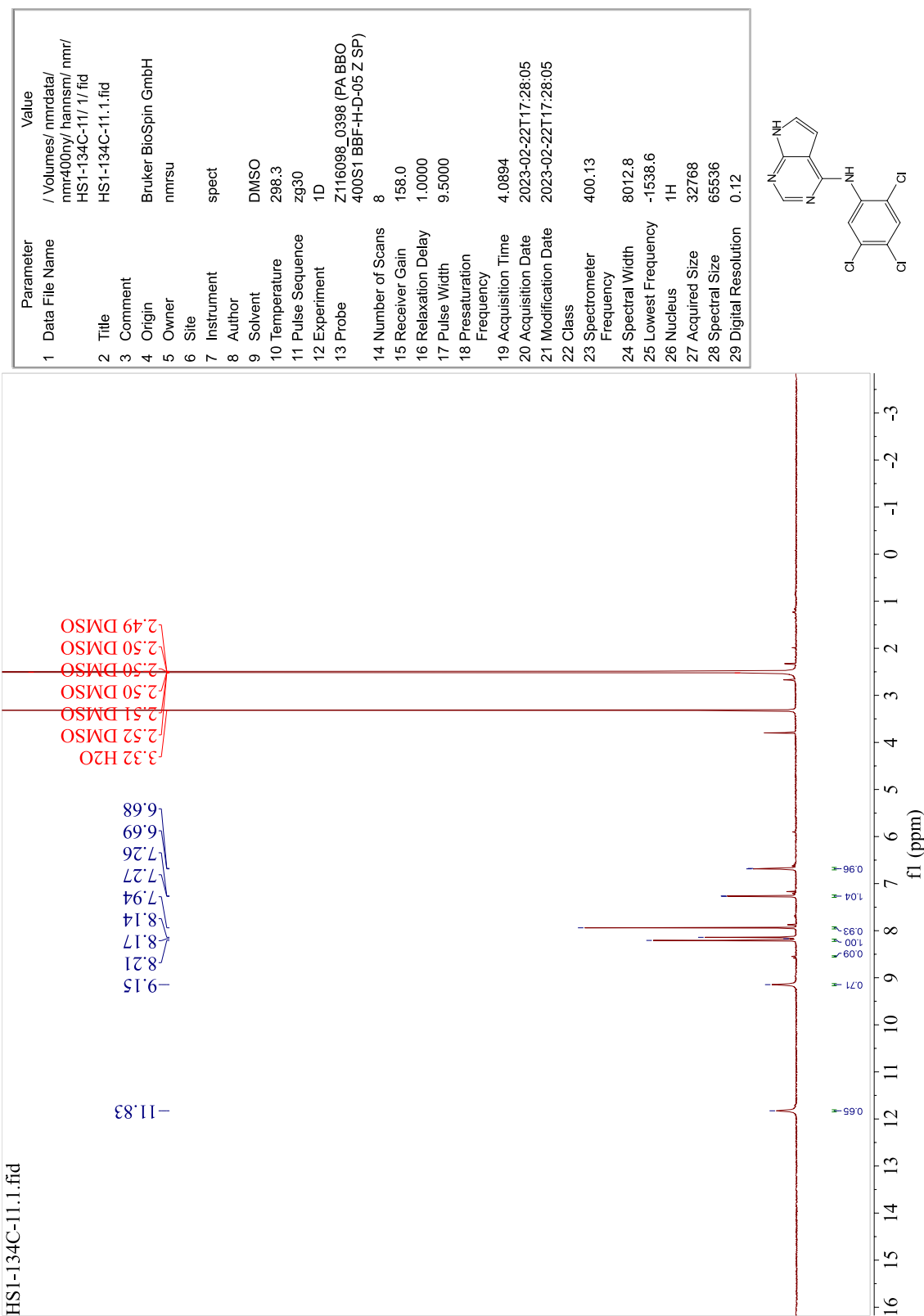


Figure E.1: ¹H-NMR spectrum of compound 34.

F Spectroscopic data – Compound 35

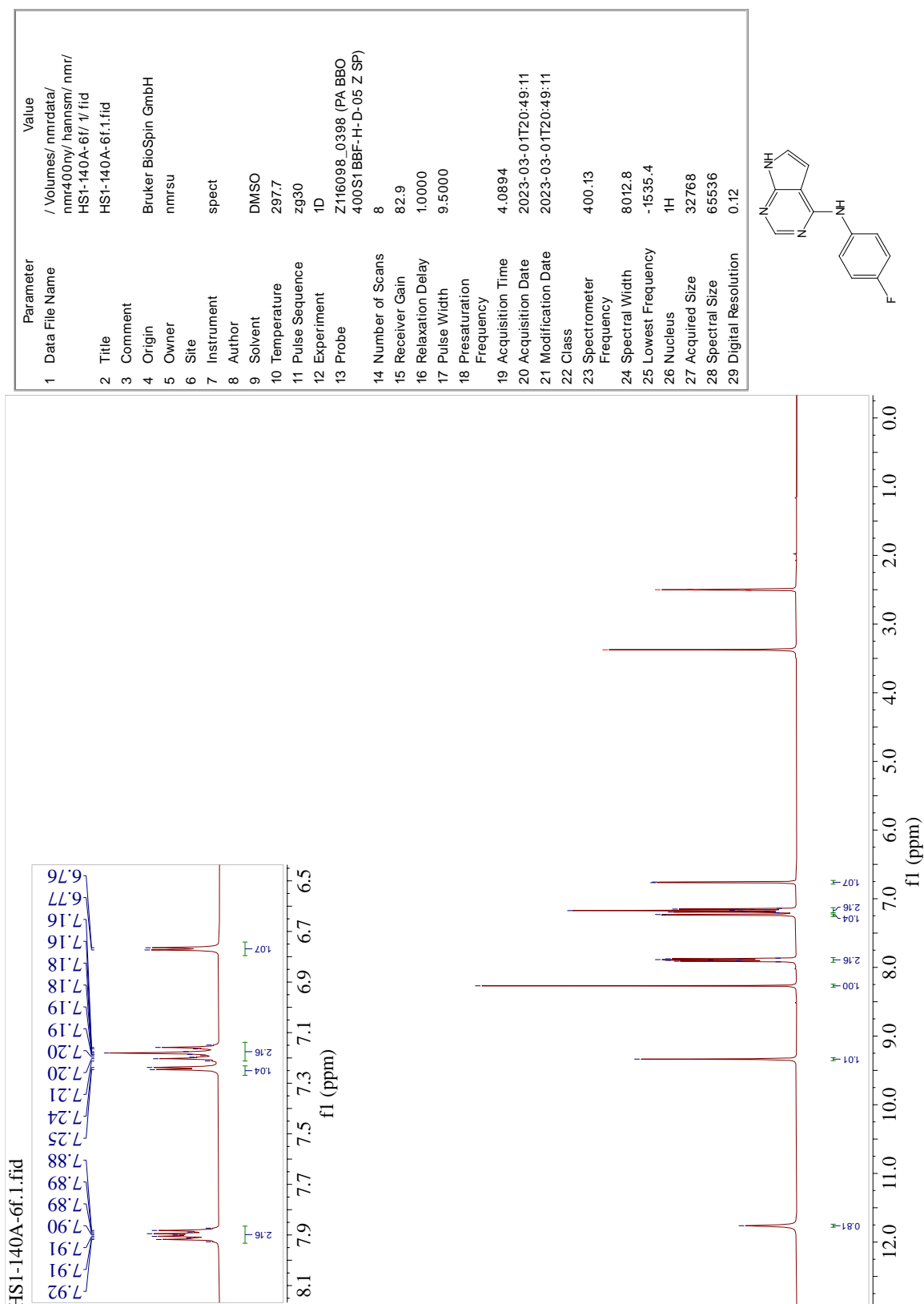
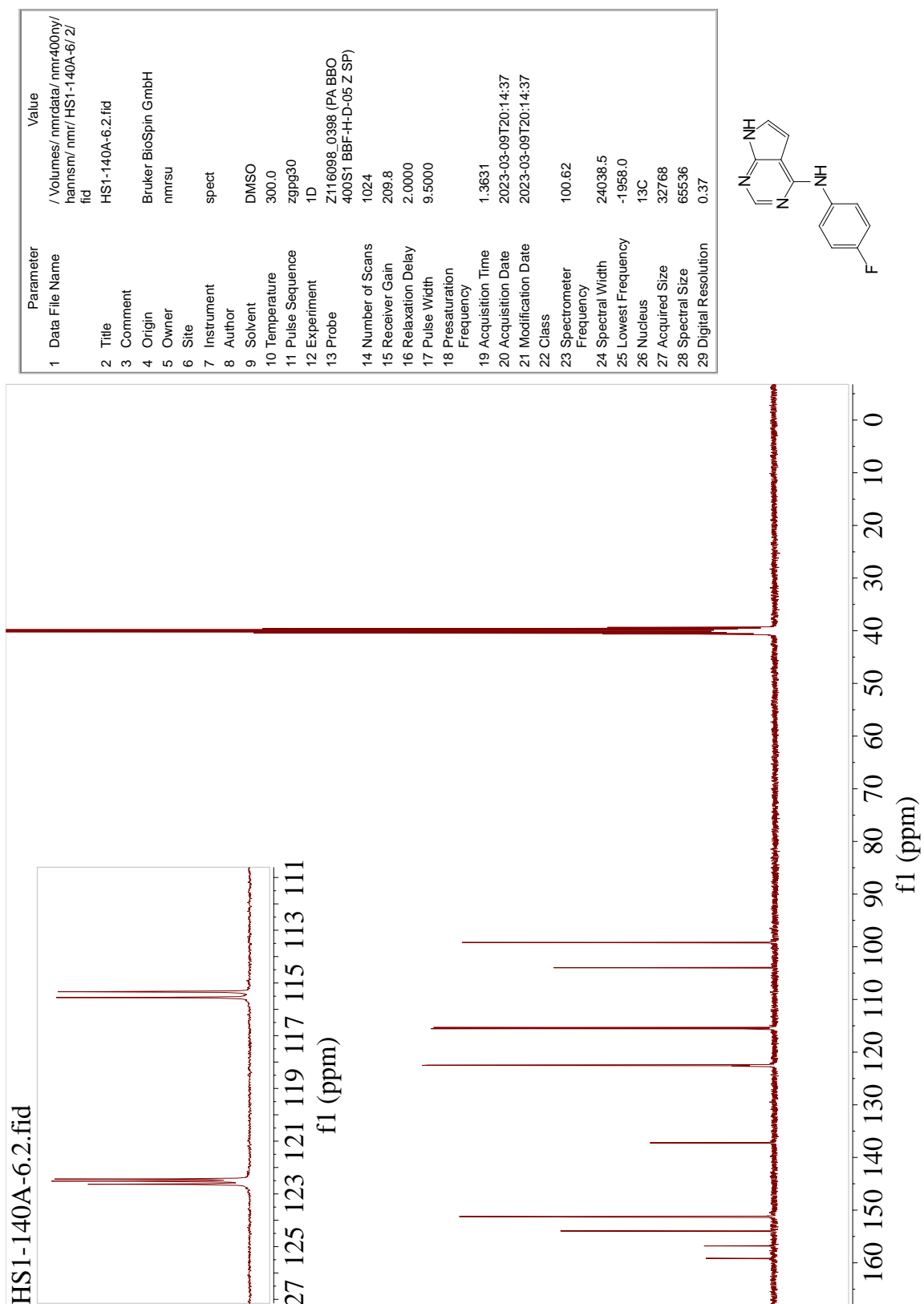


Figure F.1: ¹H-NMR spectrum of compound 35.

**Figure F.2:** ¹³C-NMR spectrum of compound 35.

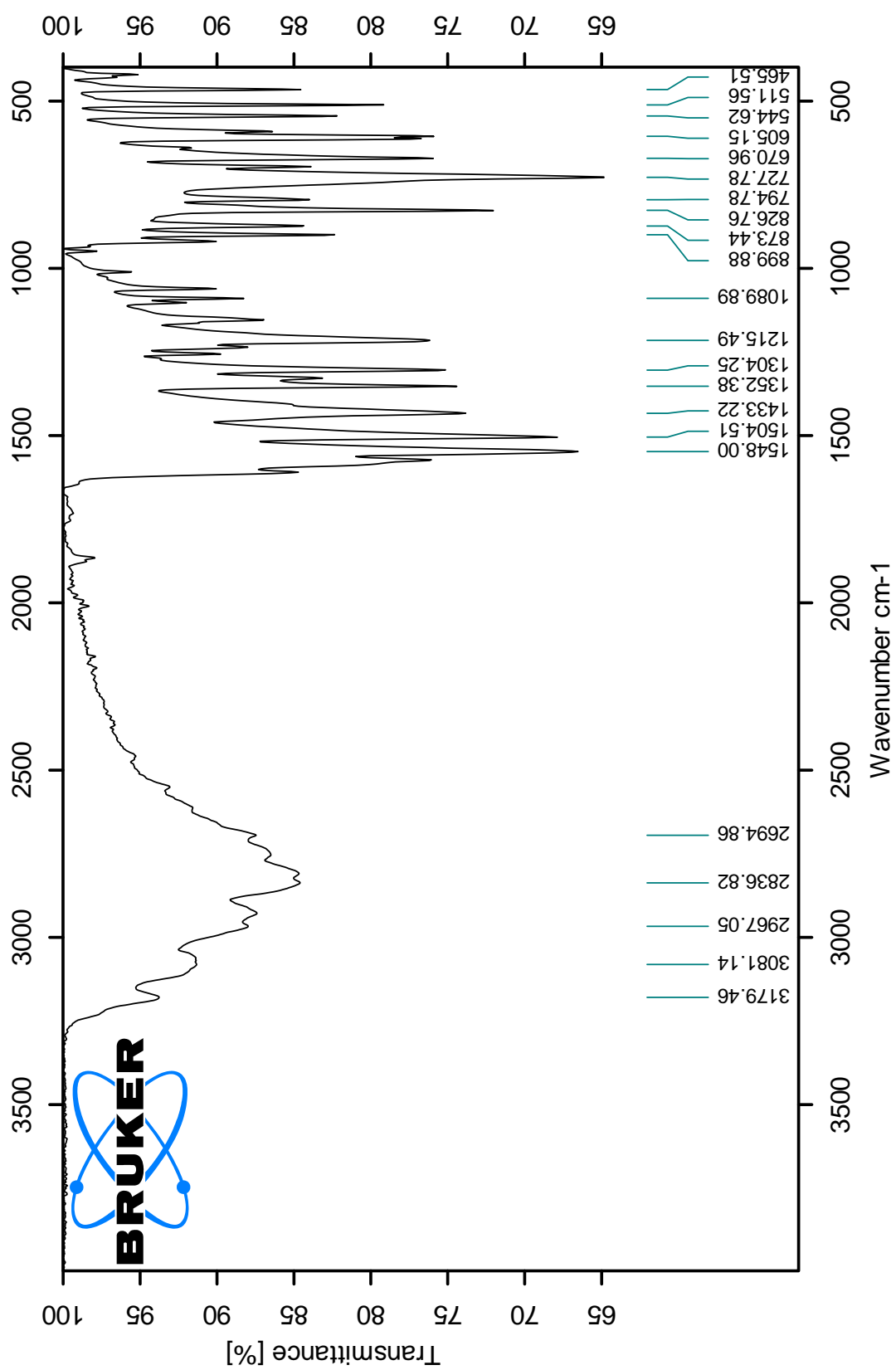


Figure F.3: IR spectrum of compound 35.

Elemental Composition Report

Single Mass Analysis

Tolerance = 2.0 PPM / DBE: min = -1.5, max = 50.0
 Element prediction: Off
 Number of isotope peaks used for i-FIT = 3

Monoisotopic Mass, Even Electron Ions
 552 formula(e) evaluated with 1 results within limits (up to 50 closest results for each mass)

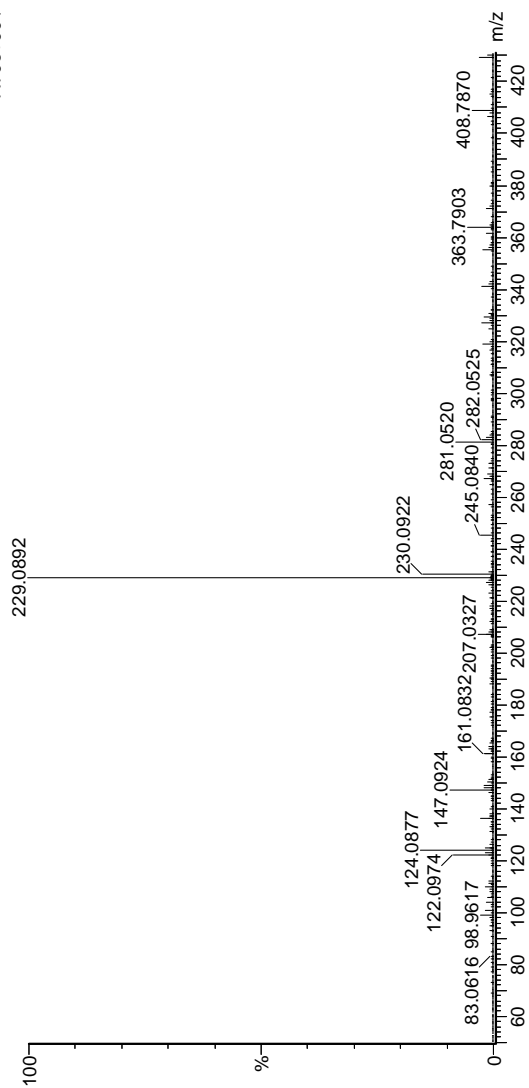
Elements Used:

C: 0-60 H: 1-1000 N: 0-5 O: 0-50 Na: 0-1 F: 0-1

ReqID2194.54 (0.618) AM2 (Ar:350000.0,0.00,0.00)

1: TOF MS ES+

7.70e+004



Minimum: -1.5
 Maximum: 50.0

Mass	Calc. Mass	mDa	PPM	DBE	i-FIT	Norm	Conf (%)	Formula
229.0892	229.0889	0.3	1.3	9.5	640.2	n/a	n/a	C12 H10 N4 F

Figure F.4: MS spectrum of compound 35.

G Spectroscopic data – Compound 36

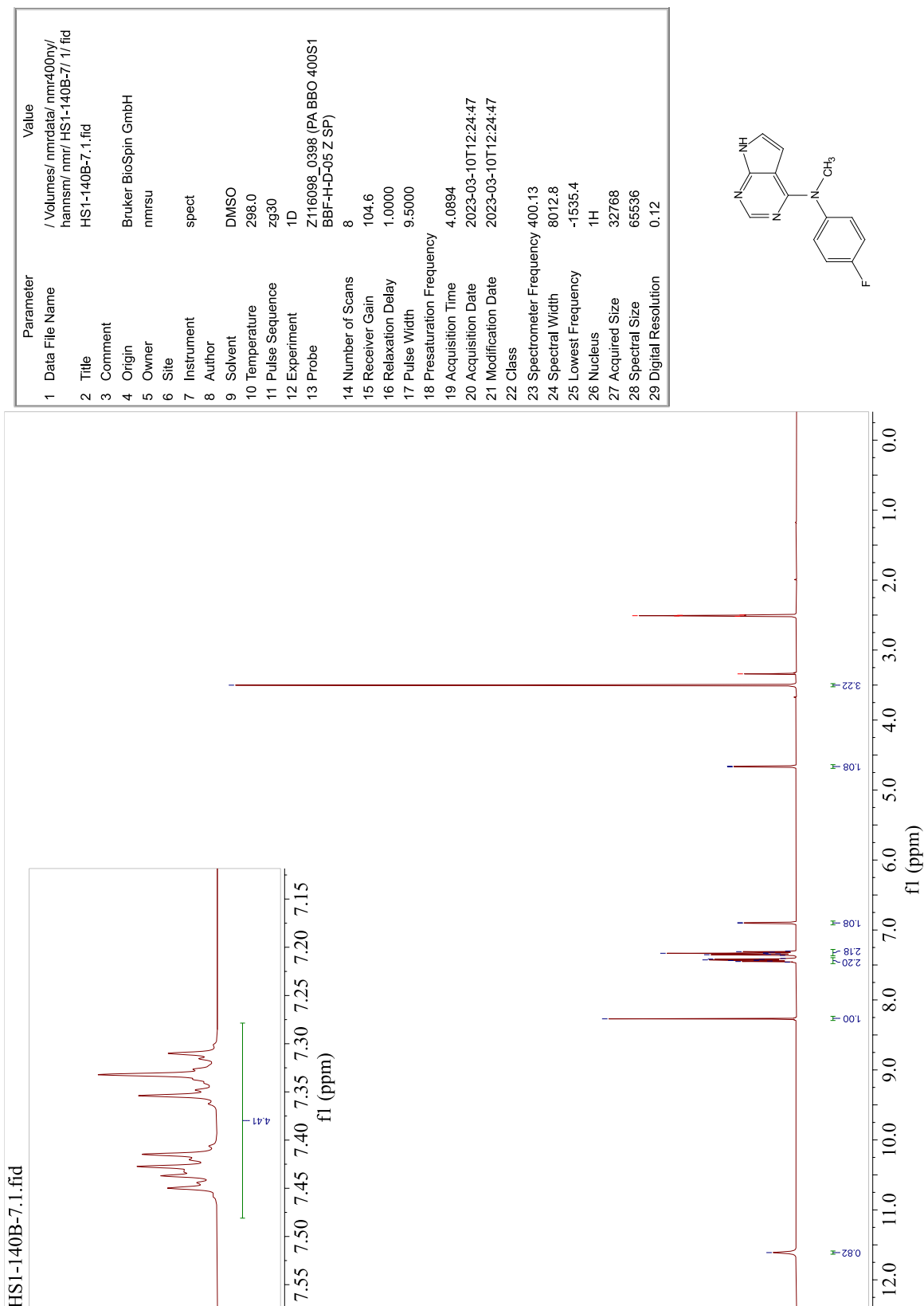


Figure G.1: ¹H-NMR spectrum of compound 36.

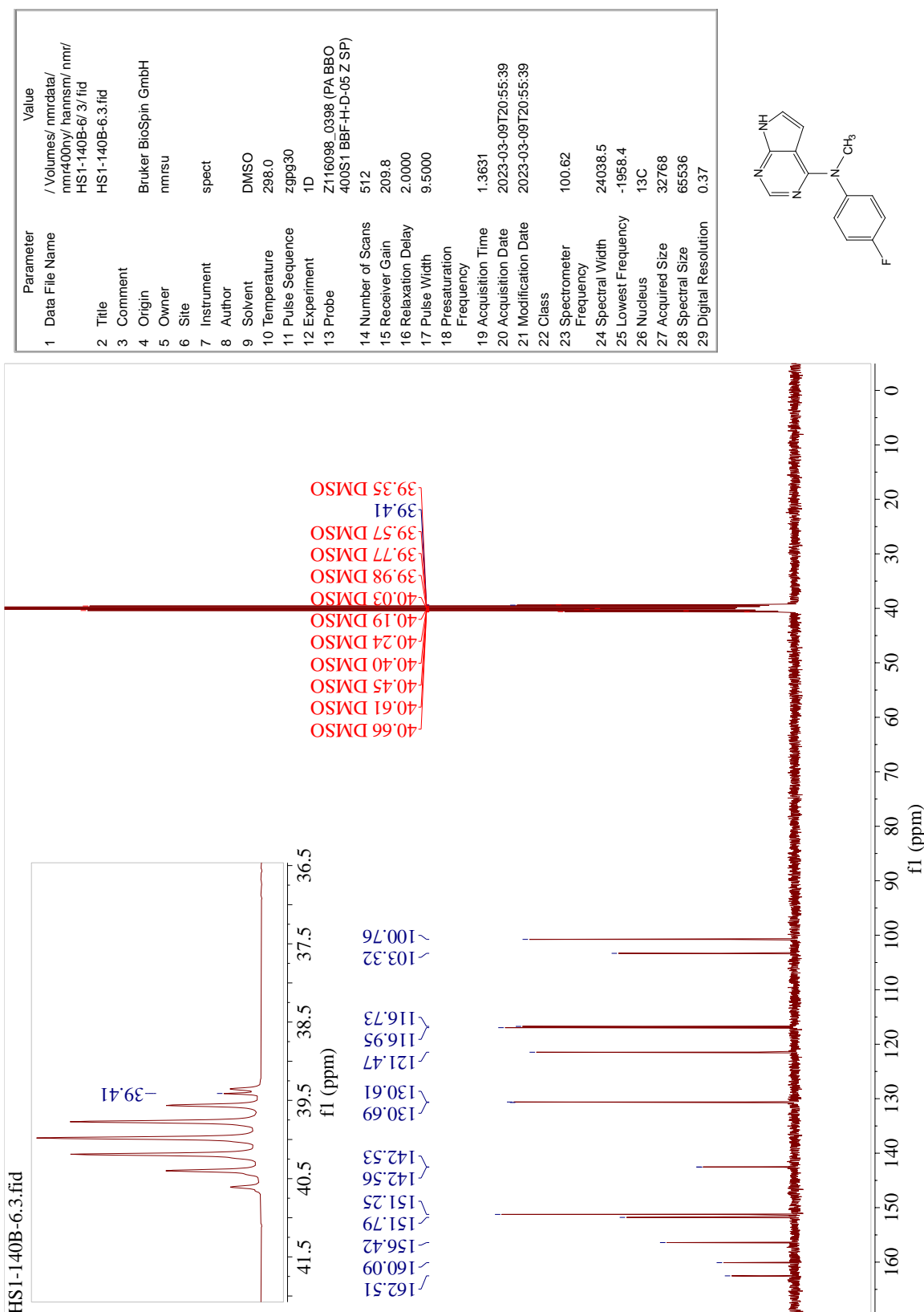


Figure G.2: ¹³C-NMR spectrum of compound 36.

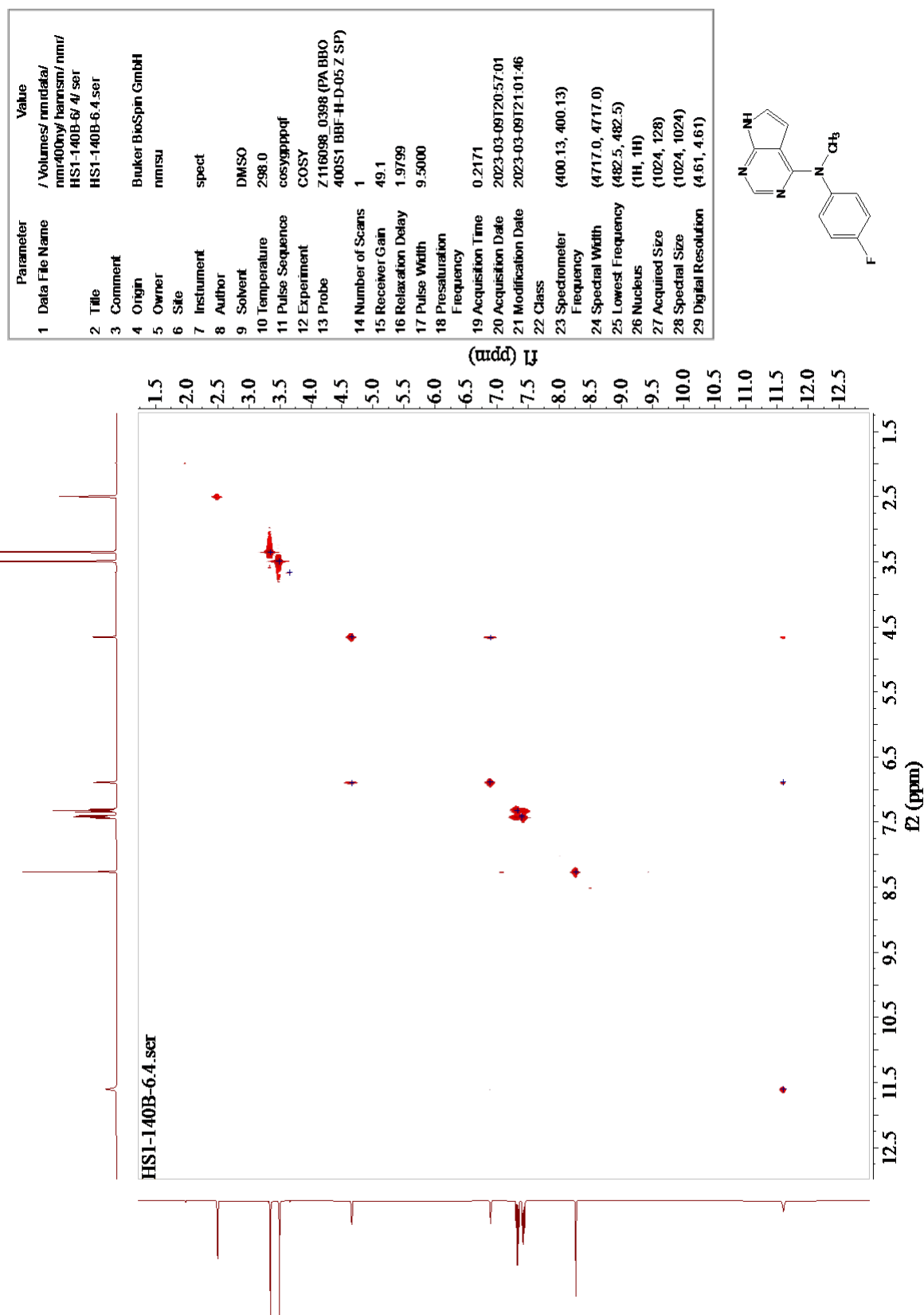
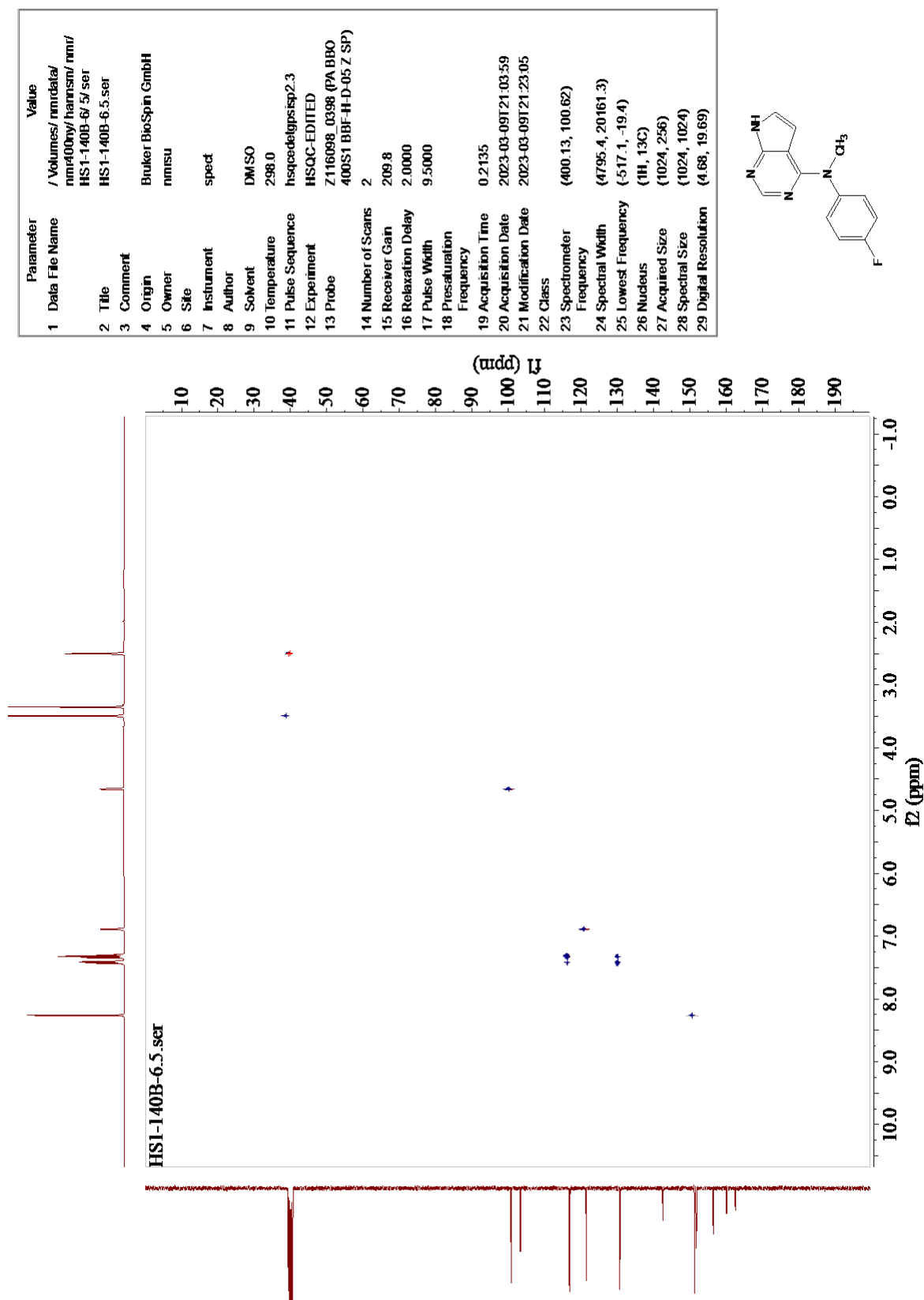


Figure G.3: COSY spectrum of compound 36.



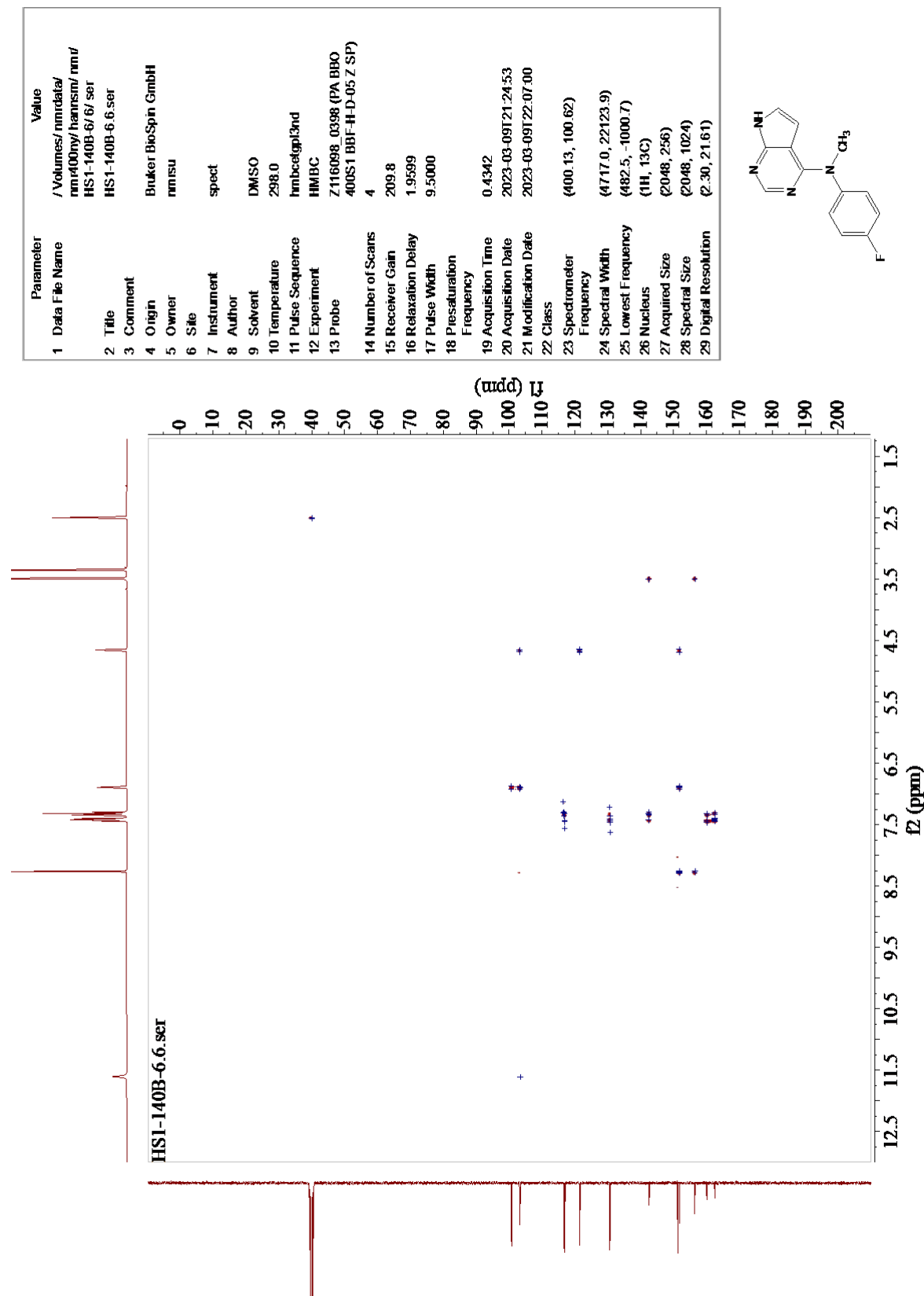


Figure G.5: HMBC spectrum of compound 36.

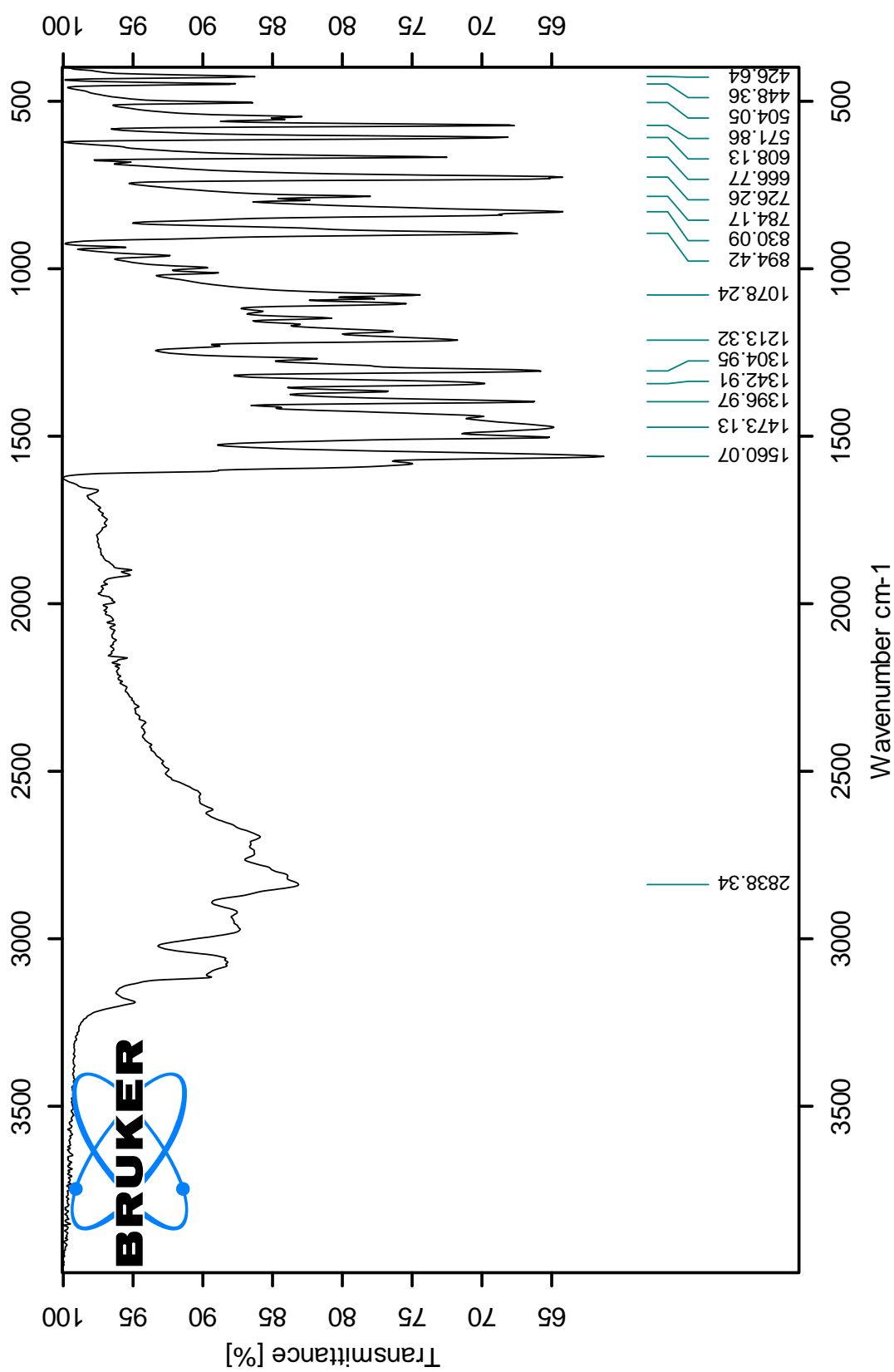


Figure G.6: IR spectrum of compound 36.

Elemental Composition Report

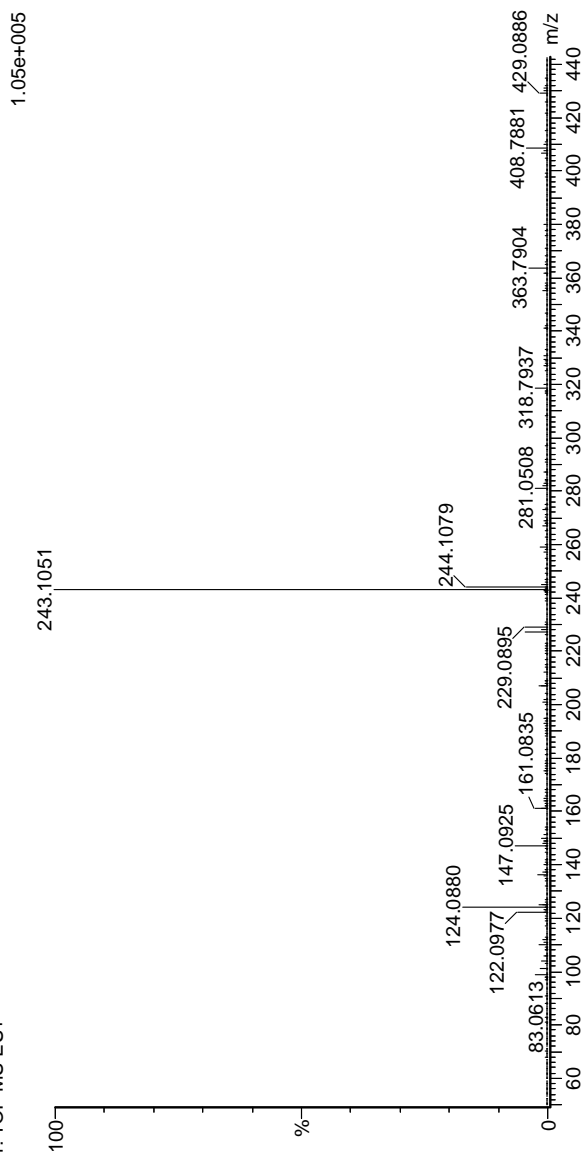
Single Mass Analysis

Tolerance = 6.0 PPM / DBE: min = -1.5, max = 50.0
 Element prediction: Off
 Number of isotope peaks used for i-FIT = 3

Monoisotopic Mass, Even Electron Ions
 615 formula(e) evaluated with 1 results within limits (up to 50 closest results for each mass)
 Elements Used:

C: 0-60 H: 1-1000 N: 0-5 O: 0-50 F: 0-1 Na: 0-1

ReqID2195.54 (0.618)AM2 (Ar:35000.0,0.00,0.00)
 1: TOF MS ES+



Minimum: -1.5
 Maximum: 50.0

Mass	Calc. Mass	mDa	PPM	DBE	i-FIT	Norm	Conf (%)	Formula
243.1051	243.1046	0.5	2.1	9.5	723.0	n/a	n/a	C13 H12 N4 F

Figure G.7: MS spectrum of compound 36.

H Spectroscopic data – Compound 37

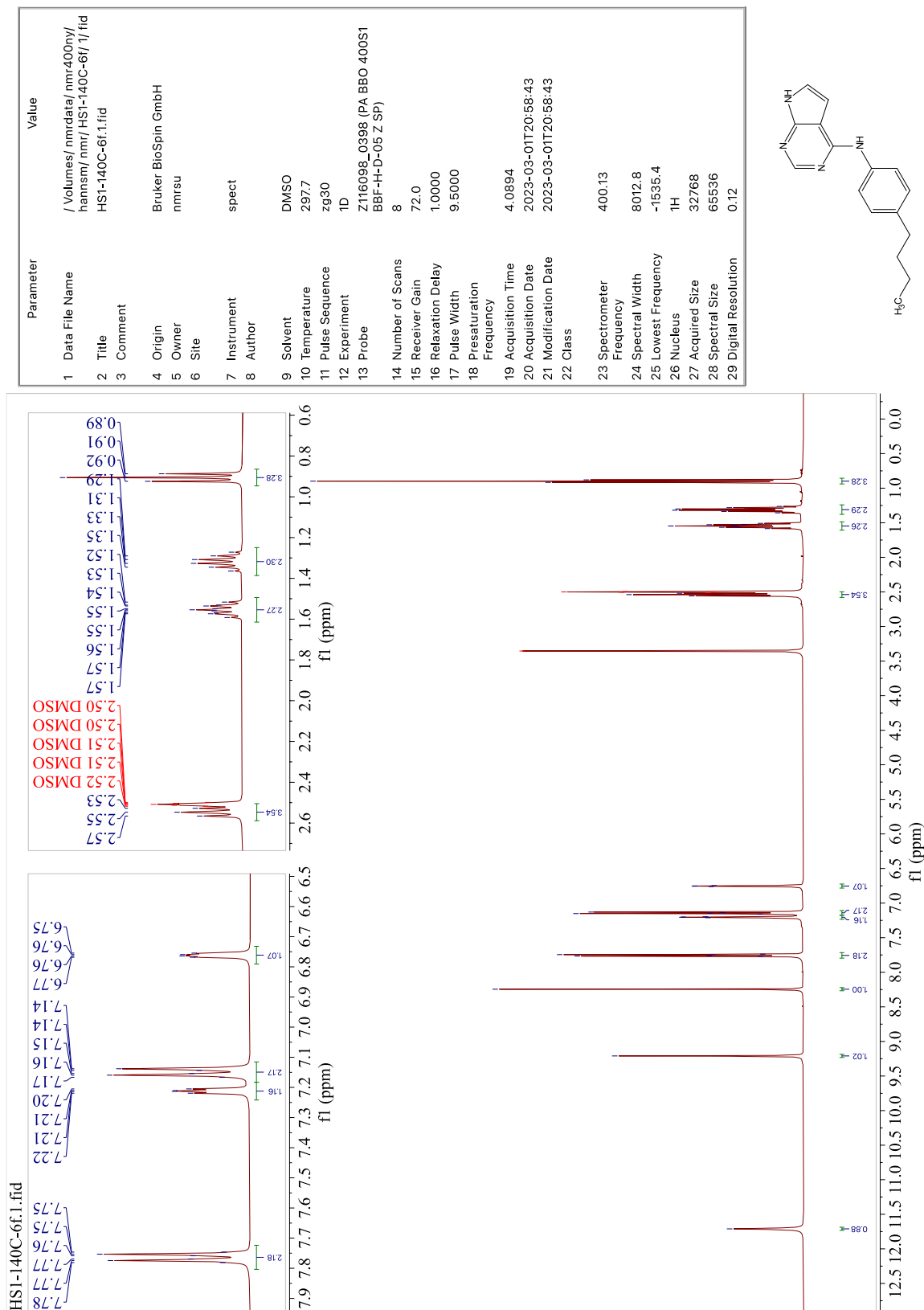


Figure H.1: ¹H-NMR spectrum of compound 37.

APPENDIX H

Parameter	Value
1 Data File Name	/Volumes/nmrdata/nmr400ny/harmsm/nmr/HS1-140C-6/3/fid
2 Title	HS1-140C-6.3.fid
3 Comment	
4 Origin	Bruker BioSpin GmbH
5 Owner	nmrsu
6 Site	
7 Instrument	spect
8 Author	
9 Solvent	DMSO
10 Temperature	298.0
11 Pulse Sequence	zgpg30
12 Experiment 1D	
13 Probe	Z116098_0398 (PA BBO 400S1 BBF-H-D-05 Z SP)
14 Number of Scans	512
15 Receiver Gain	209.8
16 Relaxation Delay	2.0000
17 Pulse Width	9.5000
18 Presaturation Frequency	
19 Acquisition Time	1.3631
20 Acquisition Date	2023-03-09T22:48:27
21 Modification Date	2023-03-09T22:48:27
22 Class	
23 Spectrometer Frequency	100.62
24 Spectral Width	24038.5
25 Lowest Frequency	-1958.4
26 Nucleus	¹³ C
27 Acquired Size	32768
28 Spectral Size	65536
29 Digital Resolution	0.37

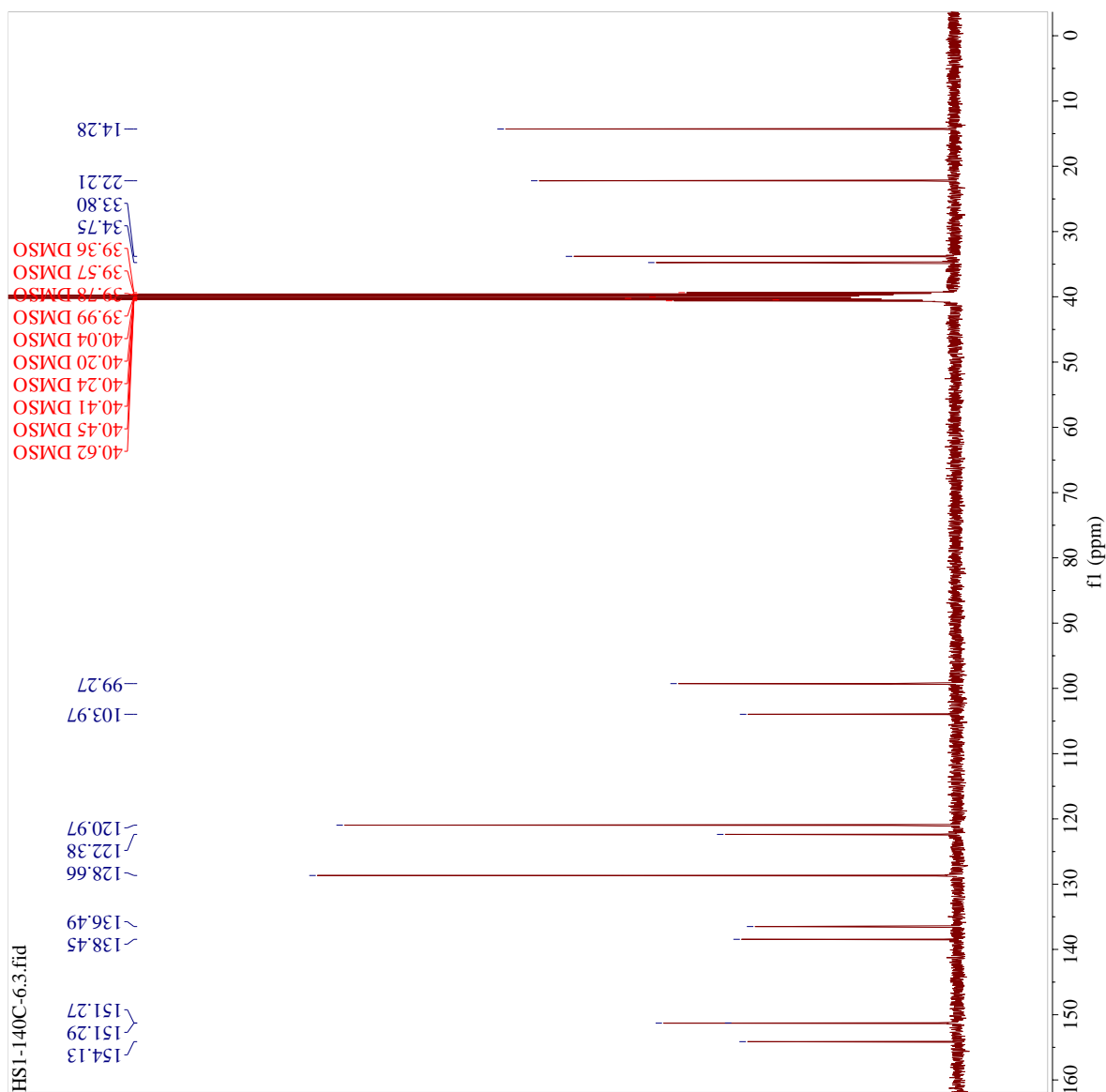
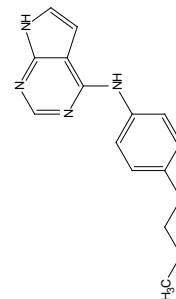


Figure H.2: ¹³C-NMR spectrum of compound 37.

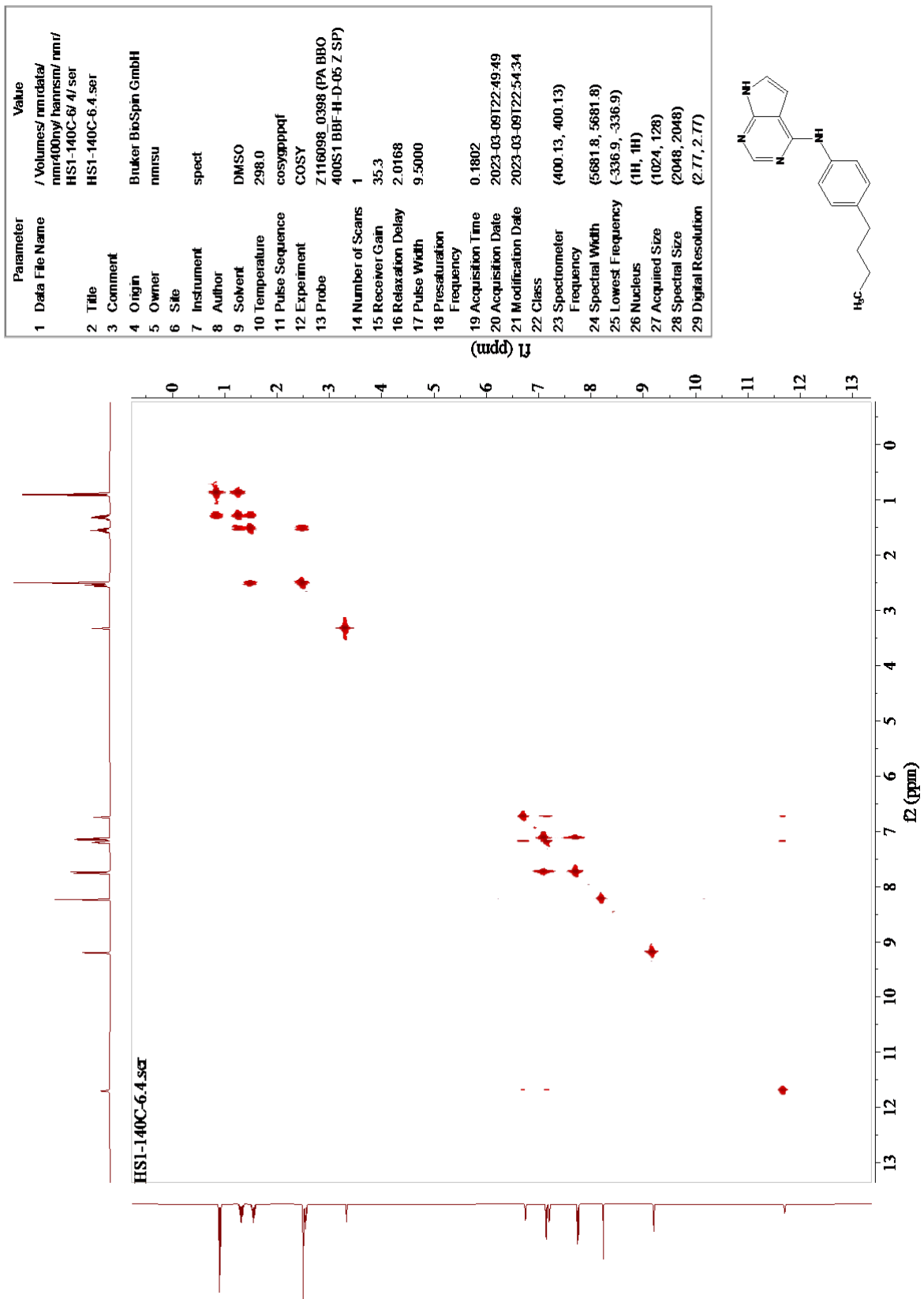


Figure H.3: COSY spectrum of compound 37.

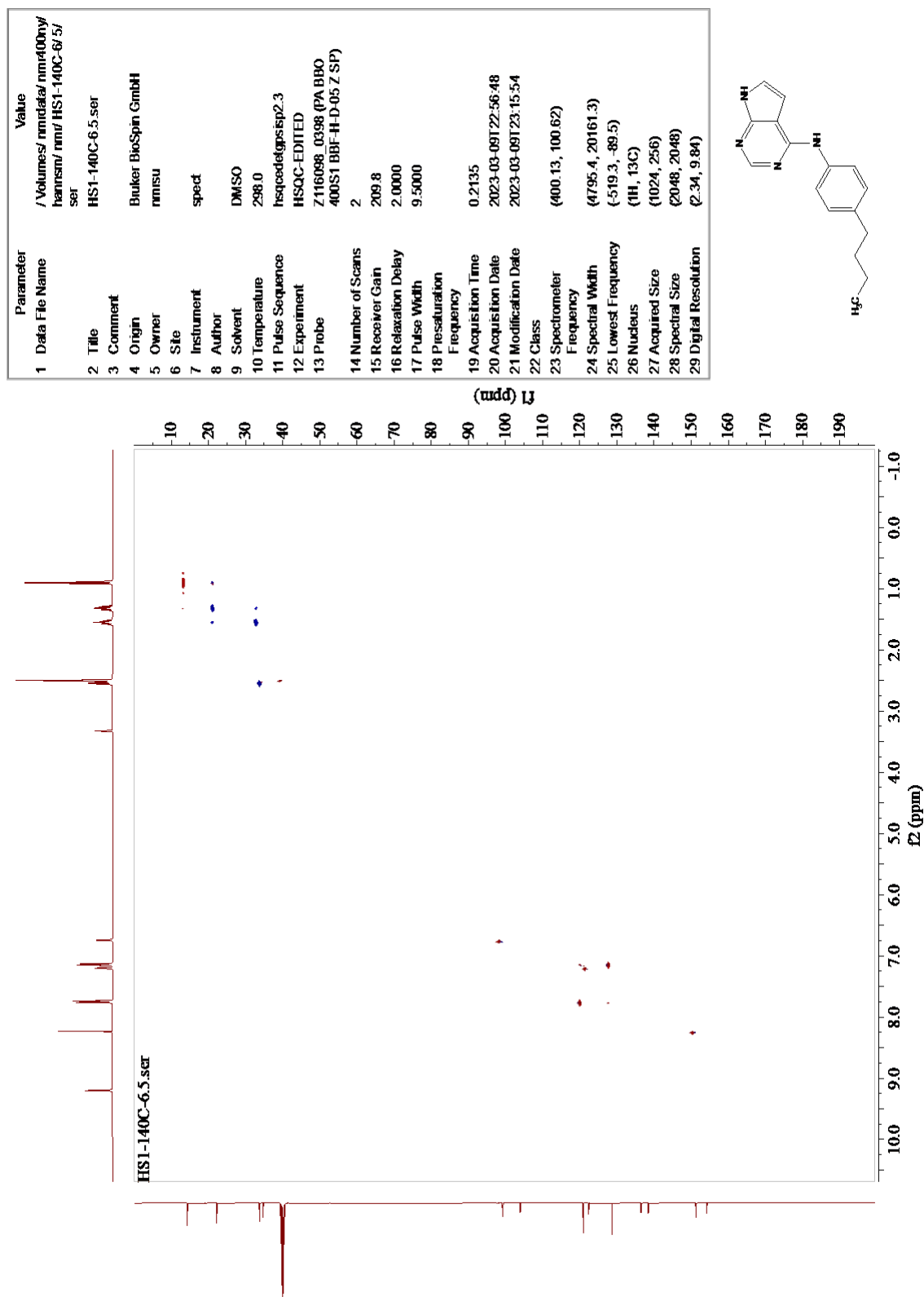


Figure H.4: HSQC spectrum of compound 37.

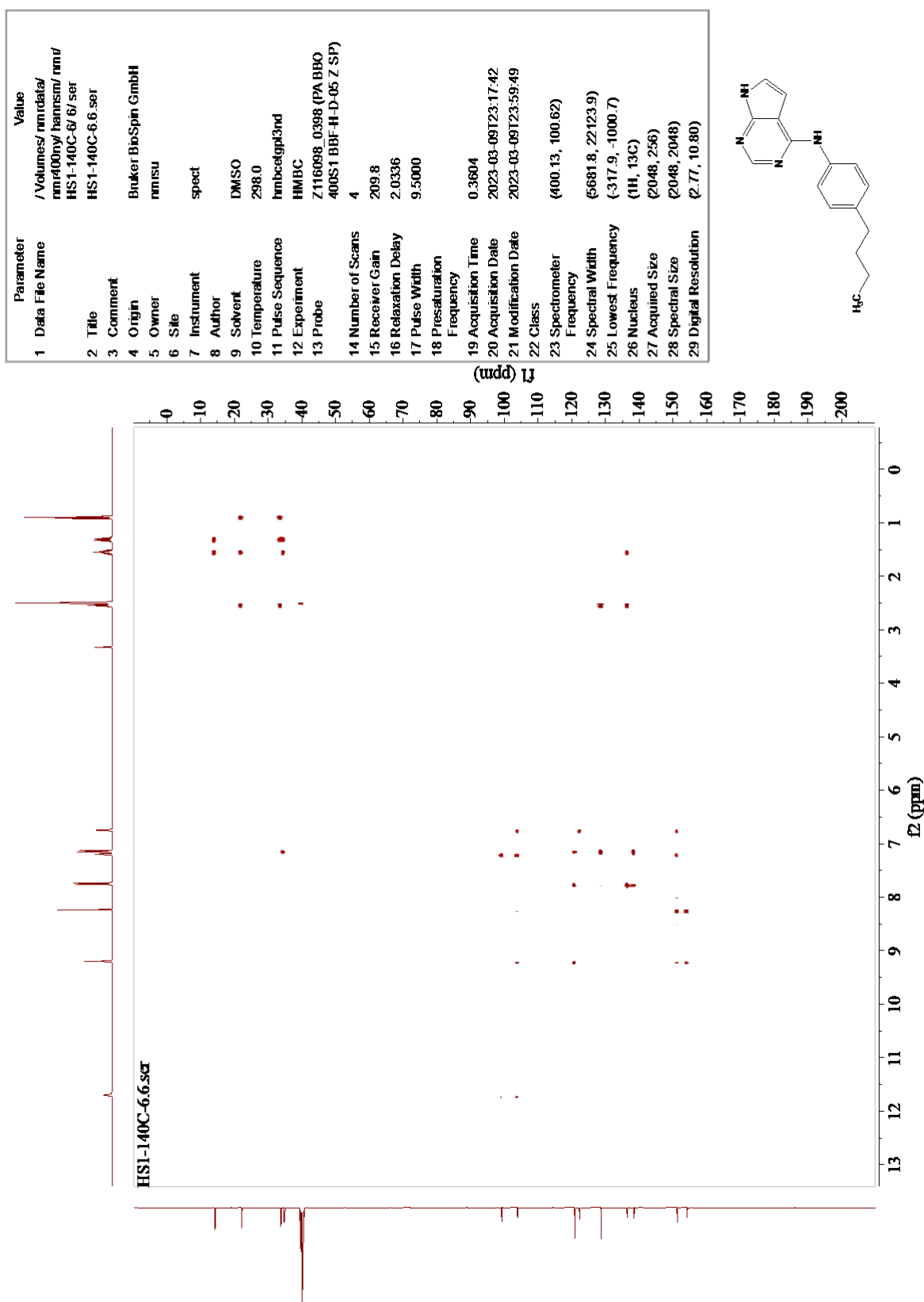


Figure H.5: HMBC spectrum of compound 37.

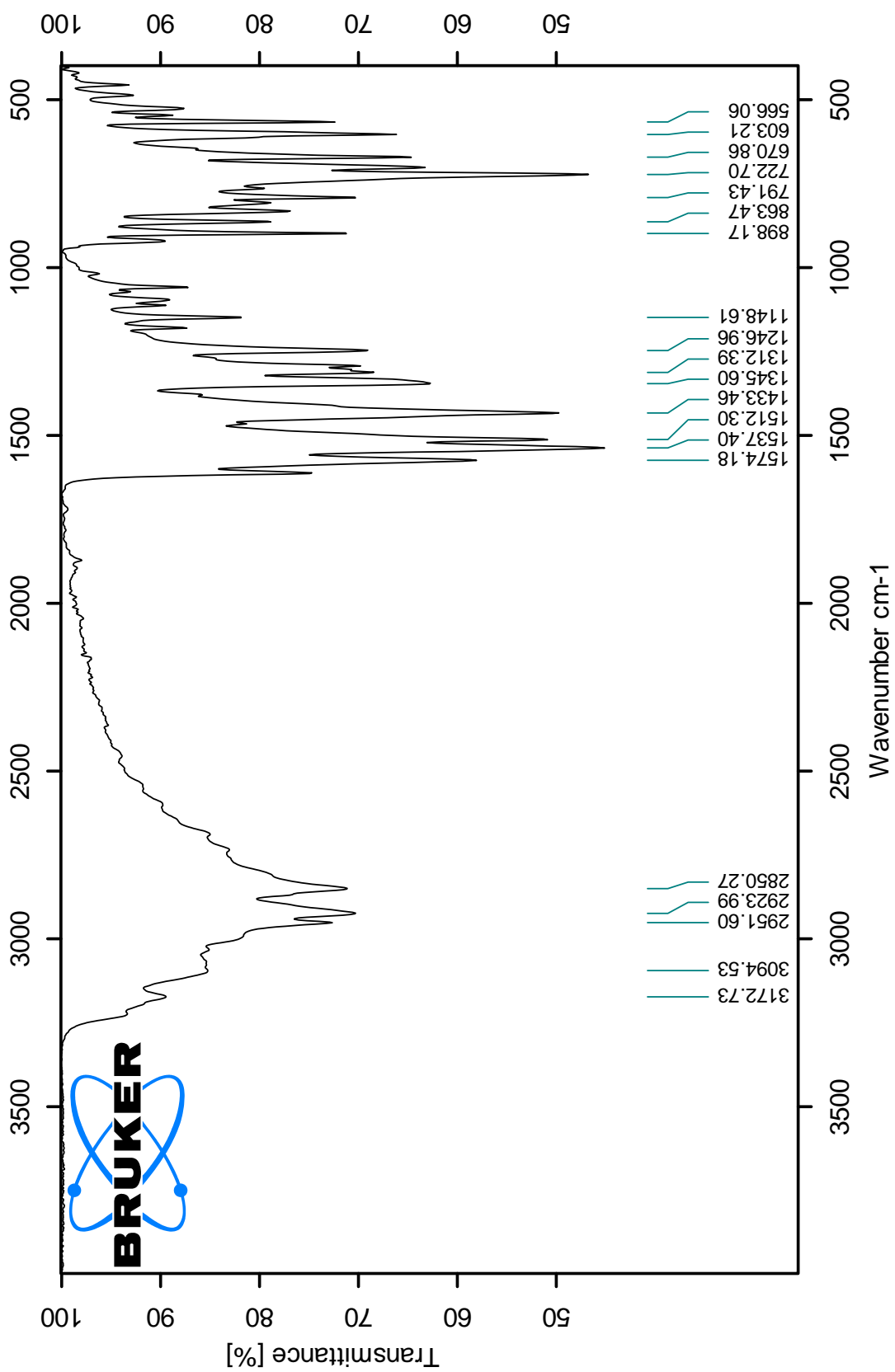


Figure H.6: IR spectrum of compound 37.

Elemental Composition Report

Single Mass Analysis

Tolerance = 6.0 PPM / DBE: min = -1.5, max = 50.0

Element prediction: Off

Number of isotope peaks used for i-FIT = 3

Monoisotopic Mass, Even Electron Ions
 397 formula(e) evaluated with 1 results within limits (up to 50 closest results for each mass)

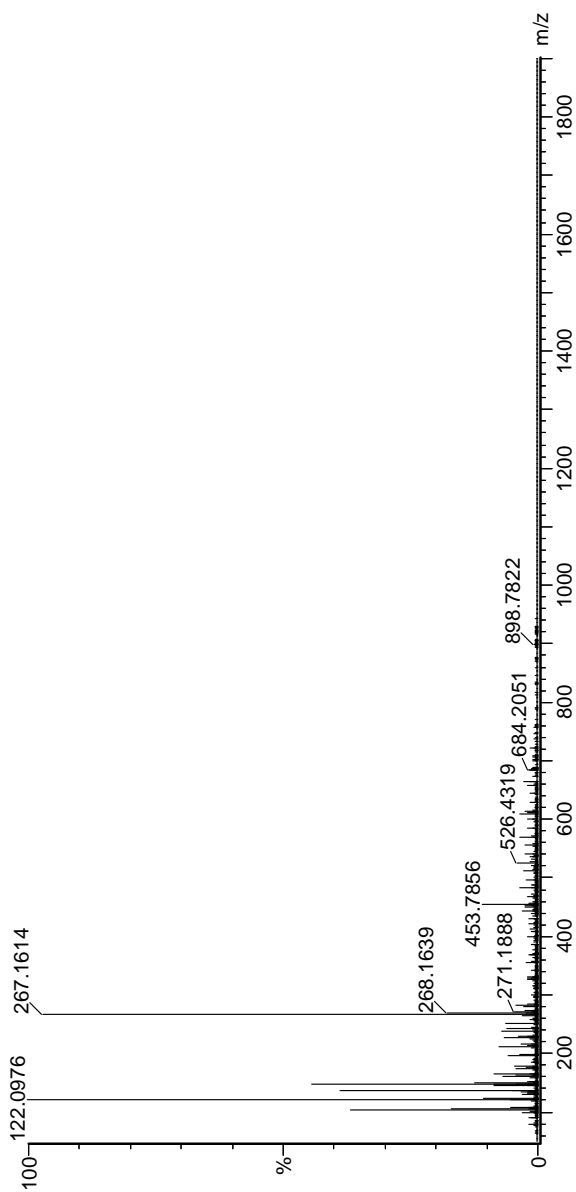
Elements Used:

C: 0-60 H: 1-1000 N: 0-5 O: 0-50 Na: 0-1

ReqID2196 152 (1.709)AM2 (Ar,35000.0,0.00,0.00); Cm (152:165)

1: TOF MS ES+

5.69e+005



Mass	Calc. Mass	mDa	PPM	DBE	i-FIT	Norm	Conf (%)	Formula
267.1614	267.1610	0.4	1.5	9.5	1316.0	n/a	n/a	C16 H19 N4
Minimum:								
Maximum:								

Figure H.7: MS spectrum of compound 37.

I Spectroscopic data – Compound 38

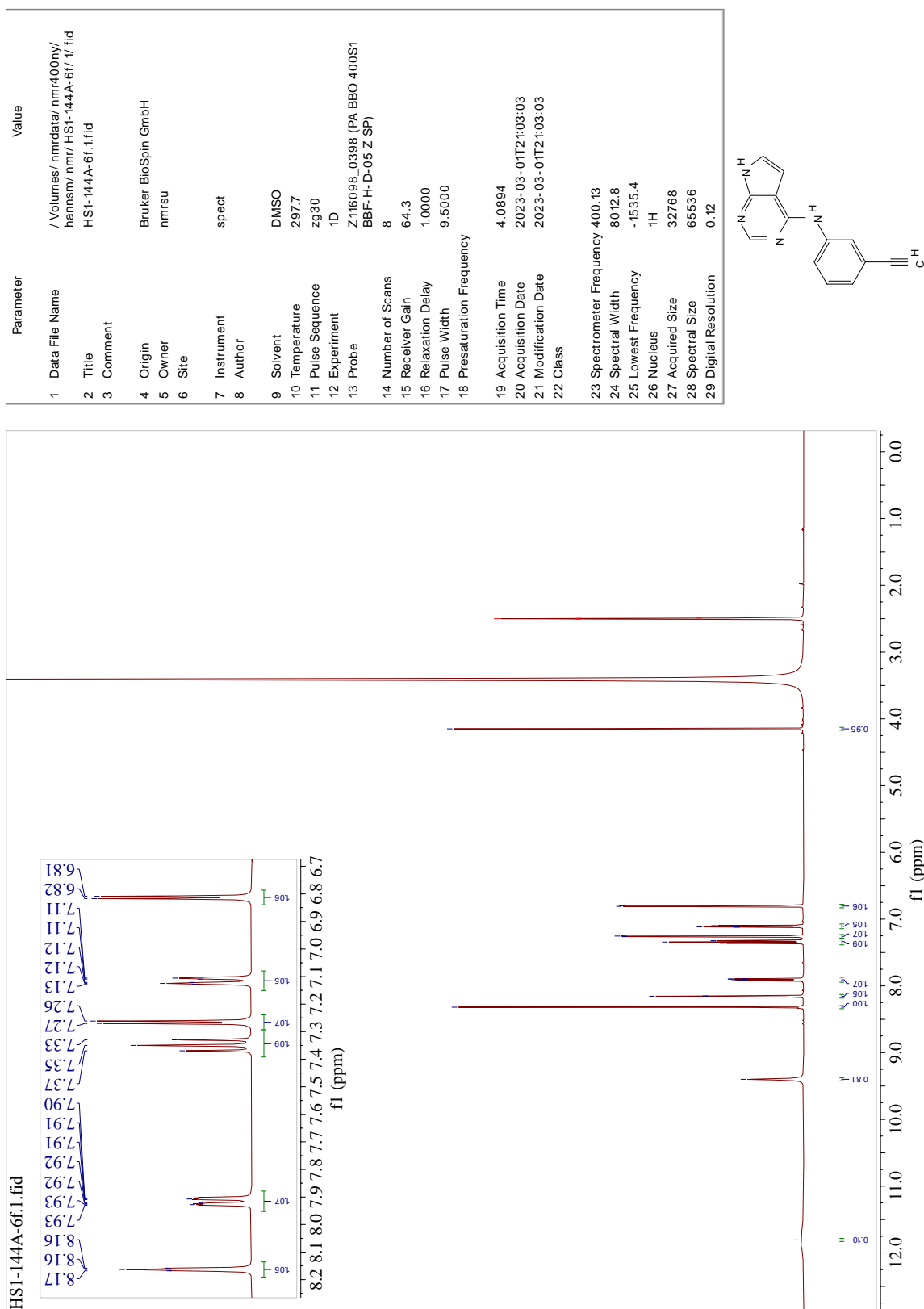


Figure I.1: ¹H-NMR spectrum of compound 38.

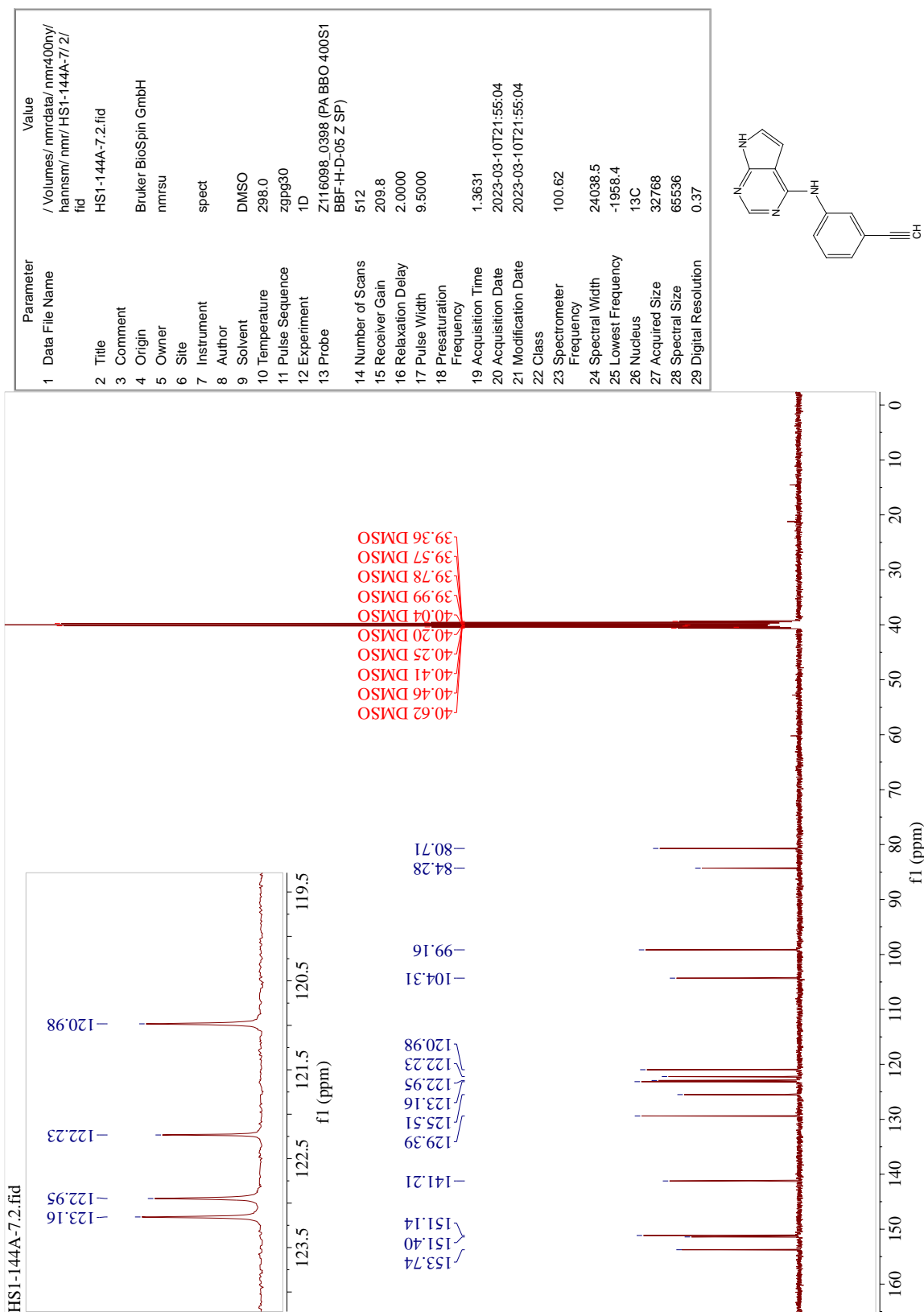


Figure I.2: ¹³C-NMR spectrum of compound 38.

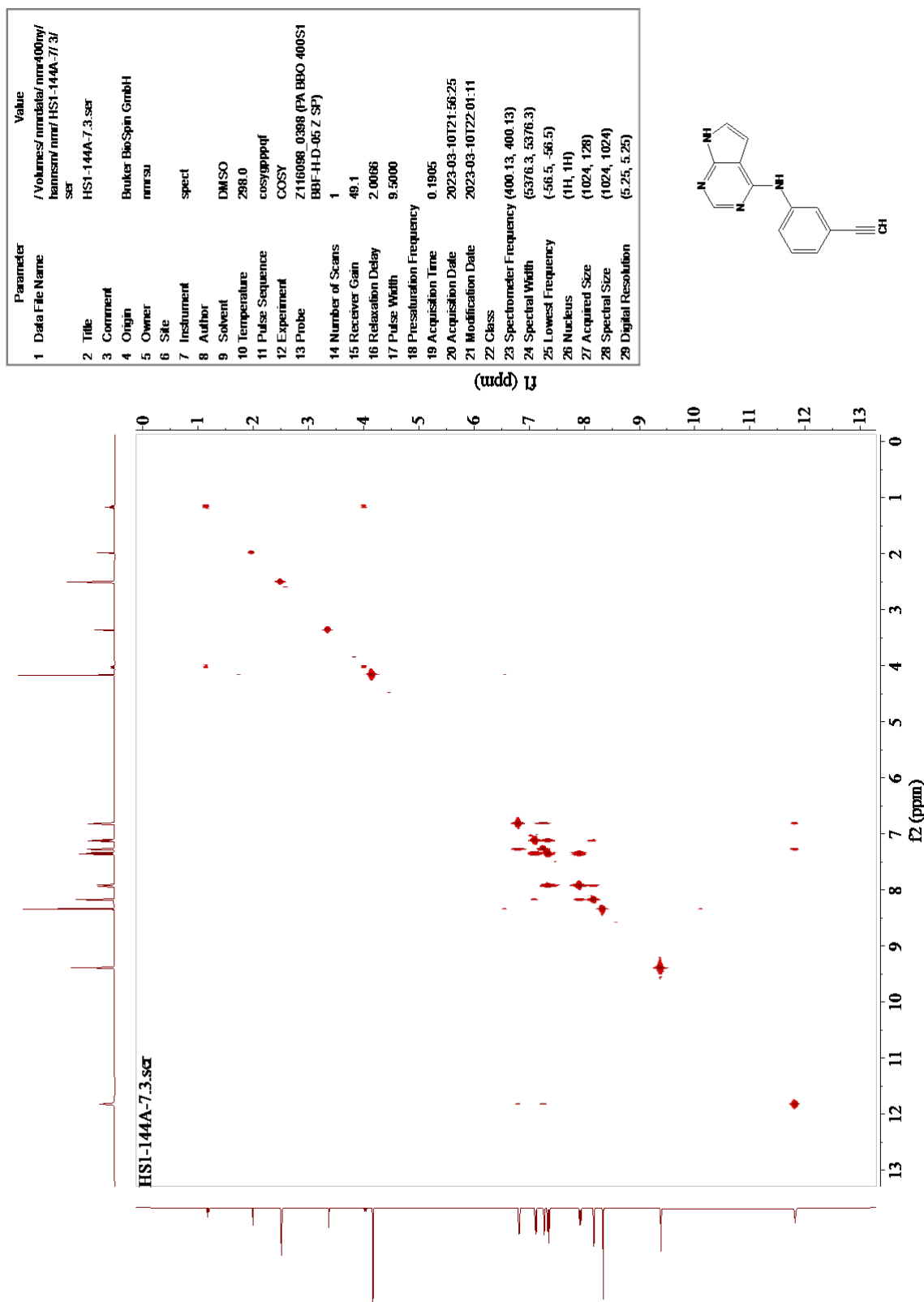


Figure I.3: COSY spectrum of compound 38.

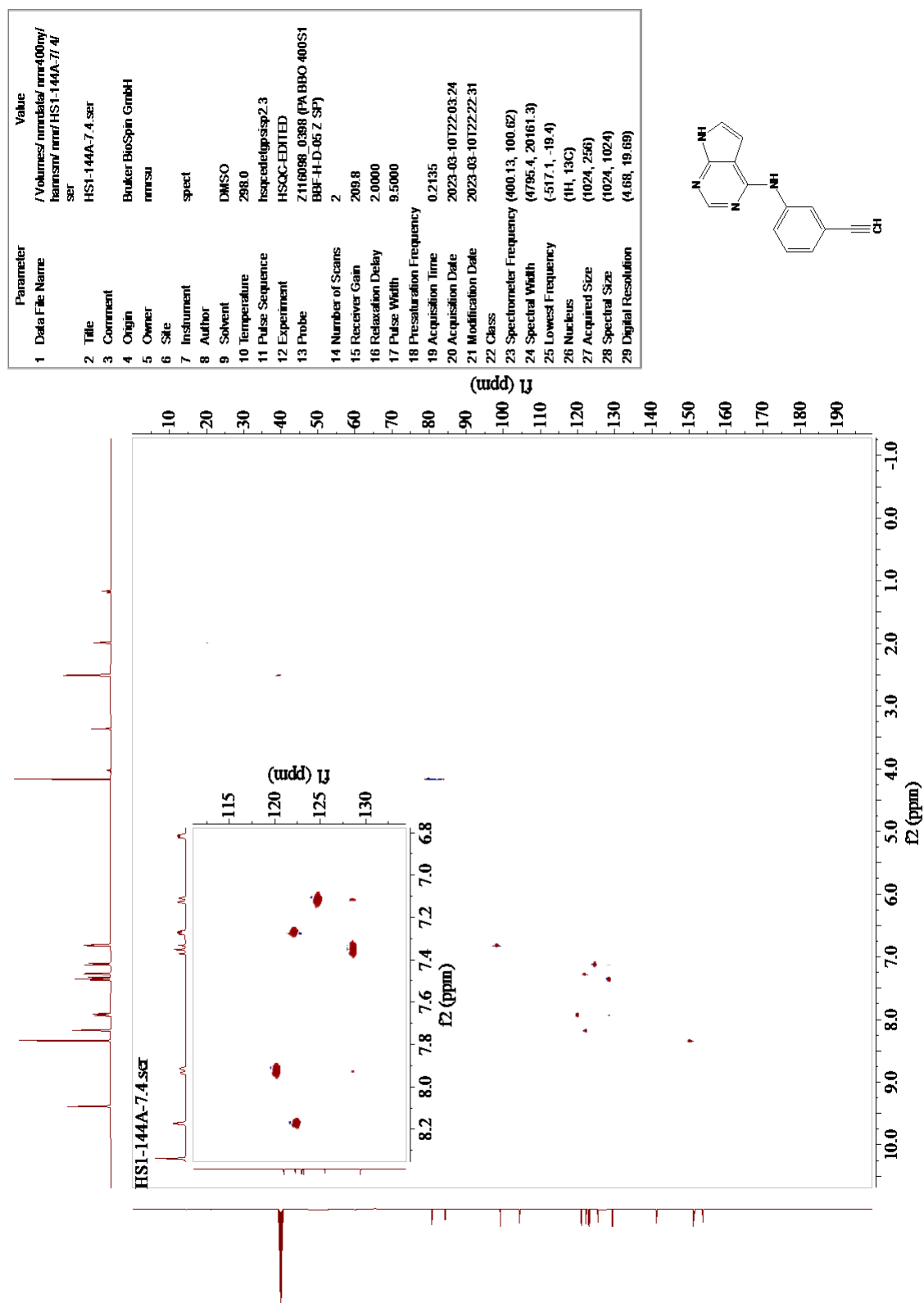


Figure I.4: HSQC spectrum of compound 38.

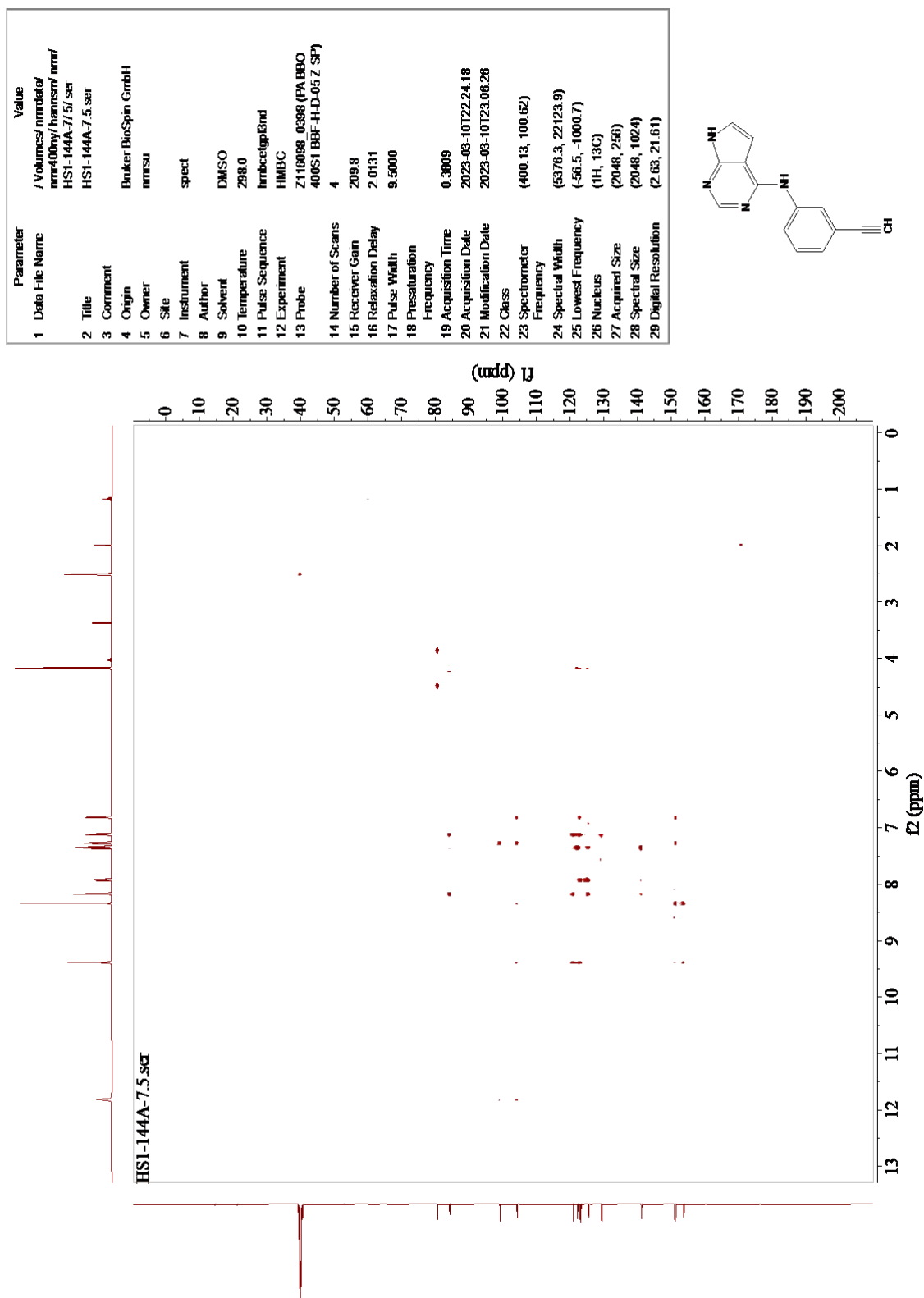


Figure I.5: HMBC spectrum of compound 38.

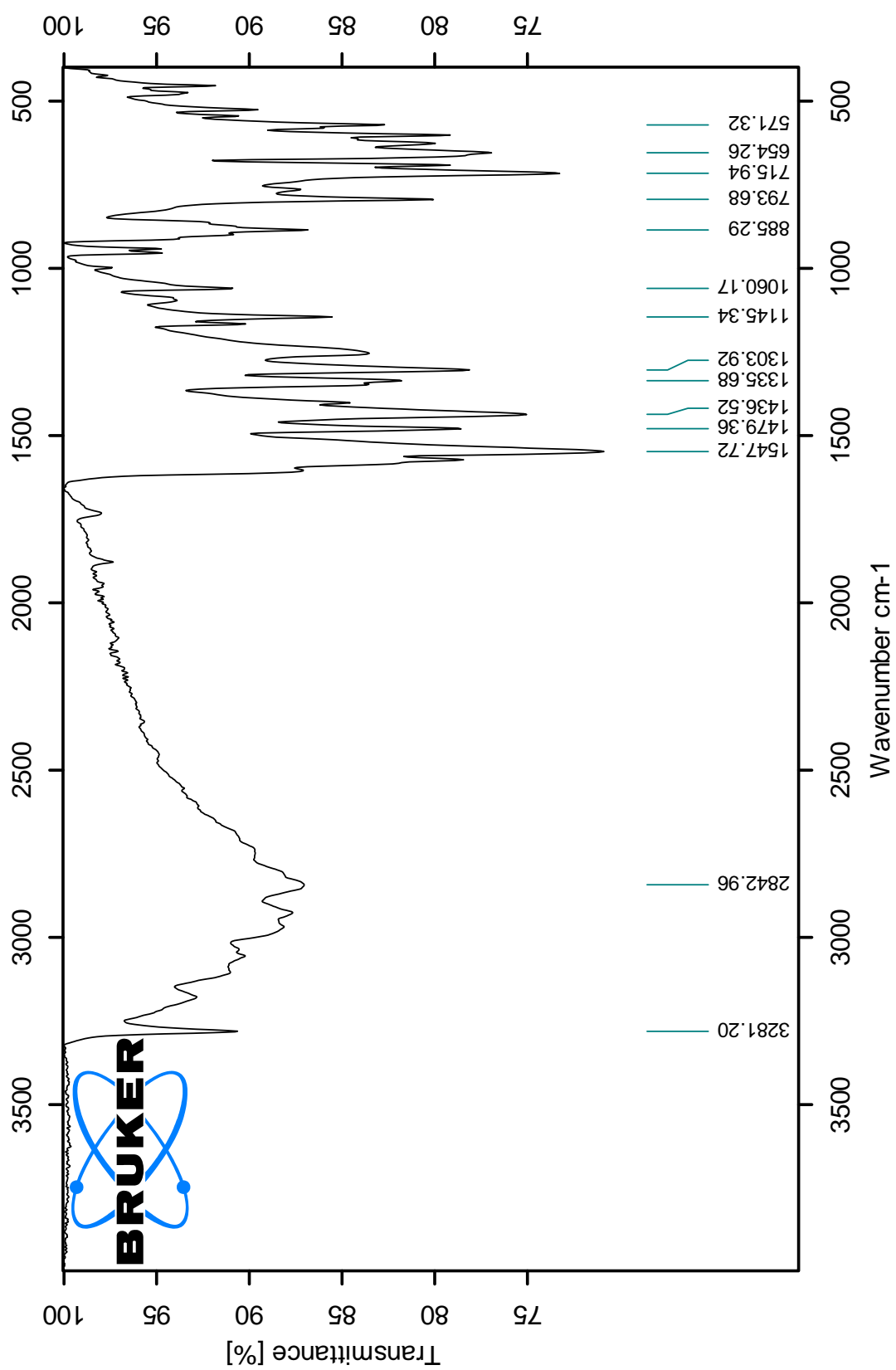


Figure I.6: IR spectrum of compound 38.

J Spectroscopic data – Compound 39

Parameter	Value
1 Data File Name	/Volumes/nmrdata/nmr400ny/hannsm/nmr/HS1-144B-10/1/fid
2 Title	HS1-144B-10.1.fid
3 Comment	
4 Origin	Bruker BioSpin GmbH
5 Owner	nmsu
6 Site	
7 Instrument	spect
8 Author	
9 Solvent	DMSO
10 Temperature	298.0
11 Pulse Sequence	zg30
12 Experiment	1D
13 Probe	Z116098_0398 (PA BBO 400S1 BBF-H-D-05 Z SP)
14 Number of Scans	8
15 Receiver Gain	128.1
16 Relaxation Delay	1.0000
17 Pulse Width	9.5000
18 Presaturation Frequency	
19 Acquisition Time	4.0894
20 Acquisition Date	2023-03-10T02:27:39
21 Modification Date	2023-03-10T02:27:39
22 Class	
23 Spectrometer Frequency	400.13
24 Spectral Width	8012.8
25 Lowest Frequency	-1535.4
26 Nucleus	¹ H
27 Acquired Size	32768
28 Spectral Size	65536
29 Digital Resolution	0.12

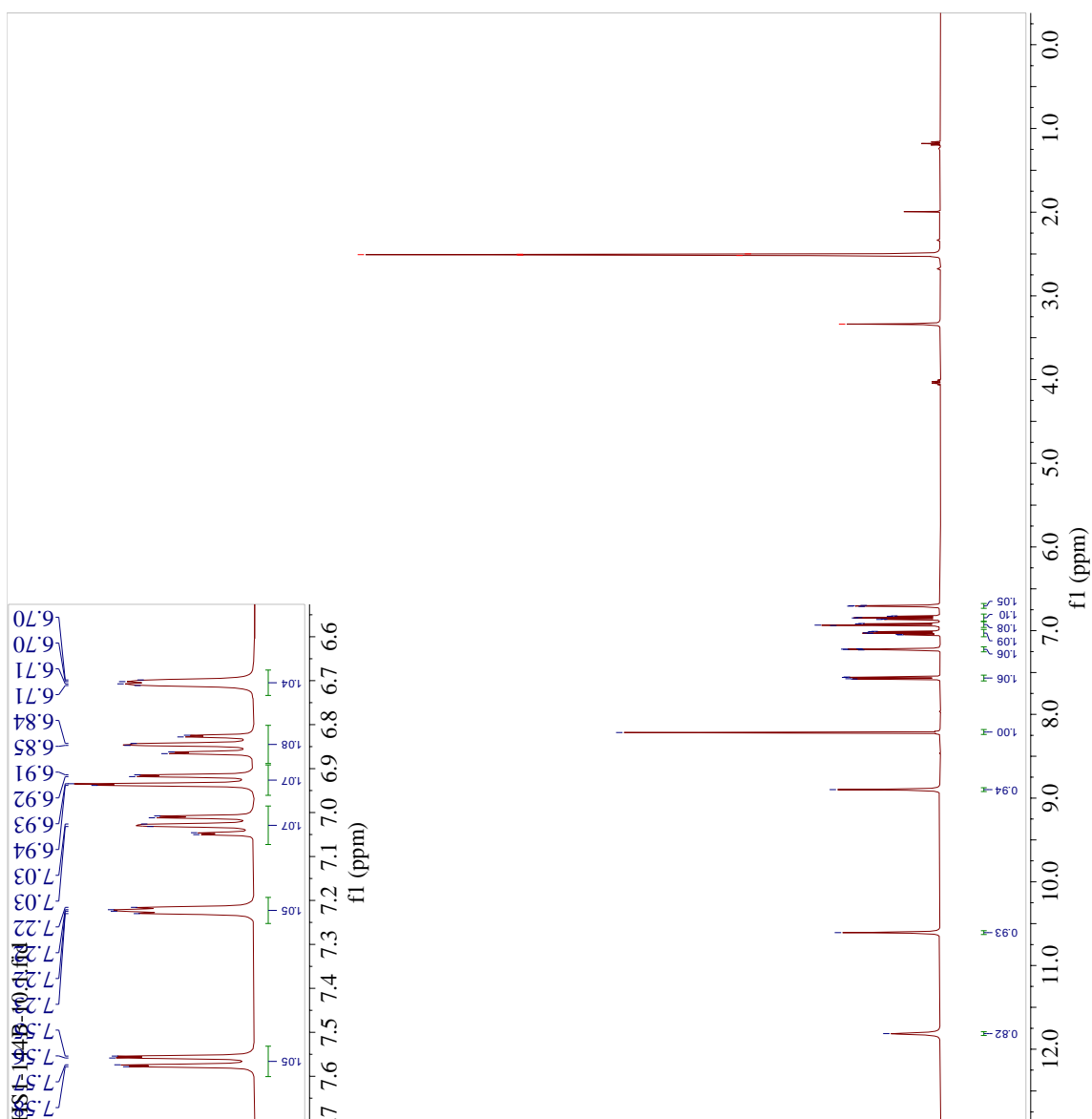
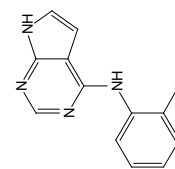


Figure J.1: ¹H-NMR spectrum of compound 39.

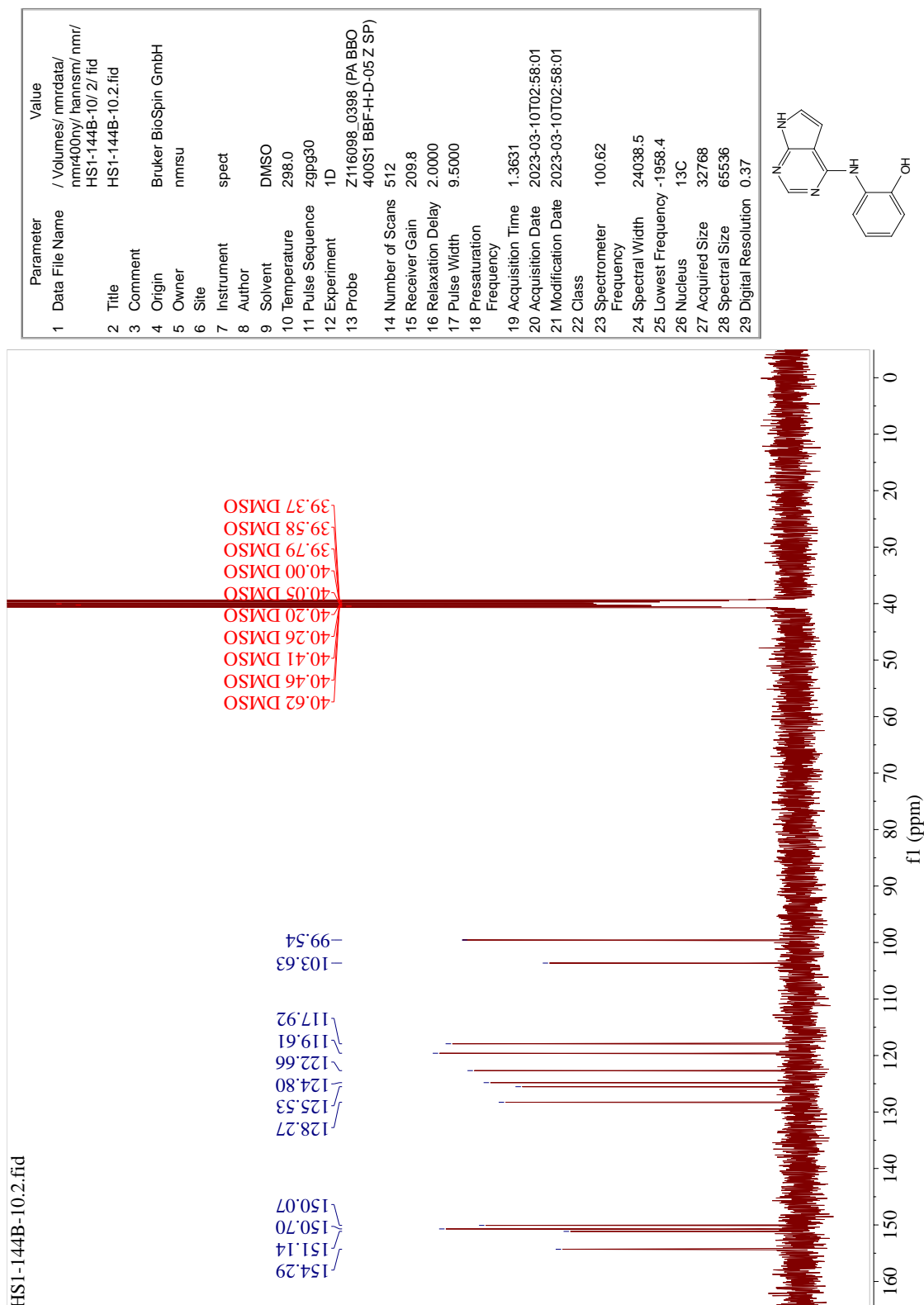


Figure J.2: ^{13}C -NMR spectrum of compound 39.

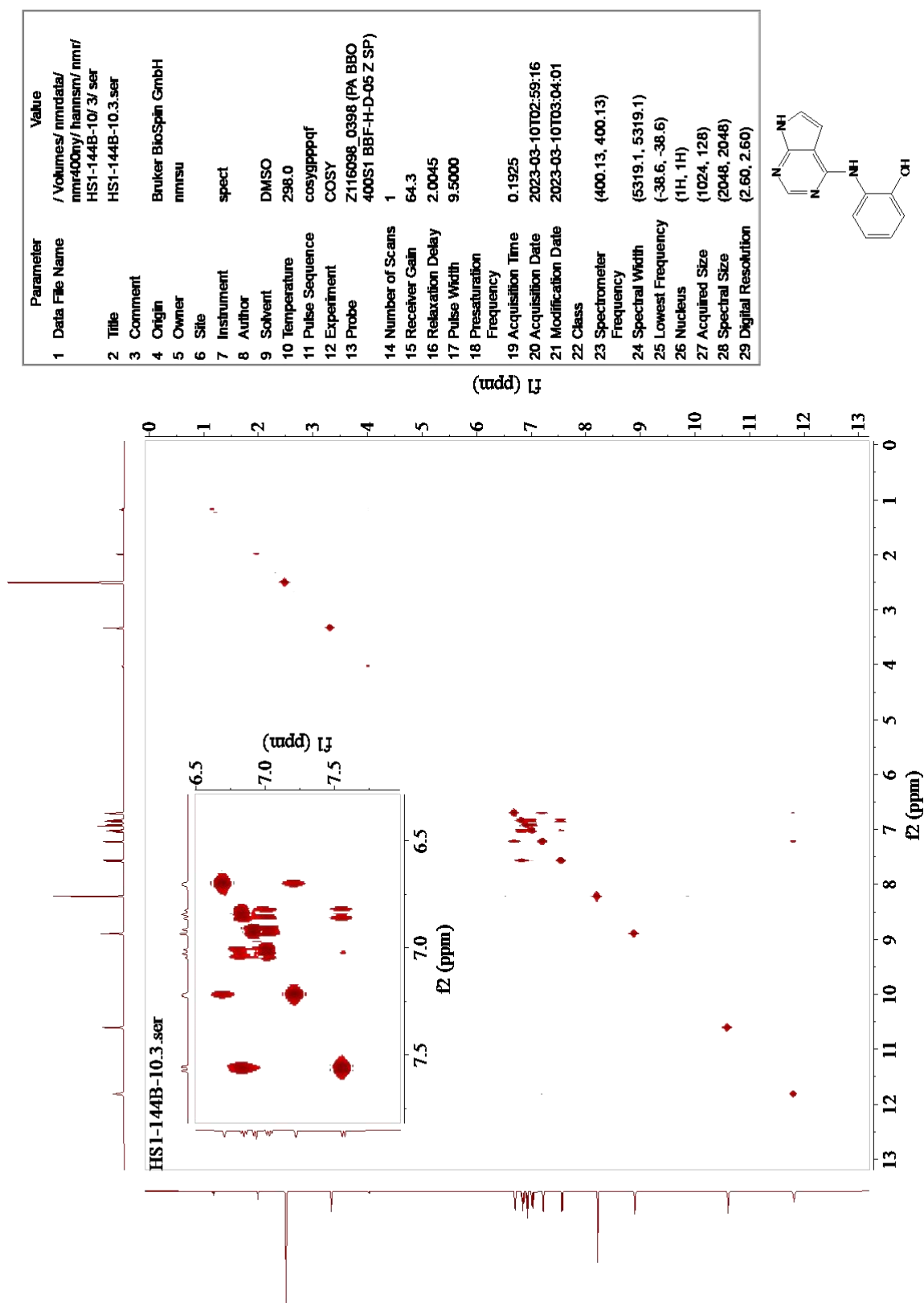


Figure J.3: COSY spectrum of compound 39.

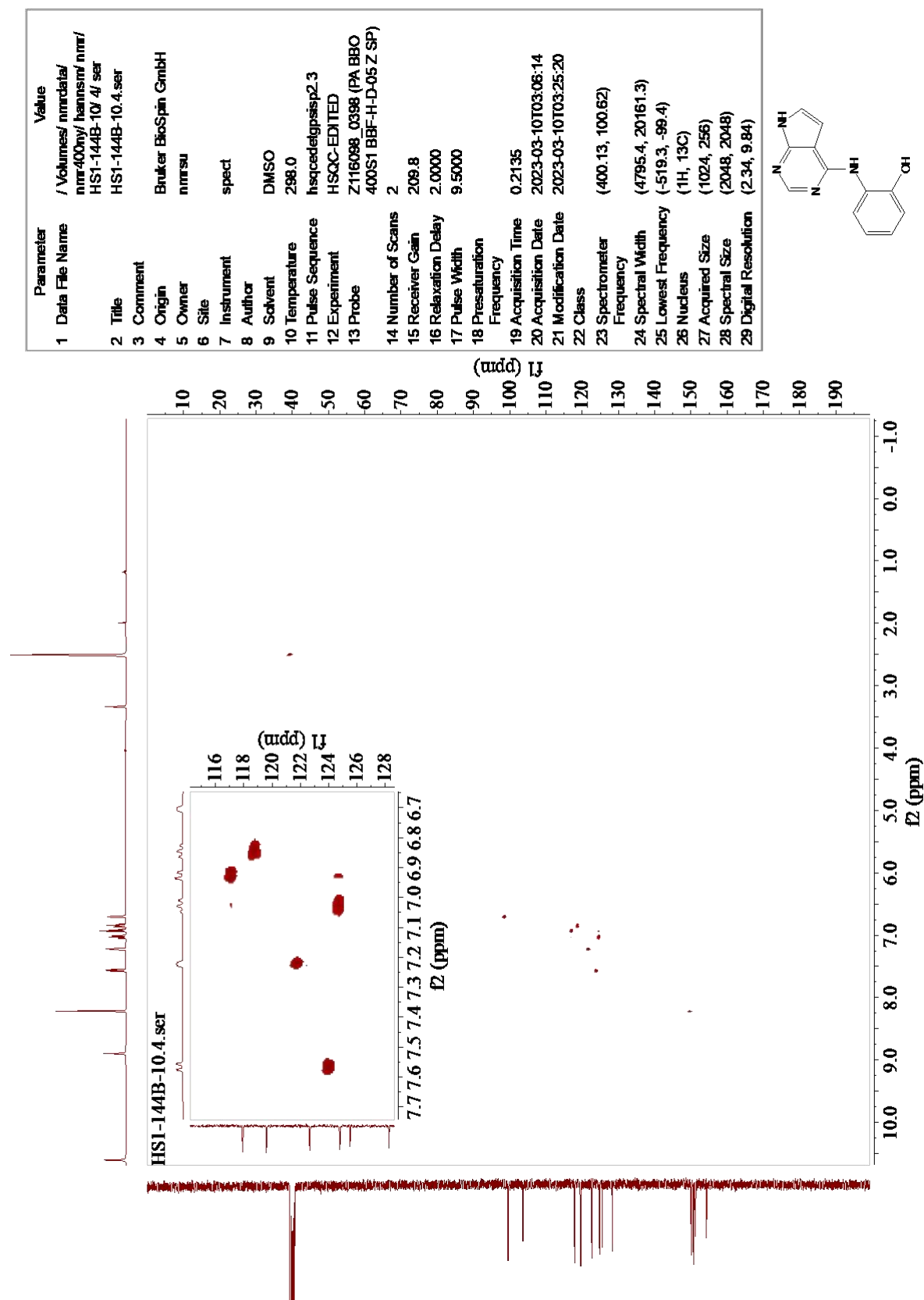
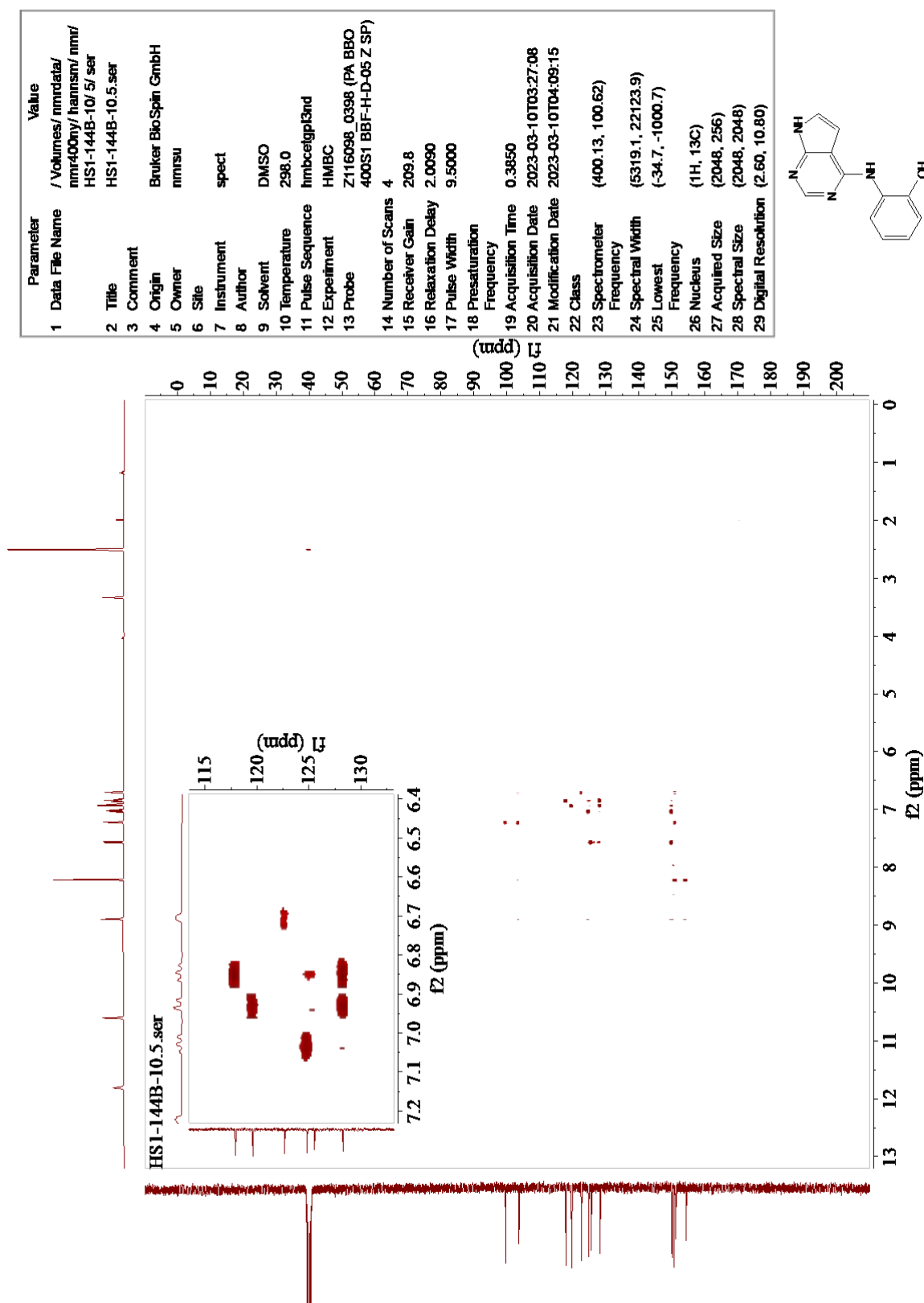


Figure J.4: HSQC spectrum of compound 39.



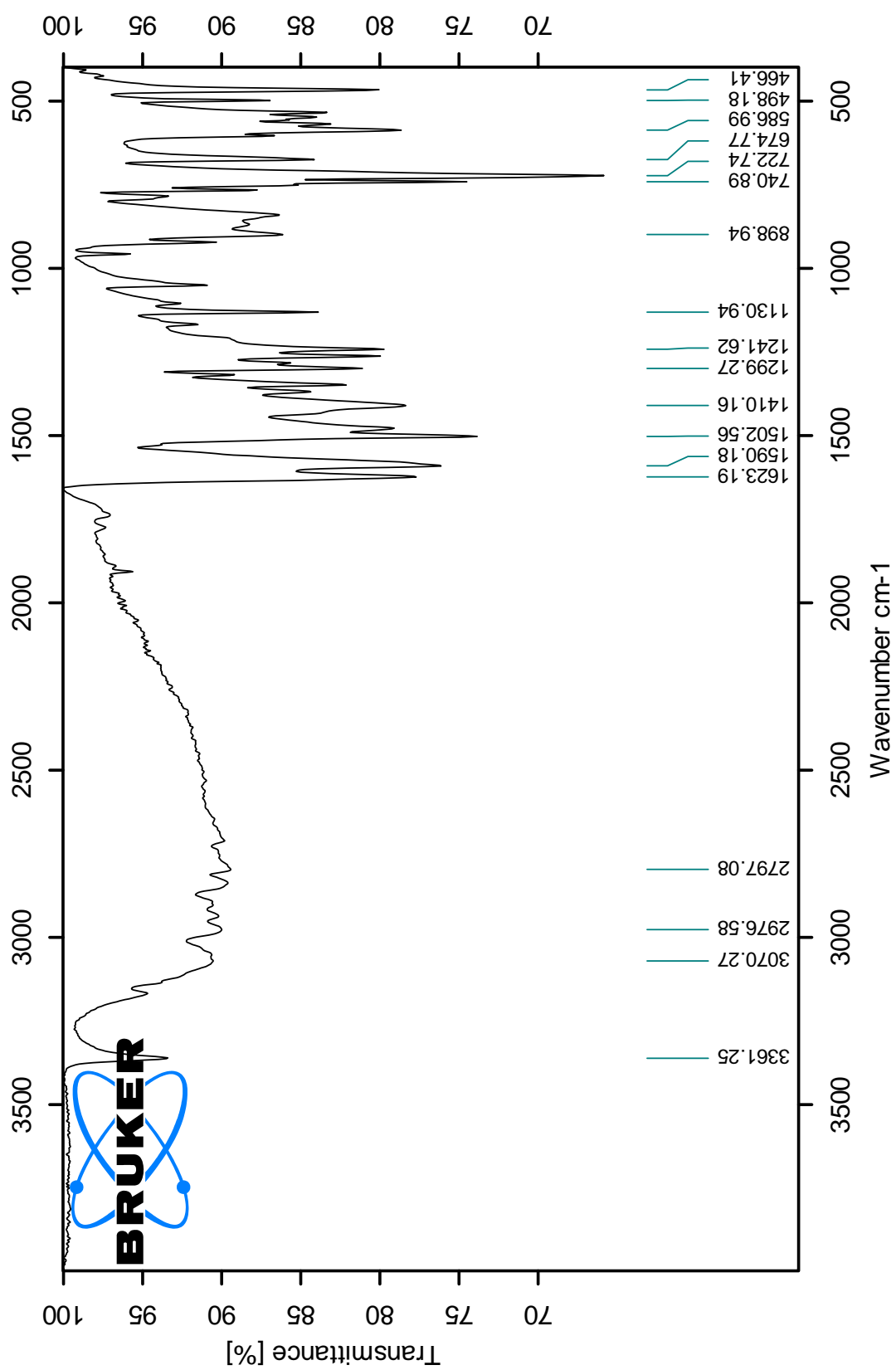


Figure J.6: IR spectrum of compound 39.

Elemental Composition Report

Single Mass Analysis

Tolerance = 5.0 PPM / DBE: min = -1.5, max = 50.0

Element prediction: Off

Number of isotope peaks used for i-FIT = 3

Monoisotopic Mass, Even Electron Ions

165 formula(e) evaluated with 1 results within limits (up to 50 closest results for each mass)

Elements Used:

C: 0-60 H: 1-1000 N: 0-8 O: 0-6

REQID2151 71 (0.674) AM2 (Ar:35000.0,0.00,0.00); Cm (71)

1: TOF MS ES+

3.21e+004

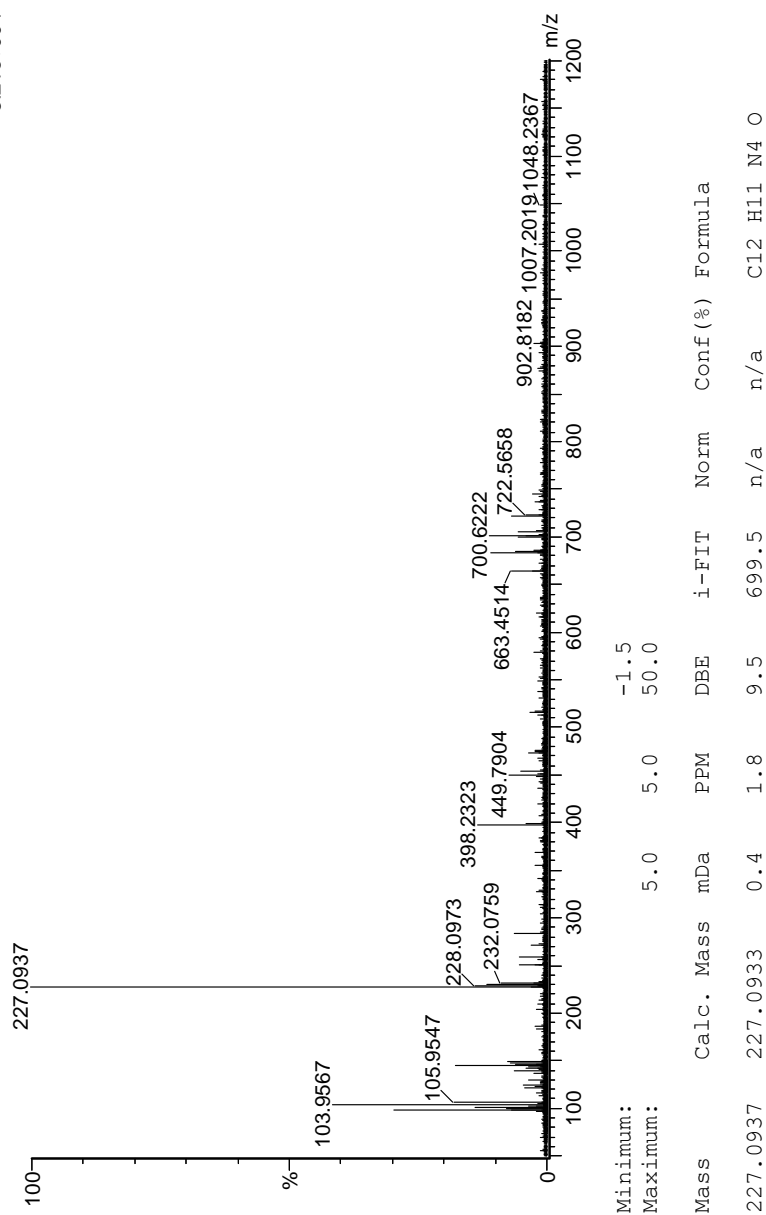
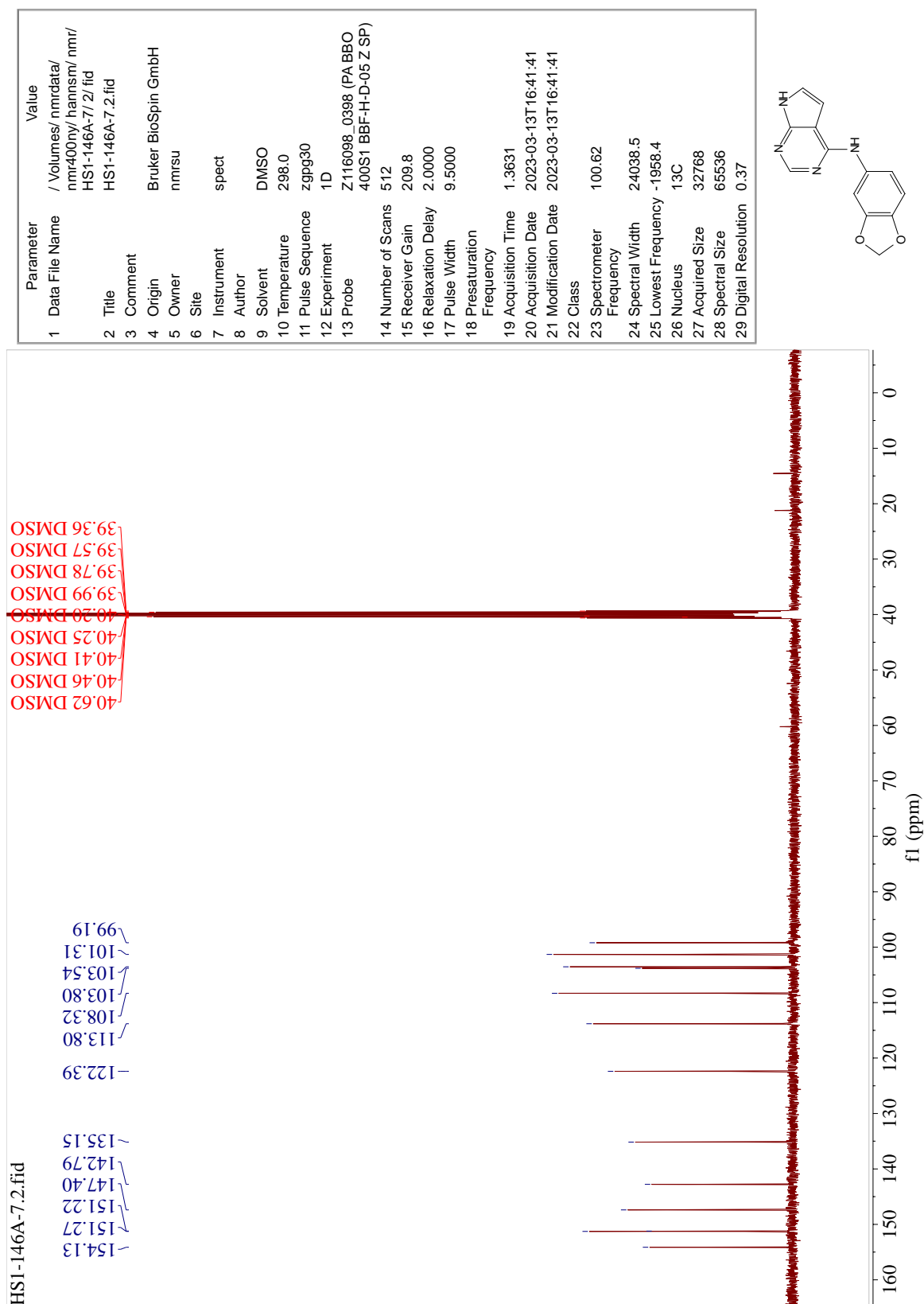


Figure J.7: MS spectrum of compound 39.

Figure K.2: ¹³C-NMR spectrum of compound 41.

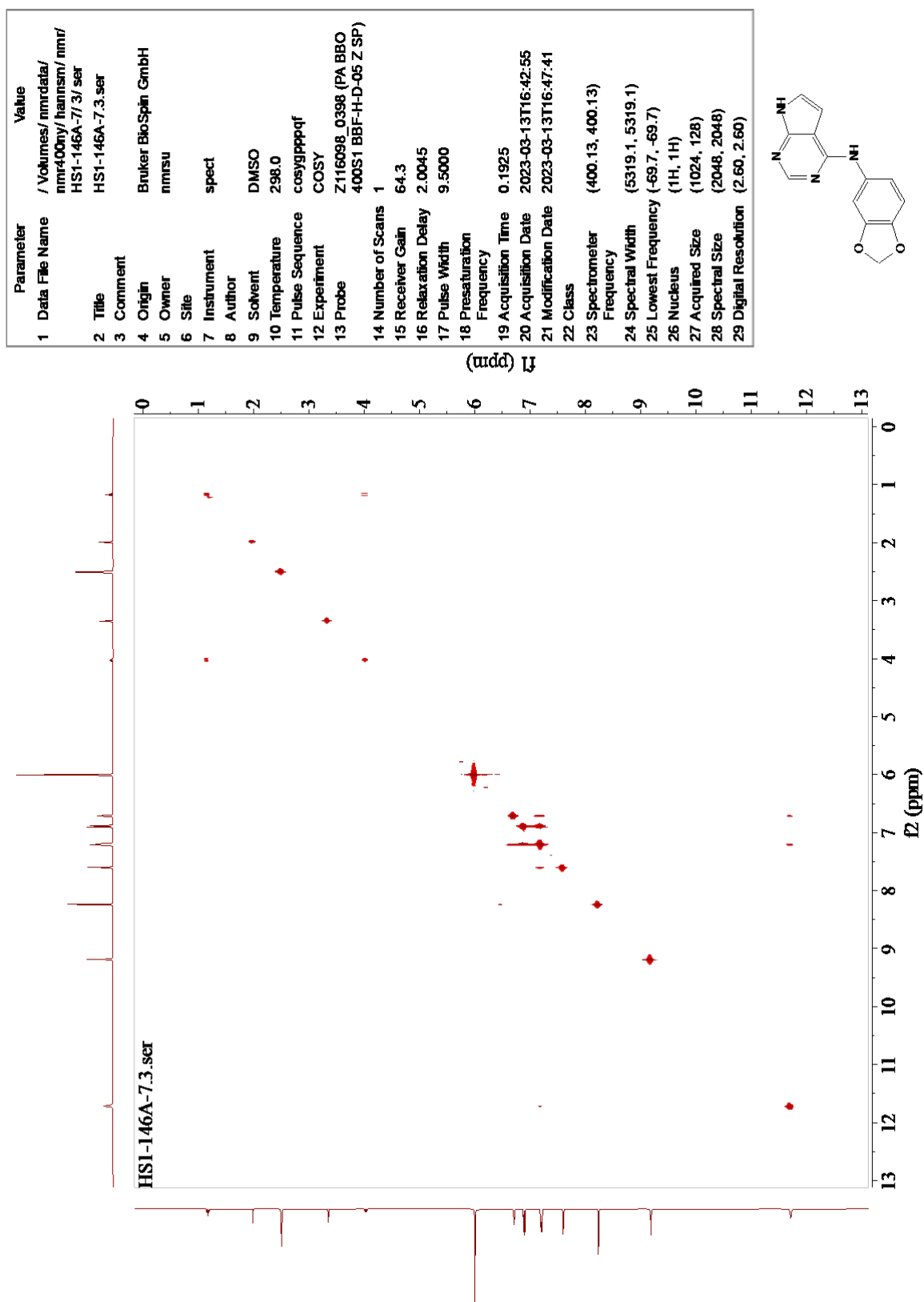
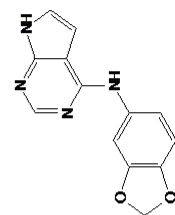
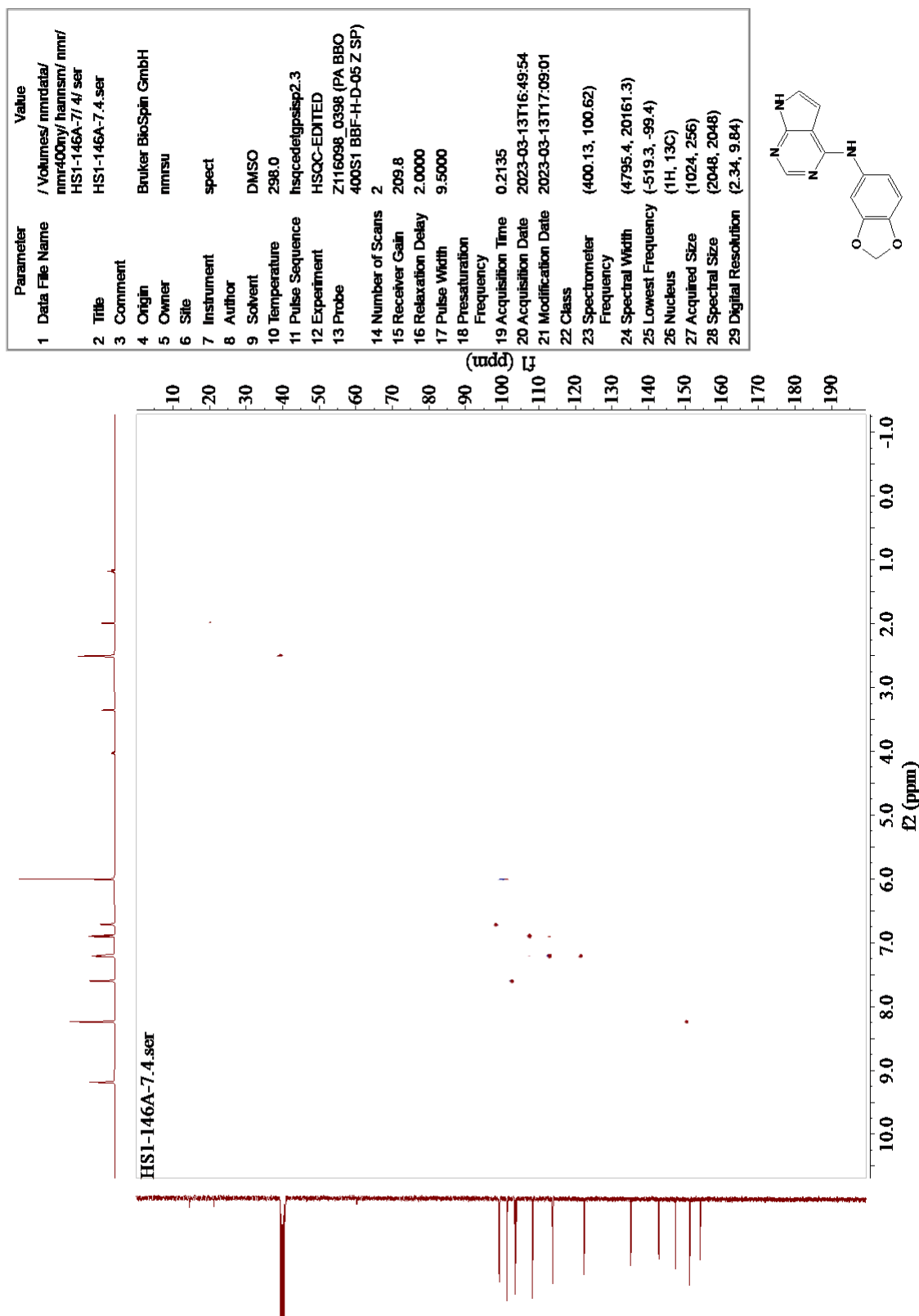


Figure K.3: COSY spectrum of compound 41.



Parameter	Value
1 Data File Name	/Volumes/nmrdata/nmr400ny/hansim/nmr/HS1-146A-7/5/ ser HS1-146A-7.5.ser
2 Title	HS1-146A-7.5.ser
3 Comment	
4 Origin	Bruker BioSpin GmbH
5 Owner	nmrsu
6 Site	
7 Instrument	spect
8 Author	
9 Solvent	DMSO
10 Temperature	298.0
11 Pulse Sequence	hmbcctgpl3nd
12 Experiment	HMBC
13 Probe	Z116098_0388 (PA BBO 400S1 BBF-H-D-05 Z SP)
14 Number of Scans	4
15 Receiver Gain	209.8
16 Relaxation Delay	2.0090
17 Pulse Width	9.5000
18 Presaturation Frequency	
19 Acquisition Time	0.3850
20 Acquisition Date	2023-03-13T17:10:49
21 Modification Date	2023-03-13T17:52:56
22 Class	
23 Spectrometer Frequency	(400.13, 100.62)
24 Spectral Width	(5319.1, 22123.9)
25 Lowest Frequency	(-65.8, -1000.7)
26 Nucleus	(1H, 13C)
27 Acquired Size	(2048, 256)
28 Spectral Size	(2048, 2048)
29 Digital Resolution	(2.60, 10.80)

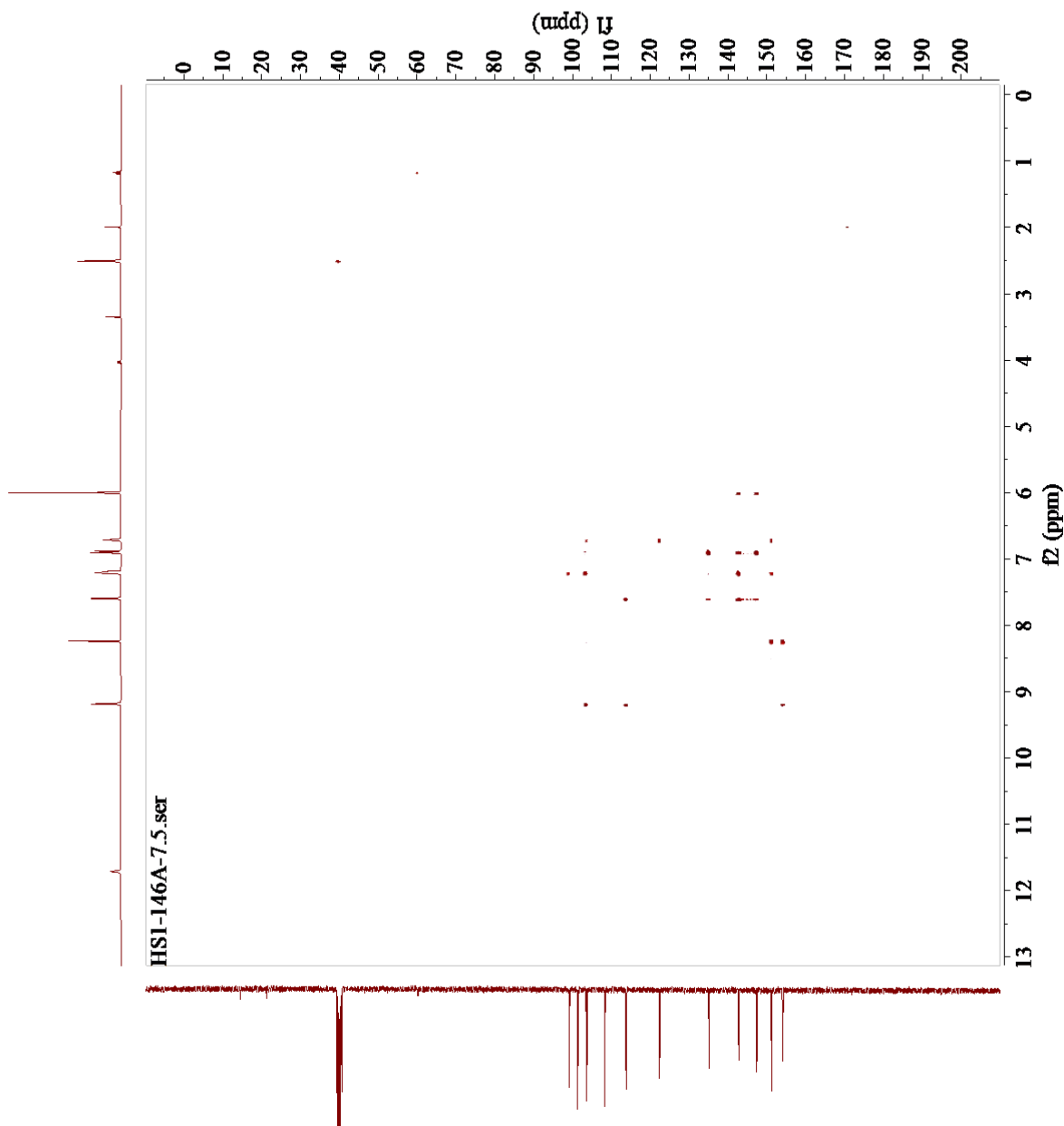
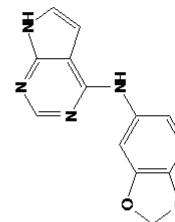


Figure K.5: HMBC spectrum of compound 41.

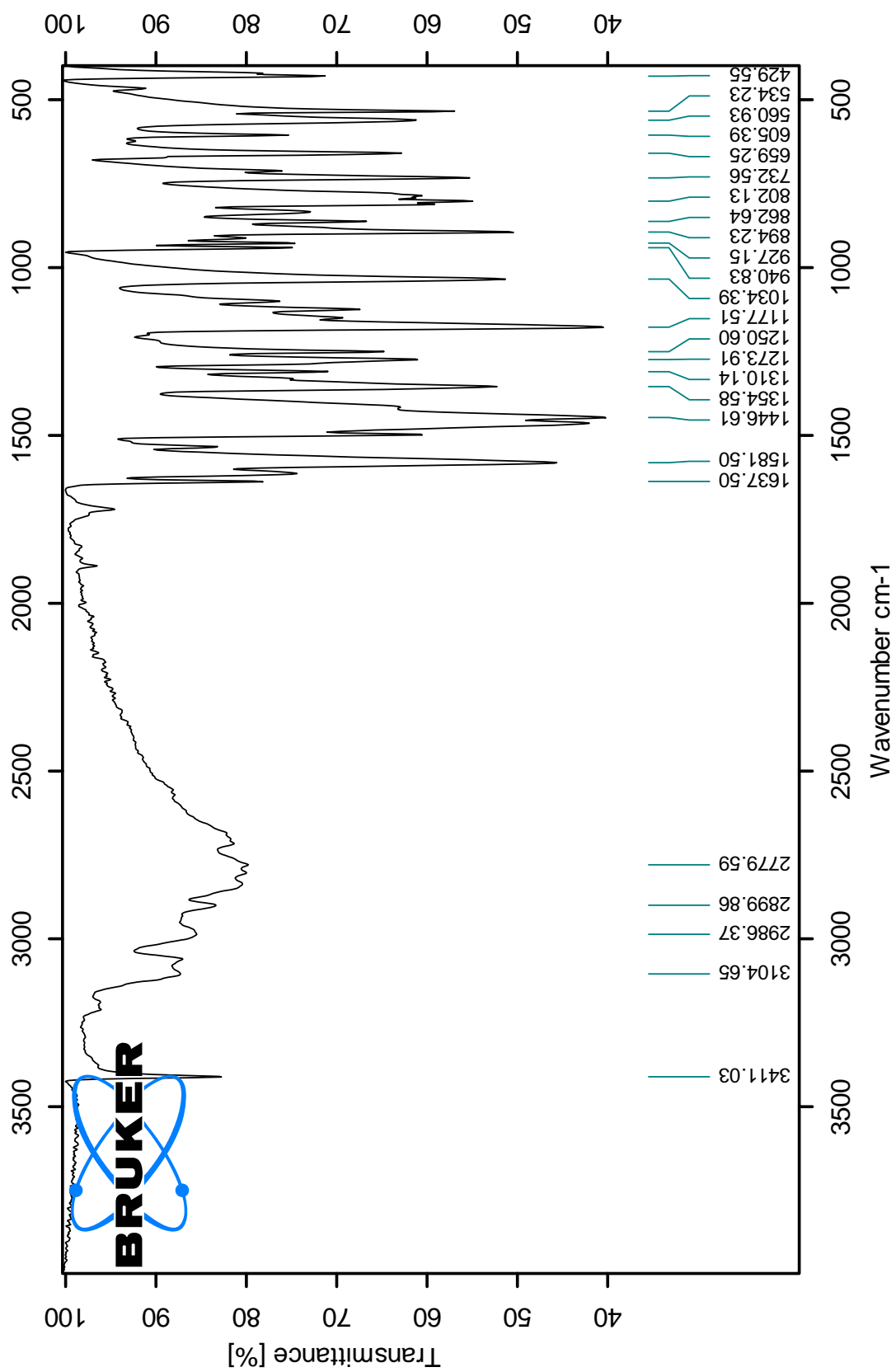


Figure K.6: IR spectrum of compound 41.

Elemental Composition Report

Single Mass Analysis

Tolerance = 6.0 PPM / DBE: min = -1.5, max = 50.0

Element prediction: Off

Number of isotope peaks used for i-FIT = 3

Monoisotopic Mass, Even Electron Ions

367 formula(e) evaluated with 2 results within limits (up to 50 closest results for each mass)

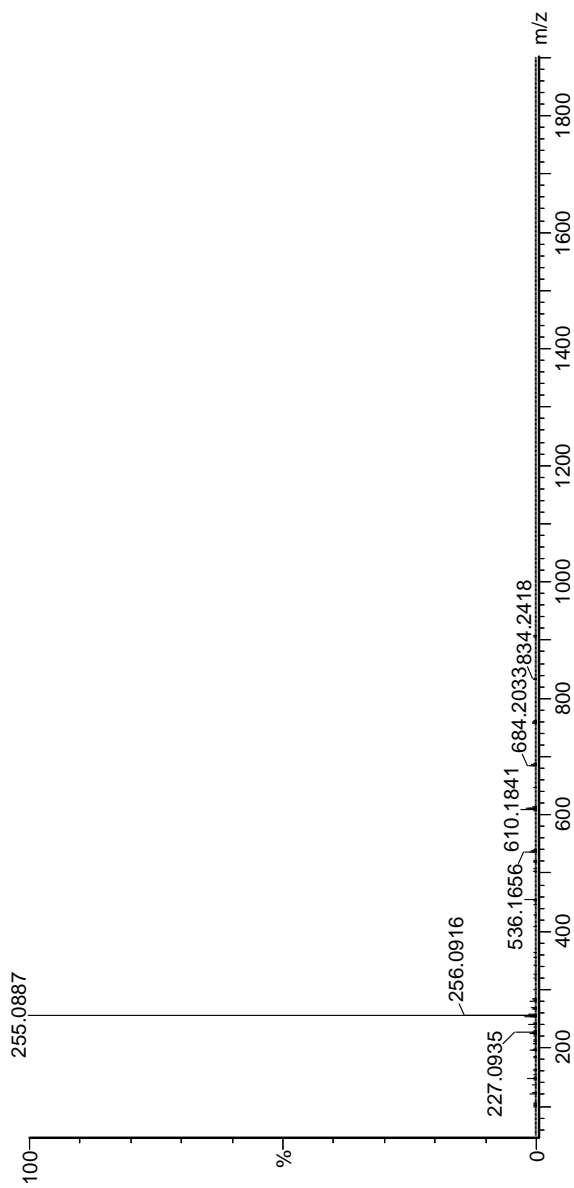
Elements Used:

C: 0-60 H: 1-1000 N: 0-5 O: 0-50 Na: 0-1

RegID: 2198.96 (1.082) AM2 (Ar: 35000.0, 0.00, 0.00); Cm (93:96)

1: TOF MS ES+

2.90e+006



Minimum: -1.5
Maximum: 50.0

Mass	Calc. Mass	mDa	PPM	DBE	i-FIT	Norm	Conf (%)	Formula
255.0887	255.0882	0.5	2.0	10.5	1349.7	0.004	99.60	C13 H11 N4 O2
255.0898	-1.1	-4.3	-4.3	11.5	1355.2	5.522	0.40	C16 H12 N2 Na

Figure K.7: MS spectrum of compound 41.

L Spectroscopic data – Compound 42

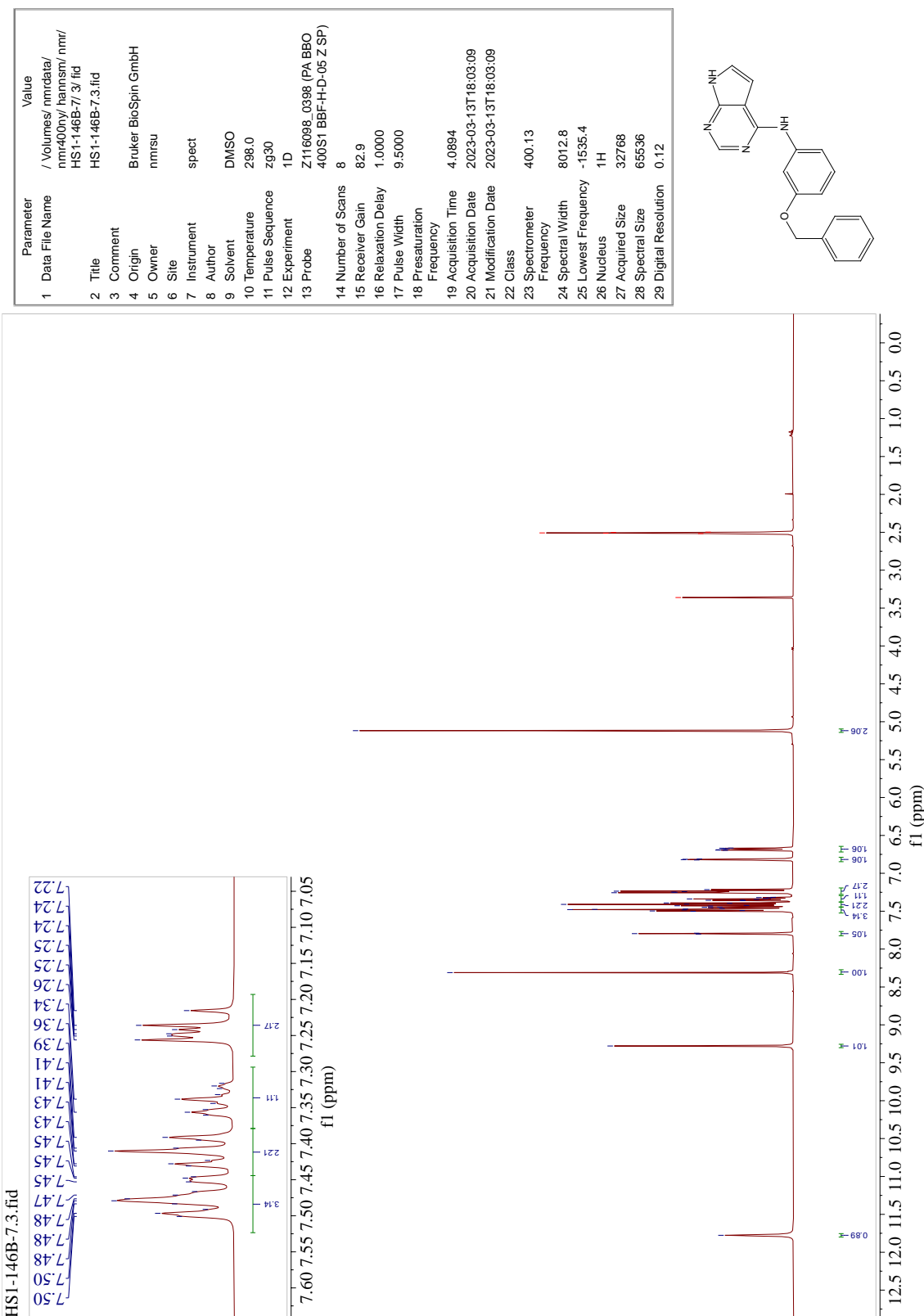


Figure L.1: ¹H-NMR spectrum of compound 42.

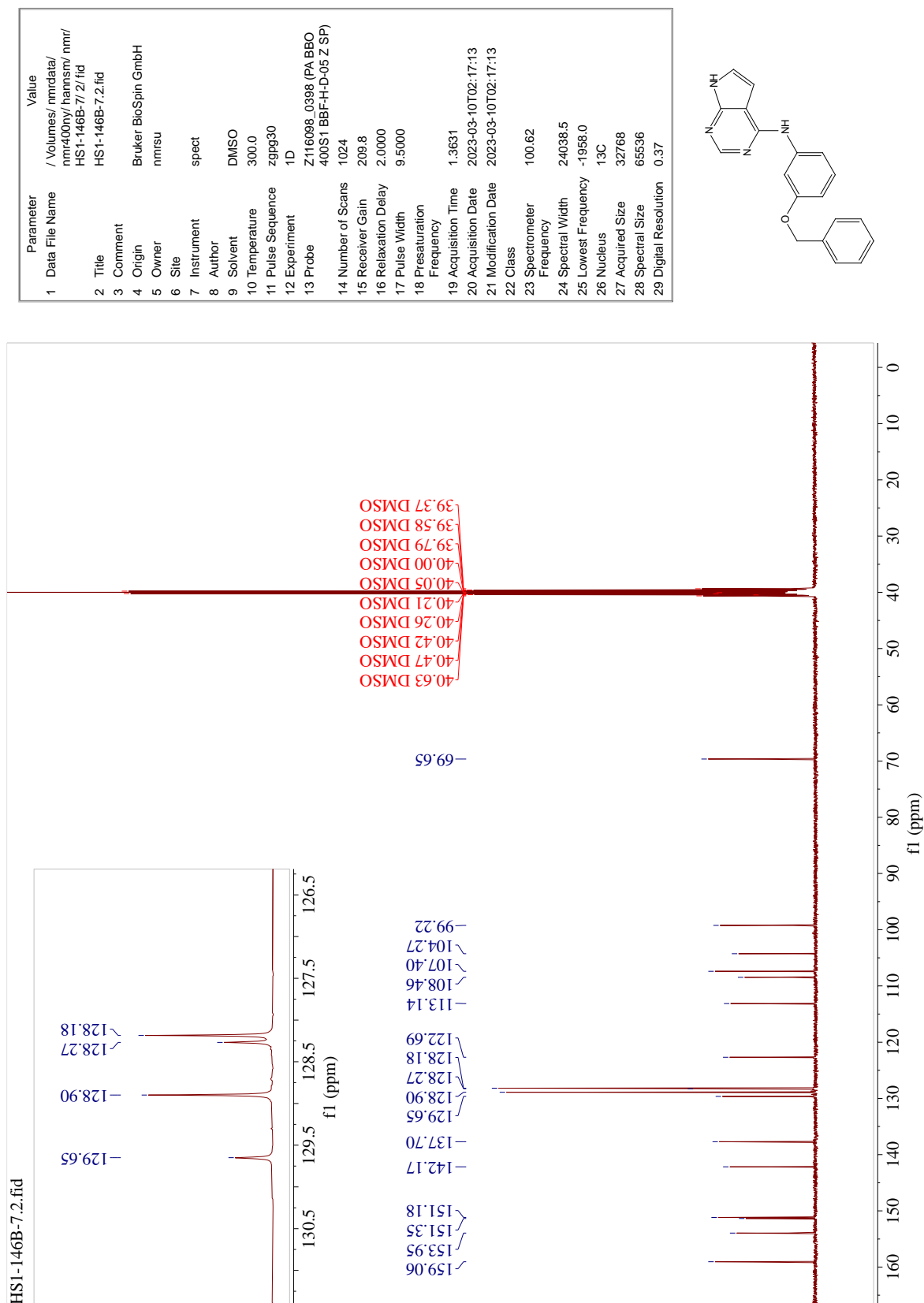


Figure L.2: ¹³C-NMR spectrum of compound 42.

Parameter	Value
1 Data File Name	/Volumes/nmrdata/nmr400ny/hanssm/nmr/HS1-146B-7.5/ser
2 Title	HS1-146B-7.5.ser
3 Comment	
4 Origin	Bruker Bio-Spin GmbH
5 Owner	nmrsu
6 Site	
7 Instrument	spect
8 Author	
9 Solvent	DMSO
10 Temperature	298.0
11 Pulse Sequence	cosyppppf
12 Experiment	COSY
13 Probe	Z116098_0398 (PA BBO 400S1 BBF-H.D-05 Z SP)
14 Number of Scans	1
15 Receiver Gain	45.5
16 Relaxation Delay	2.0066
17 Pulse Width	9.5000
18 Pressurization Frequency	
19 Acquisition Time	0.1905
20 Acquisition Date	2023-03-13T18:34:51
21 Modification Date	2023-03-13T18:39:37
22 Class	
23 Spectrometer Frequency	(400.13, 400.13)
24 Spectral Width	(5376.3, 5376.3)
25 Lowest Frequency	(-97.0, -97.0)
26 Nucleus	(1H, 1H)
27 Acquired Size	(1024, 128)
28 Spectral Size	(2048, 2048)
29 Digital Resolution	(2.63, 2.63)

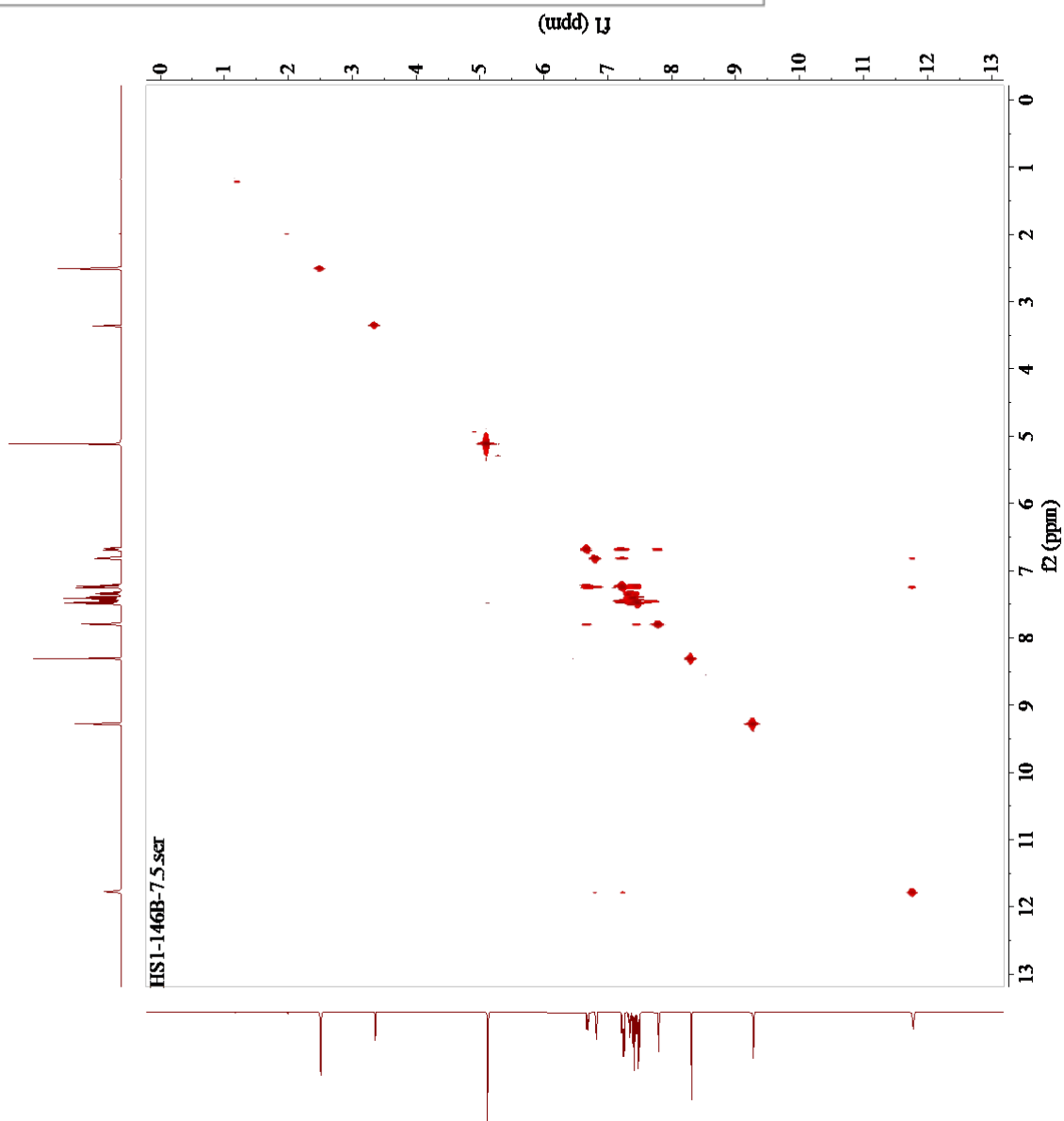
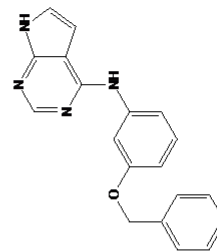


Figure L.3: COSY spectrum of compound 42.

Parameter	Value
1 Data File Name	/Volumes/nmrdata/nmr400m/kanusan/nmr/HS1-146B-7f.6.ser
2 Title	HS1-146B-7f.6.ser
3 Comment	
4 Origin	Bruker BioSpin GmbH
5 Owner	nimsu
6 Site	
7 Instrument	spect
8 Author	
9 Solvent	DMSO
10 Temperature	298.0
11 Pulse Sequence	hsqclegpsp2.3
12 Experiment	HSQC-EDITED
13 Probe	Z116098_0388 (PX BBO 400S1 BBE-HD-05 Z SPT)
14 Number of Scans	2
15 Receiver Gain	209.8
16 Relaxation Delay	2.0000
17 Pulse Width	9.5000
18 Presaturation Frequency	
19 Acquisition Time	0.2135
20 Acquisition Date	2023-03-13T18:41:50
21 Modification Date	2023-03-13T19:00:56
22 Class	
23 Spectrometer Frequency	(400.13, 100.62)
24 Spectral Width	(4795.4, 20161.3)
25 Lowest Frequency	(-519.3, -99.4)
26 Nucleus	(1H, 13C)
27 Acquired Size	(1024, 256)
28 Spectral Size	(2048, 2048)
29 Digital Resolution	(2.34, 9.84)

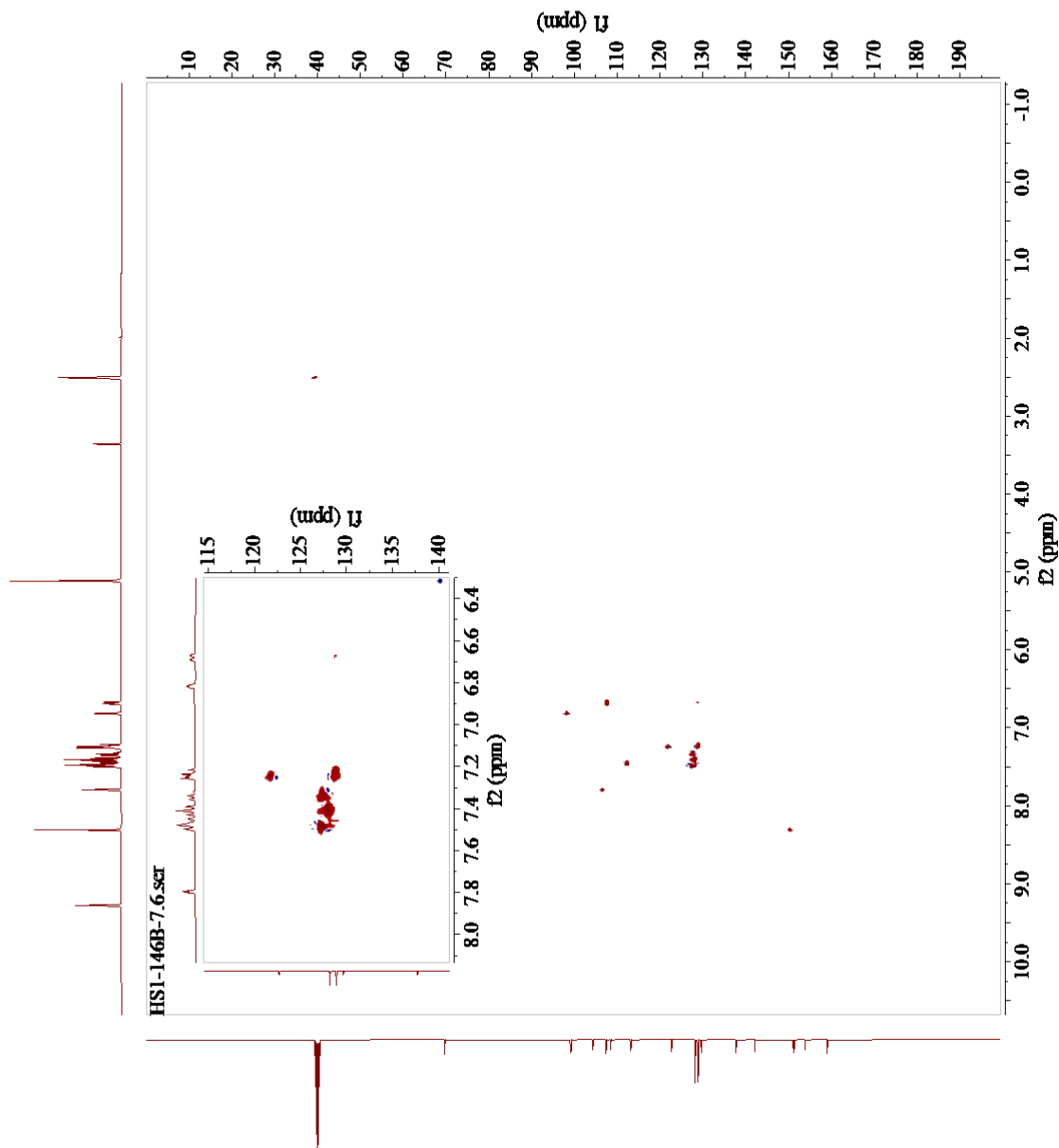
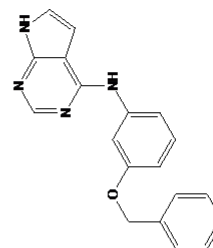


Figure L.4: HSQC spectrum of compound 42.

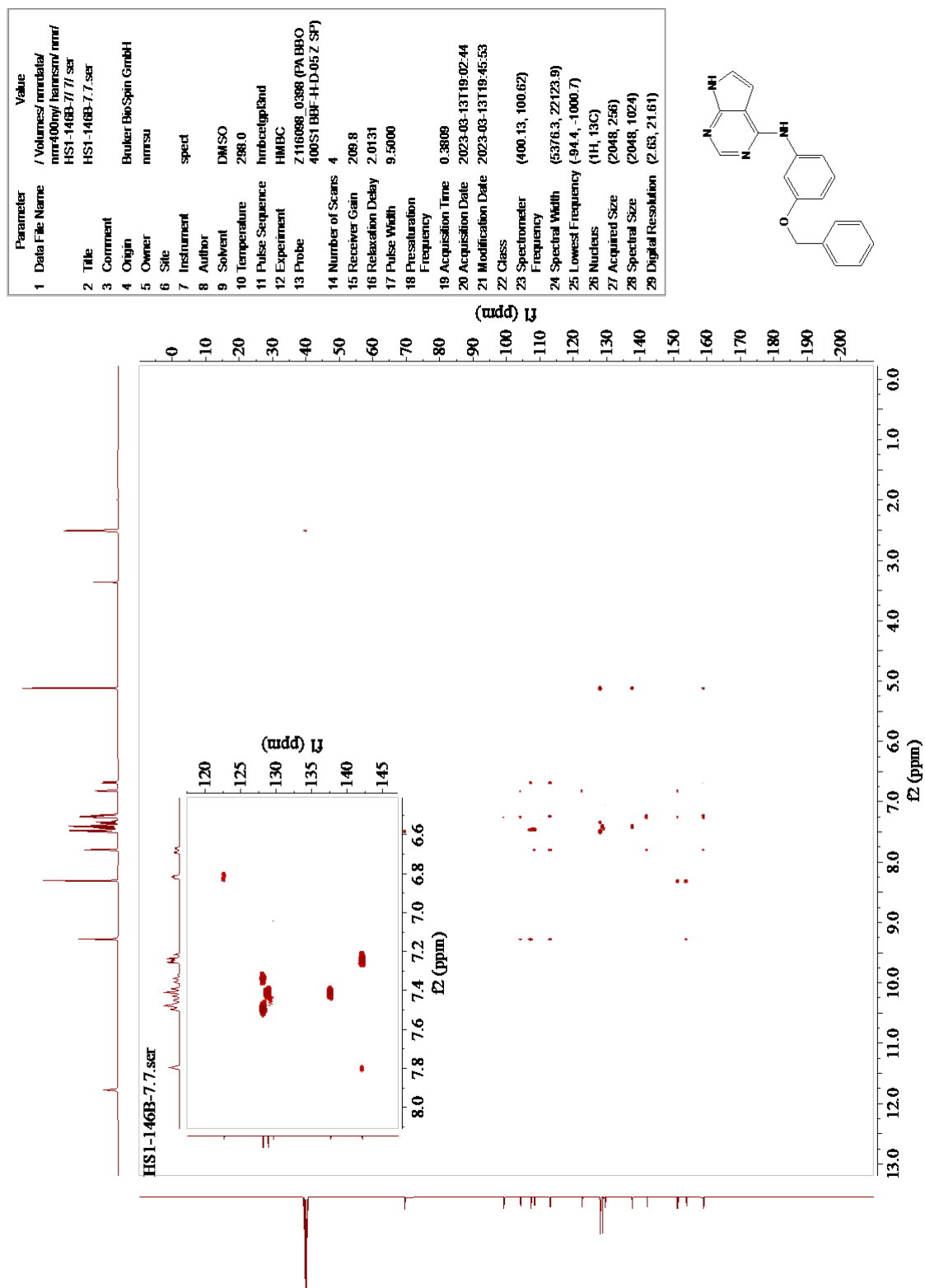


Figure L.5: HMBC spectrum of compound 42.

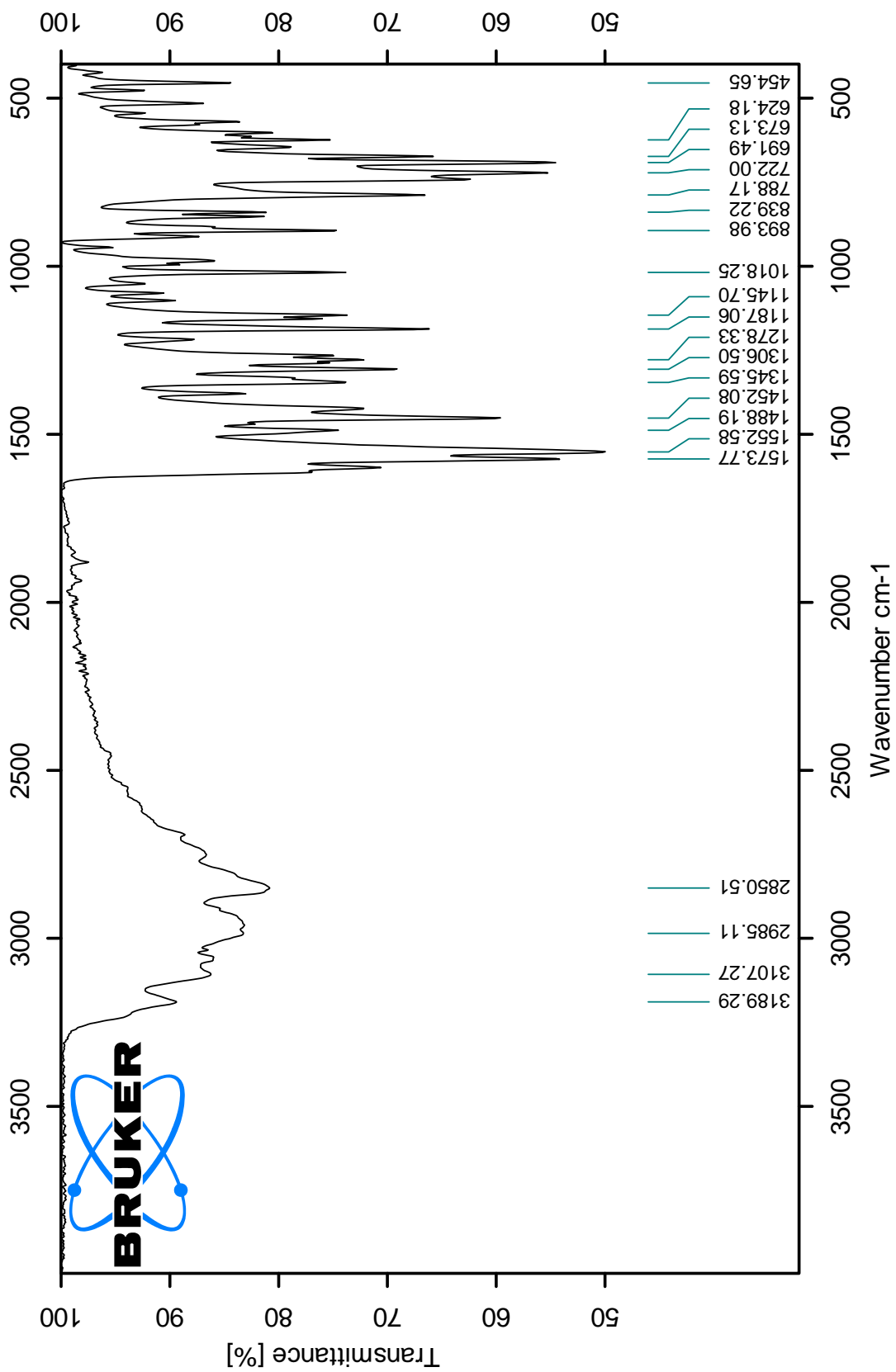


Figure L.6: IR spectrum of compound 42.

Elemental Composition Report

Single Mass Analysis

Tolerance = 3.0 PPM / DBE: min = -1.5, max = 50.0
 Element prediction: Off
 Number of isotope peaks used for i-FIT = 3

Monoisotopic Mass, Even Electron Ions
 548 formula(e) evaluated with 1 results within limits (up to 50 closest results for each mass)
 Elements Used:
 C: 0-60 H: 1-1000 N: 0-5 O: 0-50 Na: 0-1
 ReqID2199.67 (0.762) AM2 (Ar,35000.0,0.00,0.00); Cm (63:68)
 1: TOF MS ES+

2.53e+006

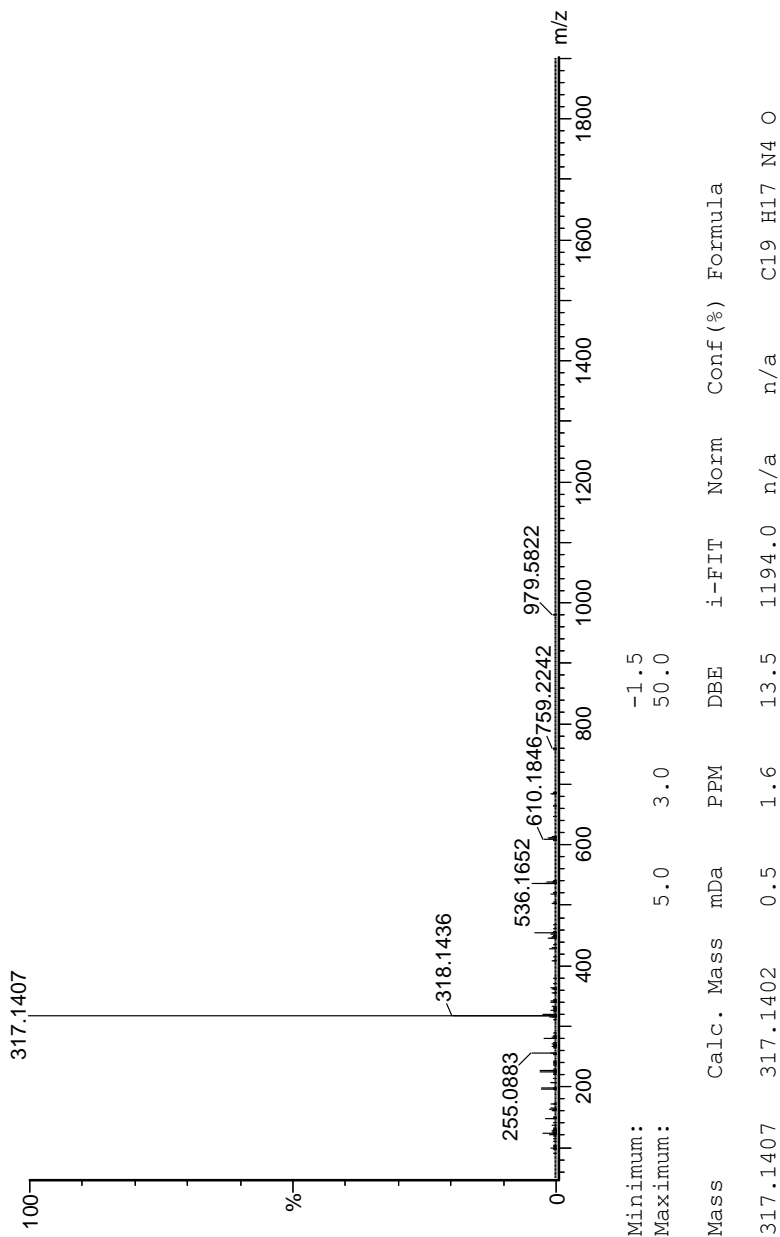


Figure L.7: MS spectrum of compound 42.

M Spectroscopic data – Compound 43

Parameter	Value
1 Data File Name	/Volumes/nmrdata/nmr400ny/hannsm/nmr/HS1-130-5/1.fid
2 Title	HS1-130-5.1.fid
3 Comment	
4 Origin	Bruker BioSpin GmbH
5 Owner	nmrsu
6 Site	
7 Instrument	spect
8 Author	
9 Solvent	DMSO
10 Temperature	298.3
11 Pulse Sequence	zg30
12 Experiment	1D
13 Probe	Z116098_0398 (PA BBO 400S1 BBF-H-D-05 Z SP)
14 Number of Scans	8
15 Receiver Gain	104.6
16 Relaxation Delay	1.0000
17 Pulse Width	9.5000
18 Presaturation Frequency	
19 Acquisition Time	4.0894
20 Acquisition Date	2023-02-10T16:05:24
21 Modification Date	2023-02-10T16:05:24
22 Class	
23 Spectrometer Frequency	400.13
24 Spectral Width	8012.8
25 Lowest Frequency	-1535.4
26 Nucleus	¹ H
27 Acquired Size	32768
28 Spectral Size	65536
29 Digital Resolution	0.12

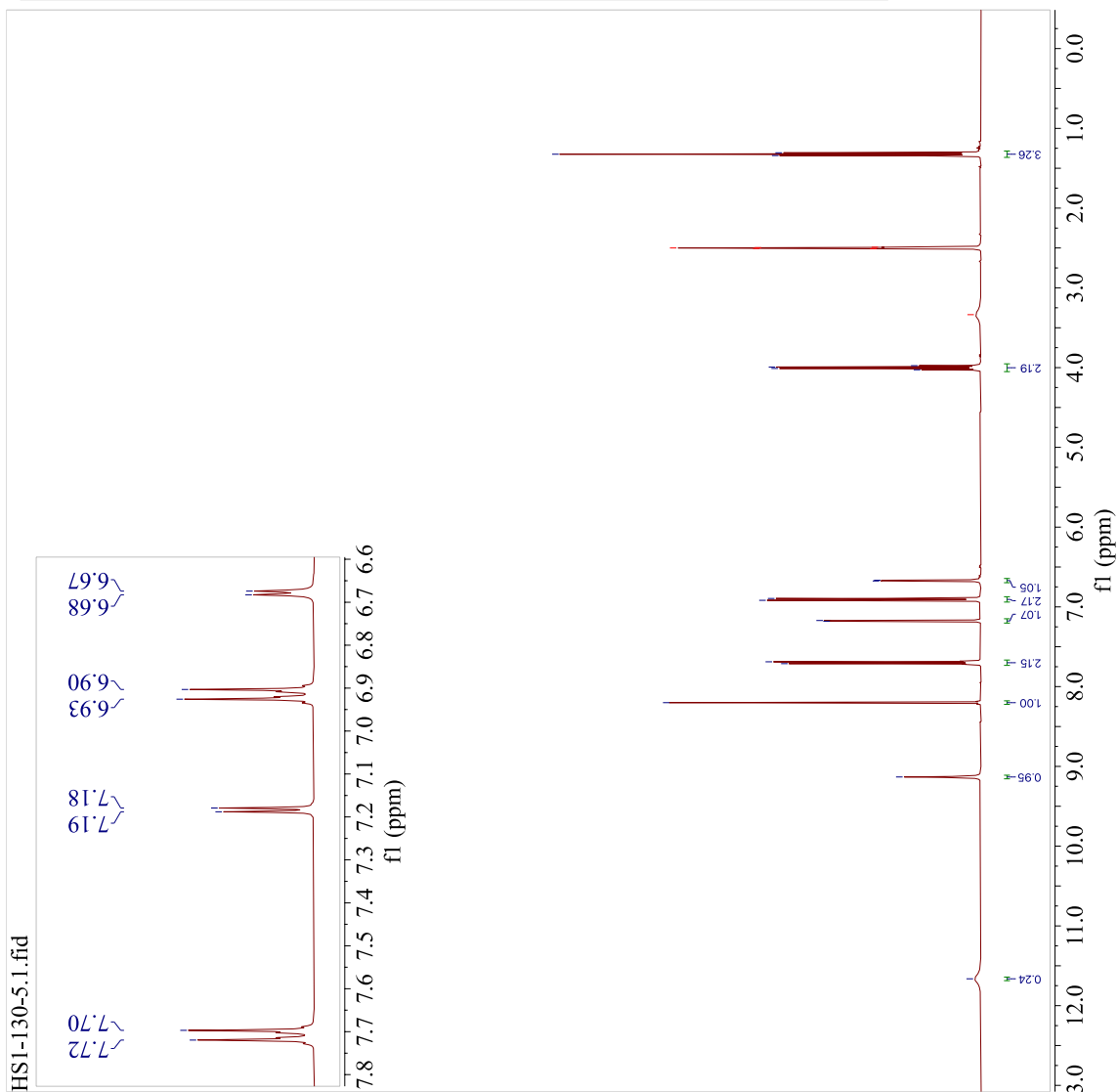
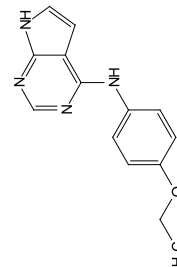


Figure M.1: ¹H-NMR spectrum of compound 43.

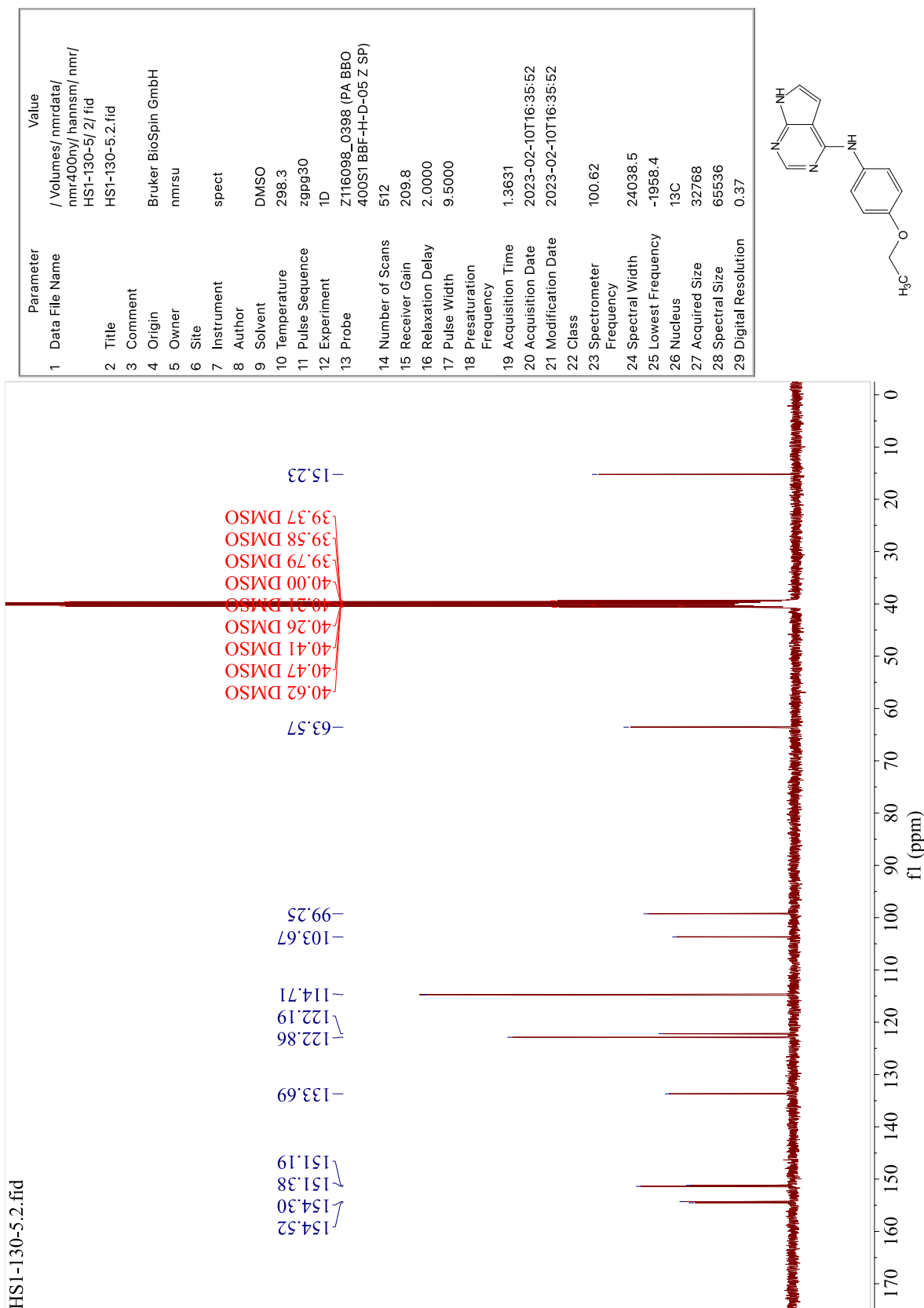


Figure M.2: ¹³C-NMR spectrum of compound 43.

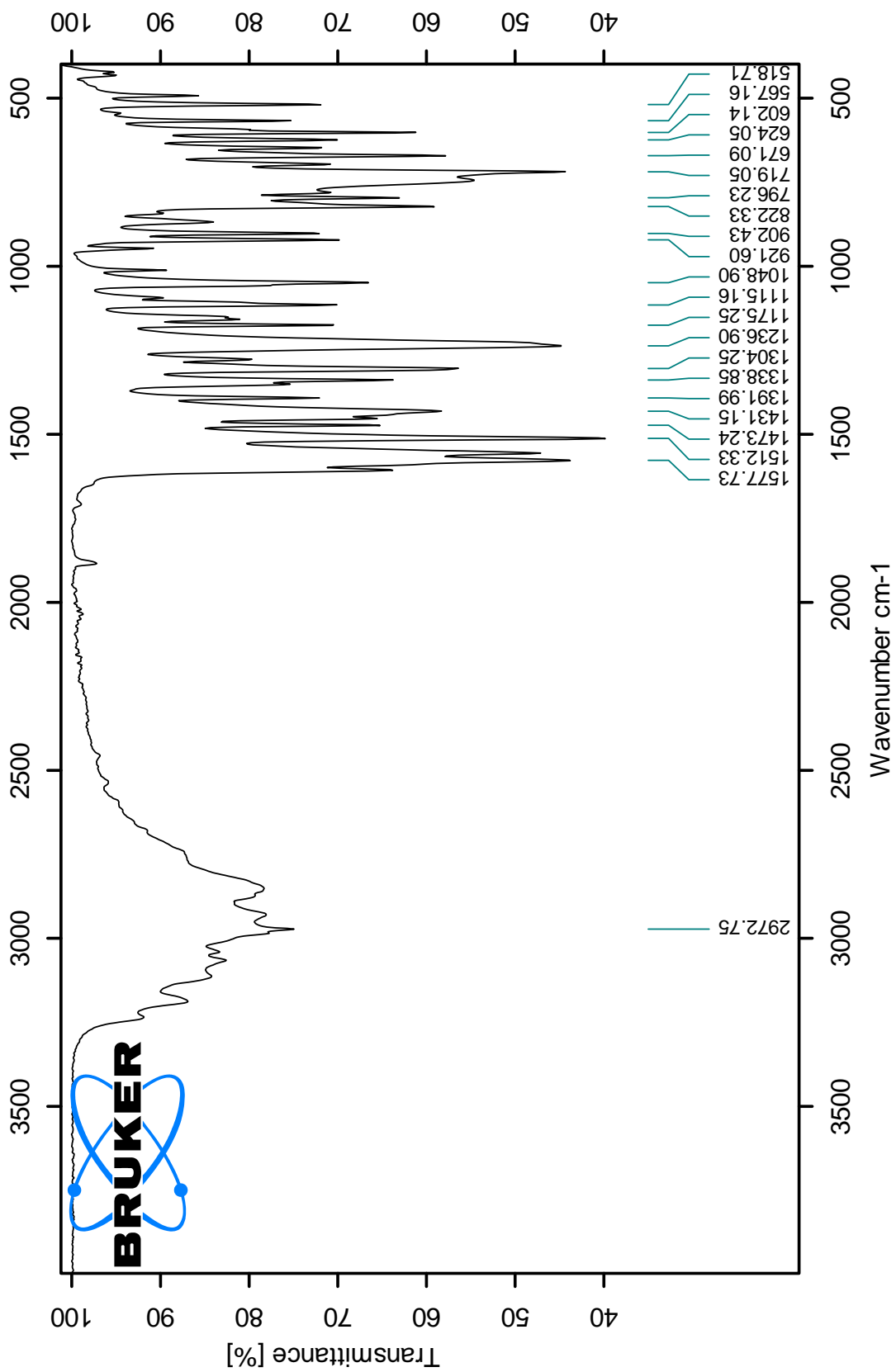


Figure M.3: IR spectrum of compound 43.

N Spectroscopic data – Compound 46

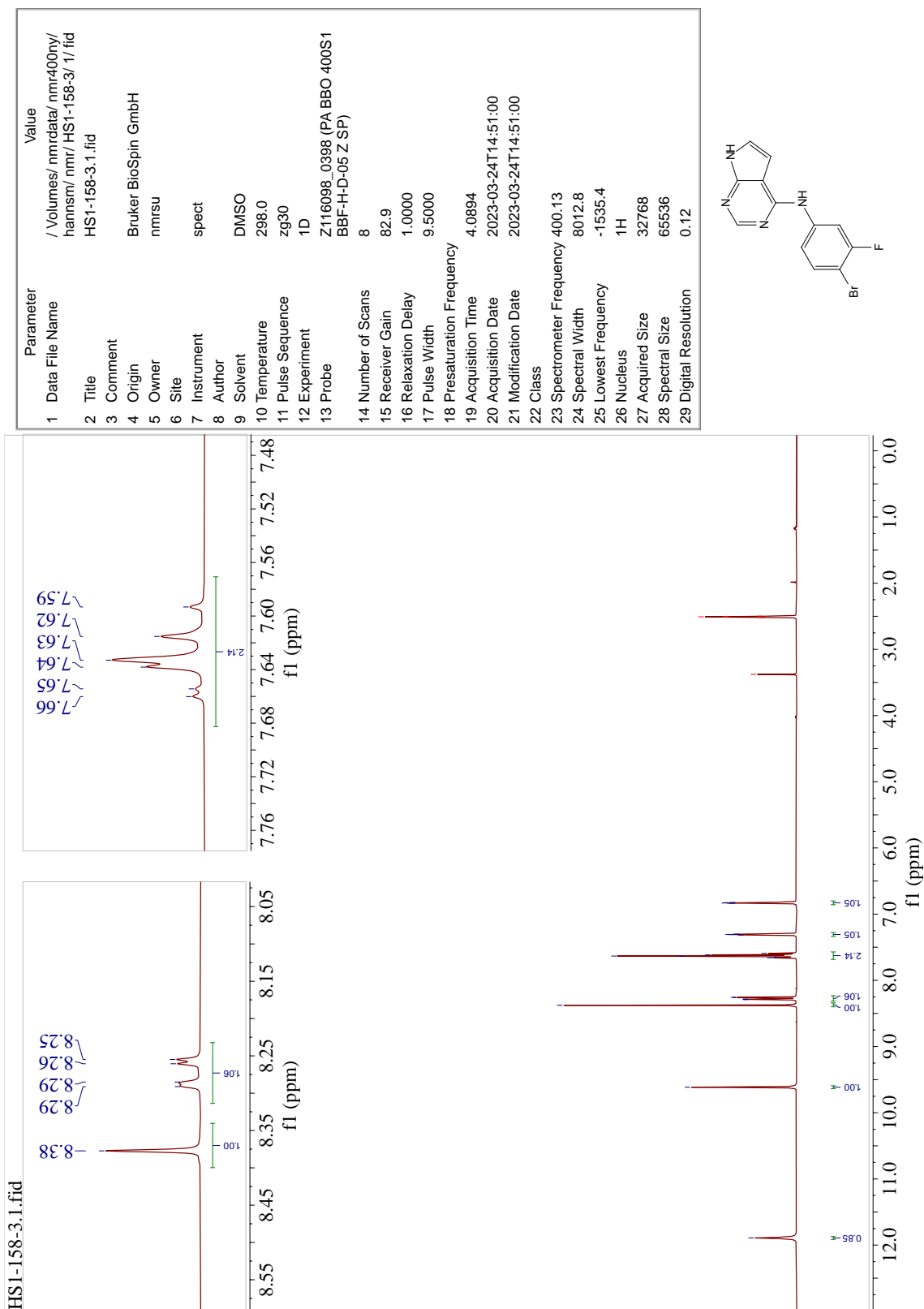


Figure N.1: ¹H-NMR spectrum of compound 46.

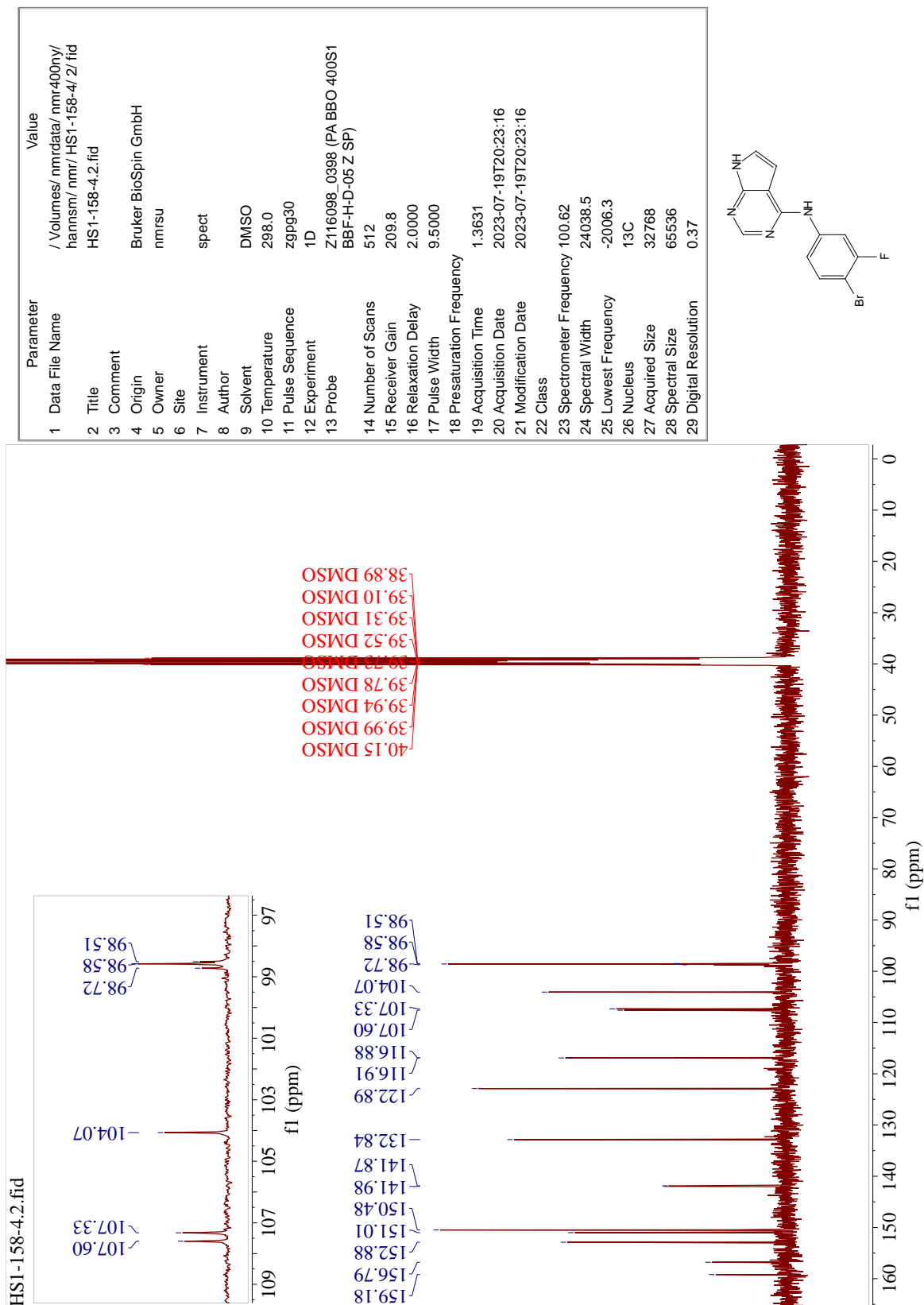


Figure N.2: ¹³C-NMR spectrum of compound 46.

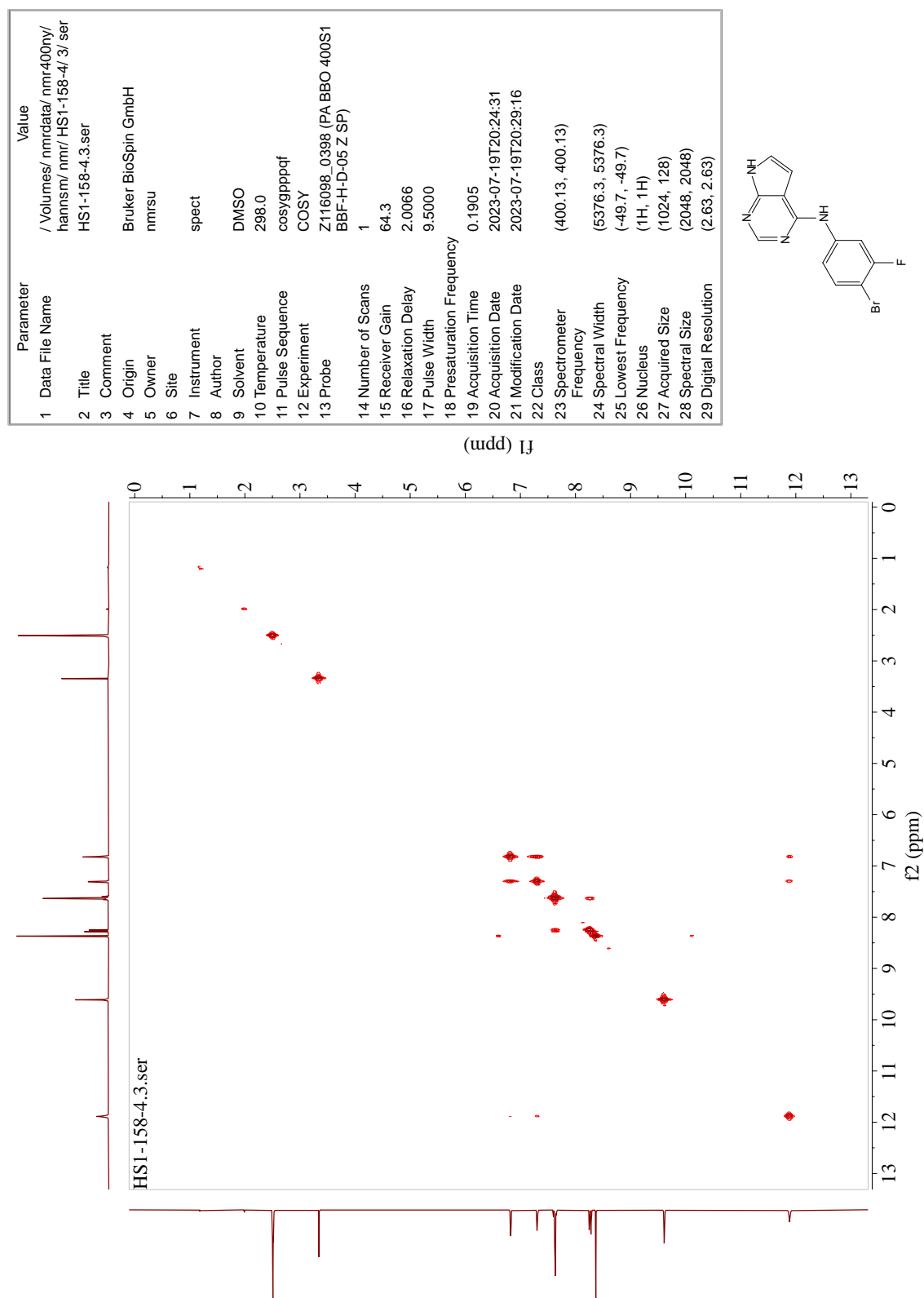


Figure N.3: COSY spectrum of compound 46.

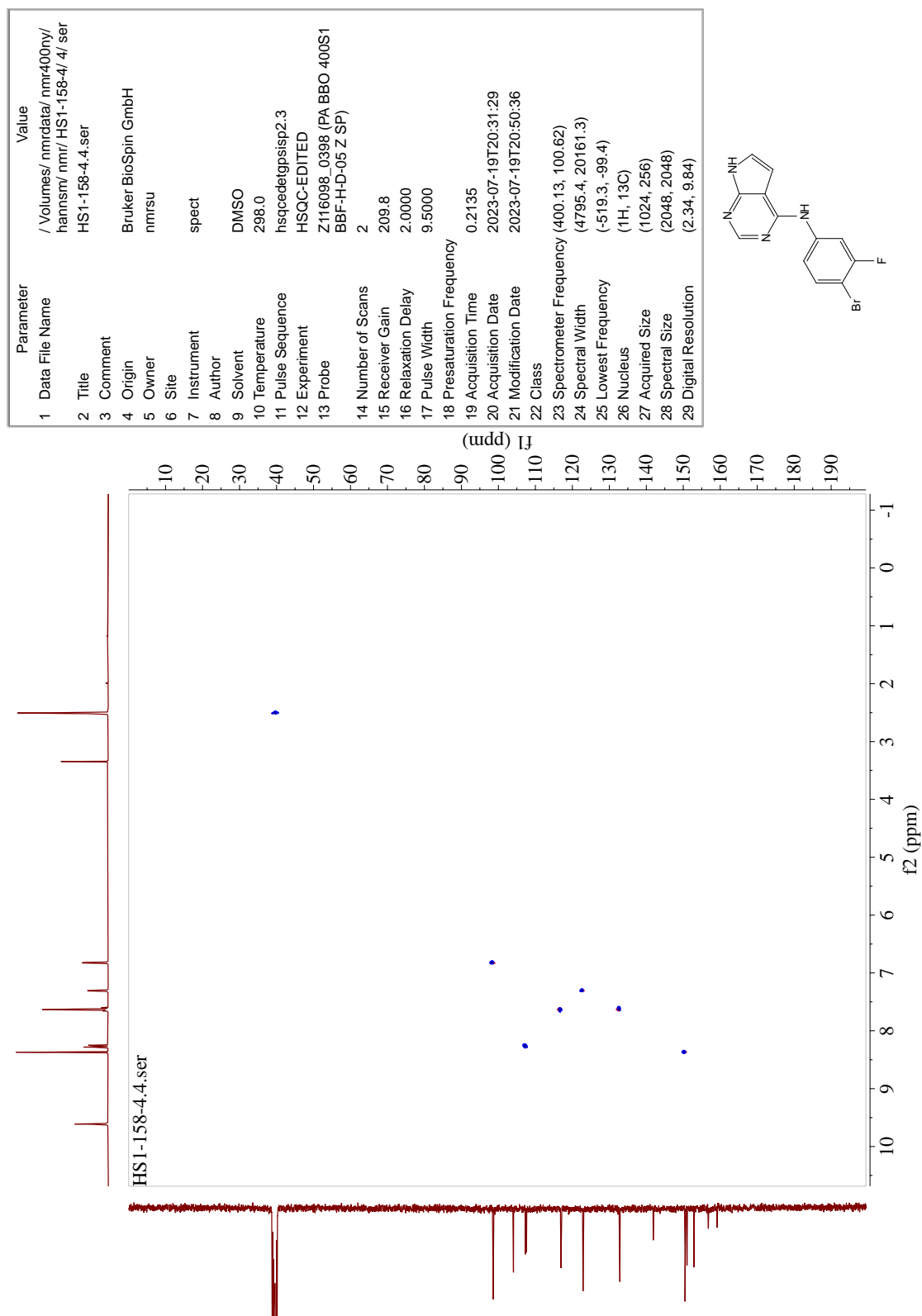


Figure N.4: HSQC spectrum of compound 46.

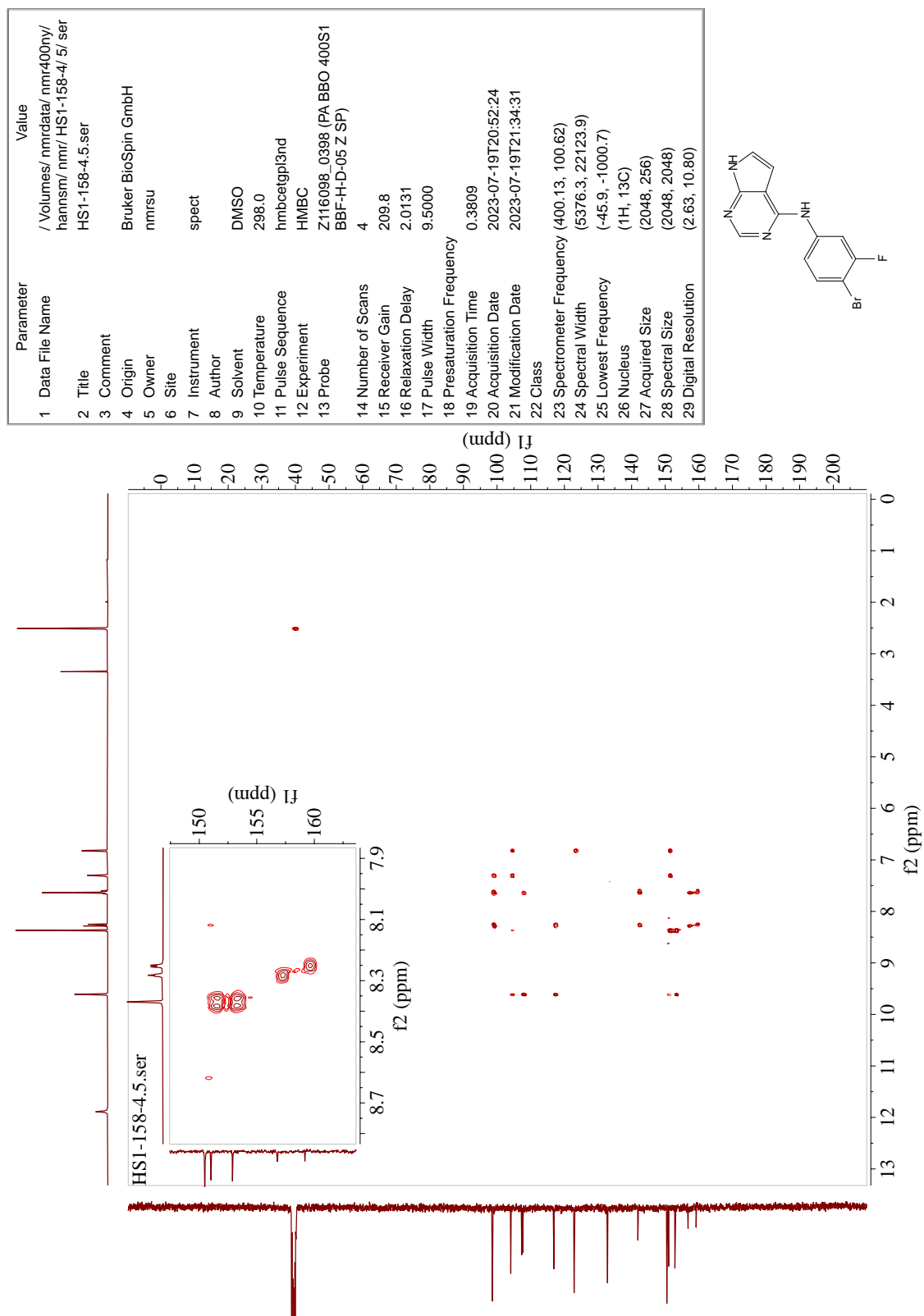


Figure N.5: HMBC spectrum of compound 46.

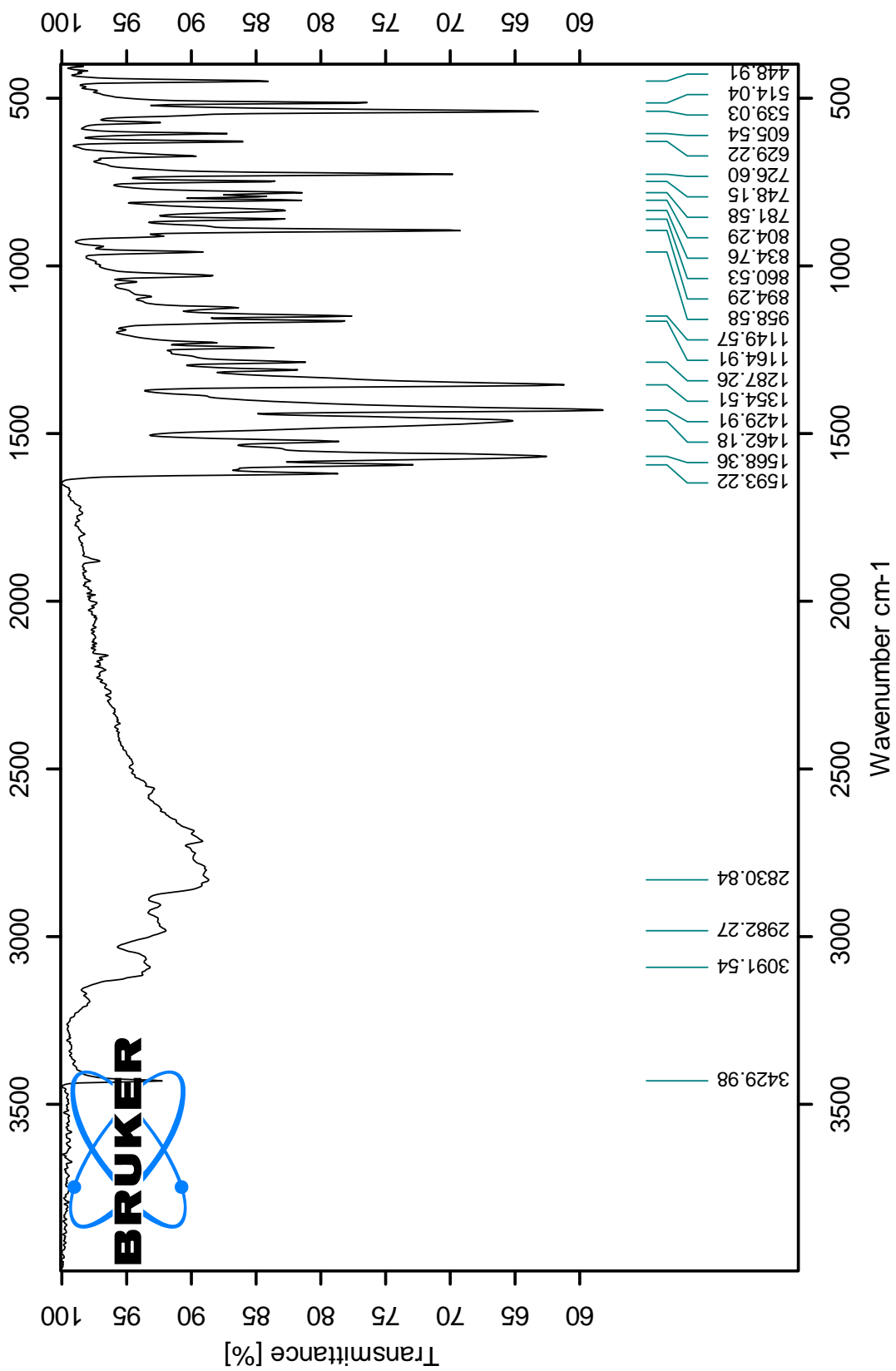


Figure N.6: IR spectrum of compound 46.

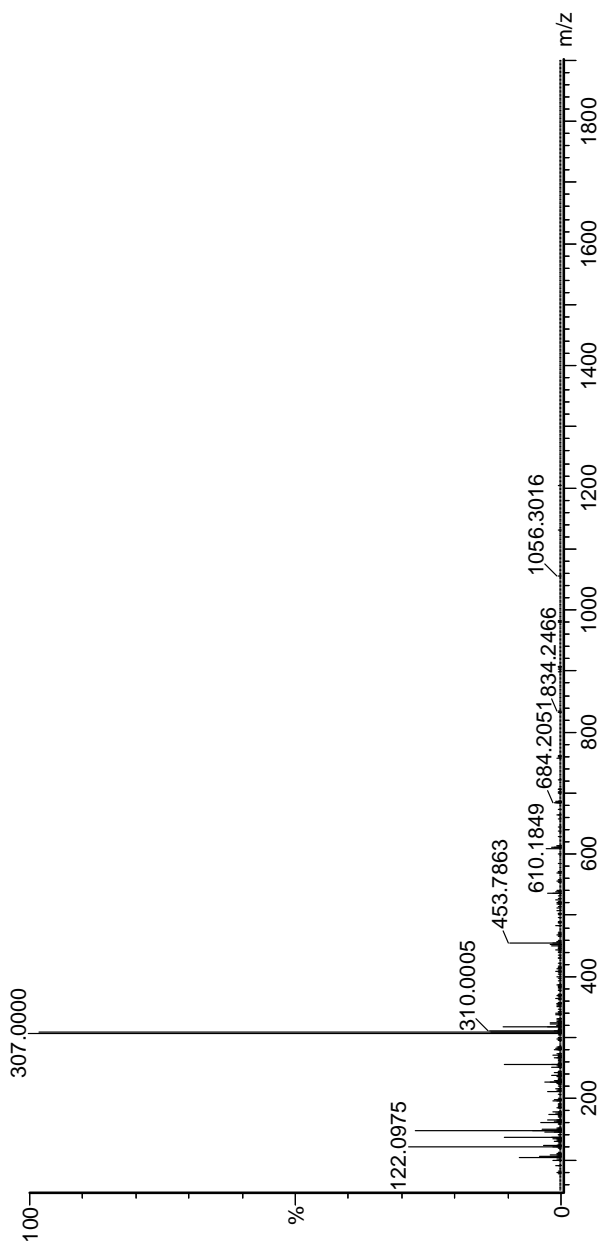
Elemental Composition Report

Single Mass Analysis

Tolerance = 5.0 PPM / DBE: min = -1.5, max = 50.0
 Element prediction: Off
 Number of isotope peaks used for i-FIT = 3

Monoisotopic Mass, Even Electron Ions
 323 formula(e) evaluated with 1 results within limits (up to 50 closest results for each mass)
 Elements Used:
 C: 0-60 H: 1-1000 N: 0-12 F: 0-1 Na: 0-1 Br: 0-1
 ReqlD2200.129 (1.452)AM2 (Ar;35000,0,0,0,0,0,0); Cm (129;136)
 1: TOF MS ES+

7.28e+005



Mass	Calc. Mass	mDa	PPM	DBE	i-FIT	Norm	Conf (%)	Formula
307.0000	306.9995	0.5	1.6	9.5	1303.8	n/a	n/a	C12 H9 N4 F Br
Minimum:				-1.5				
Maximum:			5.0	50.0				

Figure N.7: MS spectrum of compound 46

O Python code for surface plot

Listing O.1: Python code for modelling the 3D surface plot of the formation of side product in different acid amounts in Section 2.2.1 (https://github.com/TrymSaether/MH_3DSurfacePlot)

```
# Import required libraries
import numpy as np
import pandas as pd
from matplotlib import pyplot as plt
from scipy import interpolate
# Define the number of array splits for the 'biprod' column
n=6
# Read the CSV file and select relevant columns
# Replace missing values with zero
df = pd.read_csv('rx_data.csv', delimiter=';', decimal=',',
usecols=['molfrac. Pp', 'biprod', 'HCl (eq.) EtOH']).replace(n
p.nan, 0)
# Split the 'biprod' column into 'n' equally sized arrays
# Transform the list of arrays into a NumPy array for future
operations bp = np.array([np.array_split(df['biprod'].to_numpy(),
n)])
# Define HCl equivalents and reaction time arrays
eq = np.array([0, 0.1, 0.5, 1, 3, 5])
t = np.array([0, 1, 2, 3, 4, 6])
# Create a 2D grid of HCl equivalents and reaction times
T, EQ = np.meshgrid(t, eq)
# Define new, more detailed arrays for HCl equivalents and reaction
times
tnew = np.linspace(0, 6, 100)
eqnew = np.linspace(0, 5, 100)
# Create a 2D grid of the new HCl equivalents and reaction times
tnew, eqnew = np.meshgrid(tnew, eqnew)
# Perform cubic interpolation of 'biprod' onto the new grid
znew = interpolate.griddata((T.flatten(), EQ.flatten()),
bp.flatten(), (tnew, eqnew), method='cubic')
# Set the font style for the plot
plt.rcParams["font.family"] = "Times New Roman" # Define the color
```

APPENDIX O

```
style for the 3D surface plot
c_style = 'plasma'
# Create a new figure with 3D subplot
fig, ax = plt.subplots(subplot_kw={"projection": "3d"})
# Generate the 3D surface plot
hs_plott = ax.plot_surface(tnew, eqnew, 100*znew, cmap=c_style,
edgecolor='k', linewidth=0.25, alpha=1, antialiased=True,
shade=True)
# Add a color bar to the figure
cbar = fig.colorbar(hs_plott, shrink=0.5, aspect=8, pad=0,
ticks=np.linspace(0, 30, 5, endpoint=True))
# Set ticks and label for the color bar
cbar.set_ticks(np.linspace(0, 30, 5, endpoint=True))
cbar.set_label('%')
# Set labels for the x, y, and z axes
ax.set_xlabel('Reaction time (h)')
ax.set_ylabel('HCl (eq.)')
ax.set_zlabel('Side product (26, %)')
# Set the limit for the z axis
ax.set_zlim(0, 40)
# Set the initial viewing angle
ax.view_init(20, -120) # Turn off the grid
ax.grid(False)
# Adjust the padding around the plot
plt.tight_layout() # Display the plot
plt.show()
# Save the figure as a high-resolution PNG file
fig.savefig('surfaceplot_MH.png', dpi=400, bbox_inches='tight')
```



 **NTNU**

Norwegian University of
Science and Technology